SHAPE EFFECT OF SHALLOW FOOTINGS ON SEISMIC BEARING CAPACITY FOR FOUNDATIONS LOCATED NEAR SLOPES

by

Mehmet Çelebi

B.S., Civil Engineering, Istanbul University, 2007

Submitted to the Institute for Graduate Studies in
Science and Engineering in partial fullfillment of
the requirements for the degree of
Master of Science

Graduate Program in Civil Engineering

Boğaziçi University

2019

SHAPE EFFECT OF SHALLOW FOOTINGS ON SEISMIC BEARING CAPACITY FOR FOUNDATIONS LOCATED NEAR SLOPES

APPROVED BY:

Assoc. Prof. Özer Çinicioğlu ……..
(Thesis Supervisor)

Asst. Prof. Dr. Adlen Altunbaş ……..

Asst. Prof. Dr. İrem Zeynep Yıldırım ……..

DATE OF APPROVAL: 24.09.2019

To my wife,

ACKNOWLEDGEMENTS

I am very excited to present such a subject which is not discussed in the current literature up until now.

I would like to express the deepest appreciation to my thesis supervisor Assoc. Prof. Özer Çinicioğlu for his valuable help, convincingly conveyed a spirit of adventure in regard to the solution of this study and scholarship and an engineering judgement guiding me throughout the whole duration of the thesis. Without his guidance and persistent support, this dissertation would have not been possible.

I would like to thank also the members of my Master's thesis examination committee: Asst. Prof. Zeynep Yıldırım and Asst. Prof. Adlen Altunbaş for their efficient comments and supportive attitude towards me and in valuable advice.

Special thanks to Ahmet Talha Gezgin for his endless support and great patience all times.I am also thankful to Geogrup family members for their polite assistance and good wishes.

And finally, I would like to thank my wife Hacer Çelebi for her endless love, moral support and great patience at all times. I am also very thankful to my mother Emel Çelebi and my brother Orhan Çelebi since they have given me their support throughout the thesis, as always they do during my educational life.

ABSTRACT

EFFECT OF THE SHAPE OF SHALLOW FOOTINGS ON SEISMIC BEARING CAPACITY FOR FOUNDATIONS LOCATED NEAR SLOPES

In this study, the factors that are effective on the collapsing behaviour such as the soil strength which is forceful on calculating the bearing capacity under dynamic loads, the slope height and angle, the foundation geometry and the distance of the foundation to the slope were taken into consideration and studied from variety of recent studies. As a result of these studies, relations and design charts have been presented in order to calculate the seismic bearing capacity. The main aspect of all existing studies is that the problem has been investigated for the plane deformation conditions. In consequence of the adoption of the plane deformation, the presented and created charts are valid only for the continuous footings. The aim of this study is to investigate the effect of the shape effect of foundation which has not been studied in previous studies on the seismic bearing capacity of the shallow foundations constructed on or near the slopes The approach used in this study will consider the undrained behavior during the earthquake by staying on the safe side. In accordance with the purpose of this thesis, finite elements methods will be created to determine seismic bearing capacity and parametric study will be done. The factors which will be investigated in the parametric study are the shape and size of foundation, the distance to the slope, undrained strength of soil, slope height, slope angle and earthquake acceleration. The effect of the earthquake on seismic bearing capacity will be described by using the pseudo-static method The inertia effect of soil and the structural loads will be defined in the models. Design tables will be prepared by using the obtained results, and various failure systems such as the foundation sliding, bearing capacity failure, base failure and foundation failure will be discussed.

ÖZET

ŞEV YAKININDA BULUNAN TEMELLERİN DEPREMLİ TAŞIMA GÜCÜNE TEMEL ŞEKLİNİN ETKİSİ

Şev üzerinde veya yakınında bulunan temeller için dinamik yükler altında taşıma kapasitesinin hesaplanmasında etkili olan temel zemini mukavemet özellikleri, şev yüksekliği ve eğimi, temel geometrisi ve temelin şeve olan mesafesi gibi göçme davranışını etkileyen faktörler çeşitli yakın zaman çalışmalarından göze alınmış ve incelenmiştir. Bu çalışmaların sonucunda tasarıma yönelik depremli taşıma gücünün hesaplanabilmesi için bağlantılar ve tasarım abakları sunulmuştur. Tüm mevcut çalışmaların ortak yönü problemin düzlem şekil değiştirme şartları için incelenmiş olmasıdır. Düzlem şekil değiştirme kabulünün sonucunda ise sunulan ve oluşturulan abaklar sadece mütemadi temeller için geçerlidir. Bu çalışmanın amacı daha önceki çalışmalarda incelenmemiş olan temel şekil etkisinin şevler üzerine veya yakınına inşa edilen yüzeysel temellerin depremli taşıma güçleri üzerine etkisinin incelenmesidir. Çalışmada kullanılan yaklaşım, güvenli tarafta kalarak deprem sırasında drenajsız davranışı göz önüne alacaktır. Bu amaçla üç boyutlu sonlu elemanlar modelleri oluşturulacak ve parametrik çalışma yapılacaktır. Parametrik çalışmada incelenecek etkiler temel şekli, boyutu, şeve uzaklığı, zeminin drenajsız mukavemeti, şev yüksekliği, şev açısı ve deprem ivmesidir. Depremin taşıma gücü üzerinde etkisi eşdeğer-dinamik yöntemle tanımlanacaktır. Hem zeminin, hem de yapısal yüklerin eylemsizliği modellerde tanımlanacaktır. Elde edilen sonuçlar kullanılarak tasarım abakları hazırlanacak, ortaya çıkabilecek temel kayması, taşıma gücü göçmesi, şev göçmesi, toptan göçme gibi farklı göçme sistemleri tartışılacaktır.

TABLE OF CONTENTS

ACKNOWLEDGEMENTS iv
ABSTRACT v
ÖZET vi
LIST OF FIGURES ix
LIST OF TABLES xxi
LIST OF SYMBOLS xxii
LIST OF ACRONYMS/ABBREVIATIONS xxiv
1. INTRODUCTION 1
2. LITERATURE REVIEW 3
2.1 Static Bearing Capacity of Shallow Foundation Around Cohesive Slopes 4
2.2 Seismic Bearing Capacity of Foundations Around Cohesive Slopes 22
2.3 Shape Effect of Shallow Foundation On Seismic Bearing Capacity 45
3. METHODOLOGY 81
3.1 FEM in Geotechnical Engineering and Plaxis 3D 81
3.2 Definition and Assumptions of the Problem 82
3.3 Suggested Solution Method 84
3.4 Model Geometry 85
3.5 Data Input in Plaxis 3D 86
3.5.1 General Settings 86
3.5.2 Numerical Model 89
3.5.3 Boundary Conditions 90
3.5.4 Loads 91
3.5.5 Material Properties 92
3.5.6 Finite Element Mesh Generation 94
3.6 Design Steps 94
3.7 Evaluation of Plaxis 3D Outputs 98
4. RESULTS AND DISCUSSIONS 100
4.1 Determination of Influential Parameters 100
4.1.1 Influence of Horizontal Seismic Acceleration Coefficient 101

4.1.2 Influence of Slope Angle 101
4.1.3 Influence of Slope Height 103
4.1.4 Influence of Slope Soil Strength 103
4.2 Examination of Failure Mechanisms 104
4.3 Design Charts 106
5. CONCLUSIONS 124
REFERENCES 126
APPENDIX A: LIST OF RESULTS OF FINITE ELEMENTS MODELS CREATED FOR STATIC CONDITION 131
APPENDIX B: LIST OF RESULTS OF FINITE ELEMENTS MODELS CREATED FOR SEISMIC CONDITION 135

LIST OF FIGURES

Figure 2.1. Plastic zones near the strip foundation on the face of a slope (Meyerhof, 957) 5

Figure 2.2. Factors of bearing capacity for the shallow foundation on a purely cohesive and granular slope (Meyerhof, 1957) 6

Figure 2.3. Slip surfaces and plastic zones around the rough strip foundation on top of the slope (Meyerhof,1957) 7

Figure 2.4. Factors of strip foundation's bearing capacity on a purely cohesive incline (Meyerhof, 1957 8

Figure 2.5. Footings on or adjacent to a slope (Bowles,1997) 9

Figure 2.6. Failure surfaces and stress trajectories in the plastic zone beneath the footing (Bowles, 1997)..... 10

Figure 2.7. Bearing capacity factors (N'_c *and* N'_q) for footings on or adjacent to a slope (Bowles, 1997) 11

Figure 2.8. Failure mechanism adopted for the upper bound solution (Kusakabe *et al.*, 1981 11

Figure 2.9. No.1 design chart presented to calculate the dimensionless factor (μ) (Kusakabe *et al.*, 1981)..... 12

Figure 2.10. No.2 and No.3 design charts presented to calculate the dimensionless factor (μ) Kusakabe *et al*., 1981) 13

Figure 2.11. Schematic representation of the problem (Georgiadis,2010)……..... 15

Figure 2.12. Modes of failure (a) and (b) failure of bearing capacity and (c) overall failure of incline (Georgiadis, 2010)……... 15

Figure 2.13. Variation of failure mode and Nc with H/B for λ= 0 and β= 45° (Georgiadis, 2010)..... 16

Figure 2.14. Variety of Nc with λ for cu/γB= 0.5 (Georgiadis, 2010)…….. .. 17

Figure 2.15. Variety of Nc with λ for cu/γB= 1 (Georgiadis, 2010)…….. .. 17

Figure 2.16. Variety of Nc with λ for cu/γB= 1.5 (Georgiadis, 2010)……..…… 18

Figure 2.17. Variety of Nc with λ for cu/γB= 2, 2.5, and 5 (Georgiadis, 2010)……. 18

Figure 2.18. Variation of λo with β (Georgiadis, 2010)…….. 19

Figure 2.19. The applied forces and the mechanism of failure used in the examination (Castelli and Motta, 2010)..... 20

Figure 2.20. Variation of ground factors (Nc*/Nc) in a static condition with the distance of foundation from the edge of the incline (Castelli and Motta, 2010)..... 21

Figure 2.21. Both sides mechanism of failure used in the study (Kumar and Rao, 2003)……. 23

Figure 2.22. Single side mechanism of failure used in the study (Kumar and Rao, 2003)…… 23

Figure 2.23. Change of *Nq* with *αh* for various amounts of *Φ* and *β*: (a) *Φ*= 10°; (b) *Φ*= 20°; (c) *Φ*= 30°; (d) *Φ*= 40°; (e) *Φ*= 50° (Kumar and Rao, 2003) ……. 24

Figure 2.24. Change of *Nc* with *αh* for various amounts of *Φ* and *β*: (a) *Φ*= 0°; (b) *Φ*= 10°; (c) *Φ*= 20°; (d) *Φ*= 30°; (e) *Φ*= 40°; (f) *Φ*= 50° (Kumar and Rao, 2003) ……..... 25

Figure 2.25. Change of *Nγ* with αh for various amounts of *Φ* and *β*: (a) *Φ*= 10°; (b) *Φ*= 20°; (c) *Φ*= 30°; (d) *Φ*= 40°; (e) *Φ*= 50° (Kumar and Rao, 2003)…. ... 26

Figure 2.26. Graphical representation of the problem (Shiau *et al.*, 2006)……...27

Figure 2.27. Effect of *tanθ* on *p/γB* for various *Φ* (Shiau *et al.*, 2006)……... . 28

Figure 2.28. Comparison of upper bound velocity diagrams for the effect of inertia forces (Shiau *et al.*, 2006)…….. 29

Figure 2.29. Effect of q/γB on p/γB for various β (Shiau *et al.*, 2006)...…… 30

Figure 2.30. Effect of soil inertia k_h on p/γB (Shiau *et al.*, 2006)…….……30

Figure 2.31. Mechanism of failure used in the analysis (Yamamoto, 2010)……32

Figure 2.32. Mechanisms of failure for various amounts of *Φ*, *β*, *α,* and K_h (Yamamoto, 2010)…….. 34

Figure 2.33. Charts of design for N_{ce} (*Φ*= 30°, 40°, *D/B*= 0, *a*= 0.0) (Yamamoto, 2010)…….. 34

Figure 2.34. Charts of design for N_{ce} (*Φ*= 30°, 40°, *D/B*= 1, *a*= 0.0) (Yamamoto, 2010)…….. 35

Figure 2.35. Charts of design for N_{ce} (*Φ*= 30°, 40°, *D/B*= 0, *a*= 0.5) (Yamamoto, 2010)…….. 35

Figure 2.36. Charts of design for Nγe (Φ= 30°, 40°, D/B= 0, *a*= 0.0) (Yamamoto, 2010)…….. 35

Figure 2.37. Charts of design for $N_{\gamma e}$ (Φ= 30°, 40°, D/B= 1, a= 0.0) (Yamamoto, 2010)…….. 36

Figure 2.38. Charts of design for $N\gamma e$ (Φ= 30°, 40°, D/B= 0, a= 0.5) (Yamamoto, 2010)…….. 36

Figure 2.39. N_c^*/N_c rates as a function of the normalized d/B distance of incline (Castelli and Motta, 2010)……..... 37

Figure 2.40. Model geometry and a typical FELA mesh…….. 39

Figure 2.41. Comparison of the results of the present study with those presented by previous researchers (A. Keshavarz *et al.,* 2019)……..... 40

Figure 2.42. Comparison of the variation in Nc against L/B for β = 30º; H/B=1, 2, 4; and $c_{uo}/(\gamma B)$=2.5 (A. Keshavarz *et al.,* 2019)……..... 41

Figure 2.43. Variation of the $q_u/(\gamma B)$ with L/B (A. Keshavarz *et al.,* 2019)…….. 41

Figure 2.44. The effect of k_h on $q_u/(\gamma B)$ (H/B=3, $c_{uo}/(\gamma B)$=3.5, and $\beta=35^0$) (A. Keshavarz *et al.,* 2019)……..... 42

Figure 2.45. Variation of $k_h q_u/c_{u0}$ against k_h for the level ground (A. Keshavarz *et al.,* 2019)…….. 42

Figure 2.46. Typical foundation failure pattern for $c_{uo}/(\gamma B)$= 4, kB/c_{u0}=0, k_h =0.1, $\beta=45^0$, (H/B = 4) (A. Keshavarz *et al.,* 2019)…….. 43

Figure 2.47. The effect of c_{uo} / (γ B) on the failure mode (kB/c_{u0}=0, k_h =0, $\beta=45^0$, H/B = 1) (A. Keshavarz *et al.,* 2019)…….. 44

Figure 2.48. The effect of k_h on the failure mode c_{uo} / (γ B) =4, (kB/c_{u0}=0, L/B = 0, $\beta=45^0$, H/B =4) (A. Keshavarz *et al.,* 2019)…….. 44

Figure 2.49. Design charts for average values of lower and upper bounds of normalized bearing capacity of a rough strip footing located on slope with $\beta = 10^0$ (A. Keshavarz *et al.,* 2019)…….. 45

Figure 2.50. Lower bound analysis of finite element coarse mesh (H. Yang *et al.,* 2003)….. 46

Figure 2.51. Lower bound analysis of finite element fine mesh (H. Yang *et al.,* 2003)... 46

Figure 2.52. Comparison of 3-dimensional lower and bound bearing capacity Nc for strip foundations on a weightless and purely adhesive soil (H. Yang *et al.,* 2003). 47

Figure 2.53. Various solutions for 3-dimensional bearing capacity for shallow foundations (H. Yang *et al.,* 2003)..... 48

Figure 2.54. Shape and depth factors usually utilized for clays (Salgado *et al.,* 2004)… 50

Figure 2.55. Ratio of net bearing capacity factor to undrained shear strength, $\boldsymbol{q_{bL}^{net}/s_u}$, for foundations in clay (L = lower, U= upper bound) (Salgado *et al.,* 2004). 51

Figure 2.56. Constants of regression in the shape factor equation (Salgado *et al.,* 2004). 52

Figure 2.57. Shape factor for foundations of various shapes as a function of relative depth as calculated by limit analysis plotted together with best-fit lines with the form of Equation 2.25 (Salgado *et al.,* 2004)..... 52

Figure 2.58. Finite element mesh (Zhu and Michalowski, 2005)..... 53

Figure 2.59. The analogy of results: (a) factor N_c and (b) factor N_γ (Zhu and Michalowski, 2005)..... 56

Figure 2.60. Factor s_γ (finite element method) as a function of aspect ratio *L/B* and internal friction angle φ (Zhu and Michalowski, 2005)... 57

Figure 2.61. Movement in the region of squared foundation: (a) 3-D distribution of vertical displacement intensity and (b) horizontal movement at surface (Zhu and Michalowski, 2005)... 57

Figure 2.62. Model test programme (Pathak *et al.*, 2008)..... 58

Figure 2.63. Typical penetration response of a footing on strong over weak soils (Yu *et al.*,2011)... 61

Figure 2.64. Typical finite element mesh (Yu *et al.*, 2011)... 62

Figure 2.65. Factors of bearing capacity for surface rough squared foundations on smooth soils (Yu *et al.*, 2011)... 63

Figure 2.66. N_c for surface square foundations on two-layer weightless soils (small strain analyses) (Yu *et al.*, 2011)... 64

Figure 2.67. The meshing of the computational model (quarter symmetry) (Li *et al.*, 2009)..... 65

Figure 2.68. Bearing capacity for rectangular foundations of different forms (Li *et al.*, 2009)..... 66

Figure 2.69. Plan representation of the foundation's impact scope (Li *et al.*, 2009)... 67

Figure 2.70. Problem notation and potential failure mechanism (Shiau *et al.*, 2011)... ... 68

Figure 2.71. Bearing capacity of upper and lower bound for weightless slopes (smooth base, β=90°) (Shiau *et al.*, 2011)... 69

Figure 2.72. The analogy of transformed forms and swiftness profiles for smooth and rough foundations (β=90°, *L/B*=0) (Shiau *et al.*, 2011)..... 70

Figure 2.73. Upper Bound Results for Rough and Smooth Foundations (β=90^o) (Shiau *et al.,* 2011). 70

Figure 2.74. Averaged upper and lower bounds for different angles of inclination (Shiau *et al.,* 2011)... 71

Figure 2.75. Averaged upper and lower bounds for different angles of inclination (Shiau *et al.,* 2011)... 71

Figure 2.76. Velocity contours for different angles of inclination ($c_u/\gamma B$=5, *L/B=0*, flat bottom) (Shiau *et al.,* 2011)... 72

Figure 2.77. Velocity contours for different angles of inclination ($c_u/\gamma B$=1, *L/B=0*, flat bottom) (Shiau *et al.,* 2011)... 72

Figure 2.78. Impact of *L/B* on the bearing capacity (smooth base) (Shiau *et al.,* 2011)..73

Figure 2.79. Velocity contours for different L/B (smooth base, β =90o, cu/ γB=5) (Shiau *et al.,* 2011)... 74

Figure 2.80. Effect of *H/B* (flat bottom, *L/B*=0) (Shiau *et al.,* 2011)... 75

Figure 2.81. FE meshes: (a) half of a square footing; (b) half of a circular footing (Islam *et al.,* 2017)... 76

Figure 2.82. Shape factor s_c as a function of φ and *D/B* : (a) comparison with previous studies (*D/B =0)*; (b) square footing ; (c) circular footing (Islam *et al.,* 2017)... 76

Figure 2.83. The failure mechanism is shown in plan view (a and b) and elevational view (c and d): (a) circular foundation: (b) square foundation: (c) circular foundation: (d) square foundation (Islam *et al.,* 2017)... 77

Figure 2.84. Shape factor sγ as a function of φ and D/B: (a) Comparison with previous studies (D/B=0); (b) Square footing; (c) circular footing. (Islam *et al.*, 2017)... 79

Figure 2.85. Continued (Islam *et al.*, 2017)..... 79

Figure 3.1. Graphical representation of the problem.. 83

Figure 3.2. Three dimensional model of created finite elements model 86

Figure 3.3. 'Project' tab sheet of 'General Settings' window 87

Figure 3.4. 'Dimensions' tab sheet of 'General settings' window... 88

Figure 3.5. Distribution of nodes (.) and stress points (x) in a 15-node wedge element... 89

Figure 3.6. Schematic representation of created finite elements model.. 90

Figure 3.7. Finite element mesh generation 94

Figure 3.8. Typical view of "Calculation Module" window... 95

Figure 3.9. Typical view of 'Initial Phase' window... 95

Figure 3.10. Activation of inertia force applying on soil clusters 96

Figure 3.11. The load stage (Σ-Mstage) found by Calculations module of Plaxis 3D for the final limit state 97

Figure 3.12. Failure mechanism obtained for the finite element model named as C_45_4_0_16_25_0.1_D and enlarged view of the failure mechanism 98

Figure 3.13. Shear surfaces obtained for the finite element model named as C_45_4_0_16_25_0.1_D 99

Figure 4.1. Variation of N_{cse} with k_h for λ=0 (β=15^0, cu/γB =2.5) 101

Figure 4.2. Variation of Ncse with β for λ=0 (k_h=0, cu/γB =2.5)..... 102

Figure 4.3. Variation of N_{cse} with β for λ=0 (k_h=0.1, $c_u/\gamma B$ =2.5). 102

Figure 4.4. Variation of N_{cse} with β for λ=0 (k_h=0.2, $c_u/\gamma B$ =2.5). 102

Figure 4.5. Variation of N_{cse} with β for λ=0 (k_h=0.3, $c_u/\gamma B$ =2.5). 103

Figure 4.6. Variation of N_{cse} with $c_u/\gamma B$ for all k_h values (β=30°, *L/B=1*, λ=0). 104

Figure 4.7. Base failure due to self-weight of cohesive slope (β=45°, *H/B*=4.0 m, and $c_u/\gamma B$ =0.625) 105

Figure 4.8. Base failure due to self-weight of cohesive slope (β=45°, *H/B*=4.0 m, $c_u/\gamma B$ =0.625 and k_h=0.2) 105

Figure 4.9. Typical "Foundation failure" approaches for λ=0 condition (a) β=45°, *H/B*=1.0 m, $c_u/\gamma B$ =1.25 and k_h=0.2); (b) β=45°, *H/B*=2.0 m, $c_u/\gamma B$ =0.625 and k_h=0.1) 106

Figure 4.10. Variation of bearing capacity factor with horizontal seismic acceleration coefficient for $\beta=15^o$ 107

Figure 4.11. Variation of bearing capacity factor with horizontal seismic acceleration coefficient for $\beta=15^o$ 107

Figure 4.12. Variation of bearing capacity factor with horizontal seismic acceleration coefficient for $\beta=15^o$ 108

Figure 4.13. Variation of bearing capacity factor with horizontal seismic acceleration coefficient for $\beta=15^o$ 108

Figure 4.14. Variation of bearing capacity factor with horizontal seismic acceleration coefficient for $\beta=15^o$ 109

Figure 4.15. Variation of bearing capacity factor with horizontal seismic acceleration coefficient for $\beta=15^o$ 109

Figure 4.16. Variation of bearing capacity factor with horizontal seismic acceleration coefficient for $\beta=15^o$ 110

Figure 4.17. Variation of bearing capacity factor with horizontal seismic acceleration coefficient for $\beta=15^o$ 110

Figure 4.18. Variation of bearing capacity factor with horizontal seismic acceleration coefficient for $\beta=15^o$ 111

Figure 4.19. Variation of bearing capacity factor with horizontal seismic acceleration coefficient for $\beta=15^o$ 111

Figure 4.20. Variation of bearing capacity factor with horizontal seismic acceleration coefficient for $\beta=15^o$ 112

Figure 4.21. Variation of bearing capacity factor with horizontal seismic acceleration coefficient for $\beta=30^o$ 112

Figure 4.22. Variation of bearing capacity factor with horizontal seismic acceleration coefficient for $\beta=30^o$ 113

Figure 4.23. Variation of bearing capacity factor with horizontal seismic acceleration coefficient for $\beta=30^o$ 113

Figure 4.24. Variation of bearing capacity factor with horizontal seismic acceleration coefficient for $\beta=30^o$ 114

Figure 4.25. Variation of bearing capacity factor with horizontal seismic acceleration coefficient for $\beta=30^o$ 114

Figure 4.26. Variation of bearing capacity factor with horizontal seismic acceleration coefficient for $\beta=30^o$ 115

Figure 4.27. Variation of bearing capacity factor with horizontal seismic acceleration coefficient for $\beta=30^o$ 115

Figure 4.28. Variation of bearing capacity factor with horizontal seismic acceleration coefficient for $\beta=30^o$ 116

Figure 4.29. Variation of bearing capacity factor with horizontal seismic acceleration coefficient for $\beta=30^o$ 116

Figure 4.30. Variation of bearing capacity factor with horizontal seismic acceleration coefficient for $\beta=30^o$ 117

Figure 4.31. Variation of bearing capacity factor with horizontal seismic acceleration coefficient for $\beta=30^o$ 117

Figure 4.32. Variation of bearing capacity factor with horizontal seismic acceleration coefficient for $\beta=45^o$ 118

Figure 4.33. Variation of bearing capacity factor with horizontal seismic acceleration coefficient for $\beta=45^o$ 118

Figure 4.34. Variation of bearing capacity factor with horizontal seismic acceleration coefficient for $\beta=45^o$ 119

Figure 4.35. Variation of bearing capacity factor with horizontal seismic acceleration coefficient for $\beta=45^o$ 119

Figure 4.36. Variation of bearing capacity factor with horizontal seismic acceleration coefficient for $\beta=45^o$ 120

Figure 4.37. Variation of bearing capacity factor with horizontal seismic acceleration coefficient for $\beta=45^o$ 120

Figure 4.38. Variation of bearing capacity factor with horizontal seismic acceleration coefficient for $\beta=45^o$ 121

Figure 4.39. Variation of bearing capacity factor with horizontal seismic acceleration coefficient for $\beta=45^o$ 121

Figure 4.40. Variation of bearing capacity factor with horizontal seismic acceleration coefficient for $\beta=45^o$ 122

Figure 4.41. Variation of bearing capacity factor with horizontal seismic acceleration coefficient for $\beta=45^o$ 122

Figure 4.42. Variation of bearing capacity factor with horizontal seismic acceleration coefficient For $\beta=45^o$ 123

Figure 4.43. Variation of bearing capacity factor with horizontal seismic acceleration coefficient for $\beta=0^o$ 123

LIST OF TABLES

Table 2.1. Comparison of 3-dimensional upper and lower bound coefficient of bearing capacity N_c for shallow foundations on a weightless and frictional cohesive soil 48

Table 2.2. Soil characteristics 59

Table 2.3. Ultimate bearing capacity (UBC) for footings 60

Table 3.1. Physical and elastic properties of rigid plate element 90

Table 3.2. Horizontal seismic acceleration coefficients 91

Table 3.3. Properties of the cohesive slope soils employed in present study 93

LIST OF SYMBOLS

B	Footing width
c_u	Undrained shear strength of cohesive slope soil
d_{eq}	Equivalent plate thickness
D_f	Depth of footing
EA	Axial stiffness of the plate element
EI	Flexural stiffness of the plate element
E_u	Undrained elasticity modulus of cohesive soil
g	Gravitational acceleration
q_c	Seismic bearing capacity of surficial strip footings near cohesive slopes
H	Slope height
L	Length of foundation
k_h	Horizontal seismic acceleration coefficient
k_x	Permeability in horizontal direction (x axis)
k_y	Permeability in vertical direction (y axis)
Ψ_u	Undrained dilatancy angle
φ_u	Undrained friction angle
N_{ce}	Seismic bearing capacity factor for surficial strip footings on level ground
N_{cse}	Seismic bearing capacity factor of surficial strip footings near cohesive slopes
N_{cs}	Static bearing capacity factor for surficial strip footings near cohesive slopes
R_{inter}	Interface strength reduction factor
R^2	Corelation coefficient
u_x	Nodal displacement in horizontal direction (x axis)
u_y	Nodal displacement in vertical direction (y axis)
w	Weight of the plate element

β	Slope angle
W	Weight of slope
γ_{sat}	Soil unit weight below phreatic level
γ_{unsat}	Soil unit weight above phreatic level
λ	Normalized footing distance from the slope edge
ν	Poisson ratio of the plate element
ν_u	Undrained Poisson ratio of soil
$\Sigma\text{-}M_{stage}$	Magnitude of the applied load on ground

LIST OF ACRONYMS/ABBREVIATIONS

WSDOT	Washington State Department of Transportation
AASHTO	American Association of State Highway Transportation Officals
FEM	Finite Elements Method
RITSS	Remeshing and Interpolation Method with Small Strain Model
UU	Unconsolidated-Undrained

1. INTRODUCTION

Foundation is the lowest and most important part of structure that transfer the loads from structure to ground. Especially, it has become a big deal with high-rise structures touching the sky. Therefore, a well design of foundation must be deeply considered about the bearing capacity of the soil.

Foundations are divided into two main categories as shallow and deep foundations depending on the location of the load bearing layer. If the layer of soil of foundation which is satisfactory for load bearing, structure can be supported by shallow footings. Spread footings and mat foundations also can be regarded as shallow foundations. On the other hand, ıf the upper strata is not strong to carry itself in weight or more compressible, structure may be supported by deep foundations.

A shallow foundation is preferred when surface soils are enough strong and stiff to carry the applied loads. It has an important type of foundation because of utilization and affordable of it.Shallow foundations are commonly built close to the finished ground surface.

Bearing capacity is net bearing pressure that causes the foundation failure. The assumption of the bearing capacity of a shallow foundations has become a big deal for geotechnical engineering. Slopes can be exposed different loads. Seismic loads may cause serious defects to soil and foundations. Due to seismic events, foundations can tend to a decline at limit bearing pressure and increment in compressbility. Therefore, design of foundations in seismic region needs different precaution compared to the static condition.

Analytical and numerical approaches are possible to assess seicmis bearing capacity of shallow footings such as the limit equilibrium method, limit analysis and finite element analysis for the calculation of the seismic bearing capacity coefficients needed for the design of the foundation. Since the pseudo-static approach is more practical and simple, the analyses are based on pseudo-static method.

The main purpose of this study is to present suitable design charts for the determination of undrained seismic bearing capacity factor linked with various shape of shallow foundations. The method used in this study will take account the undrained conditions because undrained circumstances are related to the most significant conditions. In the present study, the finite element method is used to evaluate the seismic bearing capacity of shallow foundations on soil which satisfies Mohr-Coulomb strength criterion, different slope angles and seismic coefficients. More than 1000 analyses were carried out in PLAXIS 3D to investigate the shape effect of shallow footings on undrained seismic bearing capacity. Lastly, the final purpose is to pioneer research studies in the literature for showing the effect of different shapes when seismic bearing capacity problem is regarded for shallow foundations.

2. LITERATURE REVIEW

This thesis aims to look at the issue of ‘real life' shallow foundation states, in a foundation at nearby positions to human-made slopes consisting of pure cohesive soil. Foundations are modelled to transmit and spread their loading to the underneath soil. Three main design criteria play an essential role to ensure the stability of foundations, respectively ultimate bearing capacity, settlement, and the cost feasibility of foundation. Primarily in this dissertation, the shallow foundation's bearing capacity on cohesive soil will be handled.

When the soil backing of foundation fails in shear, bearing capacity failure happens, which can include different type of failure mechanism, namely; punching, local, and general shear failure (Bowles,1988). In geotechnical engineering, prediction and determination of the final bearing capacity are one of the most fundamental and problematic issues (Poulos *et al*.,2001)

‘Literature review' section is composed of three parts, as briefly explained in the ‘Introduction' section of the thesis. First of all, the static bearing of various shape footings will be handled using past studies. The main reason for addressing these studies is that the certainties of the advanced numerical model are investigated by comparing numerical model results with those obtained by previous researchers mentioned in Chapter 2.1.

Secondly, we will mention experimental investigations of shallow foundations seismic bearing capacity on cohesive soils around inclinations. According to the results of those studies mentioned in Chapter 2.2 are shed light on investigating the accuracy of developed numerical model results.

Lastly, research studies related to shape effects on the bearing capacity of various footings located on cohesive slopes which have been investigated so far will be examined. There are very few literature that exist related to analytical studies for circular, rectangular, and square foundations on slopes. Therefore, Chapter 2.3 will contribute to the studies and shed light on this matter.

2.1. Static Bearing Capacity of Shallow Foundation Around Cohesive Slopes

Shallow foundations which are generally referred to as footings can be divided into two types as per the following;

(i). Spread footings, which are supported by a single structural member.
(ii). Strip footings, which are supported by two or more structural members.

On slopes, near the hills or close to proposed excavation are the places where civil engineering structures are generally imposed to be built on. The investigation of bearing capacity of loaded slopes is crucial in this case because they are more susceptible to failure than other types of earth structures.

While in cohesive soil, the bearing capacity of the building may be stabilized, in the case of noncohesive soils, the bearing capacity is entirely determined by foundation failure (Saran *et al*., 1989).

Nowadays, researchers have presented a variety of techniques to establish the bearing capacity for shallow foundations on a slope, which some of them are as follows:

(i). Limit equilibrium analysis
(ii). Slip line analysis
(iii). Limit analysis
(iv). Finite element analysis

Meyerhof (1957) is the prominent research study which has been adopted by well-known design manuals such as "Standard Specification of Highway Bridges," Washington State Department of Transportation (WSDOT, 2005), "Geotechnical Design Manual.", and the American Association of State Highway Transportation Officials (AASHTO, 1996). He proposed a methodology combining bearing capacity theory for foundations on level ground with slope stability theory in order to determine the static final bearing capacity of a footing on or near cohesive and granular inclines.

Meyerhof (1957) pointed out that the final bearing capacity of a footing placed on the surface of the incline or close to the edge of the hill can be obtained using by Equation 2.1 and nature of plastic zones evolved in soil under the continuous foundation in both cases are indicated in Figure 2.1.

$$q_c = cN_{cq} + \frac{1}{2}\gamma B N_{\gamma q} \tag{2.1}$$

Ncq and Nγq are the bearing capacity factors assigned depending on inclination angle (β), angle of internal friction (Φ) and the depth of footing to footing width (D/B) ratio, and the unit weight of soil; and the footing width indicated by γ and B respectively.

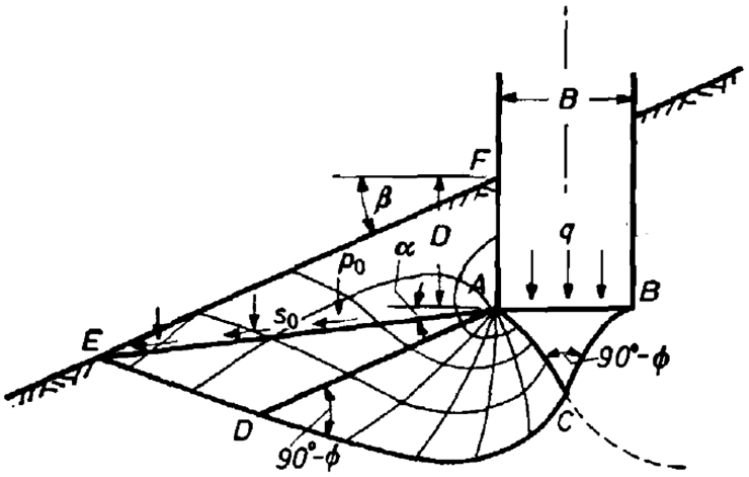


Figure 2.1. Plastic zones near the strip foundation on the face of a slope (Meyerhof, 1957).

Footing's static final bearing capacity on a cohesive incline is calculated by the given formula shown in Equation 2.2.

$$q_u = c_u N_{cq} \tag{2.2}$$

where qu is the final bearing capacity of a strip footing; cu is the undrained shear strength; Ncq is the factor of bearing capacity determined depending on slope angle (β); rate of footing depth to footing width (D/B) and slope stability number ($N_s = \gamma H / c_u$); γ is the soil's unit weight; B is the width of footing ; D is the footing depth .

The bearing capacity factor (N_{cq}) given in Equation 2.2 is determined by using design charts shown in Figure 2.2.

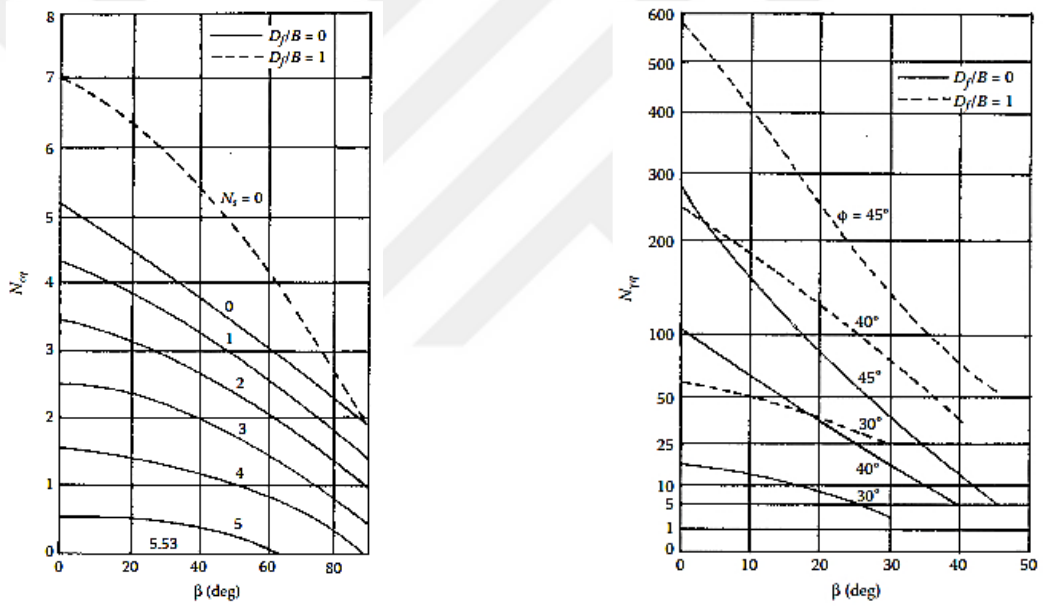


Figure 2.2. Factors of bearing capacity for the shallow foundation on a purely cohesive and granular slope (Meyerhof, 1957).

When the charts are compared, the inclination of the slope angle increases with the decrease of the bearing capacity. Furthermore, the reduction of bearing capacity on cohesive soils is less than granular soils for slope angles (β <30°) that figured by author.

The author defined that the plastic zone on the slope side is reasonably smaller compared to the similar foundation on leveled ground, which indicates that the length of the failure surface is decreased and in turn will reduce the resistance of the soil.

Ultimate footing's bearing capacity on cohesive soil located near the top edge of the incline might result in some cases on the overall stability of the slope. When the ultimate bearing capacity is exceeded, Meyerhof (1957) assumed three types of failure mechanisms for this situation . These are foundation failure, toe failure, and base failure, respectively. Foundation failure is defined as where failure surface intersects with slope surface above the slope toe level. Another two failure modes can also be called as ‘slope failure.' While the failure surface passes from the edge of the slope, base failure passes under the toe level as footing exceeds its bearing capacity. These failure modes are depicted in Figure 2.3 below.

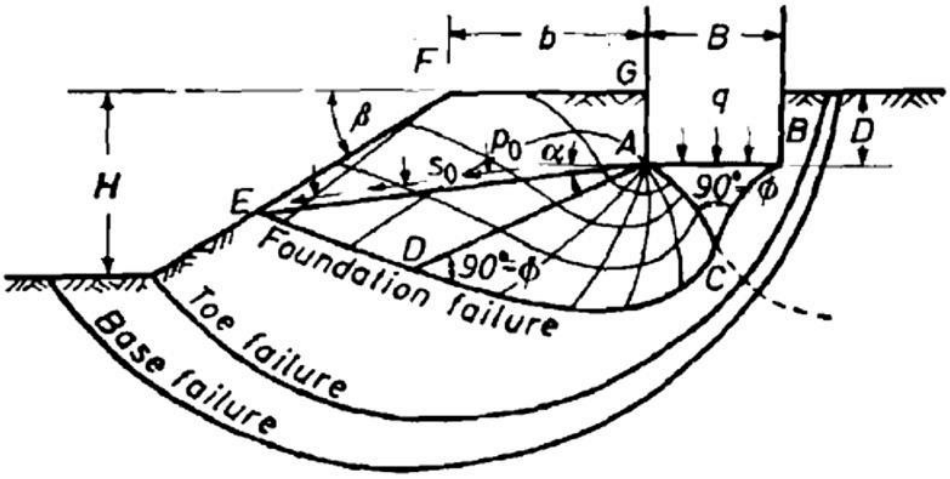


Figure 2.3. Slip surfaces and plastic zones around the rough strip foundation on top of the slope (Meyerhof,1957).

In Equation 2.2, a theoretical connection is presented for the final bearing capacity of shallow rigid foundations located on a slope (Meyerhof, 1957). In this equation, bearing capacity coefficient (N_{cq}) given in Equation 2.2 is calculated by using the design chart shown in Figure 2.4. Bearing capacity coefficient (N_{cq}) is a function rate of footing depth to width of footing (D/B),angle of slope (β), stability number of slope ($N_s=\gamma H/c_u$) and the ratio of

the distance between the footing and the slope edge to the slope height (*b/H*). As shown in Figure 2.4, the impact of slope stability is remarkable when compared to the effect of slope angle on the footing's bearing capacity in static conditions. The more distance between the footing and slope edge, the higher the bearing capacity coefficient will be. When a footing is more than twice the slope height away from the inclined edge, the static final footing's bearing capacity is not affected by the slope angle.

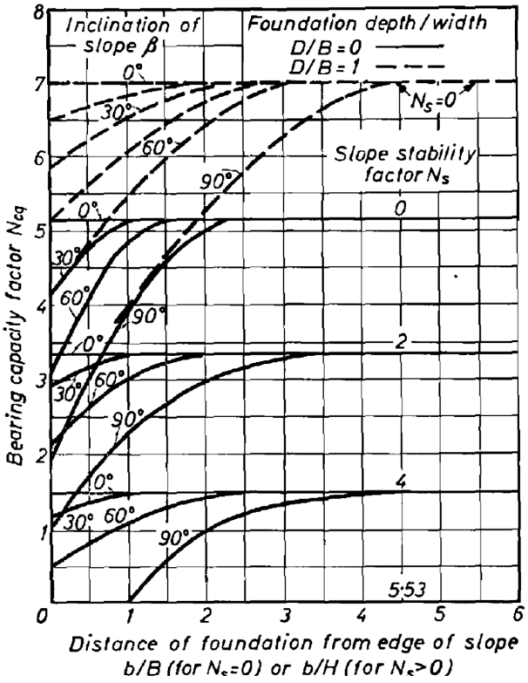


Figure 2.4. Factors of strip foundation's bearing capacity on a purely cohesive incline (Meyerhof, 1957).

Bowles (1997) proposed a model of a compiled computer code to predict the static final bearing capacity of a footing near inclines or excavations and developed the design table in Figure 2.7. Mathematical equations are shown in Figure 2.5 and have been employed after the obtained failure surface. A new bearing capacity coefficient is computed using the approach mentioned below. It should be pointed out that failure surfaces occurred under an equal footing placed on level ground (refer to Figure 2.6) are considered.

- The reduced bearing capacity factor (*Nc*) based on the failure surface ade=L_0 of Figure 2.6 and the failure surface adE=L_1 of Figure 2.5 to derive

$$N_c' = N_c \frac{L_1}{L_0} \tag{2.3}$$

- Calculate a reduced N_q based on the ratio of area ecfg (A_0) of Figure 2.6 to the equivalent area Efg=A_1 (footings on the slope) or Efgh=A_1 (footings near slope) of Figure 2.5 to derive the equation in below

$$N_q' = N_q \frac{A_1}{A_0} \tag{2.4}$$

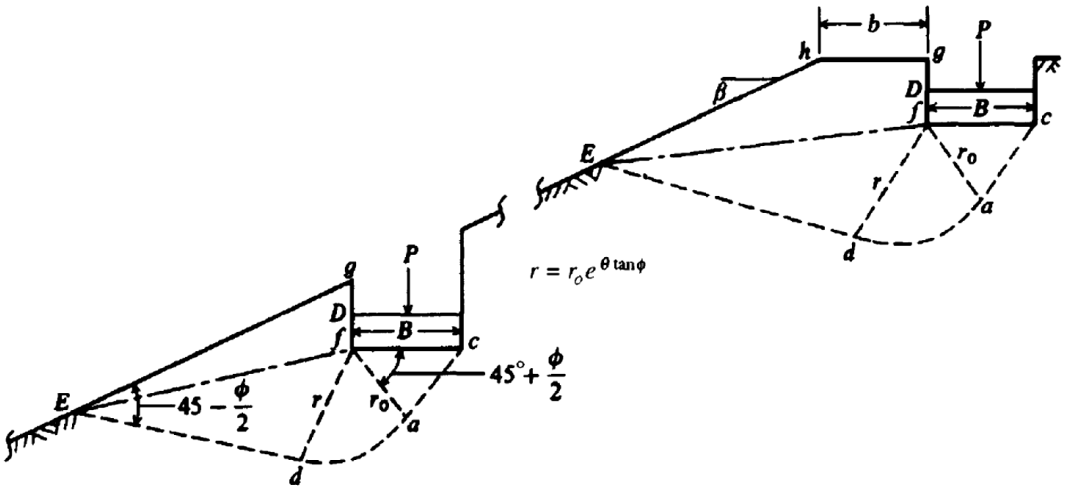


Figure 2.5. Footings on or adjacent to a slope (Bowles, 1997).

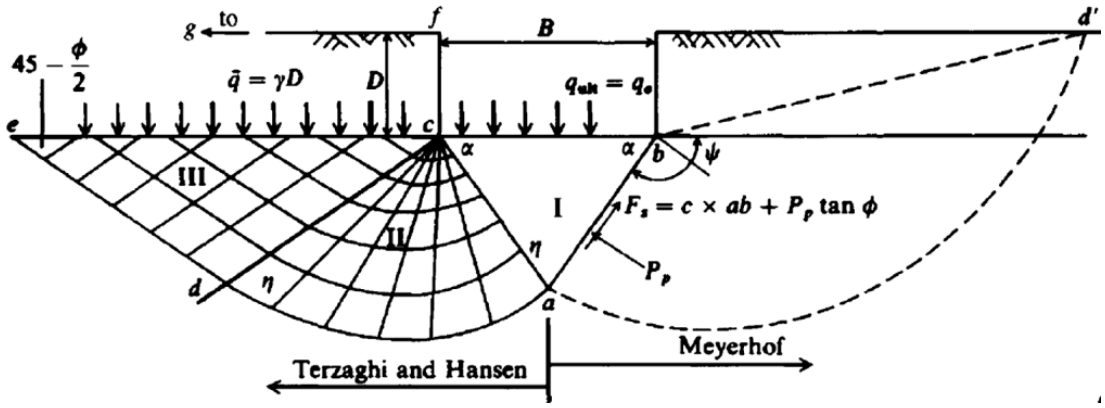


Figure 2.6. Failure surfaces and stress trajectories in the plastic zone beneath the footing (Bowles, 1997).

The design table presented in Figure 2.7. should be integrated with bearing capacity equation given by Hansen in order to calculate the static strip foundations' bearing capacity located near to cohesive inclines. In Figure 2.7., it is seen that (*N'c* and *N'q*) as bearing capacity coefficients are function of slope angle (β), rate footing depth to width of footing (*D/B*), ratio of distance between the footing and slope edge to width of footing (*b/B*) and internal friction angle ($\varphi_u=0^o$). It is noted that the area ratio given in Equation 2.4 equals to unity or the rate of (*b/B*) changes between 1.5 and 2, reducing effect because of the presence of slope on bearing capacity coefficients disappears.

$\beta\downarrow$	$\Phi\rightarrow$	*D/B* = 0			*b/B* = 0		*D/B* = 0.75			*b/B* = 0		*D/B* = 1.50			*b/B* = 0	
		0	10	20	30	40	0	10	20	30	40	0	10	20	30	40
0°	$N'_c=$	5.14	8.35	14.83	30.14	75.31	5.14	8.35	14.83	30.14	75.31	5.14	8.25	14.83	30.14	75.31
	$N'_q=$	1.03	2.47	6.40	18.40	64.20	1.03	2.47	6.40	18.40	64.20	1.03	2.47	6.40	18.40	64.20
10°		4.89	7.80	13.37	26.80	64.42	5.14	8.35	14.83	30.14	75.31	5.14	8.35	14.83	30.14	75.31
		1.03	2.47	6.40	18.40	64.20	0.92	1.95	4.43	11.16	33.94	1.03	2.47	5.85	14.13	40.81
20°		4.63	7.28	12.39	23.78	55.01	5.14	8.35	14.83	30.14	66.81	5.14	8.35	14.83	30.14	75.31
		1.03	2.47	6.40	18.40	64.20	0.94	1.90	4.11	9.84	28.21	1.03	2.47	5.65	12.93	35.14
25°		4.51	7.02	11.82	22.38	50.80	5.14	8.35	14.83	28.76	62.18	5.14	8.35	14.83	30.14	73.57
		1.03	2.47	6.40	18.40	64.20	0.92	1.82	3.85	9.00	25.09	1.03	2.47	5.39	12.04	31.80
30°		4.38	6.77	11.28	21.05	46.88	5.14	8.35	14.83	27.14	57.76	5.14	8.35	14.83	30.14	68.64
		1.03	2.47	6.40	18.40	64.20	0.88	1.71	3.54	8.08	21.91	1.03	2.47	5.04	10.99	28.33
60°		3.62	5.33	8.33	14.34	28.56	4.70	6.83	10.55	17.85	34.84	5.14	8.34	12.76	21.37	41.12
		1.03	2.47	6.40	18.40	64.20	0.37	0.63	1.17	2.36	5.52	0.62	1.04	1.83	3.52	7.80

Figure 2.7. Bearing capacity factors (N'_c *and* N'_q) for footings on or adjacent to a slope (Bowles, 1997).

Kusakabe *et al*. (1981) suggested an approach to determine the final bearing capacity of a footing located around the slope using an upper bound solution with the mechanism of failure that is shown in Figure 2.8. A failure mechanism which was responsible for this problem is shown in Figure 2.8, where β=slope angle, the αB=distance incline edge, *HB*=height of incline , *hB*=failure point depth 'A' on the face of the slope.

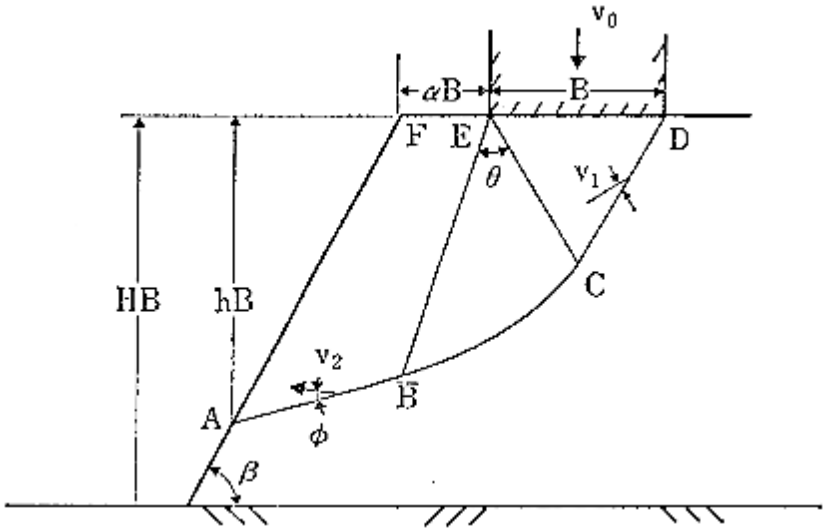


Figure 2.8. Failure mechanism adopted for the upper bound solution (Kusakabe *et al*.,1981).

The author adopted the limit analysis upper bound theorem to reach the static ultimate bearing capacity of a footing located adjacent near slope given by Equation 2.5.

$$q_s = \mu q_L \tag{2.5}$$

Authors compared their results with bearing capacities obtained from those of previous studies and concluded that results were in good agreement with previous findings. Bearing capacity factor N_c varies with $c/\gamma B$ parameter. According to the author, this parameter has

a positive impact on bearing capacity factor (N_c). $c/\gamma B$ parameter was defined as 0.5, 1, 2. It was also mentioned experimental tests, in which Kanto loam was used, can be regarded undrained due to the rapid loading capacity of the test devices. During the test period, both mechanical and physical properties were used. Details of the test apparatus can be obtained in detail in the related reference (Kusakabe *et al*., 1981).

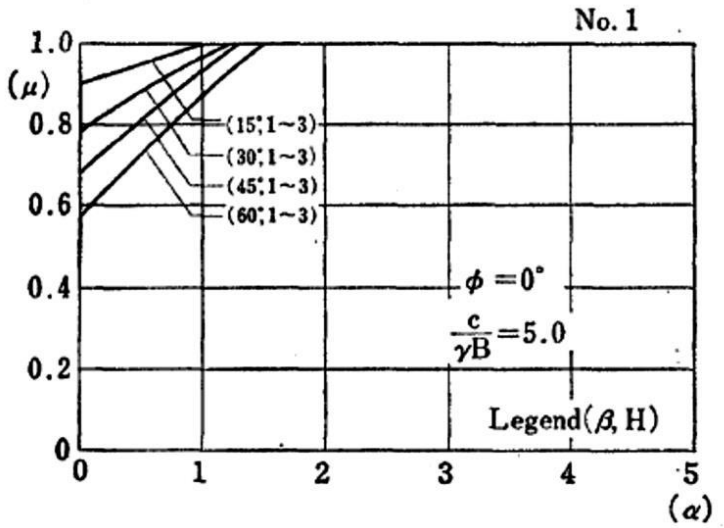
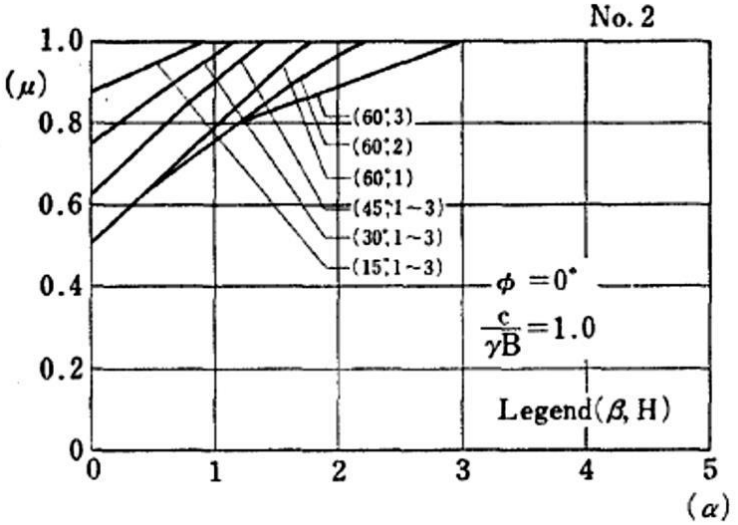


Figure 2.9. No.1 design chart presented to calculate the dimensionless factor (μ) (Kusakabe *et al.*, 1981).



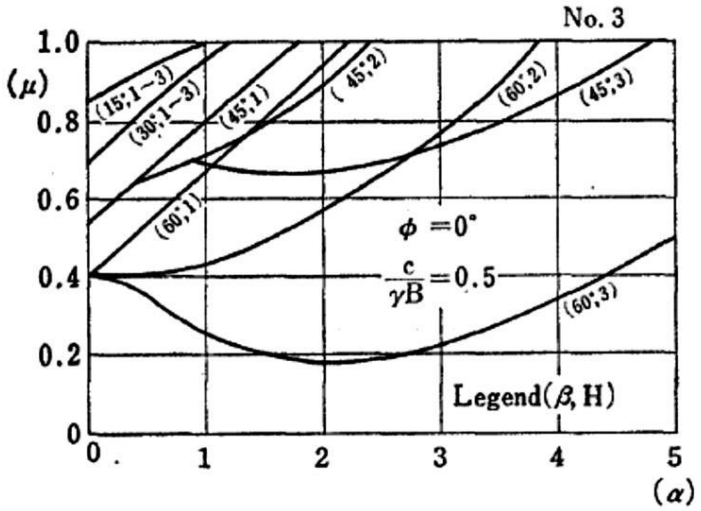


Figure 2.10. No.2 and No.3 design charts presented to calculate the dimensionless factor (μ) (Kusakabe *et al*., 1981).

Unconfined compression strengths of consolidated samples were measured in this study (Kusakabe *et al*., 1981). The results of obtained from the proposed calculation method are less than the results found during experimental model tests; failure surfaces observed the preliminary tests were in good agreement with expected failure surfaces. It is concluded that computed bearing capacity values using the proposed method are less than that found in the model tests. This is primarily based on the effect of the side friction in the test apparatus. Another reason is the variation in stress states between those assumed in the proposed methodology and those established in test models.

To study the impact of the different parameters on undrained bearing capacity, Georgiadis (2010) presented the finite element analysis of shallow foundations located around undrained soil inclines. The author suggested that undrained bearing capacity of a surficial strip footing near slopes can be computed as the following Equation 2.6.

$$q_u = \frac{V_u}{B} = c_u N_c \tag{2.6}$$

Where q_u is the near slope ultimate footing static bearing capacity ; V_u is the final vertical weight; B is the breadth of the footing; c_u is the strength of the undrained shear, and Nc is the factor of undrained bearing capacity.

Various parameters are taken into consideration in this study to determine their impact on bearing capacity. Incline angle, the distance of footing , and earth characteristics are the impacting factors of the undrained bearing capacity. The figures of the investigated study are schematically presented in Figure 2.11. Three widths for footing (respectively 1,2 and 4 m) and three different angles for inclines (15, 30, 45) were examined. In addition, some incline heights (H) and normalized distances of footing (λ) were considered to show influences of all critical parameters on ultimate bearing capacity .Slope soil material was identified by elastic-perfectly plastic Mohr-Coulomb constitutive model. The undrained shear strength was changed while undrained elasticity modulus (E_u),saturated unit weight(γ_{sat}), and Poisson's ratio(v_u) were kept constant as 30 MPa, 20 kN/m^3 and 0.49 respectively. Seven different undrained shear strength was considered to indicate the influence of undrained shear strength (c_u), respectively 20,40,100,150,200,300 and 1000 kPa. Footing, which has 1.0 m thickness, was modeled using beam element. 'Rough footing' assumption was used in all analyses.

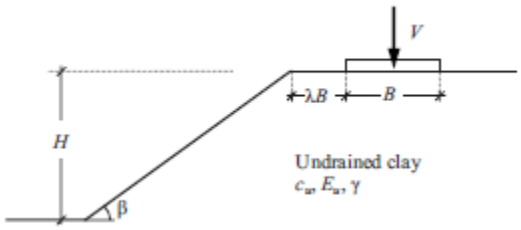


Figure 2.11. Schematic representation of the problem (Georgiadis, 2010).

Various soil characteristics and geometries were regarded. The outcomes of the investigations were correlated with those of the calculation methods presented by other writers. According to the results of previous studies, the author concluded that the results of the suggested approach obtained for specific soil and various shape combinations reflects a sensible conclusion with those given by the previous researchers. For some instances, the

differences between the results of the different calculation methods were also determined. The main reason of detected differences is that these solutions do not consider all affecting parameters . The author identified three different failure mechanisms shown in Figure 2.12 that can occur depending on the combination of soil and geometry of foundations.

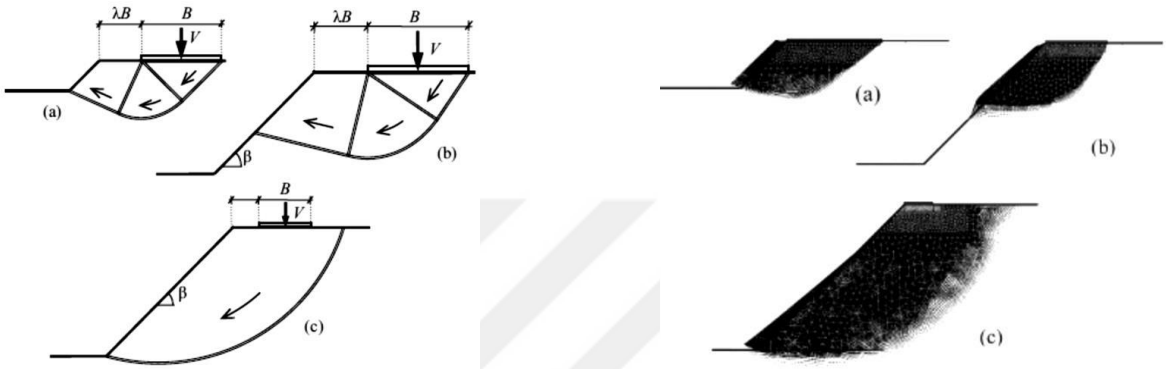


Figure 2.12. Modes of failure (a) and (b) failure of bearing capacity and (c) overall failure of incline (Georgiadis, 2010).

In this study, the FE method was used to examine all essential variables. According to the slope height normalized by the width of footing (*H/B*), the results showed that the failure mechanism could be identified . It is illustrated in the chart presented in Figure 2.13. a sheer decrease of the amount of N_c from the flat ground amount is perceived in a primary mode. Where the undrained bearing capacity representative falls quickly to 0, it is the second mode and a final mode of constant N_c. These modes of failures were sequentially outlined above as bearing capacity and overall incline failure mechanisms for the first second and third modes of failure. Moreover, the undrained bearing capacity factor N_c grows steeply with the rise of $c_u/\gamma B$. Additionally, with the rise of $c_u/\gamma B$, the second failure mode starts more aggressive.

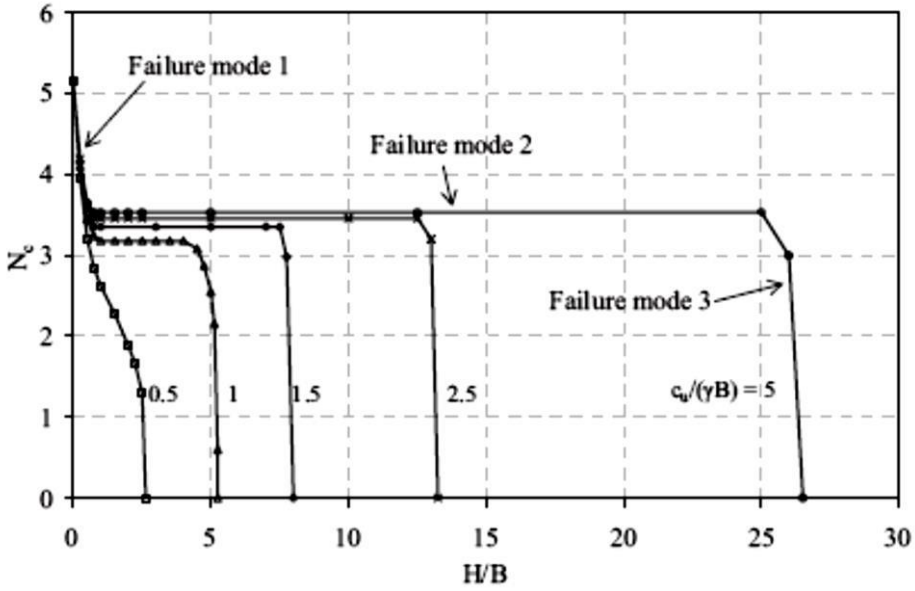


Figure 2.13. Variation of failure mode and N_c with *H/B* for λ= 0 and β= 45° (Georgiadis, 2010).

Any of these diagrams ensure trajectories for angles of incline (β) of 0°, 15°, 30°, and 45° and several rates of *H/B*. Figures 2.14, 2.15, 2.16 and 2.17 present a variety of N_c with λ for rates of $c_u/\gamma B$.

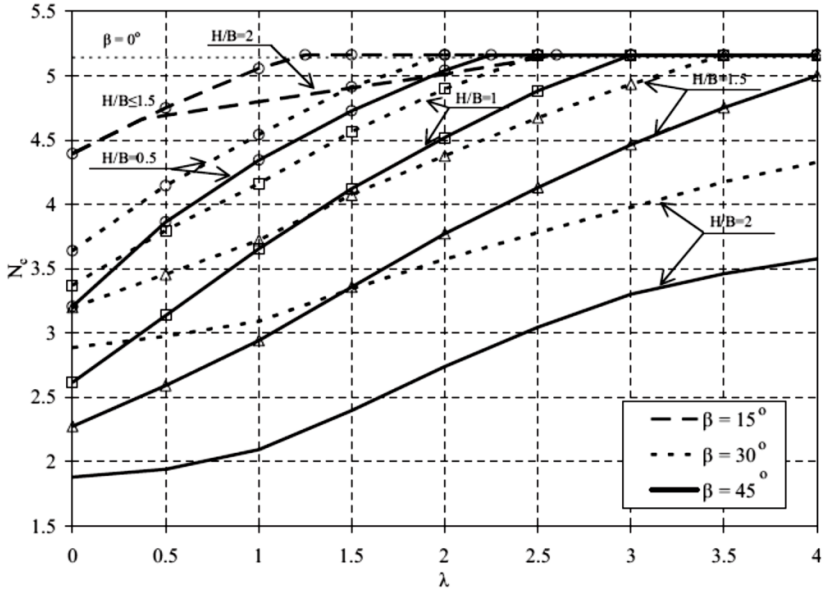


Figure 2.14. Variety of *Nc* with λ for $c_u/\gamma B$= 0.5 (Georgiadis, 2010).

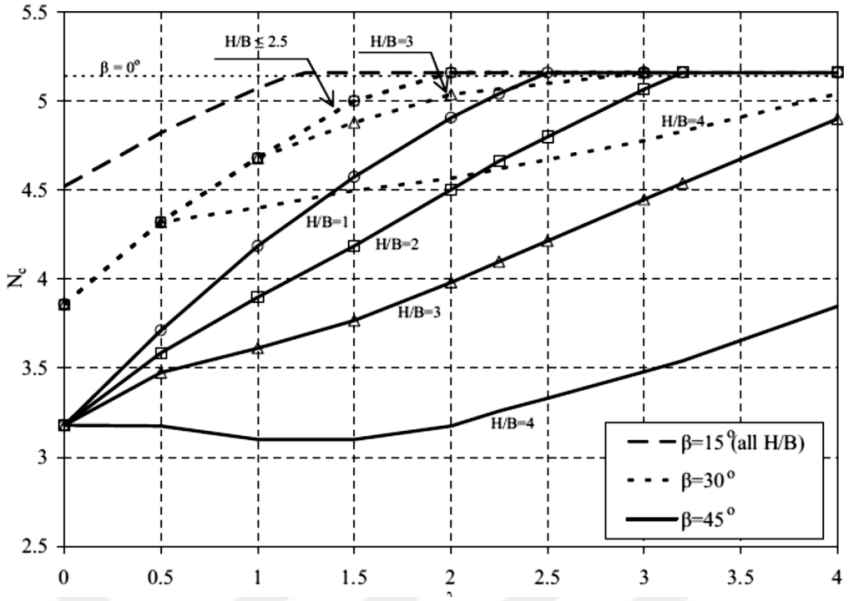


Figure 2.15. Variety of N_c with λ for $c_u/\gamma B$= 1 (Georgiadis, 2010).

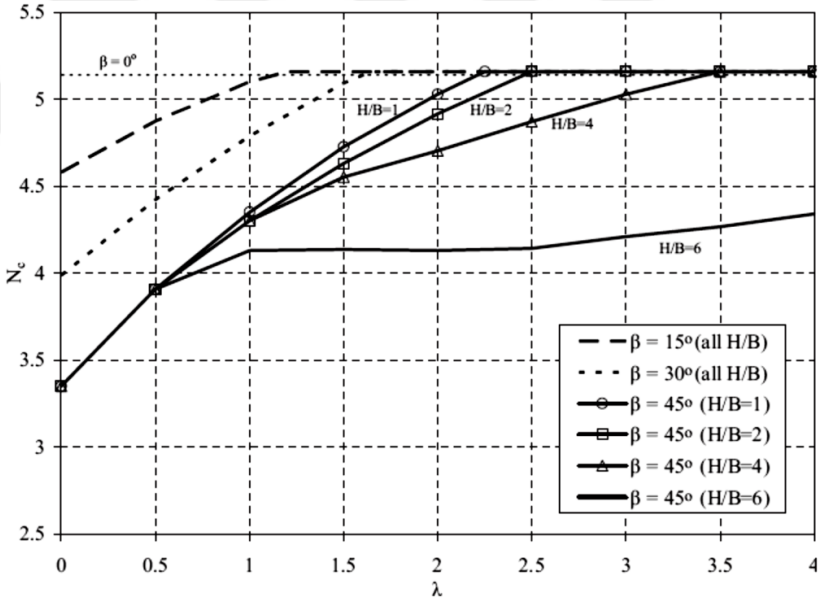


Figure 2.16. Variety of N_c with λ for $c_u/\gamma B$= 1.5 (Georgiadis, 2010).

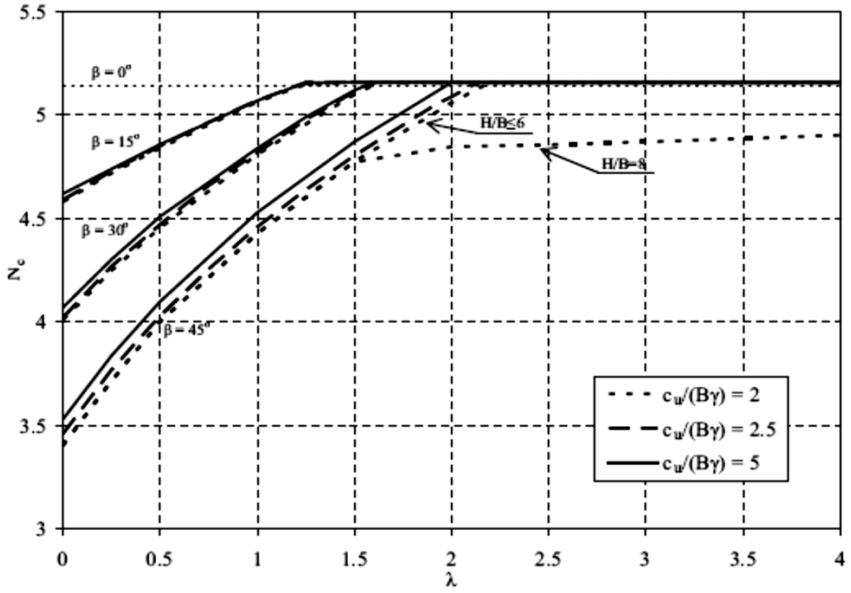


Figure 2.17. Variety of N_c with λ for $c_u/\gamma B$= 2, 2.5, and 5 (Georgiadis, 2010).

It can be clearly seen from the chart that factor of undrained bearing capacity (N_c) increase with the rise of $c_u/\gamma B$ ratio. For low amounts of $c_u/\gamma B$ and high amounts of λ and inclination angle β, it is observed that the factor of undrained bearing capacity (N_c) is related to the *H/B* rate. Since the second failure mode is regarded for large amounts of $c_u/\gamma B$, the factor of undrained bearing capacity is separated from *H/B*.

With the rising of the distance of footing from the incline, the factor of undrained bearing capacity (N_c) is also growing. If a significant amount of the normalized footing span (λ_0) is given exceeding the factor of undrained bearing capacity for the flat ground surface, the increment stops. The change of essential values of normalized span (λ_0) is presented in Figure 2.18 depending on slope angle (β) and $c_u/\gamma B$ ratio (shown for values as 2, 2.5, 3.75, 5 and 7.5). The critical value of normalized distance can be computed by using Equation 2.7.

$$\lambda_0 = \left(\frac{5.14}{2}\right)^{\beta} \tag{2.7}$$

where β is the slope angle (in radian).

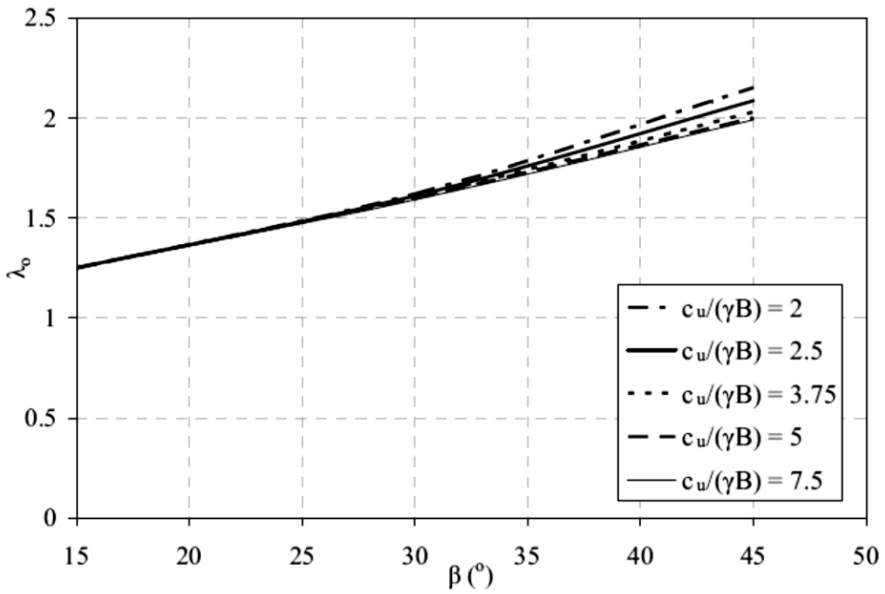


Figure 2.18. Variation of λo with β (Georgiadis, 2010).

As observed from the chart, the critical normalized distance has sharply increased with the increase of slope angle. It changes between 1.25 and 2.25 approximately.

For any returned $c_u/\gamma B$, angle of inclination , normalized footing span λ_o , and normalized height of incline H/B, the author could obtain the determinant of undrained bearing capacity from the outcomes of examinations. As stated in the methodology, by using lineer interpolation among amounts received from the plan outlines given in Figure 2.14, the bearing capacity coefficient (N_c) can be calculated - Figure 2.17 for all combinations of $c_u/\gamma B$ ratio and slope angle (β).

Castelli and Motta (2010) used the limit equilibrium method to develop a model for footing with circular failure surface .The proposed process of review is also related to a solution of an upper bound of the ultimate capacity of the footing. In this sense, circular failure surface occurs distribution from footing edge after it keeps its relative movement until reaching the sloping ground surface. The mechanism of failure and involved energies of foundation regarded as the calculation model are illustrated in Figure 2.19. The limit base pressure can be computed for an arbitrary circular failure surface based on the principle of moment equilibrium ($\Sigma M_{mobilizing} = \Sigma M_{resisting}$). In the proposed method, failure mechanism on the surface for minimum base pressure is computed the most sensitive surface among all

possible circular surfaces whose locates and radii are different. Therefore, minimum base pressure can be detected for the critical circular failure surface correlated with the shallow footing's final bearing capacity.

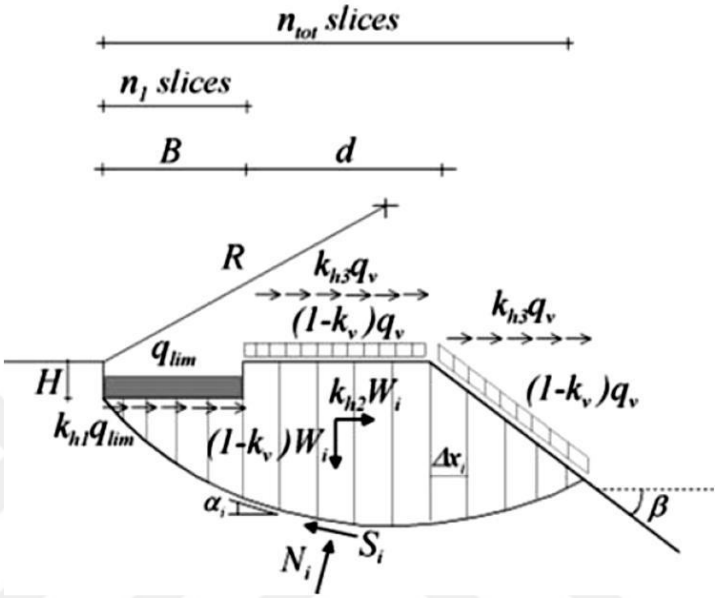


Figure 2.19. The applied forces and the mechanism of failure used in the examination. (Castelli and Motta, 2010).

When the static conditions are taken into account as $k_{h1}=k_{h2}=k_{h3}=k_v=0$, the distance between the footing and slope edge changes among 0 and 6*B* regarding higher values of internal friction angle. Besides this, angle of inclination (β) and internal angle of resistance (Φ) change in between $5^0 – 35^0$ and $0^0 – 40^0$ respectively.

The ratio of bearing capacity coefficients (N_c^*/N_c) changes with the angle of inclination (β), the normalized interval between the foundation and incline edge (*d/B*) and normalized embedment depth of footing (*H/B*) for undrained conditions. As a result, the ratio of bearing capacity coefficients is computed by using design charts shown in Figure 2.20.

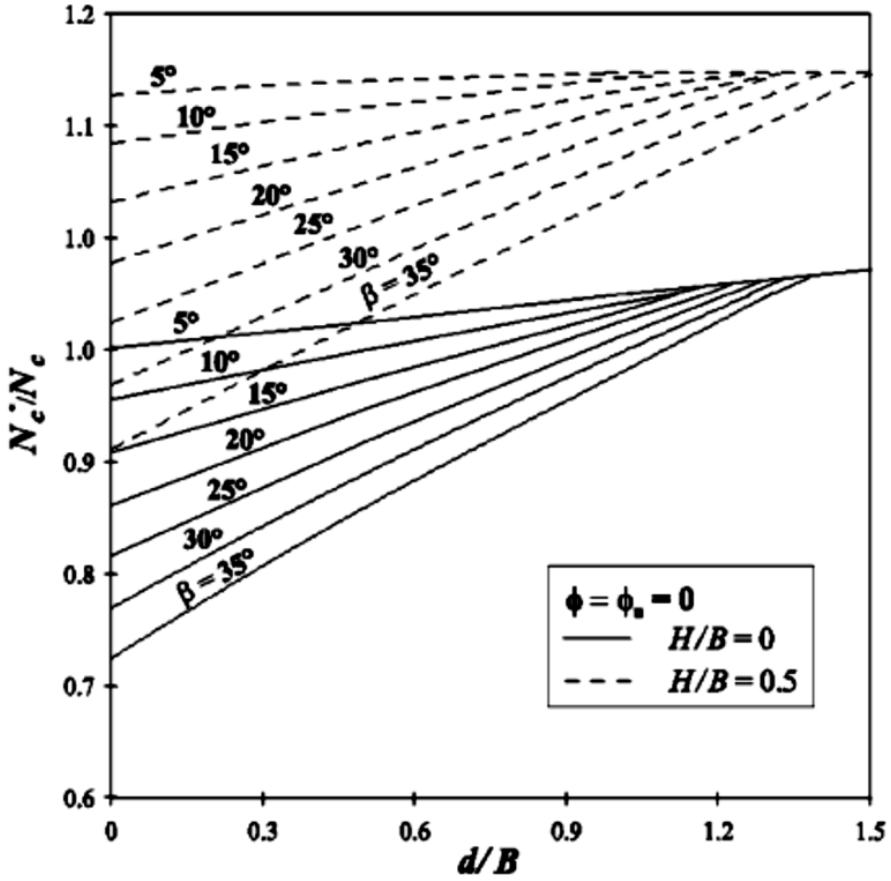


Figure 2.20. Variation of ground factors (N_c^*/N_c) in a static condition with the distance of foundation from the edge of the incline (Castelli and Motta, 2010).

When the foundation is located at the edge of the incline, the reduction in the bearing capacity reaches the maximum. As the distance between the slope edge and the foundation increases, the factors of bearing capacity rate (N_c^*/N_c) for a foundation near the slope outside and far from the slope decreases. The authors had also concluded that inclination angle (β) impacts on the distance of the threshold , whilst the embedment of the foundation (H) does not influence notably the distance of the threshold d_t/B (Castelli and Motta, 2008, 2010).Additionally, these critical distances normalized with footing width change between 1 and 1.4 depending on slope angle (β). Evidently, the addition in the footing depth only causes an increment in the calculated bearing capacity values.

2.2. Seismic Bearing Capacity of Foundations Around Cohesive Slopes

Numerous researchers have pay attention to find a permanent answer for bearing capacity of adjacent to inclines. However, these studies cover the static state while limited studies investigated the resistance of shallow foundations around inclines under earthquake situation. `Pseudo-static method' is the most popular technique for assessing the impact of an earthquake on the durability of a soil-foundation system. Actually, there are few studies available explaining the seismic impact on the foundations' bearing capacity. In this chapter, different approaches which were suggested a solution method to find the seismic bearing capacity of foundations near inclines will be referred.

The ascertainment of the seismic bearing capacity of footings located horizontally on semi-infinite slopes was determined using the technique of pressure symptoms by Kumar and Rao (2003). The fact that this study is entirely different than presented in the above methods because of the ‘semi-infinite slope' assumption. This difference can also be seen in Figure 2.21 and Figure 2.22 clearly. The main reason of addressing to this study in Chapter 2.2 is that it is compared with existing studies approaches, the present analysis describes the change of the factor of undrained *Nc* bearing capacity (Φu= 0°) with respect to the seismic acceleration coefficient (α_h) and the slope angle (β). Solution tools given in this study would be regarded for the aims of comparison to be given in the following chapter of the dissertation just for the particular case that the footing is at the slope edge (λ= 0).

Schematic mechanisms of the problem shown in Figure 2.21 and Figure 2.22 were taken into consideration, respectively. The change of N_c with variations in angle of inclination (β), the internal frictional, and the horizontal seismic acceleration coefficient (α_h) analyzed using failure mechanisms named as the single side and both sides as slope soil material obeys Mohr-Coulomb failure criterion, internal friction angle (β) used in analyses changes in between 0^o and 50^o. Additionally, the effect of slope angle (β) on seismic bearing capacity factors was studied using different slope angles.

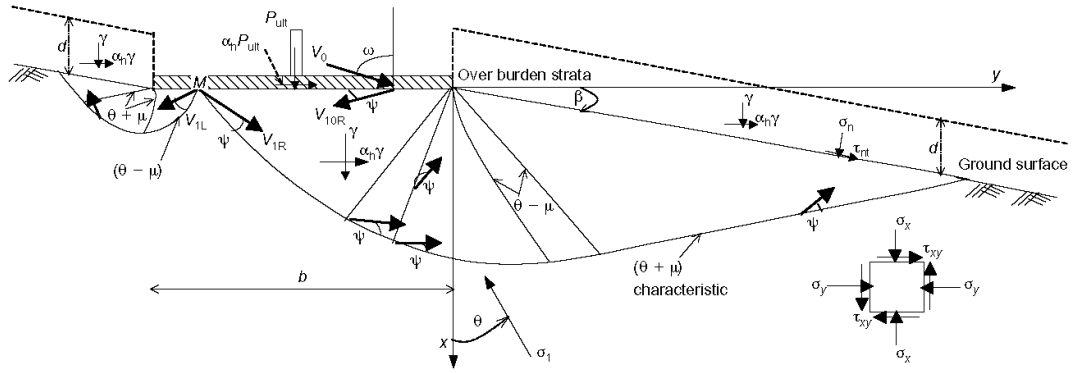


Figure 2.21. Both sides mechanism of failure used in the study (Kumar and Rao, 2003).

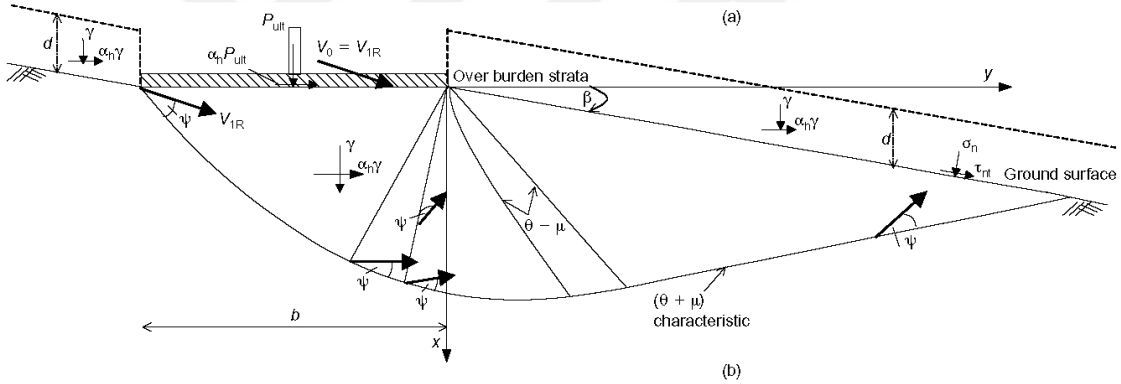


Figure 2.22. Single side mechanism of failure used in the study (Kumar and Rao, 2003).

As a result, for fewer amounts of the coefficient of earthquake acceleration (α_h), the quantity of N_c in the mechanism of both-sides failure is considerably less than that produced by the single-side mechanism. Nonetheless, with the seismic acceleration coefficient for the both-sides mechanism becomes kinematically for many situations in which the internal friction angle takes higher values. The single-side mechanism is observed statically acceptable for determining factors of bearing capacity N_c and N_q on slanted soil.

Seismic bearing capacity of footings located near the slopes can be determined using the well-known method presented by Terzaghi (1943) in this study. Furthermore, the

following design charts are shown in Figure 2.23, Figure 2.24, and Figure 2.25 that enable to calculate for various cases n which $\alpha_h \geq 0$ and $\beta \geq 0$. Two different curves obtained from the presented design graphs to reflect the effect of various $N\gamma$ factor concerning to each failure mechanism because of two different failure mechanisms. The results obtained from the presented design graphs, both sides failure mechanism gives more sensible results or smaller values of the seismic acceleration coefficient (α_h) and the slope angle (β). Briefly, when an increment in the seismic acceleration coefficient happens for different slopes, all the factors of bearing capacity decrease significantly.

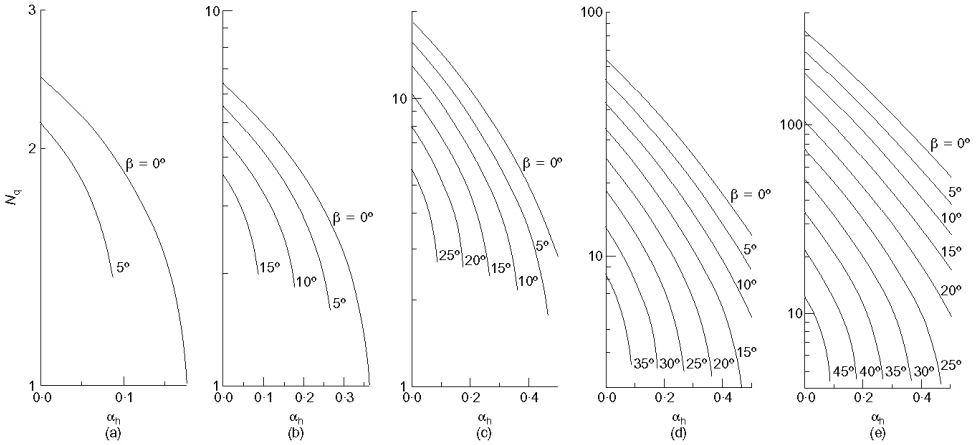


Figure 2.23. Change of Nq with α_h for various amounts of Φ and β: (a) Φ= 10°; (b) Φ= 20°; (c) Φ= 30°; (d) Φ= 40°; (e) Φ= 50° (Kumar and Rao, 2003).

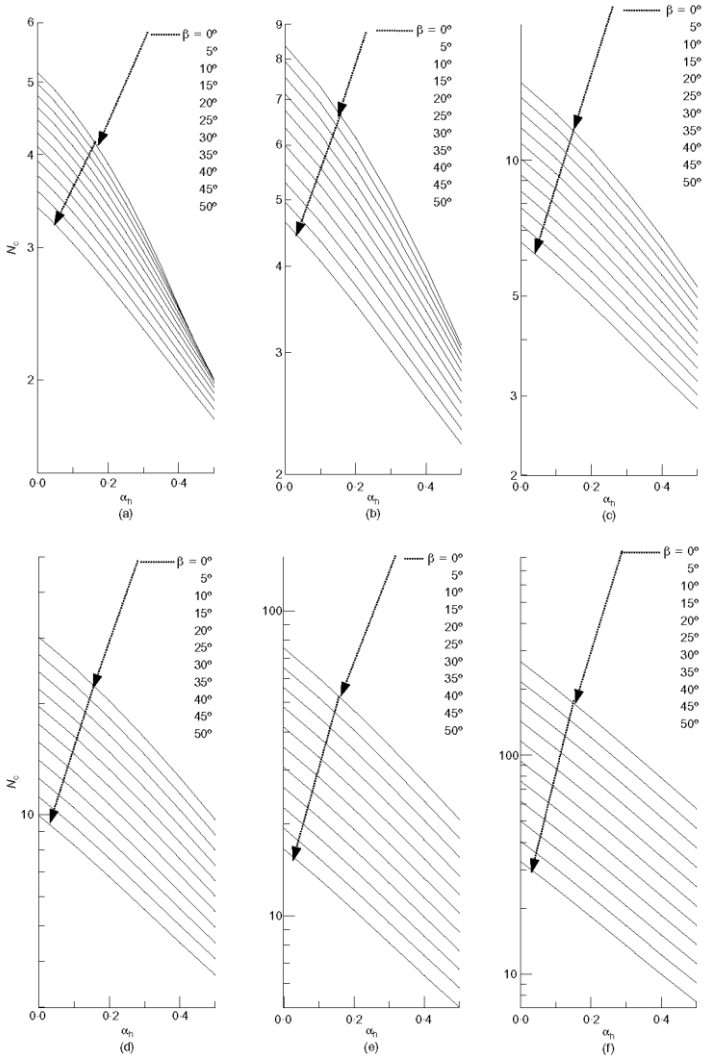


Figure 2.24. Change of *Nc* with α_h for various amounts of Φ and β: (a) Φ= 0°; (b) Φ= 10°; (c) Φ= 20°; (d) Φ= 30°; (e) Φ= 40°; (f) Φ= 50° (Kumar and Rao, 2003).

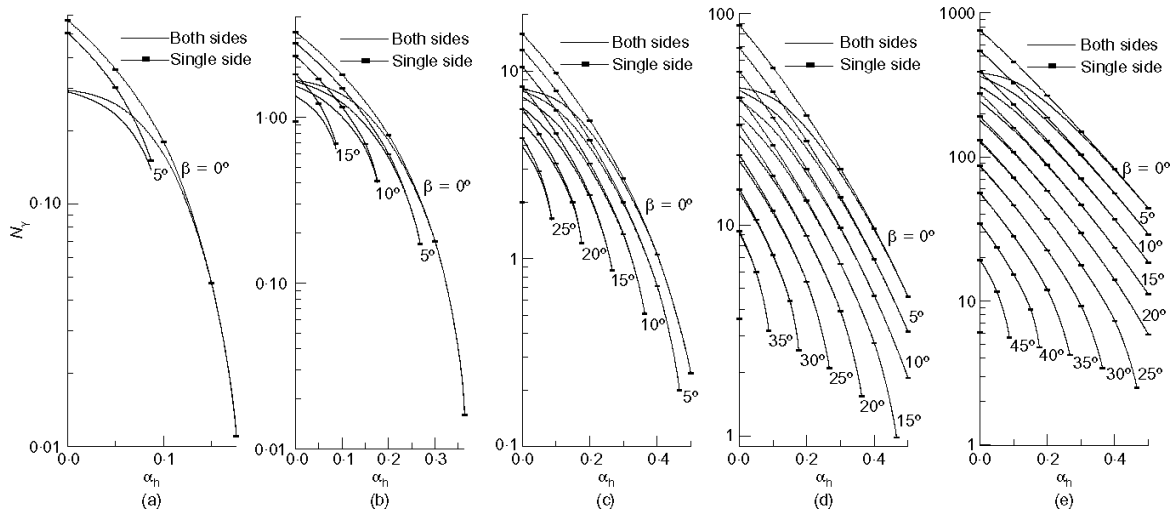


Figure 2.25. Change of $N\gamma$ with α_h for various amounts of Φ and β: (a) Φ= 10°; (b) Φ= 20°; (c) Φ= 30°; (d) Φ= 40°; (e) Φ= 50° (Kumar and Rao, 2003).

Shiau *et al*. (2006) proposed a pseudo-static method in conjuction with the limit equilibrium and upper bound limit methods for determining the capacity of the seismic bearing of shallow foundation reclining on c– Φ soil . These limitations were defined as being necessary to determine the overall state of the failure facade before the limit equilibrium method and providing higher results than specific limit loads and therefore being non-conservative for the upper bound limit examination.

The authors pointed out that upper and lower bound finite element methods are more confidential methods comparing to the existing methods in the above. As a result, these methods enable the exact limit load from over and under and thus provide a stable load interval to the design engineers for the exact limit load. The fact that the primary purpose of this study was to include the pseudo-static method in the statistical approaches developed at the University of Newcastle based on the upper and lower bound finite element methods. To confirm the results of updated numerical methods , "determination of the seismic bearing capacity of rigid footings on homogenous slopes" was one of the essential criteria chosen in this text.

Schematic diagram of the problem is presented in Figure 2.26. Homogenous soil material obeys the Mohr-Coulomb result in a pattern with the shear strength characteristics cohesion (*c*) and internal friction angle (*Φ*). Additionally, it is expected that the dynamic quake loading cannot change the shear strength of the soil. Furthermore, the impact of the water pore force is not taken into consideration. The vertical and horizontal acceleration coefficients had been chosen to be equal for slope,structure, and surcharge load, as shown in Figure 2.26. Moreover, the load of the earthquake on the structure footing acts at the foundation level, and the overturning moment due to the inertia of the structure is not considered.

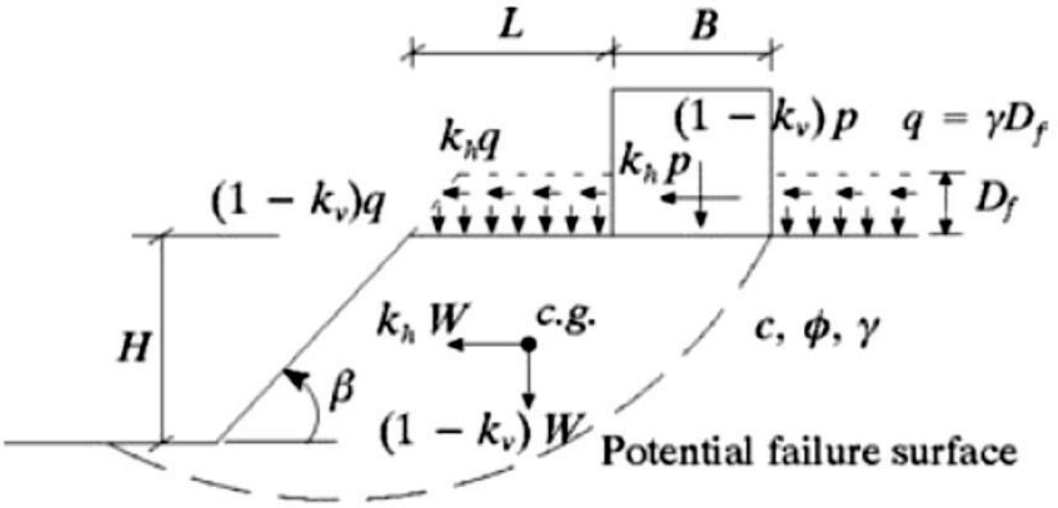


Figure 2.26. Graphical representation of the problem (Shiau *et al.*, 2006).

According to this study, the ultimate bearing capacity of unyielding foundations around inclines can be stated as following given in Equation 2.8.

$$\frac{p}{\gamma B} = f\left(\beta, \frac{L}{B}, \frac{c}{\gamma B}, \varphi, tan\,\theta\right) \tag{2.8}$$

where p is the limit pressure average below the foundation, γ is the soil unit mass, B is the width of foundation , β is the slope angle, L is the distance from the inclined edge to the edge of the foundation c is the cohesion, q is the surcharge load, Φ is the angle of inner resistance of slope soil and $tan\theta = k_h/(1-k_v)$.

As a conclusion of made estimation, it is drawn that the results given in the following have essential influence.

Seismic bearing capacity of such foundations decreases by earthquake forces. Moreover, for any angle of friction , the bearing capacity declines, while the value of $\tan\theta$ increases. The shaded area is shown in the table Figure 2.27 represents the zone that enclosed with upper and lower bound curve obtained by numerical methods which correct limit load falls into is determined. As shown in the graph given in Figure 2.27, lower and upper bound curves close to each other with the increase of $tan\,\theta$ value and therefore, the efficiency of bonding solutions goes up.

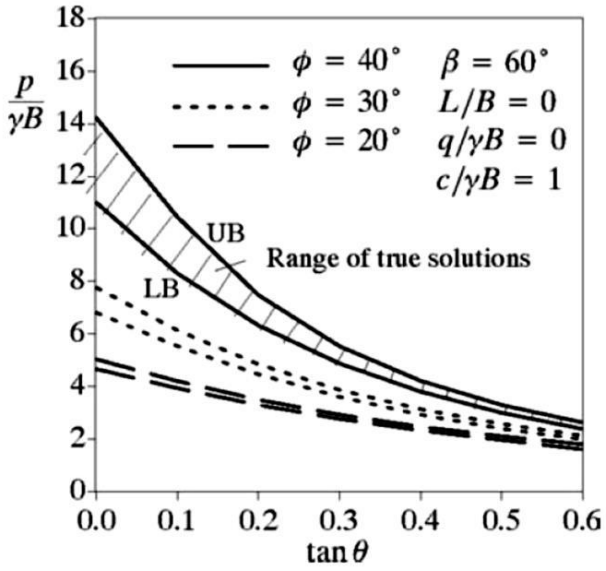


Figure 2.27. Effect of $tan\theta$ on $p/\gamma B$ for various Φ (Shiau *et al.*, 2006).

Figure 2.28. explains the change of normalized seismic bearing capacity and upper bound velocity diagrams with different values of *tanθ*. The velocity fields tend to decrease due to a horizontal earthquake load, and as tanθ increases, a decrease in normalized seismic bearing capacity can be recognized.

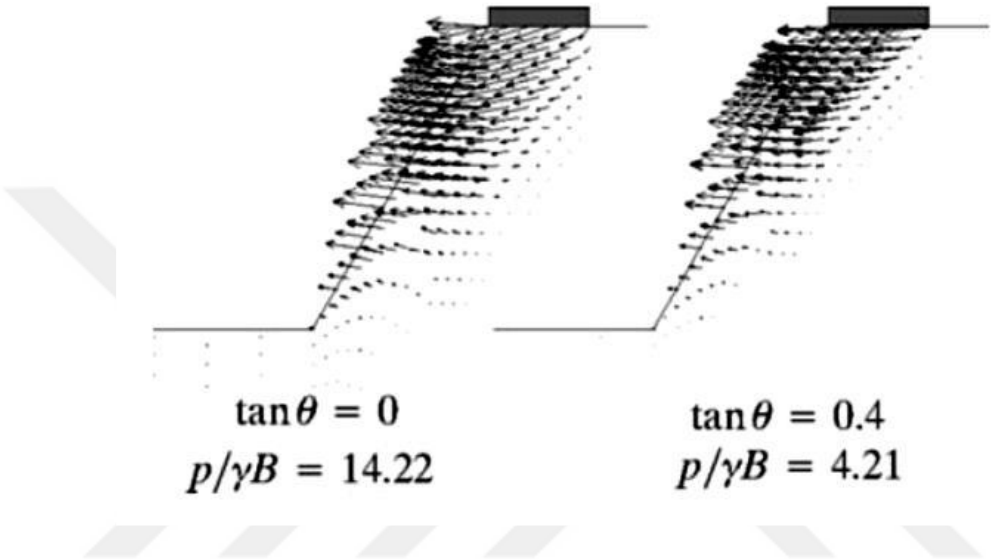


Figure 2.28. Comparison of upper bound velocity diagrams for the effect of inertia forces (Shiau *et al.*, 2006).

The presence of surcharge load on slopes based on *β*, *L/B*, and *q/γB* parameters might reduce, enhance, or does not change the foundation seismic bearing capacity. As can be understood from in the graph given Figure 2.29, a small reduction in *p/γB* is seen for a vertical incline. As the overcharge on the inclined surface provides driving energy to the failure of incline, this causes a reduction in the bearing capacity of the foundation. The influence of surcharge load the seismic bearing capacity is remarkably small. Briefly, *p/γB* ratio is constant, although the *q/γB* ratio increases.

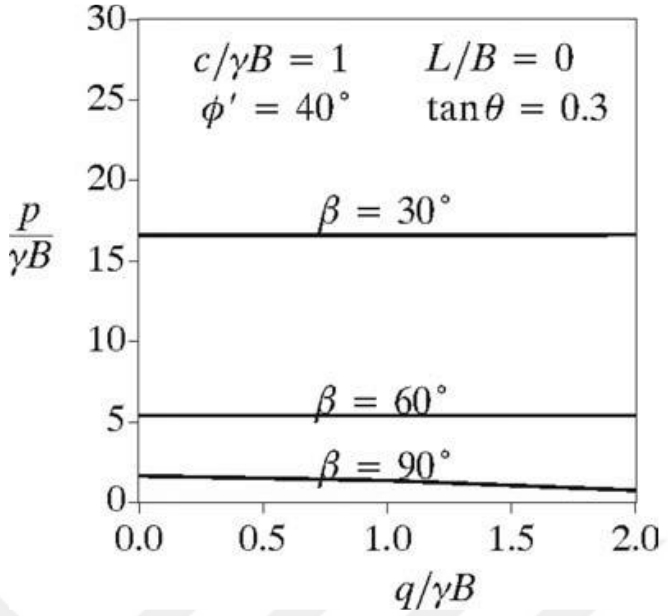


Figure 2.29. Effect of $q/\gamma B$ on $p/\gamma B$ for various β (Shiau *et al.*, 2006).

When the impact of inerti force of the soil incline is neglected, an uncertain estimation of the final bearing capacity can be achieved for all inclination angles. The result can be clearly seen in Figure 2.30.

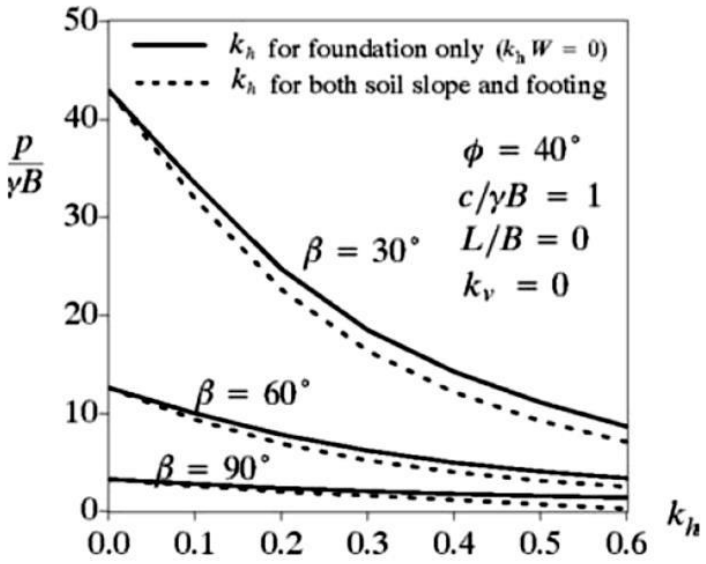


Figure 2.30. Effect of soil inertia k_h on $p/\gamma B$ (Shiau *et al.*, 2006).

The results obtained from this study indicated that numerical upper and lower bounds mostly support the right solution by %10 or more. This flow rule showed that solutions of any method have to return outcomes that are placed within upper and lower bounds.

Yamamoto (2010) has stated that Japanese ıslands have been exposed to severe seismic activities. However, the foundations have to be constructed near slopes. In recent earthquakes, the author reported that the bearing layer under the buildings had destructed and sunk, although the damage of structures was not significantly severe. Hence, he concluded that it is important to investigate both the evaluation of bearing capacity and seismic bearing capacity in such footings design process .

The purpose of this study is to investigate the seismic bearing capacity factors of shallow foundations around inclines by utilizing the upper-bound limit examination. The assumed mechanism of failure in Figure 2.31 consists of a log-spiral shear zone, an active triangular wedge, and passive wedge. The non-symmetrical failure mechanism is determined by just two ξ and η angular parameters. Furthermore, the author strongly expressed that the developed model can be adopted in the practical applications of geotechnical engineering.

In accordance with material assumptions of limit analysis, c-Φ soil is rigid-perfectly plastic material and follows correlated flow rule. Seismic effect determined by the pseudo-static approach consists of a horizontal shear force acting on the footing at the first layer of foundation and an inertia force of the sliding soil mass. In this study, the horizontal seismic acceleration coefficient (K_h) was assumed to be equal to calculate inertia force of structure running on the foundation and of the sliding soil mass. The effect of vertical acceleration onto the seismic bearing capacity was neglected.

Shear transfer coefficient (f) is introduced to regard variable shear force shift in the foundation base. The impact of footing embedment is also investigated as well.

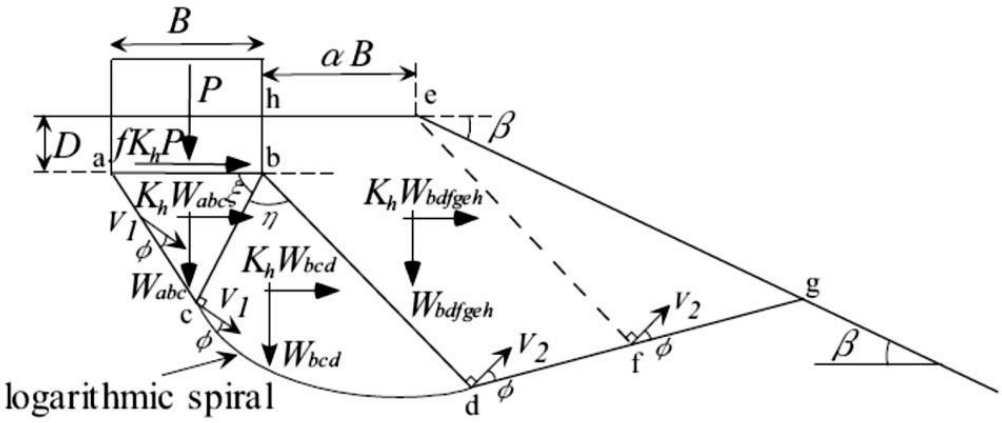


Figure 2.31. Mechanism of failure used in the analysis (Yamamoto, 2010).

Through the solution of the energy balance equation that establishes a base for upper bound limit examination, the upper limit of seismic bearing capacity is obtained through the formula given in Equation 2.9.

$$q_b = cN_{ce} + \frac{1}{2}\gamma B N_{\gamma e} \tag{2.9}$$

where *c* is the adherence, *B* is the footing width, γ is the specific weight of the soil, N_{ce} and $N\gamma e$ are the factors of seismic bearing capacity.

Nce and *Nγe* seismic bearing capacity factors given in Equation 2.17 are calculated by the equations given in Equation 2.11 and Equation 2.11 respectively.

$$N_{ce} = \frac{1}{\cos\varepsilon + fK_h \sin\varepsilon}(f_7 + f_8 + 2f_9) \tag{2.10}$$

$$N_{\gamma e} = \frac{1}{\cos\varepsilon + fK_h \sin\varepsilon}(f_1 + f_3 + f_5) + K_h(f_2 + f_4 + f_6) \quad (2.11)$$

where ξ is the angle which defines the geometry of active wedge beneath the footing, f is the shear transfer coefficient, K_h is the horizontal seismic coefficient and f_i (i= 1 to 9) are the functions of which independent variables are ξ, η, β, αB, D/B and Φ. Since seismic bearing capacity factors obtained in this study are represented by design charts, the expanded forms of fi function (i= 1 to 9) will not be given in detail. Related formulas can also be found in the reference (Yamamoto, 2010).

All possible combinations of ξ and η variables, providing a kinematically possible swiftness range were considered in this study to get the least amount of two factors (N_{ce} and $N_{\gamma e}$) individually. Thus, the use of superposition approach is, in fact, on the safe side.

The conclusion drawn in this research compared with the existing researches by earlier scholars after the validity of the method is verified for some cases. Results of the parametric study performed by using this method are summarized as follows :

- The factors of seismic bearing capacity decrease significantly by increasing horizontal seismic coefficient K_h.
- Increasing the inclination angle causes a decrease in the factors of bearing capacity magnitude.
- Seismic bearing capacity declines by the rise of the coefficient of shear transfer (*f*).
- The factors of bearing capacity quantities rise by the embedment (*D/B*) and the incline peak distance from the start of loading (αB).
- As shown in Figure 2.32, as K_h increases, the angle of active wedge increases, and the angle of the log-spiral zone also decrease. Additionally, by the rise of K_h, the overall extent of failure mechanism decreases.

Design charts for the bearing capacity factor obtained N_{ce} and $N_{\gamma e}$ with K_h for various amounts of β are presented in Figure 2.33 to 2.40 (Φ= 30°, 40°, *D/B*= 0.0 and 1.0, α= 0.0 and 0.5).

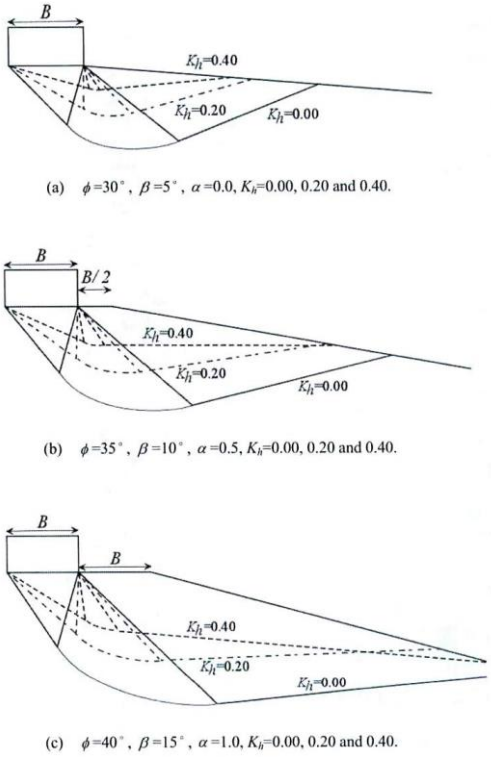


Figure 2.32. Mechanisms of failure for various amounts of *Φ*, *β*, *α,* and K_h (Yamamoto, 2010).

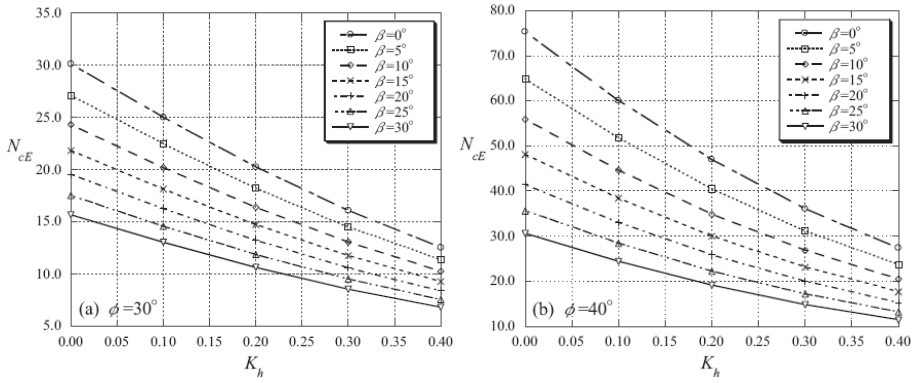


Figure 2.33. Charts of design for N_{ce} (*Φ*= 30°, 40°, *D/B*= 0, *a*= 0.0) (Yamamoto, 2010).

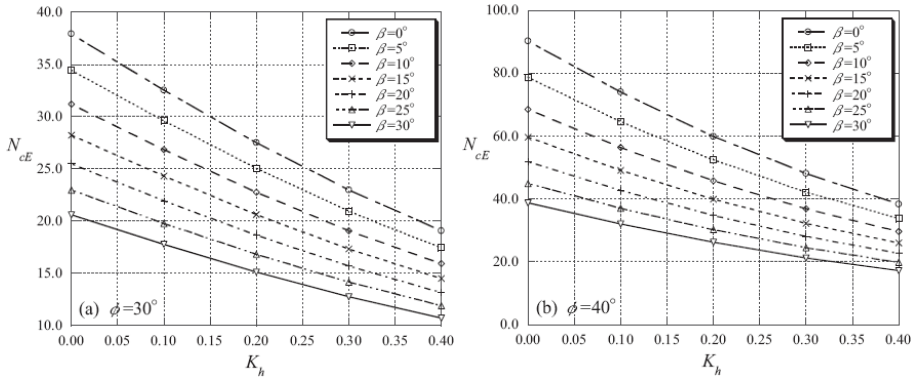


Figure 2.34. Charts of design for N_{ce} (Φ= 30°, 40°, D/B= 1, a= 0.0) (Yamamoto, 2010).

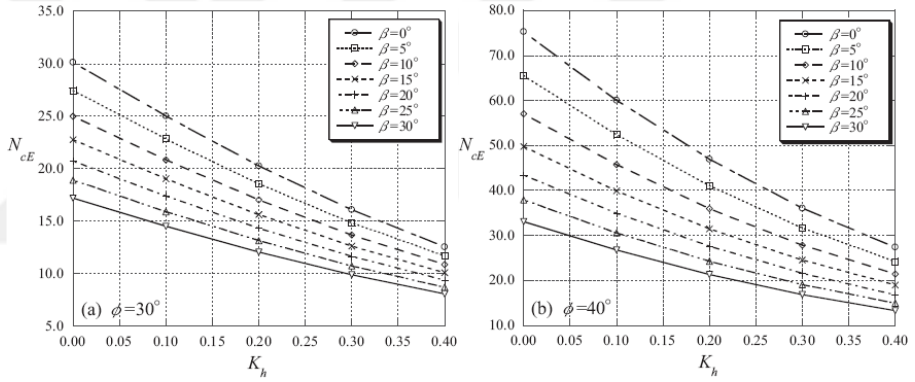


Figure 2.35. Charts of design for N_{ce} (Φ= 30°, 40°, D/B= 0, a= 0.5) (Yamamoto, 2010).

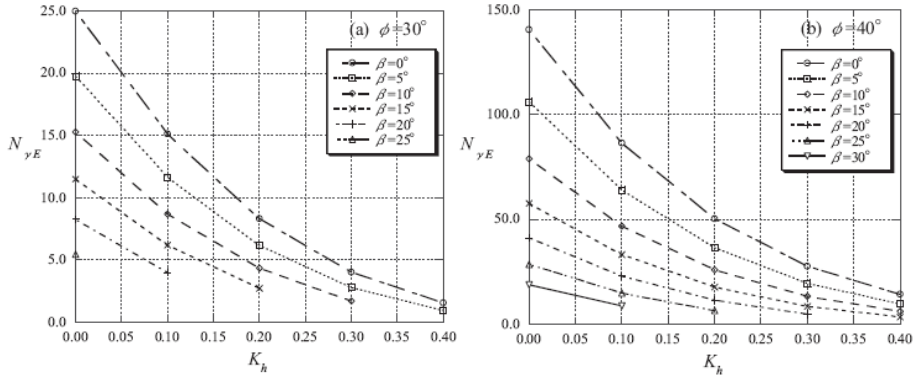


Figure 2.36. Charts of design for $N\gamma e$ (Φ= 30°, 40°, D/B= 0, a= 0.0) (Yamamoto, 2010).

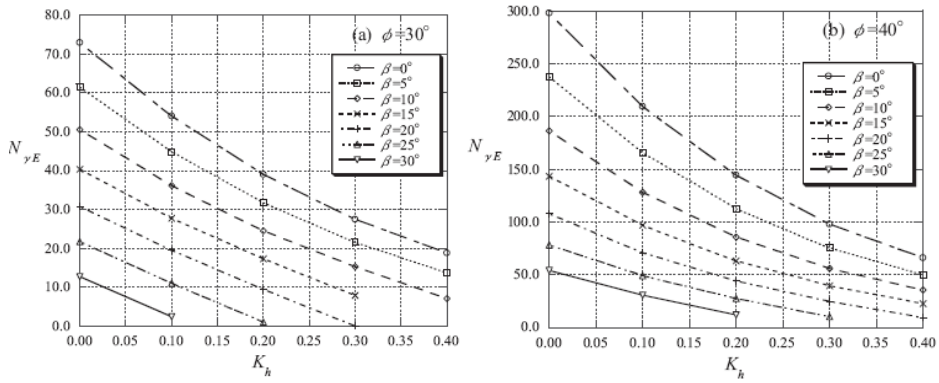


Figure 2.37. Charts of design for $N_{\gamma e}$ (Φ= 30°, 40°, D/B= 1, a= 0.0) (Yamamoto, 2010).

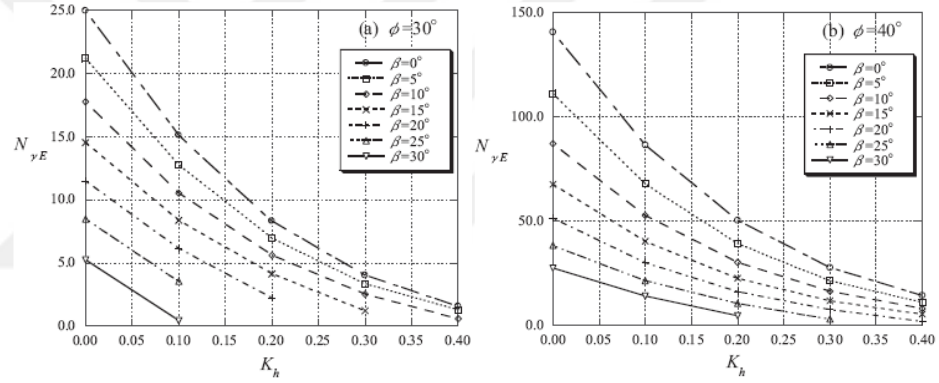


Figure 2.38. Charts of design for $N\gamma e$ (Φ= 30°, 40°, D/B= 0, a= 0.5) (Yamamoto, 2010).

Castelli and Motta (2010) had expressed that the pseudo-static approach is used to measure the factors of seismic ultimate bearing capacity. Therefore, the study intends to investigate taking into account both the impact of the foundation embedment and the span of the foundation from the inclined edge. According to this method, earthquake forces includes the inertia forces employed on the footing, sliding soil mass and surcharge. The inertia force of the surcharge and structure are computed using equal seismic acceleration coefficients (k_{h1}=k_{h3}) to each other. However, the value of the soil mass (k_{h2}) was chosen higher than the inertia of the structure because Eurocode 8 supports decreasing the seismic behavior with respect to the flexibility analysis of the constructions. Thus, pseudo-static analysis is performed regarding the subsequent coefficients of seismic as k_{h1}=0.1 and 0.2 for the inertia force of the construction, k_{h2}=0.2, and 0.4 for the inertia force of the soil body.

The author concluded that the results obtained from the proposed model are in high consistency with the obtained models of other scholars even though the simplified mechanism. In addition to, the ratio of bearing capacity coefficients in seismic conditions (*Nc*/Nc*) changes with *d/B* ratio, slope angle (*β*), *H/B* ratio as well as internal friction angle (*Φ*) and seismic acceleration coefficients (k_{h1}, k_{h2} ve k_{h3}). Moreover, *d/B* ratio, slope angle (*β*), *H/B* ratio and k_{h1} seismic acceleration coefficient plays a significant role on the *Nc*/Nc* ratio in undrained conditions ($\Phi = \Phi u = 0°$). The rates of seismic bearing capacity *Nc*/Nc* are presented in Figure 2.39 as a function of *d/B* for different angles of inclination. The presented charts show that the value of k_{h1} just takes greater than zero since the decrease in seismic bearing capacity due to the inertia force of the structure is more decisive.

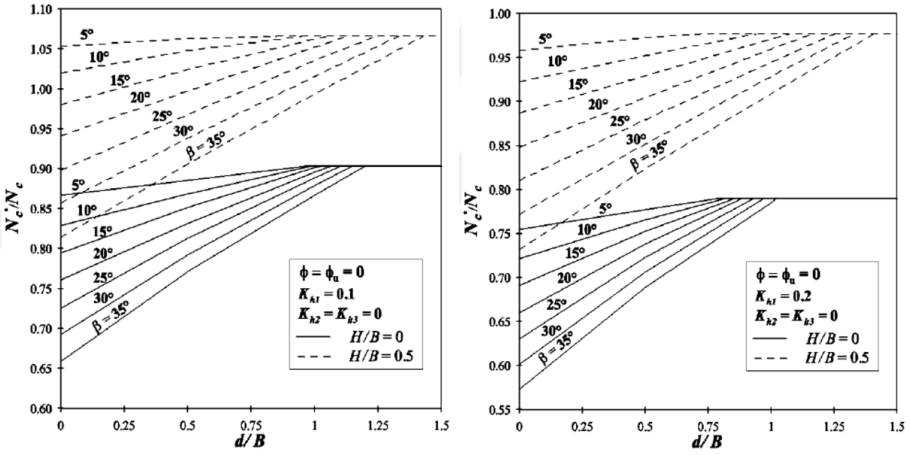


Figure 2.39. N_c^*/N_c rates as a function of the normalized *d*/*B* distance of incline (Castelli and Motta, 2010).

Results of the developed method are similar to compared with outcomes of static condition; when the foundation is located at the inclined edge, the highest decrease of the bearing capacity is observed. The bearing capacity generally tends to increase with the rise of the distance of foundation from the slope edge. As the footing reaches a certain distance from the slope edge defined as threshold distance, the presence of slope will not affect the failure mechanism. Thus, the ratio no longer takes the constant value that is diminished by the influence of inertia forces only. As shown in Figure 2.39, the threshold distance varies

in between 0.75*B* and 1.5*B*. Moreover, this distance increases with the increase of k_{h1} seismic acceleration coefficient. Besides, it is reported that the threshold distance is not changed by considering either inertia of the structure and of the sliding soil mass separately.

Amin Keshavarz *et al.* (2019) used the finite element method that is named 'FELA' to obtain the seismic bearing capacity of a strip foundation located near homogenous soil slopes. In order to find the under undrained seismic load carrying capacity of a strip footing placed on cohesionless soil, various influential factors were defined respectively; geometrical properties of the slope, the setback distance ratio (*L/B*), and the slope angle, the strength ratio ($c_{u0}/(\gamma B)$), the horizontal earthquake coefficient (k_h). Consequently, the functional description of the seismic undrained bearing capacity ($q_u/\gamma B$) and its variables parameters are given briefly in Equation 2.12.

$$\frac{q_u}{\gamma B} = f(\frac{L}{B}, \frac{H}{B}, k_h, \frac{c_{u0}}{\gamma B}, \beta, \frac{kB}{c_{u0}}) \tag{2.12}$$

In addition with homogeneous soil slope, heterogeneity soil slope effect on the undrained seismic load carrying capacity of a strip footing located close to slope. Therefore, the soil strength heterogeneity (kB/c_{u0}) is expressed as a function of seismic bearing capacity.

Graphical representation of the problem is presented in Figure 2.40. Model type is selected as plane strain. Accordingly, the undrained shear strength is assumed as a constant value for the homogeneous soil slope. The soil saturated unit weight is kept constant at 20 kN/m3. The dimensions of the model of L_x, $L_ı$ and L_z are arranged 3*B*,14*B*, and 13*B*. The reason for choosing these values is to avoid the effect of boundaries on the outcomes.

The effective parameters are choosen: (i) $c_u/(\gamma B)$=0.5, 1.0, 1.5, 2.0, 2.5, 5.0; (ii) β=10°, 20°, 30°, 40°, 50°; (iii) *L/B*=0, 0.25, 0.50, 1, 2, 3, 4, and 5 for homogeneous soil.

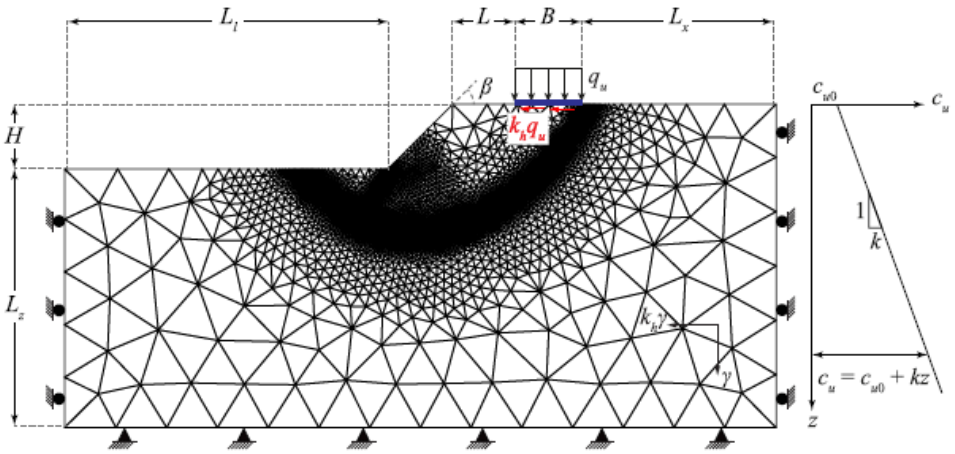


Figure 2.40. Model geometry and a typical FELA mesh.

As mentioned above, computer codes based on FELA have been used to solve the problem of the present study. Even though, FEM and FELA have the same ability to deal with problem, there is a sharp difference regarding the usage methodology. In the FEM, a relatively fine mesh must be taken account in the area where it sustains high deformation to take exact value whereas the FELA adopts automatic adaptive mesh refinement.

The results obtained from this adopted method were compared with other research works. The following outcomes were summarized in the following:

- Figure 2.41 shows that relationship between *Nc* and *L/B* obtained from the present study shows a good agreement with the finite element results of Georgiadis. On the other hand, the results of Meyerhof and Kusakabe *et al.* are noticeably higher than the results of the present study because of a face failure mechanism in their analysis. However, this hypothesis can't be true because the failure mechanism depends on location of footing from the slope crest.

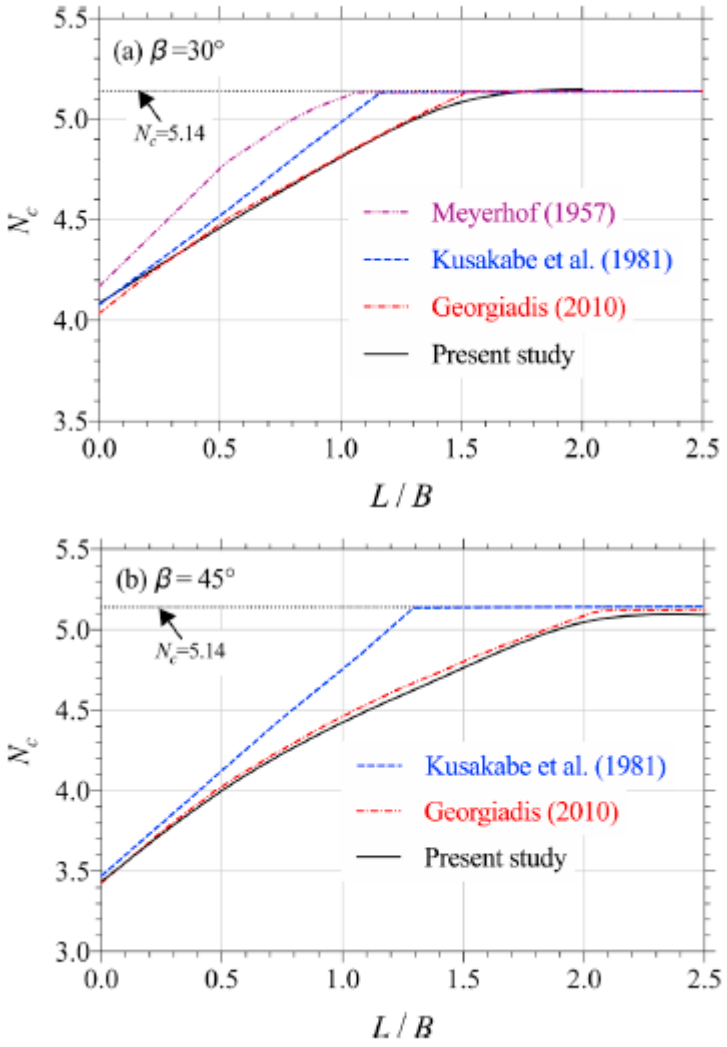


Figure 2.41. Comparison of the results of the present study with those presented by previous researchers (A. Keshavarz *et al.*, 2019).

- As depicted at Figure 2.42, the variation in seismic load carrying capacity was compared for four different values of k_h; respectively; 0, 0.1, 0.2 and 0.3. According to the results of present study are good agreement with FEM results of Cinicioglu and Erkli. Only for large values of *L/B*, the results are slightly greater than FEM results of Cinicioglu and Erkli.

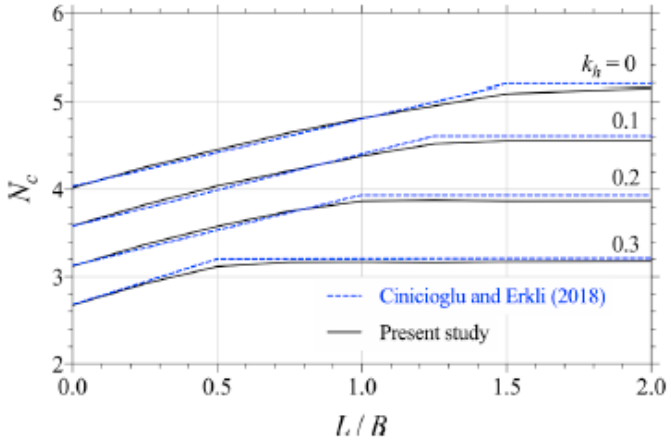


Figure 2.42. Comparison of the variation in *Nc* against *L/B* for β = 30°; *H/B*=1, 2, 4; and $c_{uo}/(\gamma B)$=2.5 (A. Keshavarz *et al.*, 2019).

- As shown in Figure 2.43, the value of $q_u/(\gamma B)$ decreases as the slope angle increases because of the shape of the failure surface under the footing. Furthermore, Figure 2.44 presents that the impact of *L/B* on $q_u/(\gamma B)$. The value of $q_u/(\gamma B)$ increases when footing distance from the slope edge increases and from a constant value of *L/B* the value to $q_u/(\gamma B)$ reaches constant.

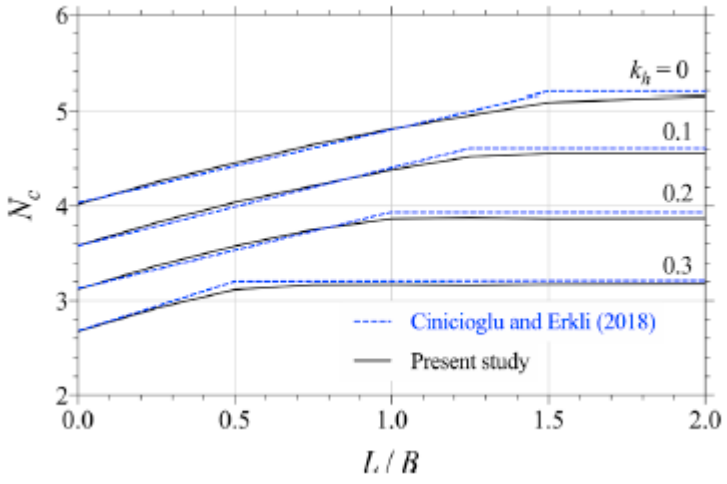


Figure 2.43. Variation of the $q_u/(\gamma B)$ with *L/B* (A. Keshavarz *et al.*, 2019).

- Figure 2.44 shows that the value of $q_u/(\gamma B)$ decreases as the value of k_h increases with a constant value *L/B*.

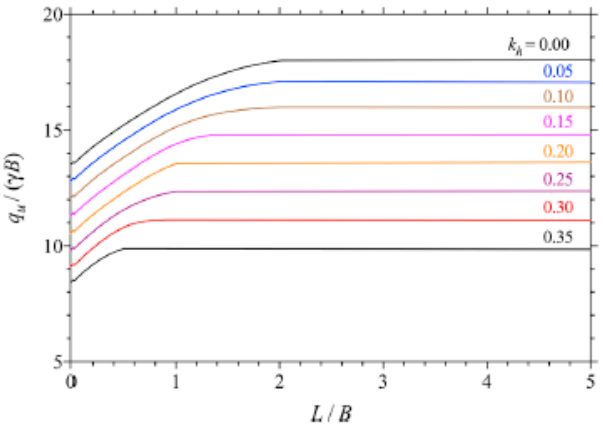


Figure 2.44. The effect of k_h on $q_u/(\gamma B)$ (H/B=3, $c_{uo}/(\gamma B)$=3.5, and $\beta=35^0$) (A. Keshavarz *et al.*, 2019).

- As mentioned beginning of the present study, pseudo-static method is used to simulate the earthquake condition. As can be seen in Figure 2.45, for any value of $k_h \geq 0.38$, $k_h q_u/c_{u0}=1$, related with foundation sliding mode of failure.

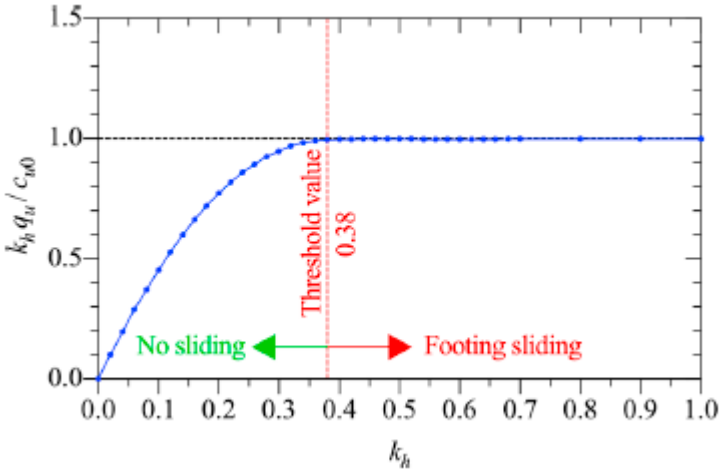


Figure 2.45. Variation of $k_h q_u/c_{u0}$ against k_h for the level ground (A. Keshavarz *et al.*, 2019).

- Result of FEM shows that the slope height ratio (*H/B*) has a direct impact on the stability problem for slopes. Based on Taylor approach for the critical value of height of the homogeneous unloaded soil slope (H_{cr}), if $H>H_{cr}$, the slope isn't stable and can't undergo any load.
- As shown in Figure 2.46, the failure modes at $L/B = 0$ is overall slope failure which initiates well behind the edge of the footing and creates a failure pattern that covers the entire model.

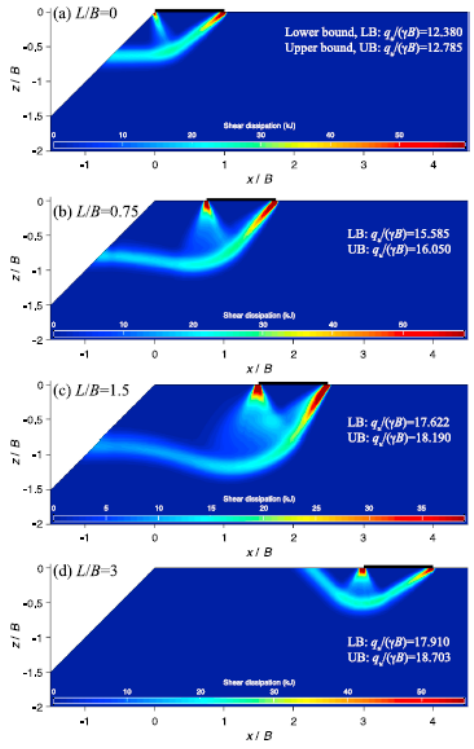


Figure 2.46. Typical foundation failure pattern for $c_{uo}/(\gamma B)= 4$, $kB/c_{u0}=0$, $k_h =0.1$, $\beta=45^0$, (*H/B* = 4) (A. Keshavarz *et al.*, 2019).

- Contrarily, the failure mode for *L/B* = 3 changes from face failure to Prandtl-type failure mode. It is also shown in Figure 2.47.
- Another failure mode is called base failure as given in Figure 2.47. Base failure correlates with bearing capacity failure. Conversely, as the value of $c_{u0} / (\gamma B)$ increases shown in Figure 2.47, the failure modes turns to be the toe failure mode.

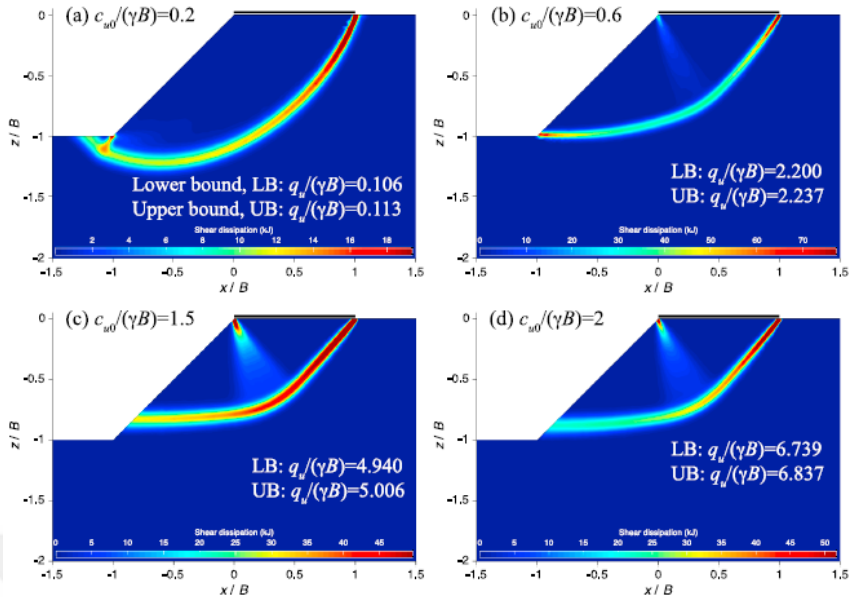


Figure 2.47. The effect of c_{uo} / (γ B) on the failure mode (kB/c_{u0}=0, k_h =0, β=45^0, H/B = 1) (A. Keshavarz *et al.*, 2019).

- It is noticed that there is a reverse relationship between k_h and the volume of failure mode. As shown in Figure 2.48, as k_h increases, the active thrust increases, the passive thrust decreases, and the wedge angles start smaller.

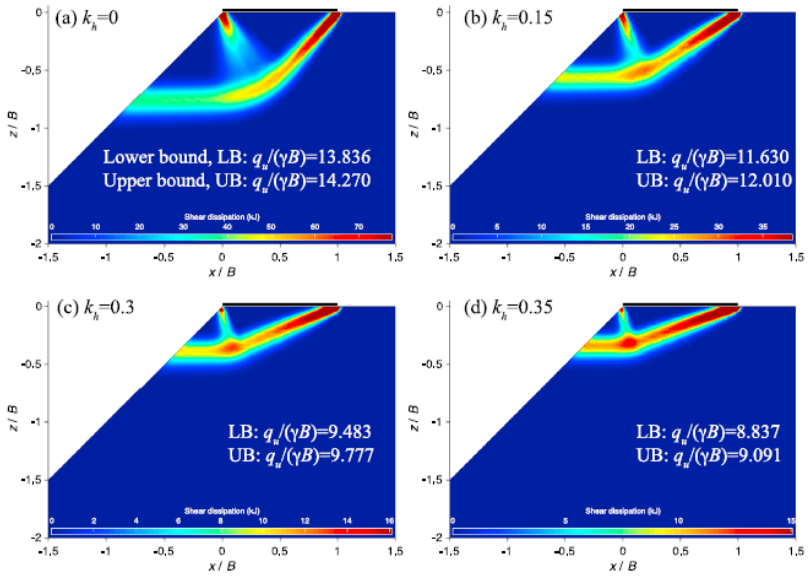


Figure 2.48. The effect of k_h on the failure mode c_{uo} / (γ B) =4, (kB/c_{u0}=0, L/B = 0, β=45^0, H/B =4) (A. Keshavarz *et al.*, 2019).

- Normalized bearing capacity $q_u/(\gamma\ B\ )$ increases linearly with the increase *L/B*. As seen from the graph given in Figure 2.49, due to the failure mode changes from face failure mode to Prandtl-type failure mode, this trend tends to go a certain value.

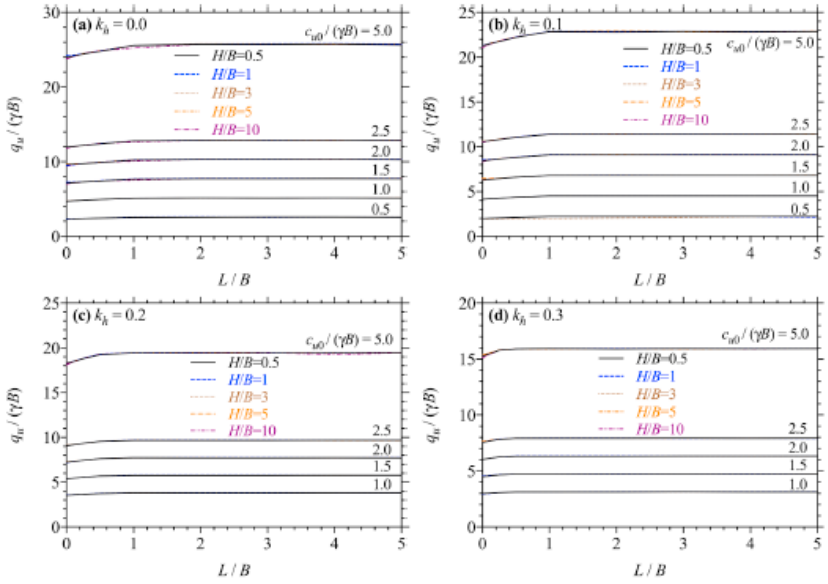


Figure 2.49. Design charts for average values of lower and upper bounds of normalized bearing capacity of a rough strip footing located on slope with $\beta = 10^0$ (A. Keshavarz *et al.*, 2019).

2.3. Shape Effect of Shallow Foundation On Seismic Bearing Capacity

Recently, both numerical and experimental analyses on the final bearing capacity of square and rectangular foundations have attracted the attention of many researchers. However, these studies were mostly performed for the footings placed on the sand. As abovementioned, few researchers have studied to investigate the ultimate loads on square or rectangular foundations resting on frictional-cohesive (*c*-φ) soil. Notably, five studies (Salgado (2004), Zhu and Michalowski (2005), Gourvenec (2006), Li et.al. (2009), Yu et.al. (2011)) suggested a solution to determine the final bearing capacity of footing within the eight studies of research that will be referred to in this section. Contrarily, the reason for

referring the other three research studies is to present brief explanations about their solution methods and their hypotheses.

Yang *et al.* (2003) proposed a technique to calculate the lower bound boundary of rectangular surface foundations' bearing capacity. A perfectly rigid plastic model was integrated to define the feature. The bearing capacity of footing was subjected to the stress boundary condition, stress discontinuity equilibrium state, stress equilibrium state, and yield state. In this study, a rectangular surface footing was taken into consideration depending on the soil internal friction angle and adherence to the bearing capacity.

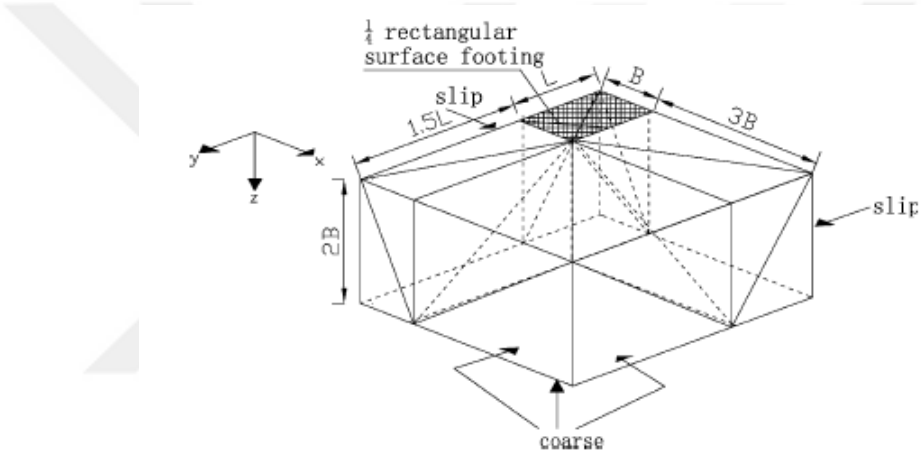


Figure 2.50. Lower bound analysis of finite element coarse mesh (H. Yang *et al.*, 2003).

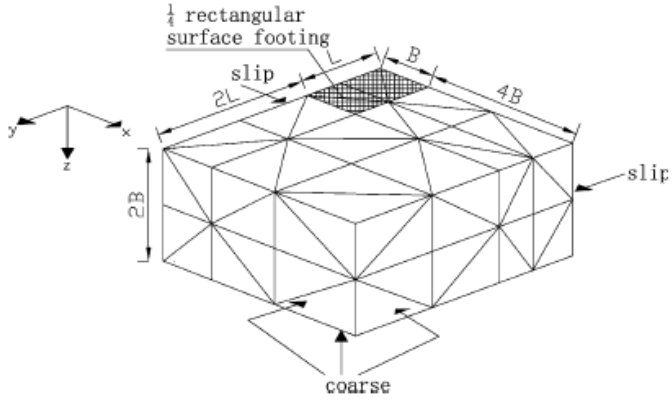


Figure 2.51. Lower bound analysis of finite element fine mesh (H. Yang *et al.*, 2003).

The 3D lower bound examination of the finite element mesh for was shown in Figure 2.50. A quarter of the whole meshes were regarded due to the symmetry. The spreading load on the rectangular foundation given in Figure 2.50 and Figure 2.51 was enlarged by exploring a statically admissible stress discontinuity between the soil underneath the strip foundation.

Within the context of this study, the square element with four nodes was used in all finite element models. It was assumed that more than one node might experience the same coordinates and statically admissible stress discontinuity is allowed at common facades among the neighboring square elements.

L/B	Author			Michalowski
	Yield condition I	Yield condition II	Yield condition III	
(a) Course mesh				
1	5.093	5.349	5.881	6.830
2	4.878	5.122	5.632	6.060
5	4.501	4.726	5.199	5.499
10	4.458	4.690	5.157	5.190
(b) Fine mesh				
1	5.256	5.567	6.174	6.830
2	5.014	5.306	5.856	6.060
5	4.782	4.952	5.354	5.490
10	4.620	4.831	5.166	5.190

Figure 2.52. Comparison of 3-dimensional lower and bound bearing capacity N_c for strip foundations on a weightless and purely adhesive soil (H. Yang *et al.*, 2003).

As seen from Figure 2.52 and Table 2.1 that coefficient of bearing capacity factor of quadrilateral foundations for utterly cohesive soil was determined by the solution of 3D lower bound. Furthermore, Michalowski (2001) gave the outcome of a similar situation utilizing 3D upper bound approach. A quadrilateral foundations' bearing capacity reduction was observed with an increment of *L/B*. As a result of analyses obtained, all results of 3-dimensional lower bound were below the identical Michalowski (2001) upper bound. However, the results should be within the upper and lower bound as the main idea of theory. It was also illustrated in Figure 2.53.

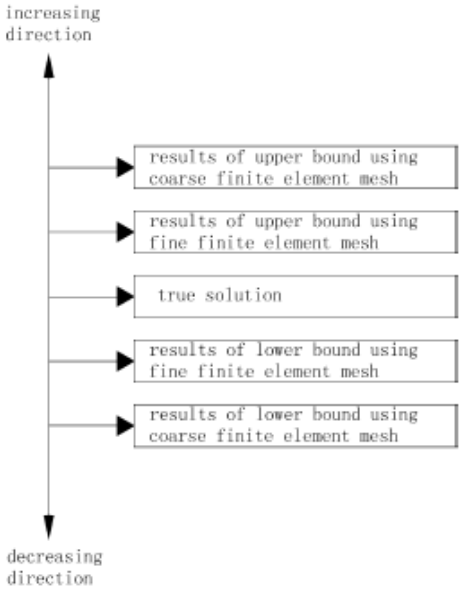


Figure 2.53. Various solutions for 3-dimensional bearing capacity for shallow foundations (H. Yang *et al.*, 2003).

The author had concluded that the accurate results of 3D condition would be more significant than the results of 2-dimensional state. Due to the dimensional outcome in the 3-dimensional state, this kind of impact was ignored entirely in the 2-dimensional state. As seen in Figure 2.53, in the lower bound methods, fine mesh gives a more significant outcome than coarse mesh, because it has matched more to the right solution.

Table 2.1. Comparison of 3-dimensional upper and lower bound coefficient of bearing capacity N_c for shallow foundations on a weightless and frictional cohesive soil.

ϕ Degrees	Author						Michalowski	
	$L/B = 1$			$L/B = 2$			$L/B = 1$	$L/B = 2$
	I	II	III	I	II	III		
(a) Coarse mesh								
10	8.651	9.489	12.037	6.011	6.647	8.363	14.365	10.733
15	10.597	11.713	16.454	8.273	9.218	13.06	22.984	15.585
20	15.862	18.621	29.971	10.247	12.195	20.09	39.199	23.912
25	20.179	25.734	49.912	11.653	14.277	29.424	71.397	38.312
30	29.598	39.759	110.823	14.437	21.479	60.452	139.337	67.099
(b) Fine mesh								
10	8.962	9.774	12.458	6.193	6.899	8.719	14.365	10.733
15	10.972	12.088	17.129	8.519	9.587	13.771	22.984	15.585
20	16.385	19.465	31.460	10.668	12.717	21.115	39.199	23.912
25	20.976	26.994	52.712	12.200	14.992	31.179	71.397	38.312
30	31.117	42.065	116.327	15.246	22.719	64.386	139.337	67.099

The coefficient of bearing capacity N_c of the exterior foundation for utterly adhesive soil was measured by the of 3-dimensional lower bound technique and compared with the results of identical Michalowski (2001) upper bound, as shown in Table 2.1. According to results, yield condition has a specific effect on 3-dimensional examination of limit lower bound. Moreover, several results can be obtained from different yield criterions. For example, the author's outcome is below Michalowski's method. This variation also grows with the increment of soil inner frictional angle Φ.

Salgado *et al.* (2004) developed a solution tool based on finite limit analysis for calculating shallow footings around inclines. These computations were conducted for rough strip, square, circular, and rectangular footings. We can represent the clay as a matter with the $c=s_u$ and $\varphi=0$ features, where s_u is the undrained shear strength of the clay. Therefore, the equation in 2.13 was presented below for a strip footing on the soil surface.

$$q_{bL} = S_u + N_c \tag{2.13}$$

where $N_c = 2 + \pi \approx 5{,}14$ (first found by Prandtl 1920, 1921)

The author has modified that equation to calculate the limit base stability of rectangle, circular, or square foundations constructed at various profundities inside the clay, revision determinants converting back to Equation 2.14.

$$q_{bL} = s_c d_c N_c s_u + q_0 \tag{2.14}$$

In accordance with material assumptions of limit analysis, *c-φ* clay is rigid, completely flexible material and follows correlated flow rule. For clays, the bearing capacity of

foundations of limited design dimension *B* and *L* have been higher than shallow foundations with breadth *B.* As the expressions for shape and depth factors given in Figure 2.54. were illustrated to get the bearing capacity of used in circular, rectangular or square foundations that multiplying $s_u N_c$.

Shape Factors	Depth Factors	Author
$s_c = 1 + (0{,}2)\, B/L$	$d_c = 1 + (0{,}2)\, D/B$	Meyerhof (1951)
$s_c = 1 + (0{,}2)\, B/L$	$d_c = 1 + (0{,}4)\, D/B\ for$ D/B<1 $d_c = 1 + (0{,}4)\tan^{-1} D/B\ forD/B \geq 1$	Brinch Hansen (1970)

Figure 2.54. Shape and depth factors usually utilized for clays (Salgado *et al.*, 2004).

Although various tables had been presented in this analysis to show the influence of shape and depth effects on ultimate bearing capacity, bearing capacity values depending on ratio of *B/L* and *D/B* were compared with examination of upper and lower bound limit presented in the following Figure 2.55. They are enough to sum up the essential results of the study. Referring to the table, the corresponding distinction among upper and lower bounds falls to approximately 12% as *B/L* declines from 1 to 0.2 for rectangular footings despite the state of *D/B*. Computations have been performed according to average amounts and lower bound of q_{bL}^{net}. However, for employment in design, it is suggested to choose lower values.

D/B	Strip		Circular		Square		Rectangular with B/L=							
							0.50		0.33		0.25		0.20	
	L	U	L	U	L	U	L	U	L	U	L	U	L	U
0.00	5.132	5.203	5.856	6.227	5.5523	6.221	5.359	6.022	5.256	5.886	5.201	5.820	5.169	5.779
0.01	5.164	5.259	5.962	6.503	5.610	6.442	5.424	6.249	5.311	6.085	5.253	6.006	5.218	5.949
0.05	5.293	5.384	6.295	6.840	5.886	6.815	5.640	6.503	5.503	6.3003	5.430	6.203	5.389	6.126
0.10	5.448	5.548	6.491	7.140	6.171	7.130	5.860	6.756	5.697	6.533	5.614	6.413	5.565	6.321
0.20	5.696	5.806	6.897	7.523	6.590	7.534	6.197	7.116	5.997	6.867	5.895	6.731	5.836	6.637
0.40	6.029	6.133	7.303	8.104	7.194	8.096	6.680	7.574	6.408	7.271	6.272	7.113	6.190	7.003
0.60	6.240	6.341	7.866	8.608	7.671	8.573	7.082	7.993	6.740	7.608	6.567	7.412	6.465	7.299
0.80	6.411	6.509	8.370	9.034	8.068	8.996	7.427	8.377	7.030	7.936	6.817	7.706	6.695	7.370
1.00	6.562	6.657	8.771	9.429	8.429	9.346	7.729	8.724	7.297	8.240	7.048	7.976	6.904	7.819
2.00	7.130	7.227	9.973	11.008	9.752	10.853	8.968	10.055	8.447	9.476	8.109	9.086	7.860	8.835
3.00	7.547	7.652	10.686	12.140	10.532	12.000	9.860	11.076	9.296	10.473	8.920	10.026	8.607	9.696
4.00	7.885	7.994	10.954	13.030	10.941	12.900	10.513	11.878	10.018	11.242	9.594	10.769	9.249	10.403
5.00	8.168	8.284	10.998	13.743	11.206	13.640	10.880	12.545	10.464	11.887	10.117	11.408	9.796	11.030

Figure 2.55. Ratio of net bearing capacity factor to undrained shear strength, $\boldsymbol{q_{bL}^{net}/s_u}$, for foundations in clay (*L* = lower, *U*= upper bound) (Salgado *et al.*, 2004).

The shape factors computed from the average of the upper and lower bound values utilizing the equation given in 2.15.

$$s_c = \frac{q_{bL}^{net}}{d_c[q_{bL}^{net}]} \tag{2.15}$$

The average value at the surface by declining *B/L* precisely falls to 1. The values of C_1 and C_2 as a dependent of *B/L* is given in Figure 2.56 to provide the best-fit lines with the equation 2.16.

$$s_c = 1 + C_1 \frac{B}{L} + C_2 \sqrt{\frac{D}{B}} \tag{2.16}$$

B/L	C_1	C_2
1(circle)	0.163	0.210
1(square)	0.125	0.219
0.5	0.156	0.173
0.33	0.159	0.137
0.25	0.172	0.110
0.2	0.190	0.090

Figure 2.56. Constants of regression in the shape factor equation (Salgado et al., 2004).

Additionally, the estimated factors of form for squared and round footings are varying from the point at *D/B*=4, the bound of the graphic. Because of the significant gap among upper and lower limit examination for *B/L* = 1 and the variation point for *D/B* > 4, results for *D/B* > 4 is not plotted in Figure 2.57.

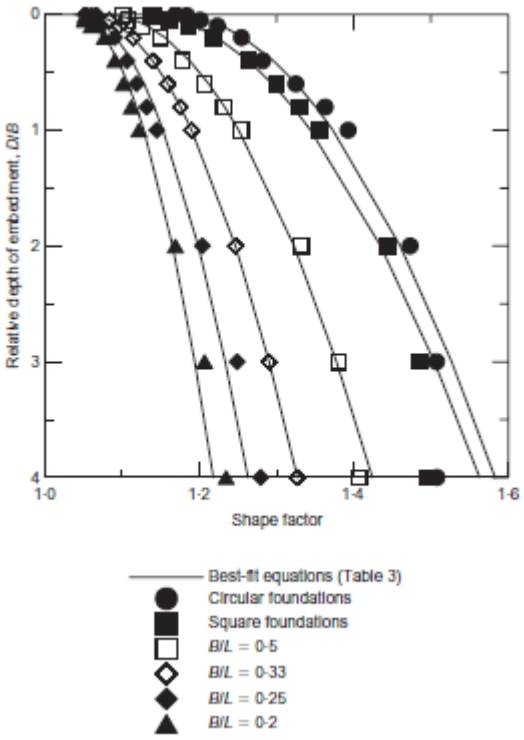


Figure 2.57. Shape factor for foundations of various shapes as a function of relative depth as calculated by limit analysis plotted together with best-fit lines with the form of Equation 2.25 (Salgado *et al.*, 2004).

The author had concluded that the equation utilized in the application for the factors of form perceived to more conservative expect for excessively low *D/B*. The equation of Meyerhof (1951) for the factor of depth was also perceived as sensible as well. On the other hand, the Brich Hansen (1970) equation was perceived to be sufficient for extremely low *D/B* values and not conservative for higher amounts of *D/B*. Based on the presented study, the uncertainties with regard to the equation of bearing capacity may cause lower factors of safety.

In order to investigate the impact of the foundation shape on the bearing capacity of a medium elasto-plastic clay, Zhu and Michalowski (2005) had used the limited element approach. The earlier proposal was according to experimental data for small foundations while a new proposal for these factors is according to the model of elasto-plastic of the clay.

In this study, ABAQUS was used to reach the maximum load of square and rectangular foundations as a finite element system. Twenty-node elements of quadratic brick with a reduced integration plan were adopted in all finite element models prepared within the context of this study. It was depicted in Figure 2.58, there is a schematic description of the finite component mesh.

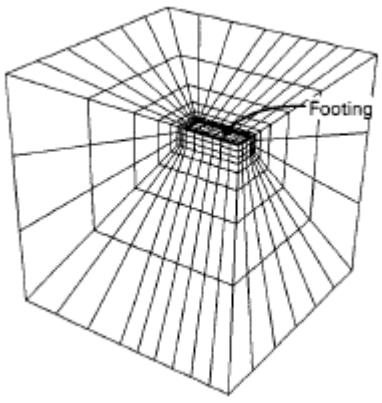


Figure 2.58. Finite element mesh (Zhu and Michalowski, 2005).

A group of computations with finer meshes were performed by the authors. The variation in coefficient of bearing capacity factor gained from computations with the coarse mesh and the fine mesh changed fewer than 1% (φ= 10º, *L/B*=2) to not actually 4% (φ= 35º, *L/B*=2). The change in *Nγ* factor was increasing to 8%. Since the coarse mesh was selected for the calculations of finite element and plane strain, the results of these calculations showed that rectangular footings are more dependent on the limit loads than the size of the mesh. The diversity in factors of form calculated for the coarse and fine meshes were quite smaller than 1%.

In essence, the approach adopted in this study is to express the *N* factor is the functions of φ, $c/\gamma B$, and $q/\gamma B$. Eventually, if these three expressions are computed independently, the sum of the three items will be the best upper bound consistent assessment. In this sense, the component of the bearing capacity based on adherence was computed considering no excessive burden (q=0) and weightless soil (γ=0) given in the following Equation 2.17.

$$p = cN_c' = s_c c N_c \tag{2.17}$$

where N_c'= factor of bearing capacity for the orthogonal foundation. Shape factor s_c was determined by the formula given in Equation 2.18.

$$s_c = \frac{N_c'}{N_c} \tag{2.18}$$

Where N_c = factor for the shallow foundation. Shape factor s_q can be measured in the same method. Hence, the factor N_q' can be obtained using the Caquot rule of equivalent states as given in Equation 2.19 and Equation 2.20.

$$N_q' = N_c' \tan \emptyset + 1 \tag{2.19}$$

and

$$s_q = \frac{N_q'}{N_q} \tag{2.20}$$

Therefore, s_q factor can be obtained if s_c is identified as given in Equation 2.21.

$$s_q = \frac{N_q'}{N_q} = \frac{N_c^! \tan \emptyset + 1}{N_c \tan \emptyset + 1} = \frac{s_c N_c \tan \emptyset + 1}{N_c \tan \emptyset + 1} \tag{2.21}$$

Results of the developed method were compared with FEM results show clearly that the upper-bound approach limit analysis produces remarkably greater factors of form, especially for small aspect ratios *L/B* and great angles of friction φ. Outcomes of this study carried out by using the FEM method are summarized in the following:

- When the earlier studies of Meyerhof (1963) and De Beer (1970) are considered, their estimates for s_c and s_q are found to be conservative. Particularly smaller amounts of s_c and s_q returns for low angles of friction and small aspect ratios of the limited element approach. Additionally, the shape factor s_γ can rise or fall according to the aspect ratio, but it also depends on the angle's internal friction of the clay.
- The shape factors and the bearing capacity computed using FEM had unsatisfactory performance compared to the kinematic boundary examination.

- Meyerhof (1963) or De Beer (1970) approaches are virtually the same, except for small φ and low *L/B.* Furthermore as shown in the graph given Figure 2.59, their results are lower than those from fine element method.

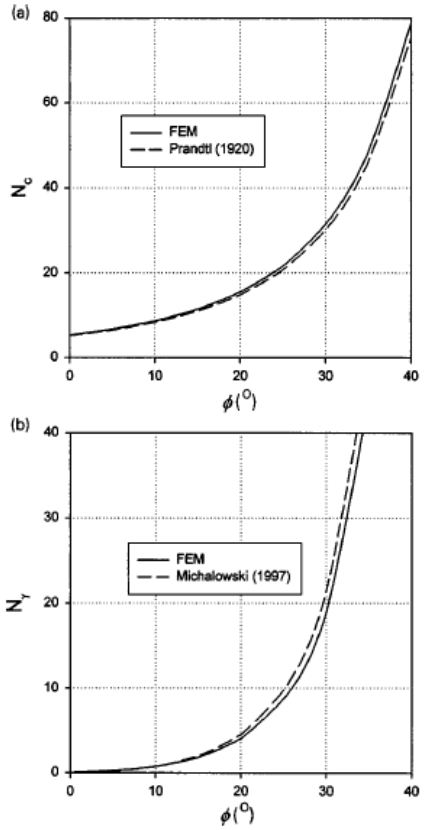


Figure 2.59. The analogy of results: (a) factor N_c and (b) factor N_γ (Zhu and Michalowski, 2005).

- Factor s_γ results are given in Figure 2.60 somewhat unusual because, by a fall in the aspect ratio for large internal angles of friction, s_γ rises. Besides this, for small angles of friction, it is reduced. S_γ has a bounded top for φ=35^o.

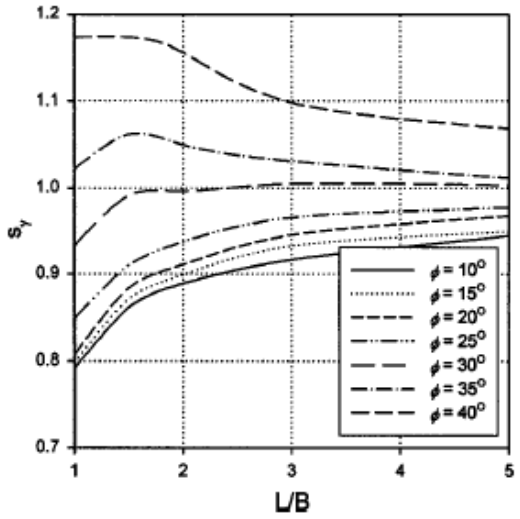


Figure 2.60. Factor s_γ (finite element method) as a function of aspect ratio *L/B* and internal friction angle φ (Zhu and Michalowski, 2005).

- As shown in Figure 2.61, the deformation scheme has diagonal symmetry, and the transformation in the zones close to the edges of the squared foundation is not flat.

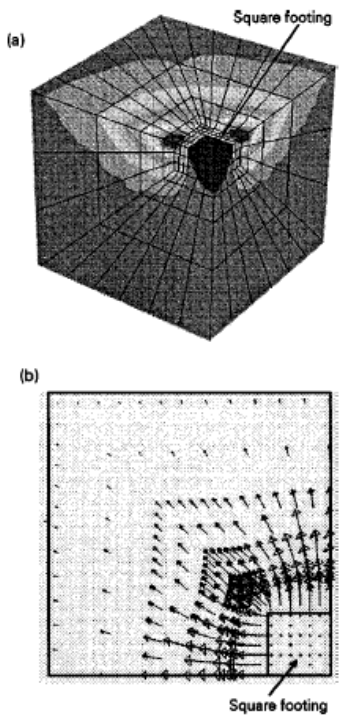


Figure 2.61. Movement in the region of squared foundation: (a) 3-D distribution of vertical displacement intensity and (b) horizontal movement at surface (Zhu and Michalowski, 2005).

Pathak *et al.* (2008) proposed a laboratory model to utilize small scale load tests on footings on *c*-*φ* clay and to find the bearing capacity of foundation on *c*-*φ* clay utilizing model test results and compare experimental data with theoretical work. The aim of the study was to investigate the impact of different parameters such as *L/B* rate, shape, and size of foundation on bearing capacity.

Sr. No.	Shape Of Foundation	Footing Designation	Size Of Footing (mm x mm)	L/B Ratio
1	Square	S1	101.6 X 101.6	1
2	Square	S2	203.2 X 203.2	1
3	Rectangular	R1	50.8 X 152.4	3
4	Rectangular	R2	50.8 X 203.2	4
5	Rectangular	R3	101.6 X 203.2	2
6	Rectangular	R4	101.6 X 304.8	3
7	Rectangular	R5	10.6 X 406.4	4
8	Circular	C1	114.3 mm dia.	-
9	Circular	C2	228.6 mm dia.	-

Figure 2.62. Model test programme (Pathak *et al.*, 2008).

The experimental test was conducted in Geotechnical Engineering Laboratory of College of Engineering. In this study, load tests were performed in the lab on two square, two circular, and five rectangular foundations on *c*-*φ* clay as given Figure 2.62. These tests were performed on square, circular, and rectangular model footings of various sizes located on the surface condition medium, prepared under arranged engineering parameters. Additionally, to show the material employed in the test plan, soil characteristics as listed in Table 2.2.

Table 2.2. Soil characteristics.

Sr. No.	Test	Name Property Name	I.S Code No.
1	Sieve Analysis	Gravel : 0%	2720-IV
		Sand : 56.99 %	
		Silt : 25.25 %	
		Clay Content: 17.76 %	
		Soil Classification: CL	
2	Standard Proctor Test	MDD: 1.764 g/cc	2720-VII
		OMC: 15%	
3	Direct shear test	C: 4 kN/m^2, φ:34^O	2720-XIII
4	Consistency Limits	Liquid limit: 34.20 %	2720-V
		Plastic limit: 22.67 %	
		Plasticity index: 11.53%	

The author compared the results of model test results with a bearing capacity of foundations evaluated by standard techniques such as Vesic's and Terzaghi's technique. As a result of the comparisons, the author concluded that both Vesic's and Terzahgi's approaches underestimate the bearing capacity of both squares as well as rectangular footings. Comparison between bearing capacity obtained from model test and conventional methods is shown in Table 2.3.

Table 2.3. Ultimate bearing capacity (UBC) for footings.

Footing No.	Footing Size Mm.	L/B Ratio	Measured UBC, kN/m^2	UBC by Vesic's Approach, Kn/m^2	UBC by Terzaghi's Approach, Kn/m^2
S1	101.6 x 101.6	1	377.81	308.88	299.98
S2	203.2 x 203.2	1	406.87	331.35	326.24
R1	50.8 x 152.4	3	271.25	224.13	246.92
R2	50.8 x 203.2	4	244.13	214.94	241.93
R3	101.6 x 203.2	2	324.43	257.49	271.68
R4	101.6 x 304.8	3	321.3	240.36	262.24
R5	101.6 x 406.8	4	319.68	231.79	257.53
C1	114.3 dia.	-	372.28	311.69	295.87
C2	228.6 dia.	-	404.81	336.94	317.03

The author had concluded that by an increment in *L/B* rate of foundation, the ultimate bearing capacity values of foundations with the same width decrease. Moreover, limit loads increase with an increase in footing size for the same *L/B*.

As anticipated, the ultimate bearing load raises with a rise in the size of the footing. On the other hand, this study based on *c-φ* soil has shown that size effects are minimal for square and circular footings while they are noticeable on rectangular footings.

To assume the forcing answers of squared foundations over soft soils, Yu *et al.* (2011) had proposed that to employ the 3D large deformation finite element examinations during 3D RITSS technique. Additionally, the impacts of surface soil heave and soil layer interface deformation in weightless soil during foundation penetration were examined.

In this study, as being different from foundation failure previously obtained, 'punch-through' failure was considered. It was defined that the foundation drops freely to point A' to balance the load, whenever the preload surpasses the first top capability illustrated at point A in Figure 2.63.

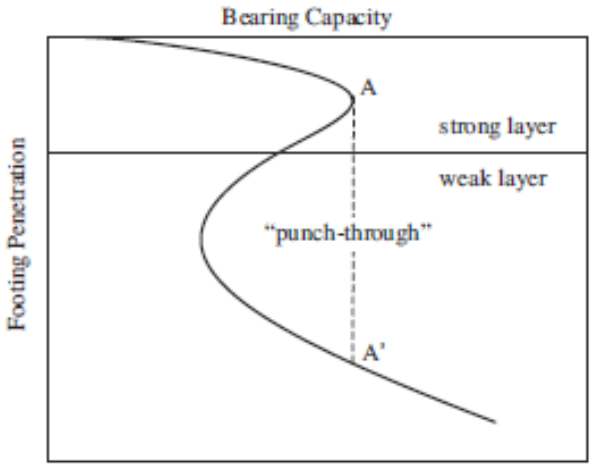


Figure 2.63. Typical penetration response of a footing on strong over weak soils (Yu *et al.*, 2011).

The author also carried out small strain finite element analyses to compare with the available solutions. Using 3D small strain analyses to solve the problem, we can use AFENA finite element computer program (Carter and Balaam 1995).The undrained soil followed Tresca rule. Accordingly, undrained total stress parameters were used. The Poisson's rate was taken v= 0,49. Young's modulus' proportion to clay shear strength was set to E/c= 500. The undrained shear strength of the first layer was defined fixed as c_1=100kPa, and the strength of underneath layer, c_2, changed to produce the proper clay layer strength ratio, c_2/c_1, which is smaller than 1.0.

The soil area was implemented as 10B in width and 6B in depth to prevent boundary effect. A standard mesh representation accepted in this research was depicted in Figure 2.64.

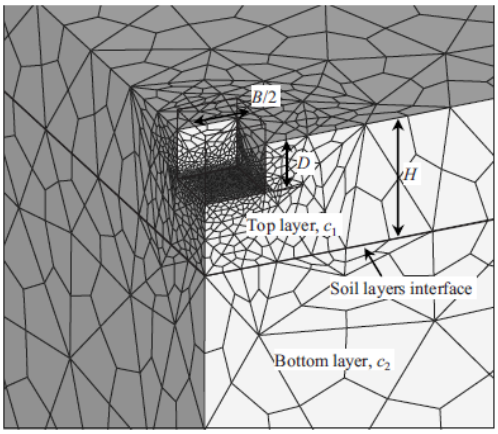


Figure 2.64. Typical finite element mesh (Yu *et al.*, 2011).

The author had also proposed that a useful large deformation method from the inside of the free Lagrangian-Eulerain class called RITSS (remeshing and interpolation method with small strain model). Different 2D plain-strain and axisymmetrical finite element examinations have employed this method (Hu and Randolph 1998a; Wang and Carter 2002; Lu *et al.*, 2004; Thorne *et al.*, 2004; Hossain *et al.* 2005a). Therefore, the 2D RITSS approach has been developed for 3D RITSS FE *approach (Yu et al.* 2008). In order to calculate the factor of bearing capacity of a surface foundation on a uniform,the following Equation 2.31 was used.

$$N_c = \frac{q}{c} = \frac{F}{Axc} \tag{2.31}$$

q is the bearing stress of a foundation near slope; c=undrained shear strength of the soil; F is net bearing pressure; A= foundation space. The area of squared foundations examined in this study. Hence $A/4=(B'/2)^2$, where B'=effective foundation breadth which is extended by half of the least component volume on each edge $(B'/2=B/2+h_{min}/2)$.

The author compared the analyses of FE with those of existing solutions presented by previous researchers. As a result of the comparisons, the author concluded that all FE analyses remain within the lower and upper bound methods of Salgado *et al.* (2004).

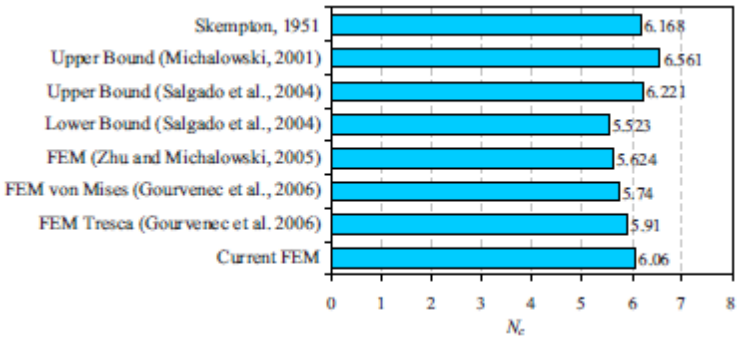


Figure 2.65. Factors of bearing capacity for surface rough squared foundations on smooth soils (Yu *et al.*, 2011).

When the determinant of bearing capacity of an exterior foundation is considered for two-layered clays, it related to the corresponding top layer width, *H/B*, and the soils power rate, c_2 /c_1. The author concluded that the current finite element results were in good agreement with the existing methods of Wang and Carter (2002) and Zhu and Michalowski (2005).

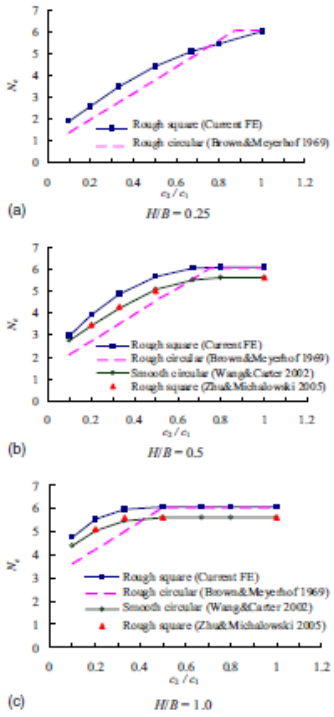


Figure 2.66. N_c for surface square foundations on two-layer weightless soils (small strain analyses) (Yu *et al.*, 2011).

Li *et al.* (2009) had used a three-dimensional finite difference program to simulate the bearing capacity of rectangular footings. Mohr-Coulomb failure criteria were used to define the soil strength.In the three-dimensional analysis model developed within the scope of this study, according to a dimensionless parameter,soil mass factor, and aspect ratio, calculated outcomes are shown as the function of dimensionless bearing capacity. Additionally, the mechanism of failure in limit conditions is examined.

According to conventional bearing capacity methods for rectangular foundations can be calculated by using empirical modification estimate impacts of foundation form. This equation is represented by Equation 2.22.

$$p_u = cN_c s_c + qN_q s_q + \frac{1}{2}\gamma B N_\gamma s_\gamma \tag{2.22}$$

Where the factors of bearing capacity N_c , N_q, and N_γ shows the impacts of soil adherence *c*, overcharge *q*, and soil unit mass γ, sequentially; s_c , s_q, and s_γ are shape factors with respect to N_c , N_q, and N_γ , sequentially; and *B* is the breadth of the foundation.

In this context, for investigating nonlinear response of elements and associated mechanism of vulnerability and collapse, a computer program named as 'FLAC^{3D}' was prepared by authors for three-dimensional analysis. In this study, all three correspondent directions have established the vertical edges and the base. In the general direction, the movements of equal levels are constant. Calculations are carried out for a rough soil foundation interface. Undrained Young's modulus E=2 x 10^5 , Poisson rate v= 0.3 was assumed. Additionally, the dimensionless soil mass factor changed to 100 from 0.1. In order to show the form impact on bearing capacity *L/B* =1 (squared), 1.5, 2, 3, and 5 were used in the analyses.

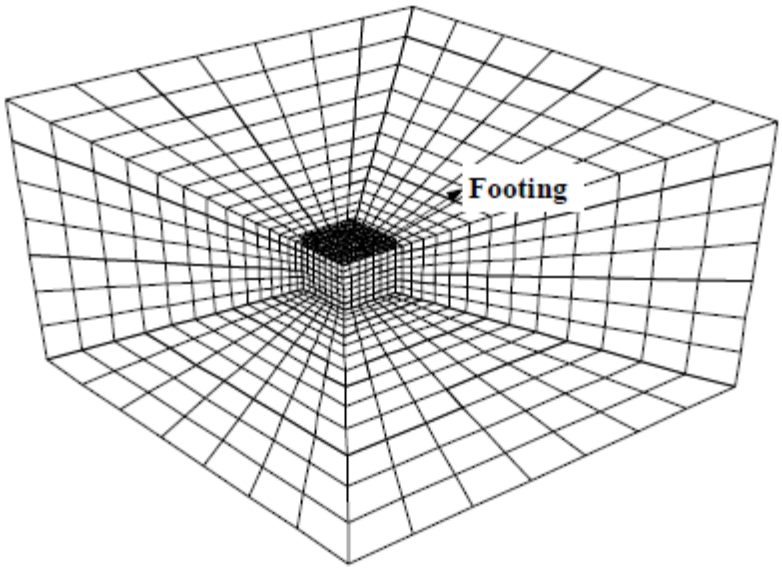


Figure 2.67. The meshing of the computational model (quarter symmetry) (Li *et al*., 2009).

The normalized soil unit mass is $G = \frac{\gamma B}{2c}$. Besides this, soil unit mass and soil adherence are considered as a function of *G*. It also shows the kind of soil. Lower *G* means the matter adherence is high, while a higher *G* means the matter adherence is low. Variation in the normalized vertical bearing capacity factor for a series of foundation aspect ratios

varies from 1 to 5 with the normalized soil mass factor from 0.1 to 100 that is shown in Figure 2.68.

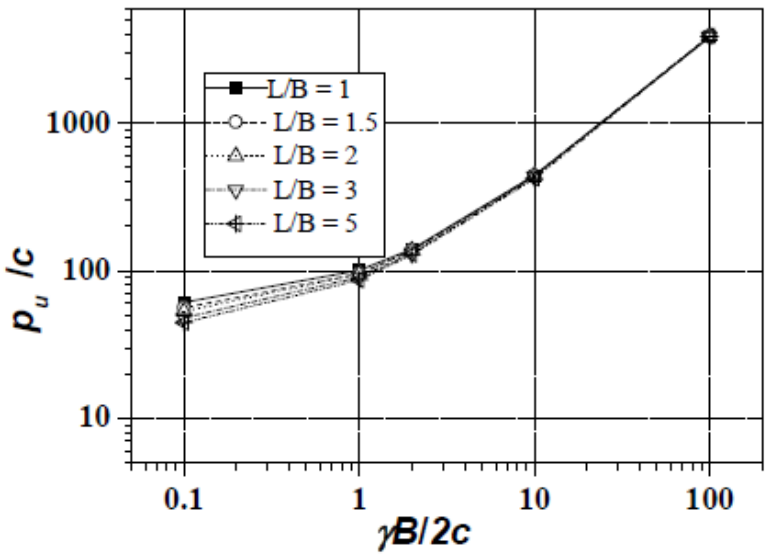


Figure 2.68. Bearing capacity for rectangular foundations of different forms (Li *et al.*, 2009).

Consequently, different shape of footings has a decisive impact on the bearing capacity of the soil, whereas it slightly changes the low adherence clay. The impact scope of the two clays can describe the reason for this effect. This result can easily be seen in Figure 2.69.

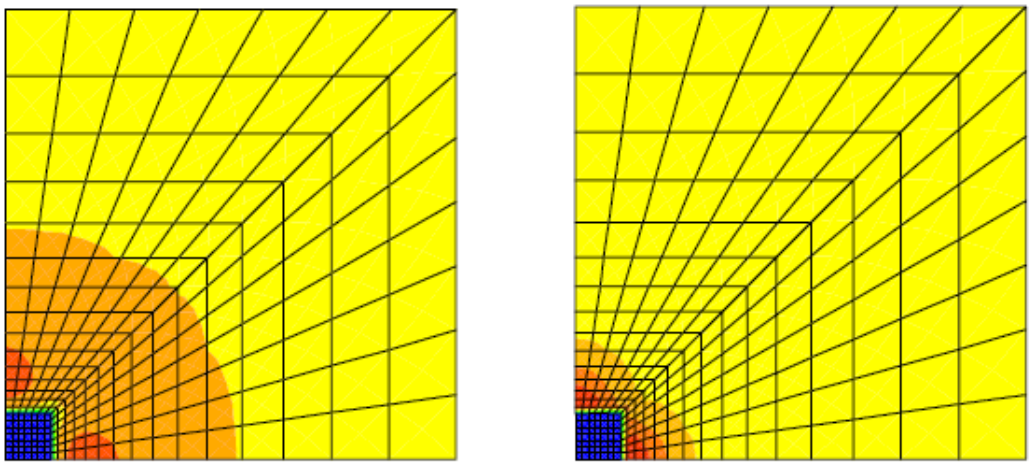


Figure 2.69. Plan representation of the foundation's impact scope (Li *et al.*, 2009).

The author had concluded that the range of failure in less adherence clay is not as extensive as very adhesive clay; therefore, the failure mechanism is influenced merely through foundation form. Put another way, and a more extensive impact scope has an essential impact on shape effect. Result of the presented method was compared with those presented by Salgado *et al.* (2004), Zhu and Michalowski (2005) and Lyamin *et al.* (2007) then the accuracy of the phenomena was confirmed. As a result of their works, s_c is influenced by form noticeably and s_γ lead to 1 for any forms. Finally, the sensitivity of form influence on bearing capacity is estimated by influencing range.

Shiau *et al.* (2011) had derived that the undrained bearing capacity of a strip foundation located close to the side of an incline and cohesive slopes. The final bearing capacity of footings on inclines depending on different influential parameter have been computed owing to the finite element examination calculations of the upper and lower bound methods.

The graphical representation given by the author is illustrated in Figure 2.70 to define the problem. B is the breadth of a wall foundation placed on granular clay with an inclination angle β and inclination altitude H at a span L from the side of the incline. In accordance with material assumptions of limit analysis, c-φ soil is rigid-perfectly plastic and obeys the Tresca

yield model with a shear strength c_u. *H/B* was chosen as three in all examinations, which leads to ‘over the toe collapse' that is discussed in this study.

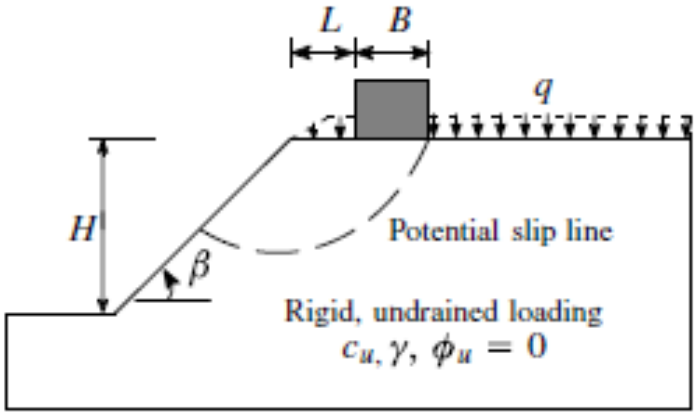


Figure 2.70. Problem notation and potential failure mechanism (Shiau *et al.*, 2011).

As a conclusion, as a function of dimensionless factors, bearing capacity influencing the durability of the system, which is expressed as given in Equation 2.23.

$$\frac{p}{\gamma B} = f\left(\beta, \frac{L}{B}, \frac{c_u}{\gamma B}, \frac{q}{\gamma B}, \frac{H}{B}\right) \quad (2.23)$$

P is the average boundary stress running on the foundation; *q* is the overcharge weight for sloping ground. The author compared the results of derived finite-element limit analyses shown in Figure 2.71 with those of calculation analytically presented by Davis and Booker (1973). As a result of the comparisons, the author concluded that the vertical cut has no significant impact on the bearing capacity of the foundation for conditions with $L/B \geq 4$. Notably, the bearing capacity is diminished by a factor of 2.5, whereas the aspect ratio of footing *L/B* reduced from 4 to 0.

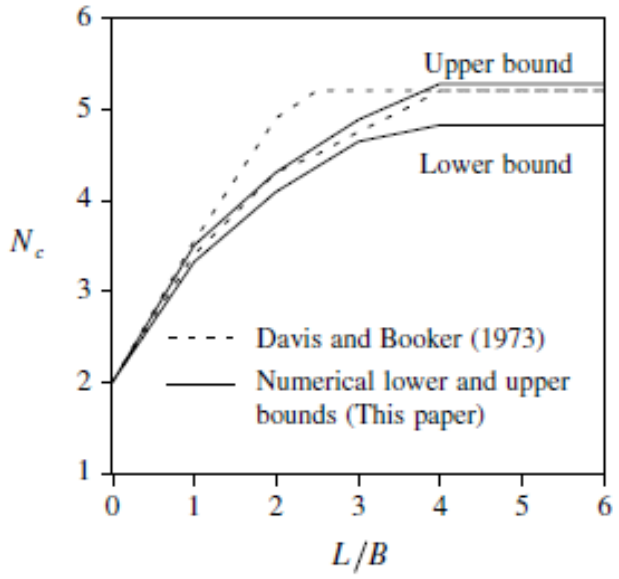


Figure 2.71. Bearing capacity of upper and lower bound for weightless slopes (smooth base, β=90^o) (Shiau *et al.*, 2011).

The author also concluded that curved shapes and swiftness areas depending on different strength rates $c_u/\gamma B$ of an vertical inclination (L/B=0, β=90^O). Results showed that for both coarse and firm clays, the bearing capacity should be the same, which is presented in Figure 2.72. Whereas for a smaller strength ratio $c_u/\gamma B$ =1, the footing may be governed overall slope failure, the mechanism of failure is composed of a rigid triangular wedge for more significant values $c_u/\gamma B \geq 2$.

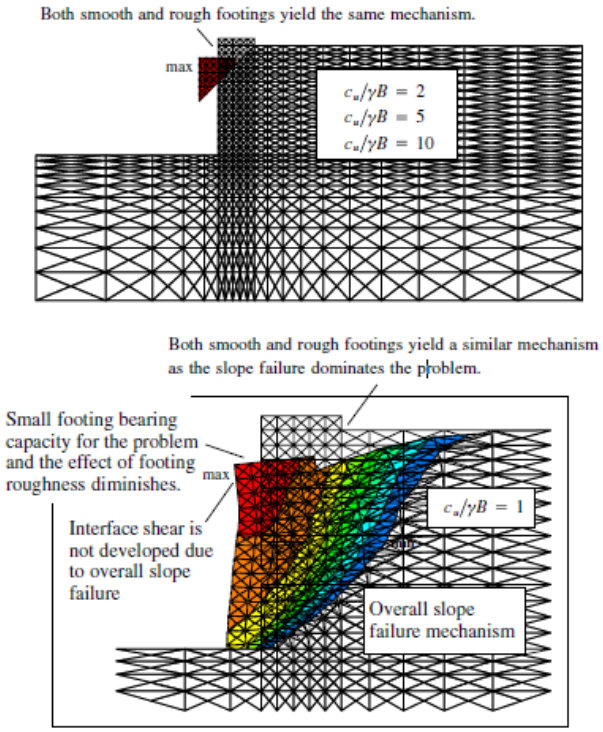


Figure 2.72. The analogy of transformed forms and swiftness profiles for smooth and rough foundations (β=90°, L/B=0) (Shiau *et al.*, 2011).

	$p/\gamma B$							
	$L/B = 0$		$L/B = 1$		$L/B = 2$		$L/B = 3$	
$c_u/\gamma B$	Smooth	Rough	Smooth	Rough	Smooth	Rough	Smooth	Rough
10	19.95	19.95	33.75	33.79	41.31	41.33	47.30	47.32
5	9.50	9.50	16.12	16.17	19.64	19.65	22.73	22.74
3	5.50	5.50	9.01	9.01	10.85	10.88	12.72	12.78
1	1.32	1.32	1.20	1.20	1.46	1.46	1.99	1.99

Figure 2.73. Upper Bound Results for Rough and Smooth Foundations (β=90°) (Shiau *et al.*, 2011).

The average upper and lower bound assumptions of the normalized bearing capacity $p/\gamma B$ are displayed in Figures 2.74. The dimensionless bearing capacity $p/\gamma B$ diminishes linearly with the strength rate $c_u/\gamma B$ until it starts nonlinear and fastly reaches 0 at a specific $c_u/\gamma B$.

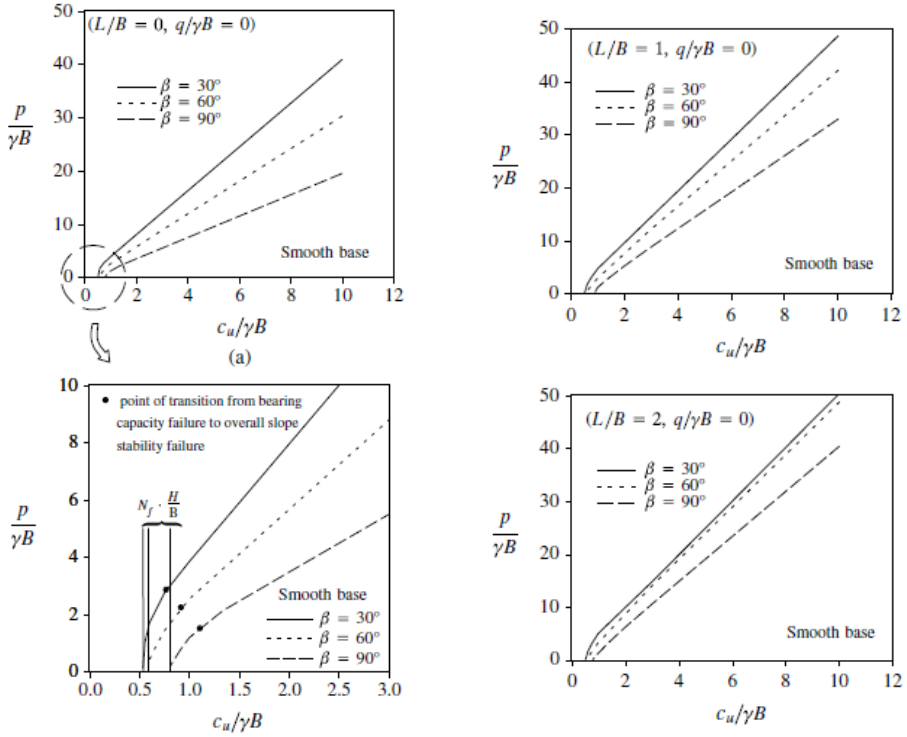


Figure 2.74. Averaged upper and lower bounds for different angles of inclination (Shiau *et al.*, 2011).

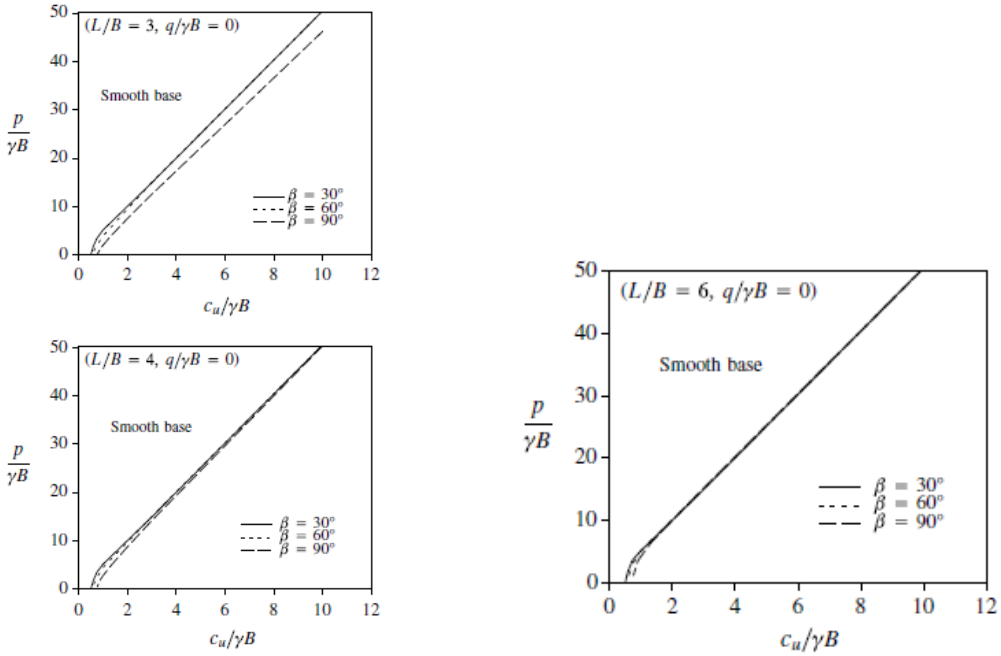


Figure 2.75. Averaged upper and lower bounds for different angles of inclination (Shiau *et al.*, 2011).

Presented design charts are drawn for showing failures of bearing capacity, which is included inside the front of the incline; therefore, the *H/B* rate has no impact. The assumed failure mechanism is shown in Figures 2.76 and 2.77.

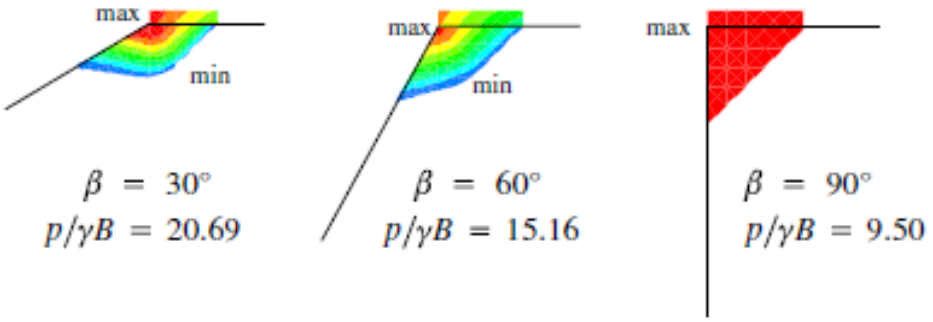


Figure 2.76. Velocity contours for different angles of inclination ($c_u/\gamma B$=5, *L/B=0*, flat bottom) (Shiau *et al.*, 2011).

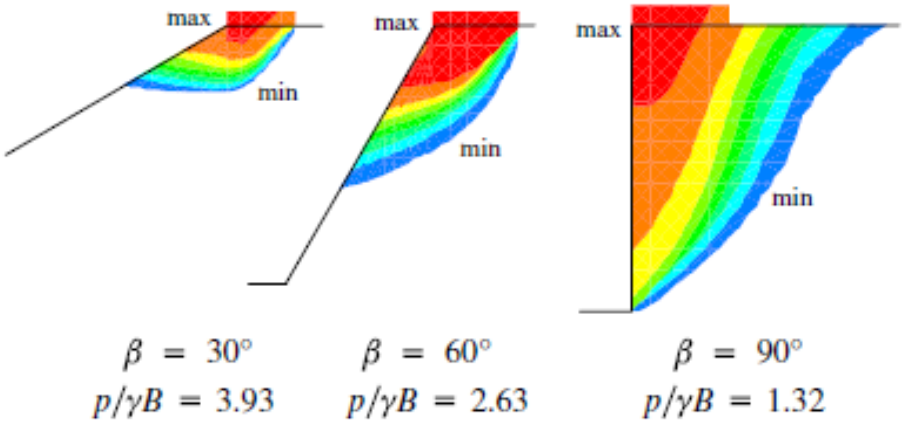


Figure 2.77. Velocity contours for different angles of inclination ($c_u/\gamma B$=1, *L/B=0*, flat bottom) (Shiau *et al.*, 2011).

Additionally, the effect of slope angle can be obtained graphically in Figure 2.78 for *L/B*=0. As the angle of inclination rises, the footing bearing capacity decreased.

Moreover, it is determined that for all slope angle, the rise in footing capacity prone to hold at a specific point of *L/B.* The impact of *L/B* is illustrated in Figure 2.78 for examples of an upright portion with $c_u/\gamma B$= 5.0. It depicts that at *L/B*=5, the figure of the swiftness plan is typically the same for a foundation located on a flat earth. This means that the vertical cut doesn't affect the performance of the foundation.

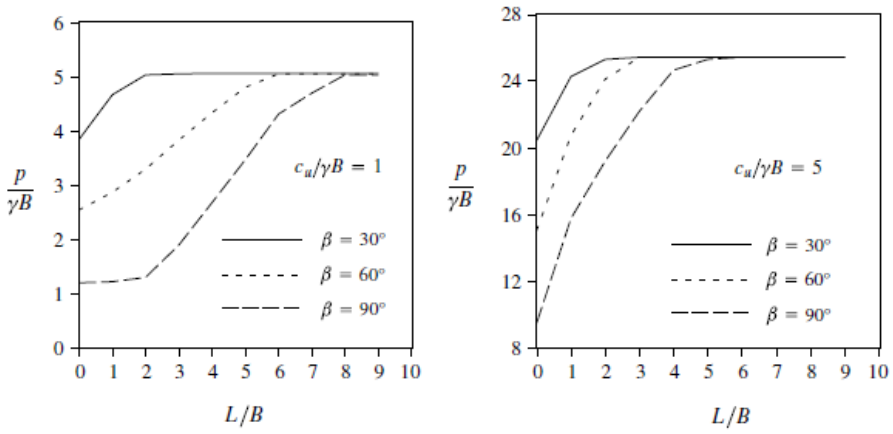


Figure 2.78. Impact of *L/B* on the bearing capacity (smooth base) (Shiau *et al.*, 2011).

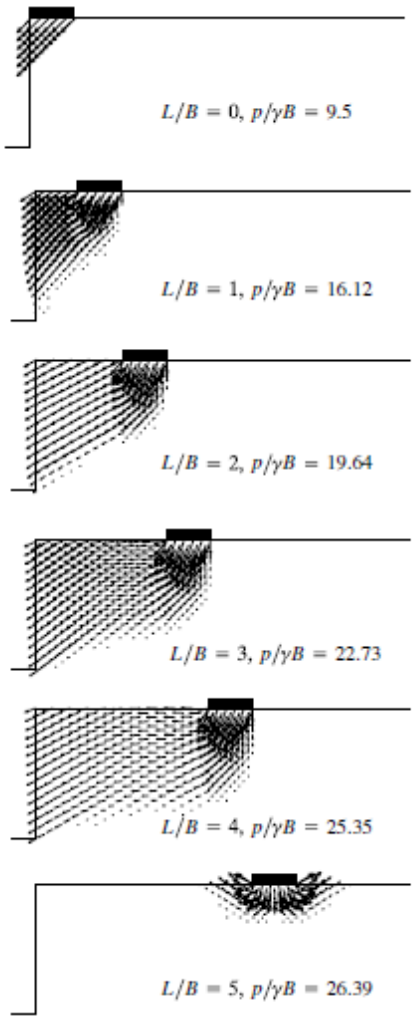


Figure 2.79. Velocity contours for different *L/B* (smooth base, β =90^{o}, $c_u/\gamma B$=5) (Shiau *et al.*, 2011).

The author had also examined the influence of *H/B,* which was also shown in Figure 2.80. It was observed that all failure mechanisms weren't especially affected by the toe of the incline when the ratio of *H/B* more significant than 3. As shown in Figure 2.80, the position of the toe was affected by the collapse load minimal. On the other hand, for minimum amounts of *H/B*, the effect of the incline on the failure system becomes trivial, hence the incline would be a portion of the mechanism of the bearing capacity.

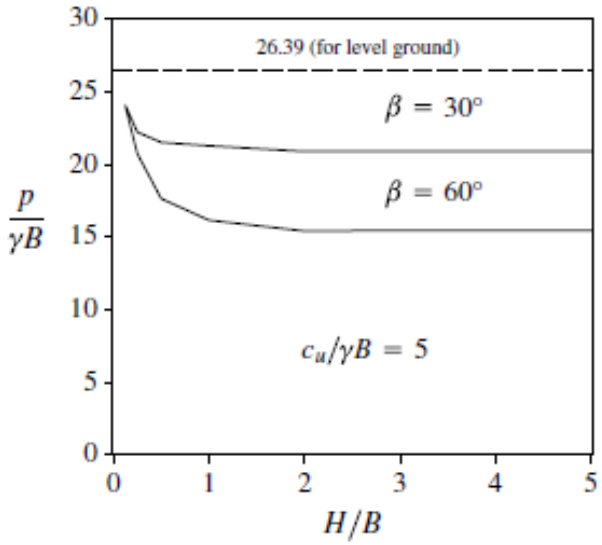


Figure 2.80. Effect of *H/B* (flat bottom, *L/B*=0) (Shiau *et al.*, 2011).

Islam *et al.* (2017) had used three-dimensional finite element method including a Mohr-Coulomb elasto-plastic material model that accepted for the consideration of the form impact of the circular and squared surface foundation below upright loading in cohesive soil. In addition that the shape of the failure mechanism and the advanced failure around the foundations were examined with regard to the shape effect. In this study, the finite-element computer program, which is called ‘ABAQUS' employed to find the ultimate bearing capacity of square and circular foundations. Finite element mesh used for the examination of the square and circular footings was illustrated in Figure 2.81.

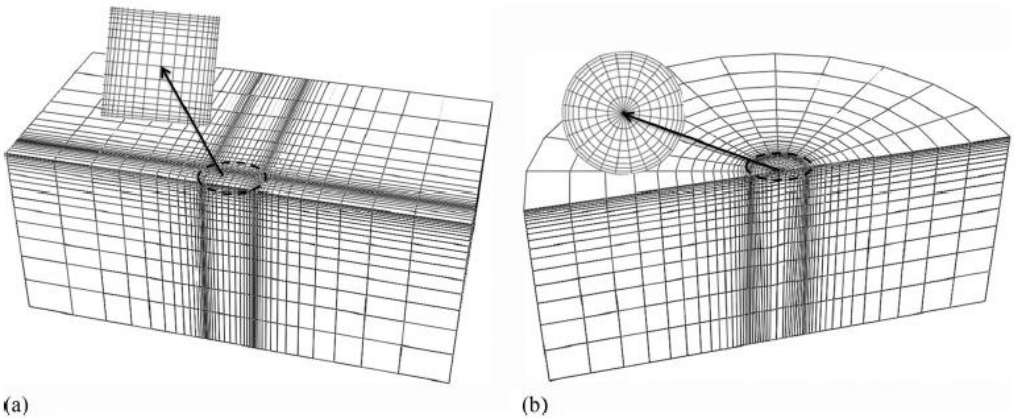


Figure 2.81. FE meshes: (a) half of a square footing; (b) half of a circular footing (Islam *et al.*, 2017).

The author compared the result of the developed method with those presented by previous researchers so far. As a result of the comparisons, the failure load of the square footing was 1.21 times bigger than that of circular footing. The results were also shown in Figure 2.82.

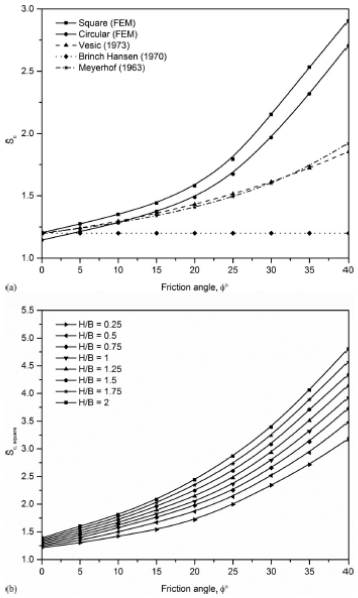


Figure 2.82. Shape factor s_c as a function of φ and D/B : (a) comparison with previous studies ($D/B = 0$); (b) square footing ; (c) circular footing (Islam *et al.*, 2017).

The assumed failure mechanism is shown in Figure 2.83 presents the plan view of the contours of the resultant displacement of rough circular and square footings at failure and display the change in soil displacement depending on the shape of footing. While the displacement contours of circular footings were created at the side of the foundation and moved to the outward orientation of the footing, the behavior for square footing was created at the corners and moved to the edges. It was concluded that the failure of the circular footing was found to be much shallower than that of the square footing.

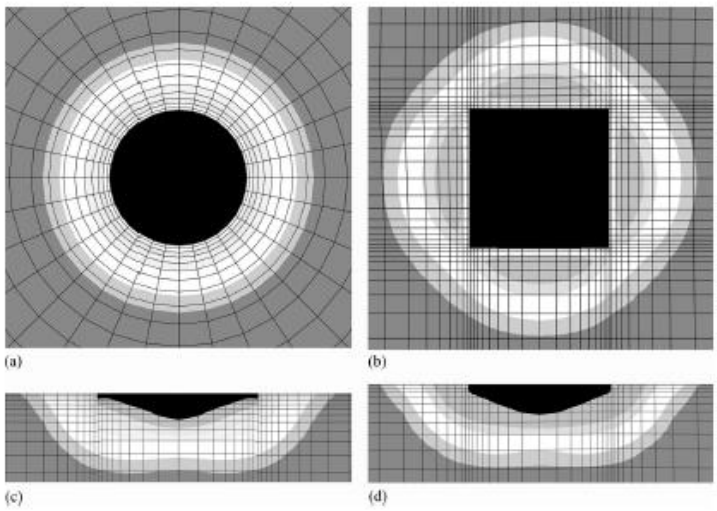


Figure 2.83. The failure mechanism is shown in plan view (a and b) and elevational view (c and d): (a) circular foundation: (b) square foundation: (c) circular foundation: (d) square foundation (Islam *et al.*, 2017).

According to this study, the influence of soil cohesion on the shape factor s_c can be obtained as given in Equation 2.24.

$$s_c = \frac{N_{c(square\ or\ circular)}}{N_{c(strip)}} \tag{2.24}$$

The analysis results also are presented graphically in Figure 2.85. The cohesion shape factors for square and circular footing are calculated by the equations given in Equation 2.25 and Equation 2.26 respectively,

$$s_{c,square} = 1 + (3.5\emptyset^2 + 0.192) \tag{2.25}$$

$$s_{c,circular} = 1 + (3.1\emptyset^2 + 0.15) \tag{2.26}$$

The author also stated the impact of soil mass on shape factor. The modified bearing capacity factor (N_γ) and shape factor (s_γ) can be computed following Equations 2.27 and 2.28,

$$N_\gamma = \frac{(q_{ult} - cN_c)x2}{\gamma B} \tag{2.27}$$

$$s_\gamma = \frac{N_{\gamma(square\ or\ circular)}}{N_{\gamma(strip)}} \tag{2.28}$$

When the ponderable soil is regarded, the shape modifier can be expressed as given in Figure 2.84 for φ ranging from 5^o to 40^o.

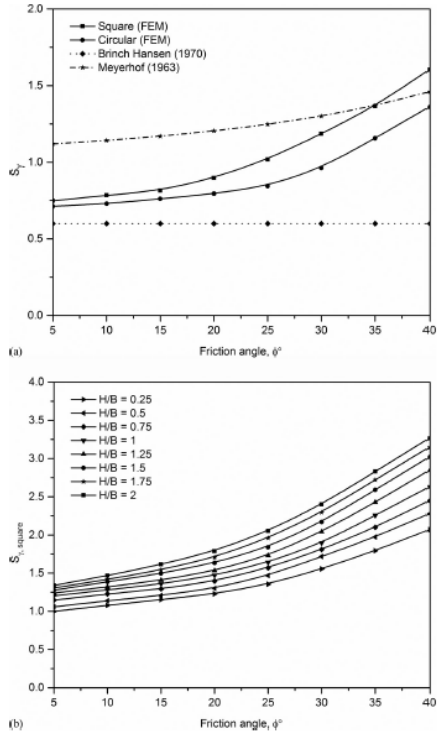


Figure 2.84. Shape factor s_γ as a function of φ and *D/B*: (a) Comparison with previous studies (*D/B*=0); (b) Square footing; (c) circular footing. (Islam *et al.*, 2017).

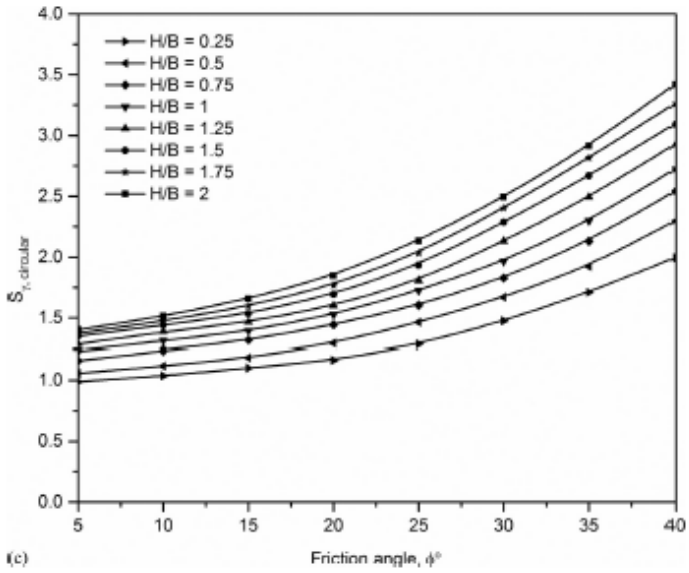


Figure 2.85. Continued (Islam *et al.*, 2017).

The author compared the results of the developed numerical model with those of calculation techniques presented by previous researchers so far. As a result of the comparisons, the author concluded that the results of the proposed method obtained for specific soil and geometrical combinations show a slight difference with those presented by the previous researchers. However, differences between results of the various calculation methods were also found for lower values of friction angle. Therefore, the shape factor s_c is not only a part of φ but also a function of *D/B.* Additionally, the shape factor s_γ is shown in Figure 2.85 also increased with the friction angle.

3. METHODOLOGY

The aim of this study is to investigate the effect of the shape effect of foundation which has not been studied in previous studies on the seismic bearing capacity of the shallow foundations constructed on or near the slopes. Numerous finite element models are defined under plane strain conditions and analyzed using Plaxis 3D.

This chapter includes important details regarding to development of the numerical model for determination of seismic bearing capacity of foundations near cohesive slopes. Model geometry, constitutive modelling of slope soil, mesh generation, loading and boundary conditions, material properties and mesh generation will be presented in detail in this chapter. After, the solution expressed by a simplified formula and the stages of the parametric study will be described. Additionally, the numerical approach adopted is the method of finite elements, using a commercial Plaxis 3D software. Therefore, thirdly, steps to be followed in order to make required activities within three Plaxis 3D sub modules (called Initial Phase, Calculation Module and Output) will be addressed with in detail.

At the end of this chapter is presented for verification of results obtained. This validation will be carried out for different shape of foundations. Seismic bearing capacity coefficient obtained by previous researcher for strip footings in undrained conditions will be compared with those obtained by Plaxis 3D. This comparison will be made only for one condition in which the footing is on the slope edge ($\lambda=0$).

3.1 FEM in Geotechnical Engineering and Plaxis 3D

The technique of finite element (FEM) is a numerical method to solve engineering and a wide variety of industries. Therefore, computer codes based on FEM have been designed to deal with difficulties including soil-structure interaction, foundation structures, seepage, and soil dynamics.

Most common methods of analysis generally use approaches that based on presumptions which oversimplify the problem at hand. These methods don't have the ability to consider all of the parameters and factors the design engineer meets and can acutely constrain the results of solution. FEM can deal with many of these deficiencies, therefore it offers many advantages to traditional methods (USACE,1995). Their ability to accurately reflect field conditions essentially depends on the ability of the constitutive model to represent real soil behavior and correctness of the boundary conditions imposed. The user has to describe the model geometry, construction step, soil parameters and boundary conditions. Structural components may be considered during the numerical analysis to model field conditions. Shallow foundations consist of different shape foundations, associated by structural members, can be regarded and, because the soil slope is modelled in the analysis, the relationship between slope angle or slope height and the soil can be taken into consideration. No hypothesized failure instrument or mode of behavior of the problem is not necessary because these are anticipated by the analysis. It enables the background of the boundary condition of problem to be assumed and a single analysis can give information on all design specifications. (Potts *et al.*, 2002)

PLAXIS 3D is a three dimensional finite element computer program that designed for the analysis of various shape foundation structures and stability analyses for different types of geotechnical implementations. The program combines simple graphical input procedures which empower the user to automatically generate complex finite element models. The advanced output facilities give a detailed presentation of computational results. The calculation itself is completely automated and based on robust numerical procedures. (Brinkgreve *et al.*, 2006)

3.2 Definition and Assumptions of the Problem

Graphical representation of the problem is shown in Figure 3.1. The purpose is to obtain seismic earing capacity (q_f) of shallow footings (D_f=0) located near cohesive slopes under undrained conditions using pseudo-static approach.

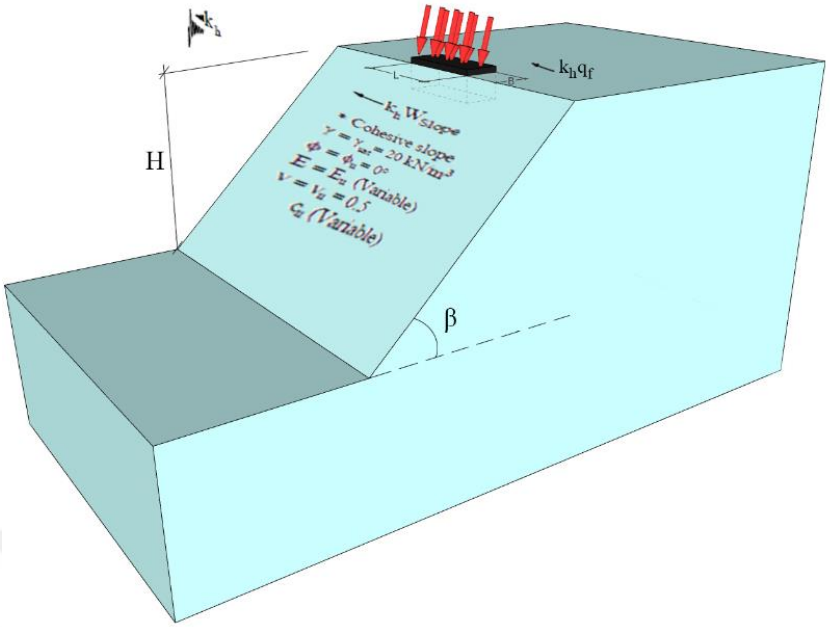


Figure 3.1. Graphical representation of the problem.

Presumptions made for the solution of the problem prensented at Figure 3.1, are summed up below. Accordingly;

- The footing is shallow footing. Thus, the effect of embedment depth onto seismic bearing capacity of such footings will not be examined in this study.
- The footing is represented by a rigid plate element and the interface is accepted to be rough.
- Seismic bearing capacity of such footings is determined by using pseudo-static approach. It is estimated that inertia force of structure acts at the base level of footing. Overturning moment due to the inertia force acting on structure is neglected as well.
- Horizontal seismic acceleration coefficients used for calculating the inertia force of structure and of slope soil are chosen to be equal (k_h).
- Effect of vertical component of earthquake acceleration onto seismic bearing capacity is neglected (k_v= 0).
- Mohr-Coulomb constitutive model is used to define soil behavior.
- Undrained shear strength of soil does not change due to complex, temporary and dynamic earthquake loading.

- Slope soil is uniform and undrained shear strength of soil does not change with depth as well.

3.3 Suggested Solution Method

Seismic bearing capacity of shallow foundations can be obtained using Plaxis 3D according to the assumptions abovementioned in Chapter 3.2. Initially, requirement data input should be integrated with input module of the software. Later, calculation module of the software should be performed to interpret the problem at hand. Moreover, failure mechanism will be shaped at the ultimate state that can be observed within Output module of the software while the foundation reaches to the seismic bearing capacity failure.

On the other hand, an available mathematical approach which correlates between seismic bearing capacity (q_f) and undrained shear strength of cohesive slope soil (c_u) may be described is examined in this study. If the form of equation defined by Skempton (1951) is taken as a reference, seismic bearing capacity of shallow footing can be computed using the formula given in Equation 3.1.

$$q_f = c_u N_{cse} \tag{3.1}$$

where q_f is the seismic bearing capacity of shallow footings near cohesive slopes, c_u is the undrained shear strength of cohesive slope soil and N_{cse} is the seismic bearing capacity factor of shallow footings located near slopes.

Undrained shear strength of cohesive soils can be obtained via several testing methods (UU triaxial compression test, unconfined compression test and etc.) or can be assumed with sufficient certainty using correlations developed for in-situ tests such as vane shear test, standart penetration test (SPT), cone penetration test (CPT) and etc. It will be enough to determine the ultimate footing capacity according to the approach given herein. The only thing to do next is to determine influential parameters on the seismic bearing capacity factor and, if possible, to prepare design charts or to obtain equations for the determination of seismic bearing capacity factor. Therefore, all the details related with parametric study will be given in Chapter 3.4.

3.4 Model Geometry

As it was referenced above, it is necessary to constitute a numerical model to set a definite approach and to obtain all influential parameters onto seismic bearing capacity factor. Respectively, parameters that are defined as variables can be classified by three groups.

Initially, it is required to define the geometry of the slope. For this reason, slope height (H) and slope angle (β) are enough to generate the geometry of the slope which foundation is located close. In order to show the influence of the slope angle variation, different slope angles chosen for β; 15^o,30^o,45^o. Moreover, different slope heights were selected for H; 2, 4 and 8m. Additionally, (λ), factor that defines footing distance from the slope edge, is normalized with footing breadth. Besides these, in order to examine the impact of shape effect on foundation, various lengths chosen for L; 2, 4, 8, 16 m. The normalized footing distance (λ) from the slope edge were selected for λ;0. The relationship between seismic bearing capacity coefficient and normalized footing distance will be represented in the subsequent chapter of this thesis and also to find out threshold distance values as precise as possible for different cases.

Second group is correlated with the strength characteristic of the soil. This factor is taken accounted as variable because the soil strength is described by undrained shear strength according to the material model selected. Undrained shear strength of cohesive slope soil (c_u) is 25, 50,100,200 kPa.

Lastly, the horizontal seismic acceleration coefficient (k_h) is only defined on the models for seismic conditions. Horizontal seismic acceleration coefficient (k_h) changes in between 0.1 and 0.3.

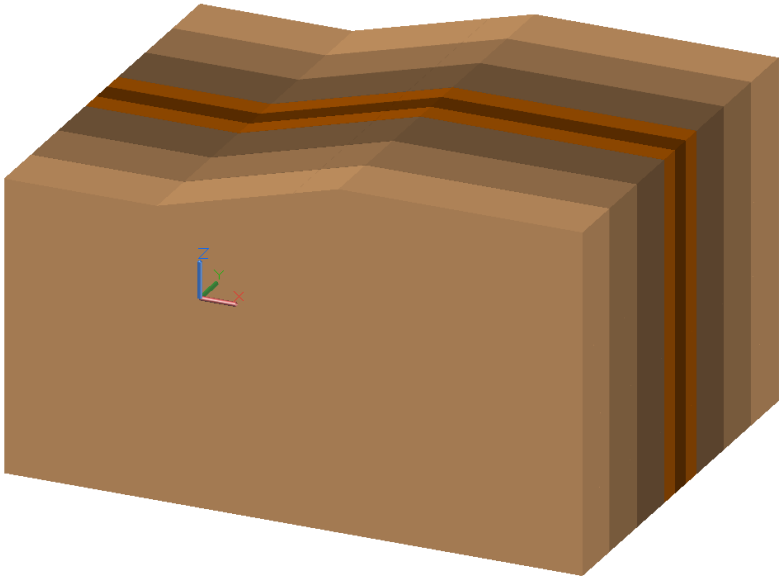


Figure 3.2. Three dimensional model of created finite elements model.

3.5 Data Input in Plaxis 3D

As previously noticed that the selected problem in the field of this thesis can be examined by Plaxis 3D software and so, seismic bearing capacity of a shallow foundation located close cohesive soil can be obtained using by a set of geometric, strength and seismic parameters. To deal with the problem, the issues linked with the necessary steps for the Input modules of the software are separated into six subheadings in this section.

3.5.1 General Settings

When a new project has to be defined, the ‘General Settings’ window will be appeared as shown in Figure 3.3. This window consists of two tabs named as ‘Project’ and ‘Dimensions’. If a filename has not been defined in the first tab, this can be done when saving the project. Additionally, a brief description of the problem as the name of the project as well as a more detailed explanation can be given in the ‘Comments’ box.

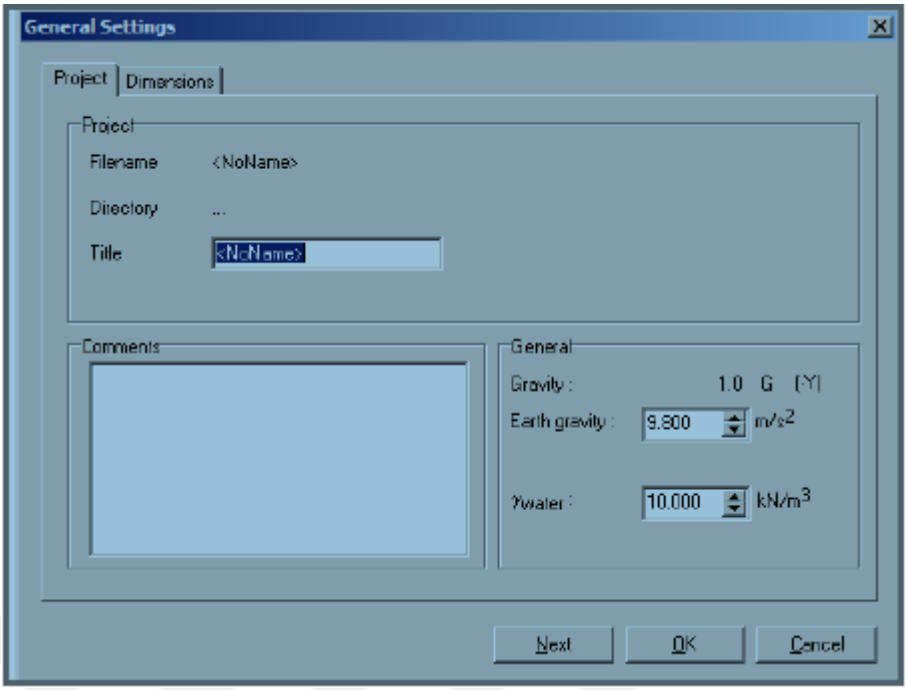


Figure 3.3. 'Project' tab sheet of 'General Settings' window

On the other hand, the basic units of Length, Force and Time, the minimum dimensions of the draw area are shown under 'Dimensions' tab as shown in Figure 3.4. In addition, there are four input data boxes in the same tab sheet that enable the definition of outer boundaries of the drawing area into which the geometry model fits. X_{min} is the lowest x-coordinate of model, X_{max} the highest x-coordinate, Z_{min} the lowest z-coordinate and Z_{max} the highest z-coordinate of the model.

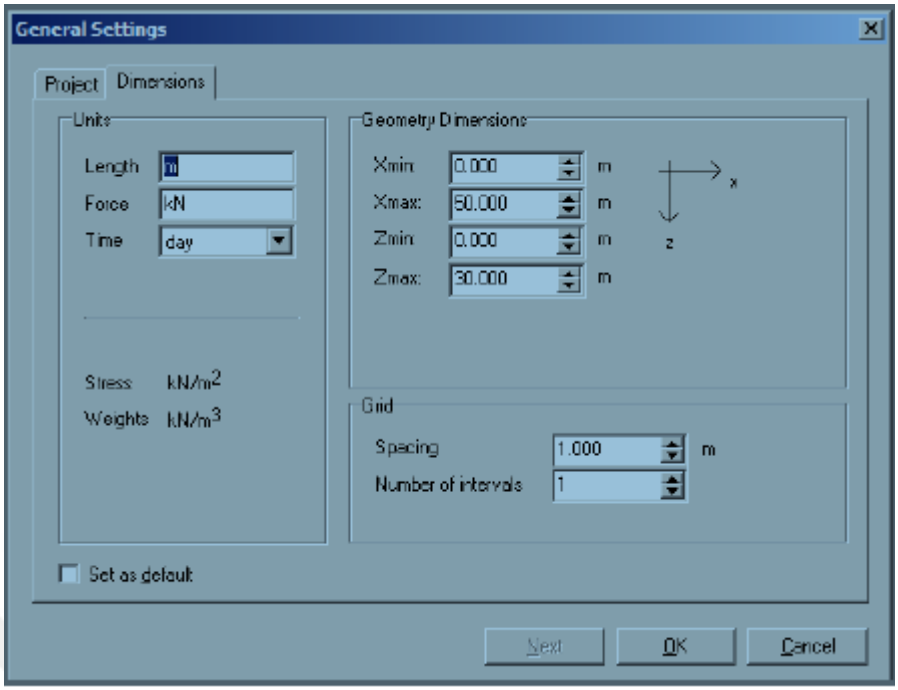


Figure 3.4. ‘Dimensions’ tab sheet of ‘General settings’ window

The wedge elements used in Plaxis 3D software consist of 15 nodes. Displacements (u_x, u_y and u_z) are computed at the nodes during finite element analysis. Contrary to displacements, stresses and strains are computed at individual Gaussian integration points rather than at the nodes. To obtain more reliable outcomes, 15-node triangular elements were used to generate a finite element as shown in Figure 3.5.

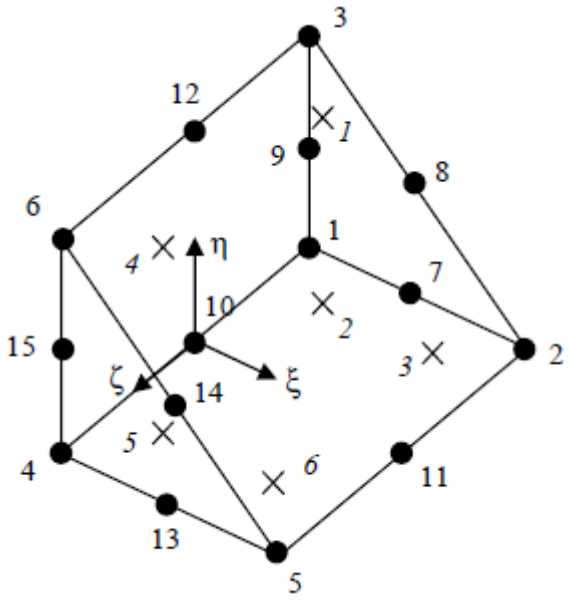


Figure 3.5. Distribution of nodes (.) and stress points (x) in a 15-node wedge element.

3.5.2 Numerical Model

While creating the finite element model, the main aspect should be that boundary limits of exterior should not influence footing failure loads computed by computer program. Therefore, exact model shape was obtained by trial and error method. As a conclusion, the model geometry shown in Figure 3.6 is convenient and suitable for all numerical models generated in this present study. According to Figure 3.6, horizontal distance between right footing edge and right vertical boundary changes with breadth of footing (8*B*). On the other hand, the horizontal distance between bottom edge of slope and left vertical boundary and the vertical distance between bottom edge of slope and horizontal bottom boundary were selected as constant, and took the value of 25m and 12m accordingly.

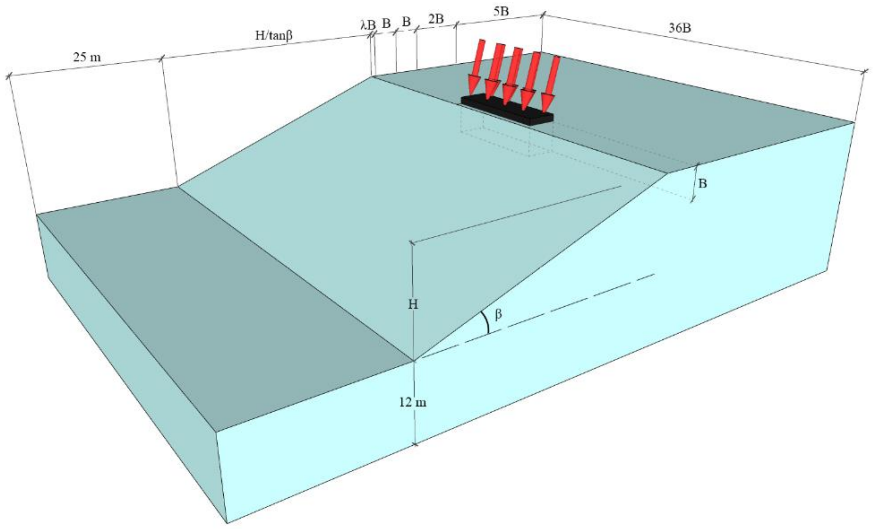


Figure 3.6. Schematic representation of created finite elements model.

Shallow foundation defined by a rigid plate element in finite element models is 2.0 m wide. The plate element is supposed to be weightless and elastic material type is assigned to it. Stiffness parameters that are commonly used for the plate element and equivalent plate thickness (d_{eq}) values considered in all analyses are given in Table 3.1. Furthermore, it was noticed that shallow foundation is supposed to be 'fully rough'.

Table 3.1. Physical and elastic properties of rigid plate element.

Material Type	Elasticity Modulus E (kN/M)	d_{eq} (m)	Weight, w (kN/m/m)	Poisson ratio, v (Unitless)
Elastic	$3x10^7$	1.0	0	0.2

3.5.3. Boundary Conditions

'Standart fixities' boundary condition is more suitable for geotechnical problems and is used in all prepared finite element analyses. It is easily chosen with a shortcut given on Input menu of the Plaxis 3D. As shown in Figure 3.5, full fixity ($u_x=u_y=0$) is defined across horizontal geometry line located at the bottom of model y coordinate is minimum while horizontal fixity ($u_x= 0$) is specified across two geometry lines whose x coordinates are minimum and maximum.

3.5.4. Loads

The present analyses are made through the pseudo-static approach. The seismic forces are characterized by the horizontal loads applying to the foundation, surcharge and the underlying soil in this method. The multiplication of the horizontal seismic coefficient (k_h) by foundation load (P), surcharge (q), and soil weight (W) gives us the horizontal load. The present study explains only the horizontal seismic coefficient (k_h). Furthermore, an inclined load placed on the foundation applied with a horizontal component to trigger seismic force, "Soil inertia" (k_hW) is the term which means the pseudo-static force applying to the soil mass. Table 3.2 as below presents the schematic diagram of the problem. In this study, horizontal seismic acceleration coefficients were selected as 0.1, 0.2, 0.3.

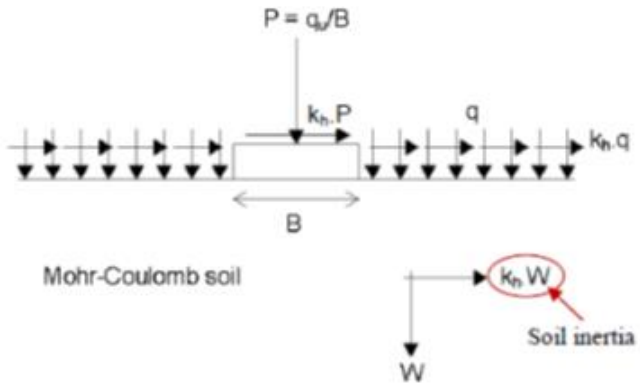


Table 3.2. Schematic diagram of the problem.

As mentioned above, the effect of horizontal earthquake acceleration was considered in this study. Vertical component of the earthquake acceleration was neglected in previous studies as mentioned Chapter 2.2. Only one study in the literature took the influence of vertical earthquake acceleration into consideration. Shiau *et al.* (2006) incorporated the effect of horizontal and vertical earthquake acceleration ($tan\theta = k_h/1-k_v$). On the other hand, Kramer (1996) noticed that vertical pseudo-static force can decrease or increase at the same time both driving and resisting forces depending on its direction. According to Kramer's results, the effect of vertical pseudo-static force is negligible compared to the effect of horizontal pseudo-static force. For that reason, the effect of vertical earthquake acceleration is generally underestimated in studies when the pseudo-static approach is used.

3.5.5. Material Properties

It is essential to recognize drained and undrained conditions. Failure might occur drained and undrained in the event of saturation of the soil pores with water standing on the size of the soil pore, the water saturation's degree and time included. The probability of the undrained failure characteristics increases when the pores are smaller and the loads are applied faster.

An undrained analysis can be made through 3 methods in Plaxis 3D 2018. These are, Undrained A, B and C, can be outlined as follows:

1. Undrained A: Undrained effective stress analysis with effective strength parameters. The undrained shear strength stands on the effective stress state and effective strength parameters.
2. Undrained B: Undrained effective stress analysis with undrained strength parameters. The undrained shear strength is exactly explained by the user and independent of the effective stress state.
3. Undrained C: Undrained total stress analysis with undrained strength parameters. All parameters are pointed out in undrained terms.

As mentioned in Chapter 3.2, all models created in this study are described by Mohr-Coulomb failure criterion under seismic events. Total stress elastic features of the soil (E_u and ν_u) were considered in the alayses because of the requirement of employing in total stress terms for undrained conditions. The third undrained modelling option enables to monitor the effect of material properties on seismic bearing capacity. Undrained C,therefore, is used in this study.

Due to the necessity of using undrained stiffness and strength parameters, Mohr-Coulomb material model turns into Tresca model. In order to define Tresca model, necessary stiffness and strength parameters are originally undrained elasticity modulus (E_u), undrained Poisson ratio (ν_u) and undrained shear strength of cohesive soil (c_u). Apart from that,

undrained internal friction angle (Φu) and undrained dilation angle (ψ_u) should be described as zero. Theoretically, the value of undrained poisson should be 0.5. However, it was selected as 0.35 in all carried out finite element calculation because of the singularity in stiffness matrix.

Four different soil types were employed in this study. These data sets link with different cohesive soil stiffness (soft, medium, stiff, hard). Related parameter details are presented in Table 3.3. Moreover, saturated unit weight of soil (γ_{sat}) was assigned as constant (20 kN/m^2). Due to the rough footing assumption, interface strength reduction factor (R_{inter}) was assigned as 1.

Table 3.3. Properties of the cohesive slope soils employed in present study.

Parameter			Cohesive Soil Stiffness			
			Soft	Medium	Stiff	Hard
	Name	Unit	Value	Value	Value	Value
Material Model	Model	-	MC	MC	MC	MC
Type of material behavior	Type	-	Undrained C	Undrained C	Undrained C	Undrained C
Soil unit weight above phreatic level	γ_{unsat}	kN/m^3	20	20	20	20
Soil unit weight above phreatic level	γ_{sat}	kN/m^3	-	-	-	-
Permeability in horizontal direction	k_x	m/day	-	-	-	-
Permeability in horizontal direction	k_y	m/day	-	-	-	-
Undrained elasticity modulus	E_u	kN/m^2	5000	10000	20000	40000
Undrained Poisson ratio	v_u	-	0.35	0.35	0.35	0.35
Undrained shear strength	c_u	kN/m^2	25	50	100	200
Undrained friction angle	Φ_u	^{o}	0	0	0	0
Undrained dilatancy angle	¥$_u$	^{o}	0	0	0	0
Interface strength reduction factor	R_{inter}	-	1	1	1	1

3.5.6. Finite Element Mesh Generation

The model used in this study was divided into finite number of elements to achieve finite element examinations. To obtain more reliable results, 15-node triangular elements

were chosen to create a finite element mesh. The soil layer subdivided into three different zones depending on the density of finite elements. The densest mesh zone was placed beneath the footing and bordered along the foundation-soil interfaces and the edge of incline for more exact values. Mesh density decreases as it moves away from the foundation.

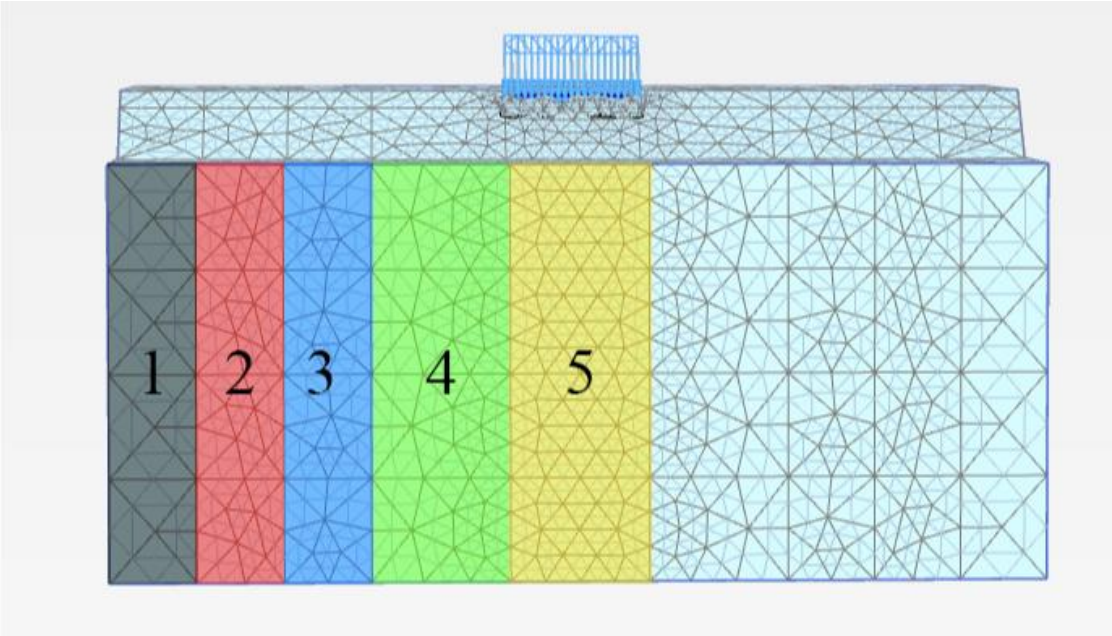


Figure 3.7. Finite element mesh generation.

3.6 Design Steps

Design steps consisted of two phases which were respectively the initial phase and second phase which is used for the calculation of undrained seismic bearing capacity of the shallow foundation using by the load factor (Σ-M_{stage}) until soil body breakdown seems to collapse. First phase includes the activation of inertia force applying on soil clusters.

Typical view of Calculation modules of Plaxis 3D software in which above mentioned calculation steps were defined is given in Figure 3.8 and Figure 3.9, respectively.

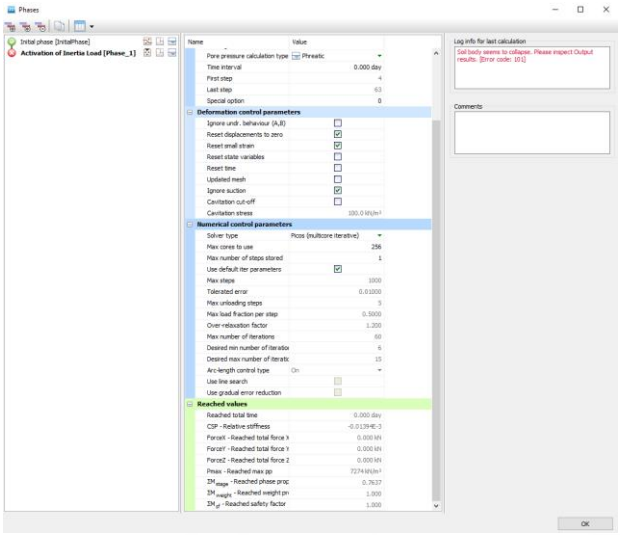


Figure 3.8. Typical view of “Calculation Module” window.

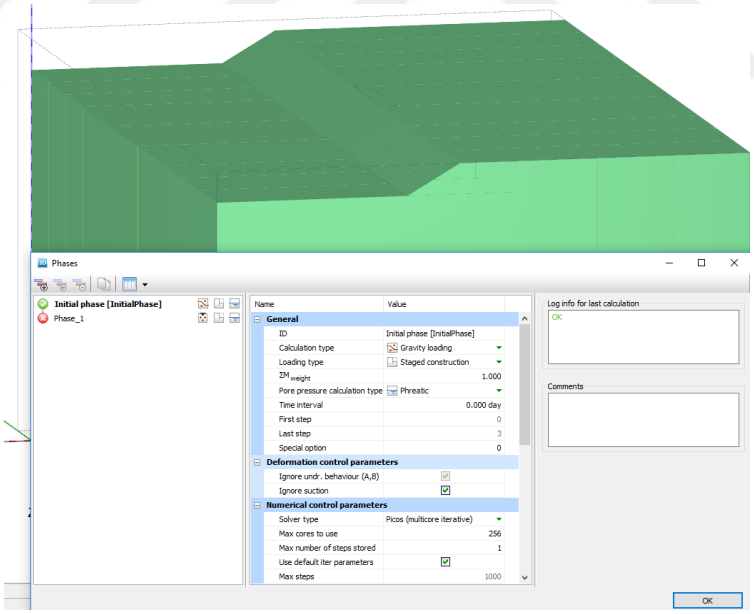


Figure 3.9. Typical View of ‘Initial Phase’ window.

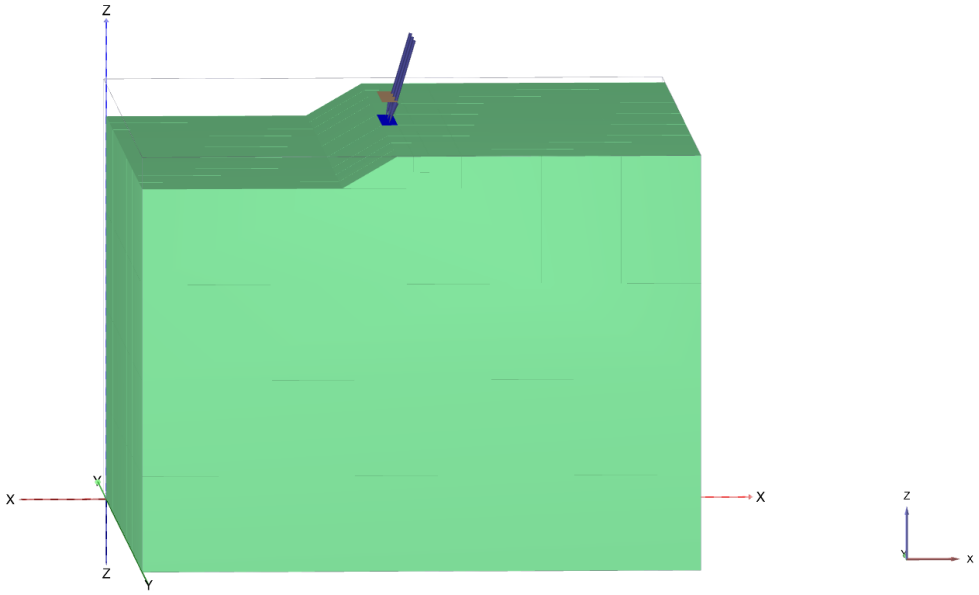


Figure 3.10. Activation of inertia force applying on soil clusters.

Failure was monitored at the initial calculation phase in all numerical examinations generated in this study. Detection of soil failure at the end of the initial stage shows that cohesive slope may not carry its weight under the impact of gravity. Lastly, detection of the failure at the end of the second calculation step shows that a footing located on face of a slope reaches ultimate limit bearing pressure with different foundation failure systems. The ultimate seismic bearing capacity was only computed for all numerical examinations that failure was found at the end of the first calculation phase.

Ultimate seismic bearing pressure coefficient (N_{cse}) is obtained by means of the load stage (Σ-M_{stage}) computed by Plaxis 3D. It relates to the magnitude of the applied load on ground. For example, as presented in Figure 3.10, the value of computed load stage at the end of the first calculation phase is 0.424 for the numerical model which is *C*_45_2_0_2_25_0.1_*D* ($\beta=45^0$, $H=2.0m$, $L=2$, $\lambda=0$, $c_u=25\ kPa$, $k_h=0.1$).

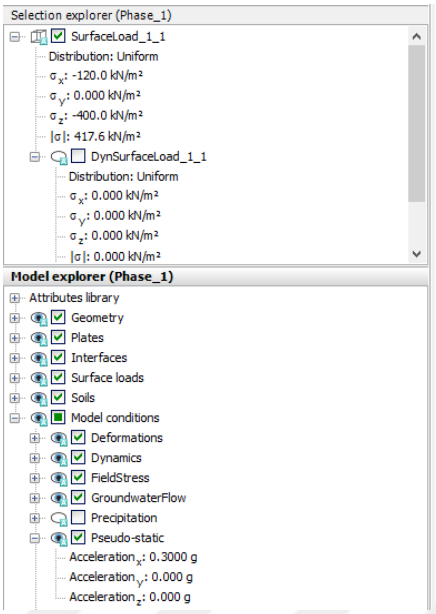


Figure 3.11. The load stage (*Σ-Mstage*) found by calculations module of Plaxis 3D for the final limit state.

Seismic bearing capacity of footing located on face of slope system (q_f),

q_f (kPa)= Magnitude of vertical component of unit load (kPa) x Σ-M_{stage}

$$q_f = 300x0.424 = 127.2\ kPa \tag{3.2}$$

Based Equation 3.2, seismic bearing capacity factor (N_{cse}),

$$N_{cse} = \frac{q_f}{c_u} = \frac{127.2}{25} = 5.09 \tag{3.3}$$

3.7 Evaluation of Plaxis 3D Outputs

According to Chapter 3.6, the load stage using Calculations tab of the software can find ultimate seismic bearing pressure and seismic bearing coefficient. On the other hand, shape of failure mechanism and shear surfaces under the foundation should be deeply considered. Different failure systems and shape of shear surfaces can be viewed by selecting 'Total Deviatric Strain' and 'Incremental Displacements' from Output results of the software. For example, for the numerical model which is *C*_45_2_0_2_25_0.1_D (β=45^0, *H*=2.0m, *L*=2, λ=0, c_u=25 kPa, k_h=0.1), the failure system at the final stage is given in Figure 3.11.

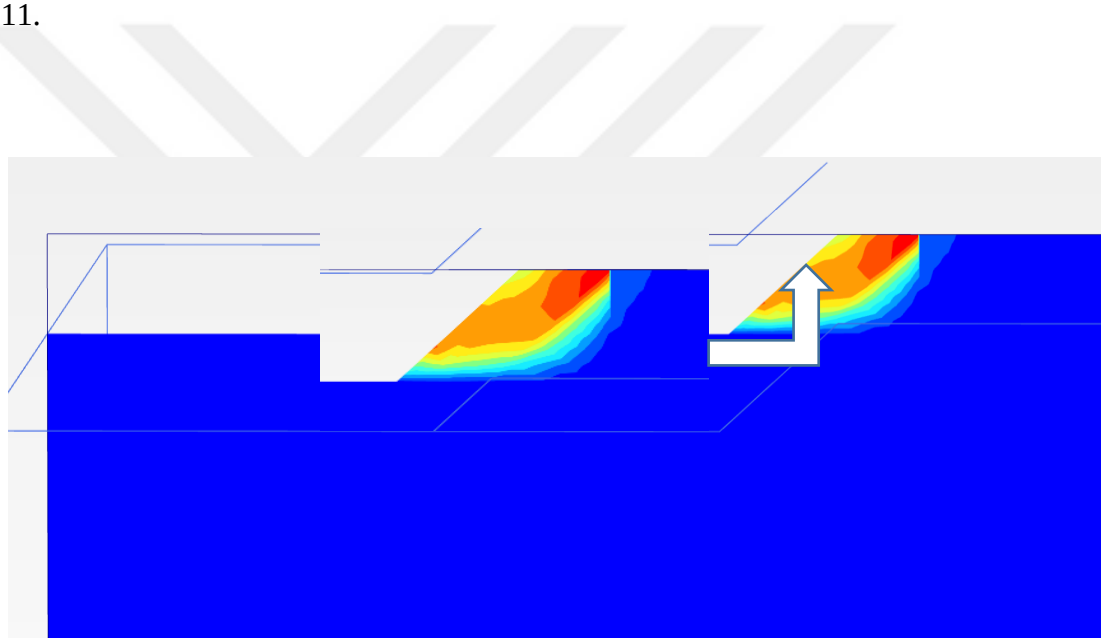


Figure 3.12. Failure mechanism obtained for the finite element model named as C_45_4_0_16_25_0.1_D and enlarged view of the failure mechanism.

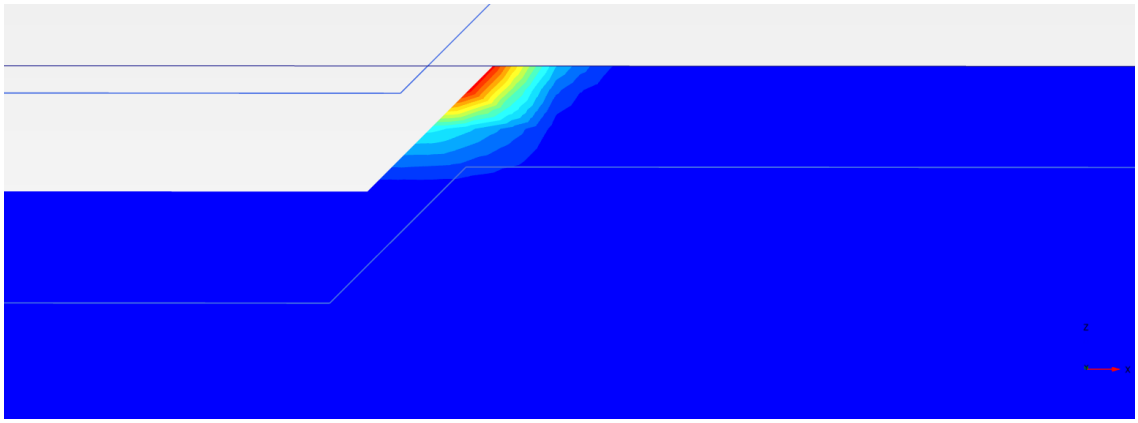


Figure 3.13. Shear surfaces obtained for the finite element model named as C_45_4_0_16_25_0.1_D.

4. RESULTS AND DISCUSSIONS

Outcomes of the parametric study which are conducted will be discussed in this section. The main goal is to reflect the relationship of the parameters with seismic bearing capacity factor (N_{cse}) of shallow foundations located close to cohesive slopes. Additionally, seismic bearing capacity coefficient can be defined as a function of different influential factors. With the definition to be made, it would be possible that various types of failure mechanisms that reached the final state by the effect of inertia forces under the foundation or within the cohesive slope.

All numerical models carried out in Plaxis3D were defined systematically. For instance "C_15_2_0_2_25_0.1_D", the first capital letter expresses that the soil material type which was the cohesive soil, the second number is the slope angle (β), the third number is the slope height (H), the forth number is the distance between the footing's near edge, the fifth number is the length of foundation, the sixth number is the undrained strength, and the last number is the horizontal seismic coefficient (k_h).

Different from the results mentioned above, shape effects of shallow foundation on seismic bearing capacity will be examined with design charts. Seismic bearing capacity can be determined by design charts given in the next part of this section as well. Also, these design charts will show the relationship between 2D and 3D.

4.1 Determination and Influential Parameters

This study is based on various influential parameters. Therefore, these parameters can be effective directly or indirectly on seismic bearing capacity factor. Horizontal seismic acceleration coefficient (k_h), normalized slope height (H/B), normalized undrained cohesive slope soil strength ($c_u/\gamma B$) and slope angle (β). The effect of each factor on seismic bearing capacity factor will be explained in a more comrepehensive way in the following section.

4.1.1 Influence of Horizontal Seismic Acceleration Coefficient

Seismic bearing capacity factor (N_{cse}) drops remarkably with the increase of horizontal seismic acceleration coefficient (k_h). As seen from the graph given in Figure 4.1, it is clear that horizontal seismic acceleration factor has a diminishing impact on seismic bearing capacity factor. Additionally, shape effect has become a minor impact on bearing capacity for the values greater than 0.3g.

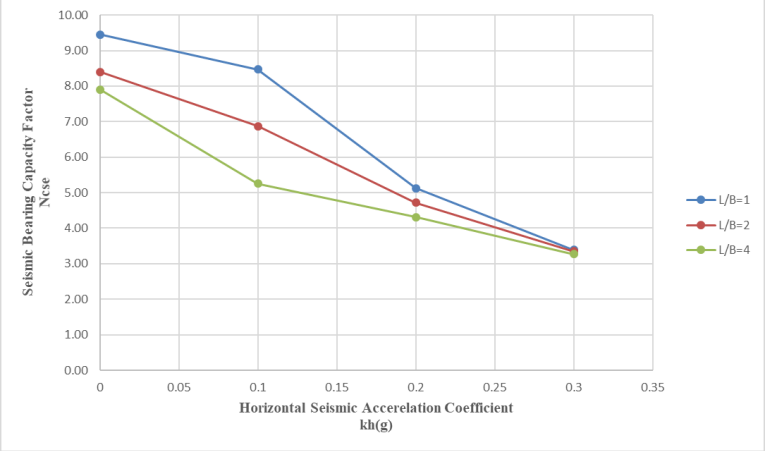


Figure 4.1. Variation of N_{cse} with k_h for λ=0 (β=15^0, $c_u/\gamma B$ =2.5).

4.1.2 Influence of Slope Angle

Seismic bearing capacity factor (N_{cse}) drops dramatically with the increase of slope angle *(β).* However, it is obvious that for bigger values of the normalized length of foundation (*L/B*), seismic bearing capacity factor decreases sharply with the increase of slope angle for foundations located close to slope edge. (λ=0)

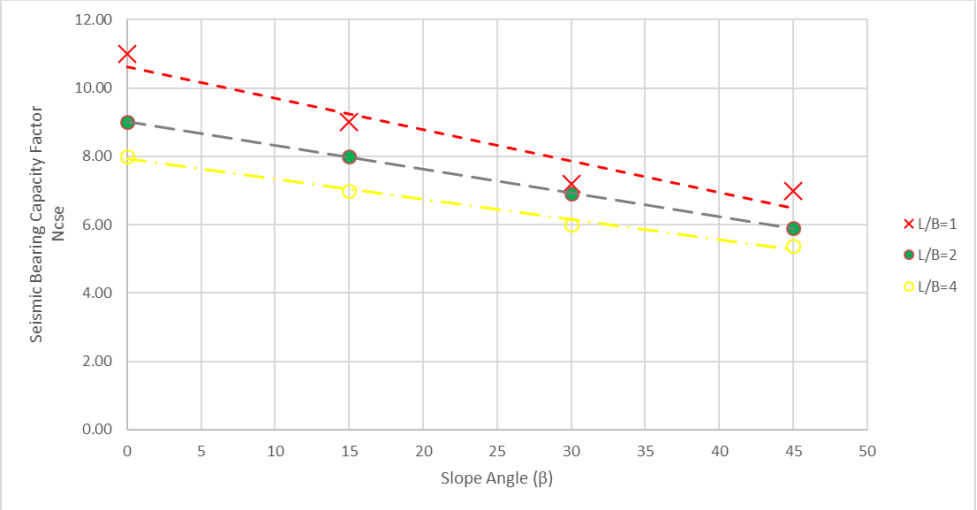


Figure 4.2. Variation of Ncse with β for λ=0 (k_h=0, cu/γB =2.5).

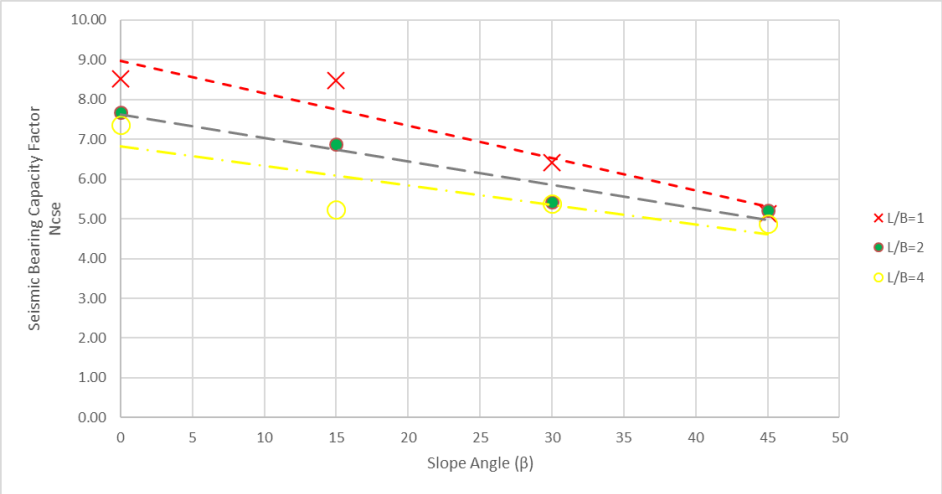


Figure 4.3. Variation of N_{cse} with β for λ=0 (k_h=0.1, $c_u/\gamma B$ =2.5).

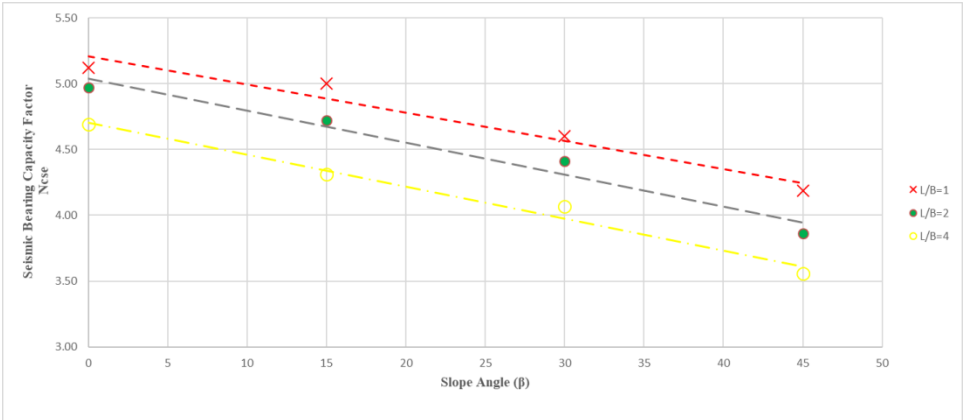


Figure 4.4. Variation of N_{cse} with β for λ=0 (k_h=0.2, $c_u/\gamma B$ =2.5).

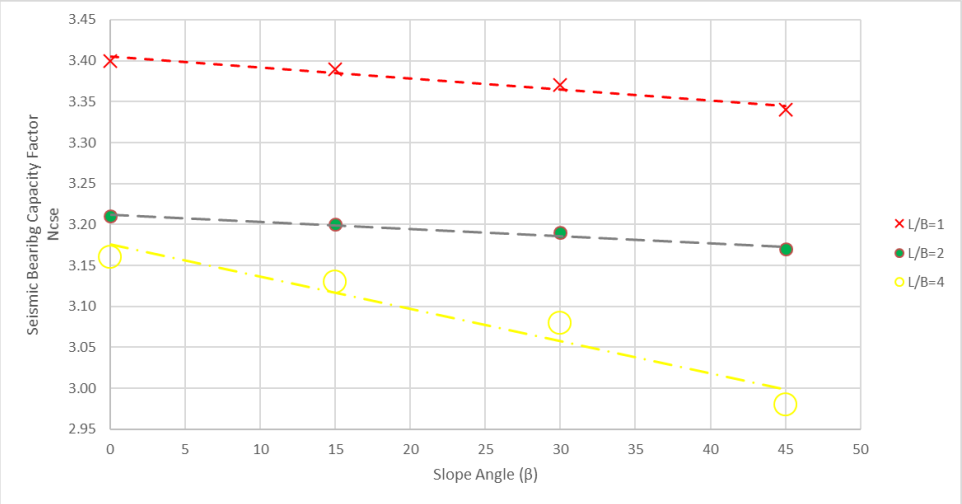


Figure 4.5. Variation of N_{cse} with β for λ=0 (k_h=0.3, $c_u/\gamma B$ =2.5).

4.1.3 Influence of Slope Height

Additionally, the effect of the *H/B* ratio was examined. Actually, the effect of normalized slope height on seismic bearing capacity can be ignored for conditions that the foundation reaches to its ultimate limit bearing pressure with "foundation failure" mode.

On the other hand, the failure mode changes as *H/B* ratio raises for the smaller values of $c_u/\gamma B$ ratio. When *H/B* ratio raises, it was firstly observed that failure form changes from "foundation failure" to "base failure due to earthquake". Later, this evolution continues to another failure form called "base failure due to self-weight of slope". They are also shown in the lists given in Appendix B.

4.1.4 Influence of Slope Soil Strength

As shown in the chart presented in Figure 4.6, seismic bearing capacity factor (N_{cse}) raises with the decrease of $c_u/\gamma B$ ratio. On the other hand, it is observed from presented chart that the influence of this factor is very limited for the values bigger than 1.25. Due to the effect of *H/B* ratio, there is a exact evolution between different failure approaches as $c_u/\gamma B$ ratio drops.

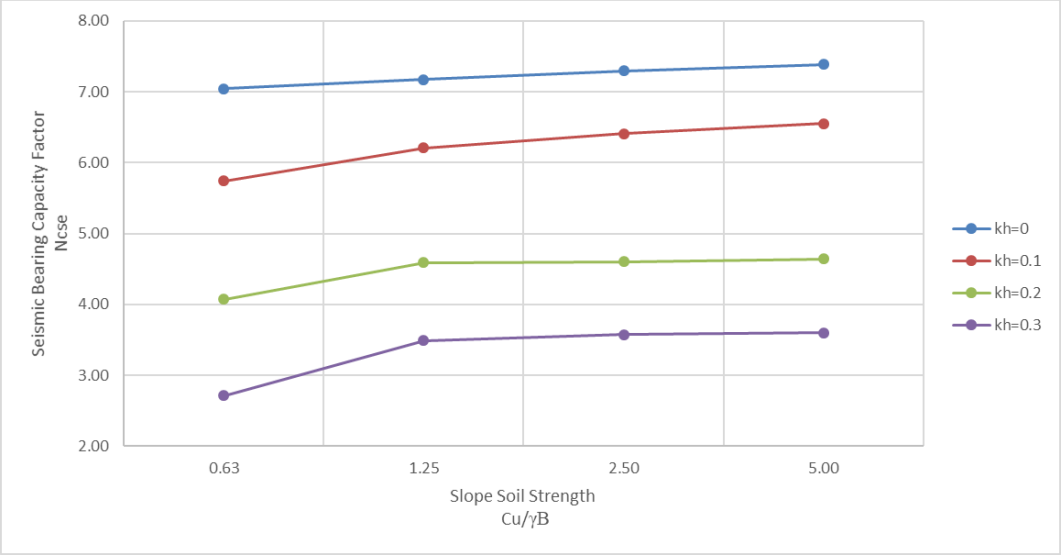


Figure 4.6. Variation of N_{cse} with $c_u/\gamma B$ for all k_h values (β=30°, $L/B=1$, λ=0).

4.2 Examination of Failure Mechanisms

As a result of numerical examinations which were carried out, it was obtained that there are three major failure shapes that can occur either under the foundation or within cohesive slope at the final state for seismic conditions. As explained before, while the dedication of failure at the end of second phase means that cohesive slope cannot ensure its stability by the effect of earthquake inertia force applying on slope, the dedication of failure at the end of the first phase means that the cohesive slope cannot control its stability under the impact of gravity. These failure modes are described as “base failure” in the present study. Failure mechanism of each of them are given in Figure 4.7 and Figure 4.8 respectively.

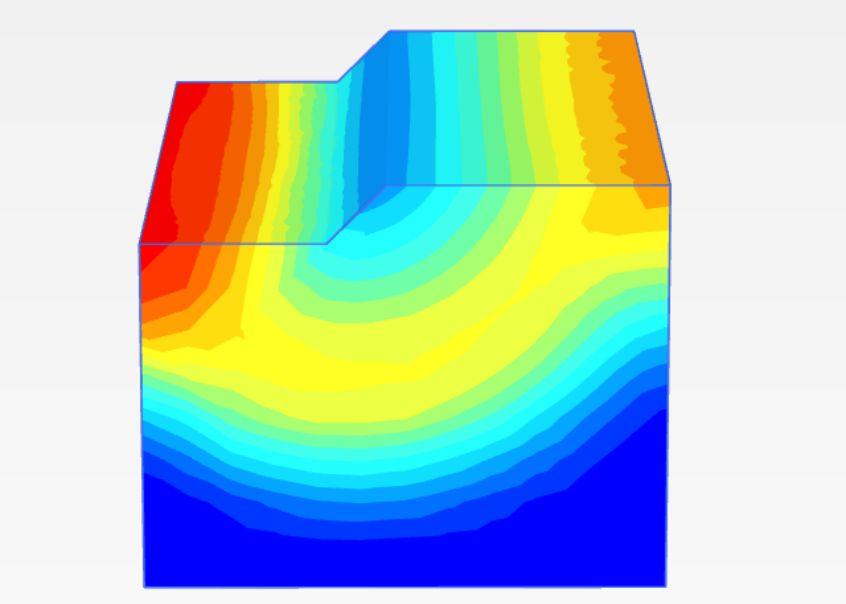


Figure 4.7. Base failure due to self-weight of cohesive slope (β=45^o, H/B=4.0 m and $c_u/\gamma B$ =0.625).

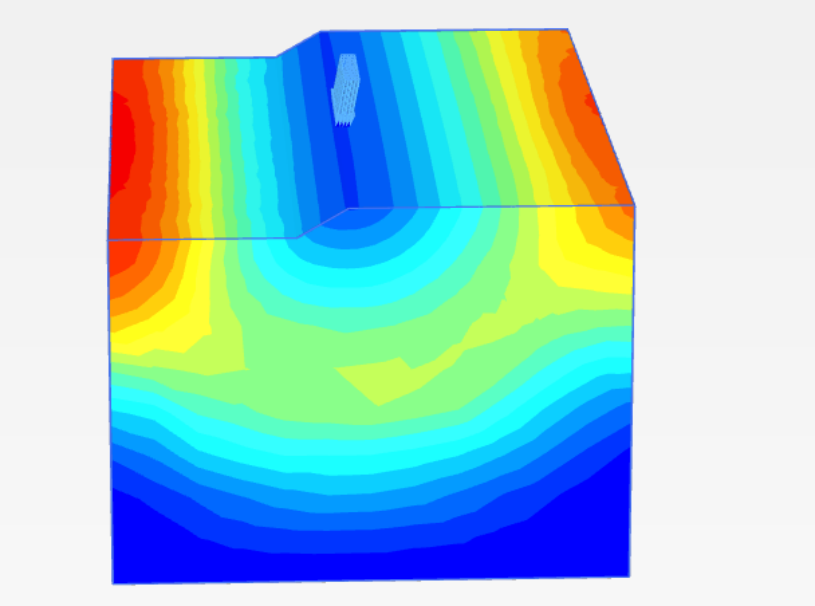


Figure 4.8. Base failure due to self-weight of cohesive slope (β=45^o, H/B=4.0 m, $c_u/\gamma B$ =0.625 and k_h=0.2).

Except from failure modes mentioned above, the dedication of failure at the end of the second phase means that the foundation comes to ultimate limit bearing pressure with a failure approach formed under the foundation. It is called as “foundation failure” in all lists given in Appendix B. Failure shapes starts distribution from the foundation edge and afterwad crosses with line of slope, moves from the incline toe or cuts at any point with upper horizontal line of the slope if the foundation is located far enough from the slope edge. This approach is virtually the same with failure mechanism definition made by Meyerhof (1957) and Farzaneh *et al.* (2013).

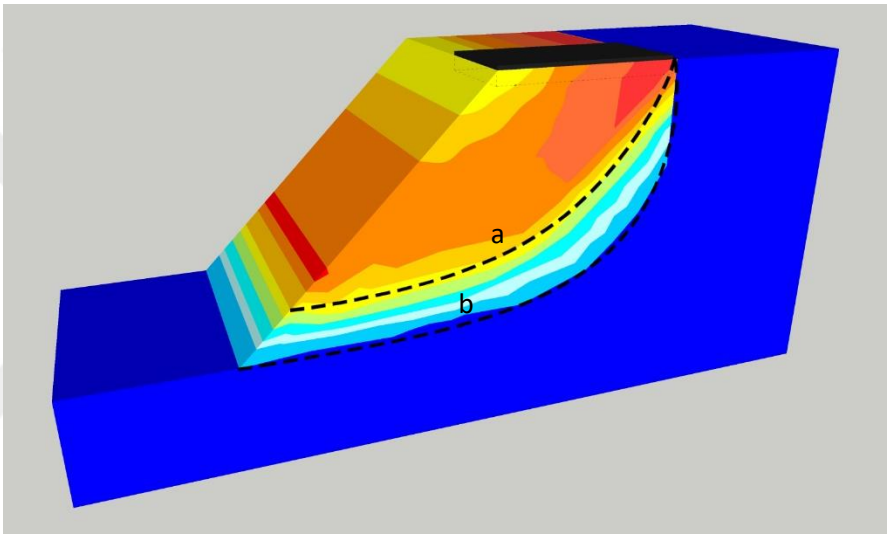


Figure 4.9. Typical “Foundation failure” approaches for λ=0 condition (a) β=45^o, H/B=1.0 m, $c_u/\gamma B$ =1.25 and k_h=0.2); (b) β=45^o, H/B=2.0 m, $c_u/\gamma B$ =0.625 and k_h=0.1).

4.3 Design Charts

Actually, seismic bearing capacity of shallow foundations located close to cohesive slopes can be obtained from Equation 3.1. Using the outcomes of parametric study, a new approach can be developed by geotechnical engineers and designers. Design charts that will shed light for this approach are given in between Figure 4.10 and Figure 4.43.

According to design charts, it is clearly expressed that the correlation between seismic bearing capacity coefficient (N_{cse}) and horizontal seismic acceleration coefficient is drawn as linear. The impact of B/L will be also examined as given design charts.

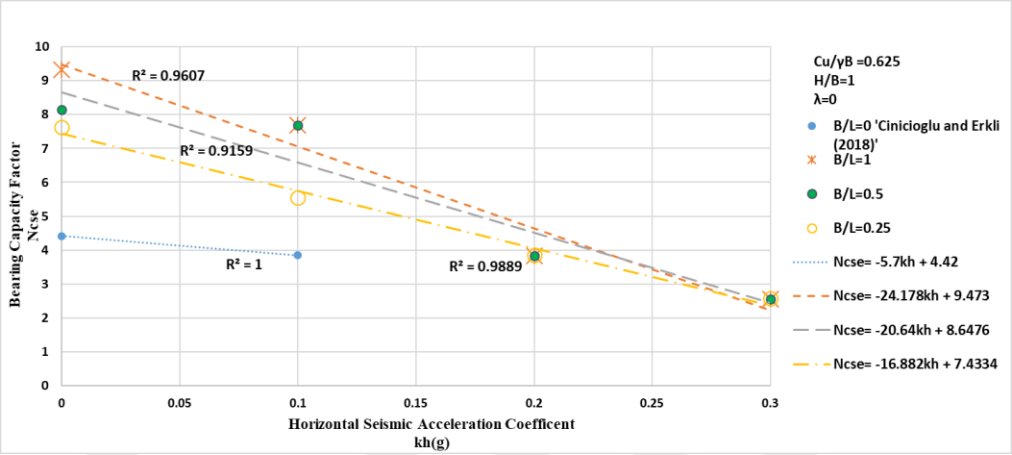


Figure 4.10. Variation of bearing capacity factor with horizontal seismic acceleration coefficient for $\beta=15^{o}$.

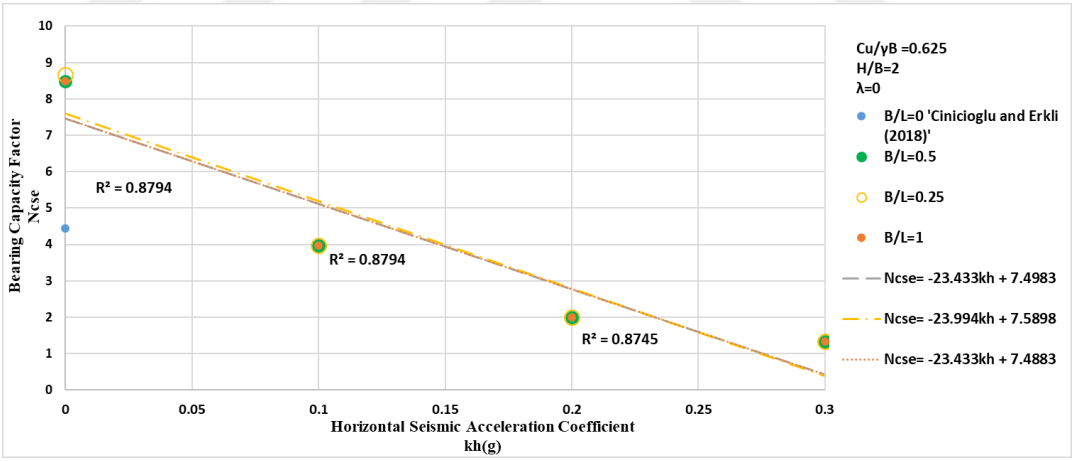


Figure 4.11. Variation of bearing capacity factor with horizontal seismic acceleration coefficient for $\beta=15^{o}$.

.

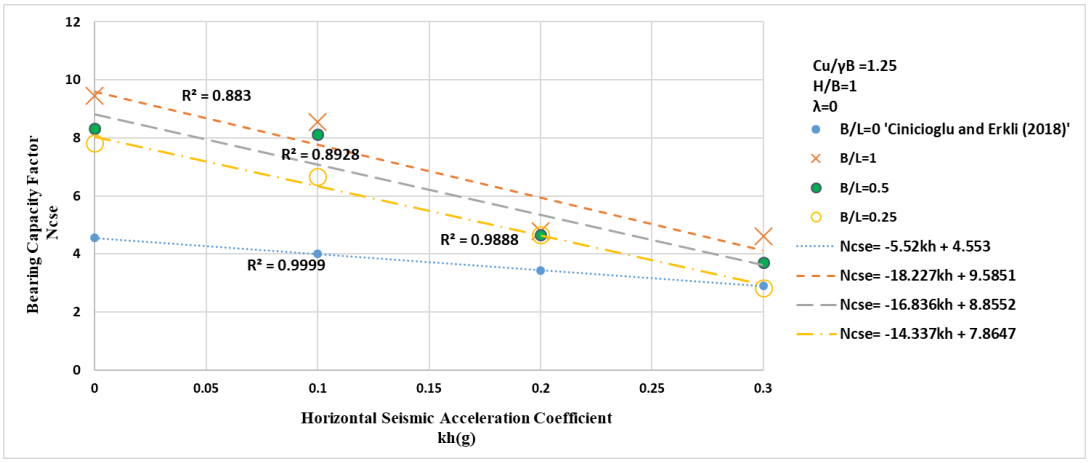


Figure 4.12. Variation of bearing capacity factor with horizontal seismic acceleration coefficient for $\beta=15^{o}$.

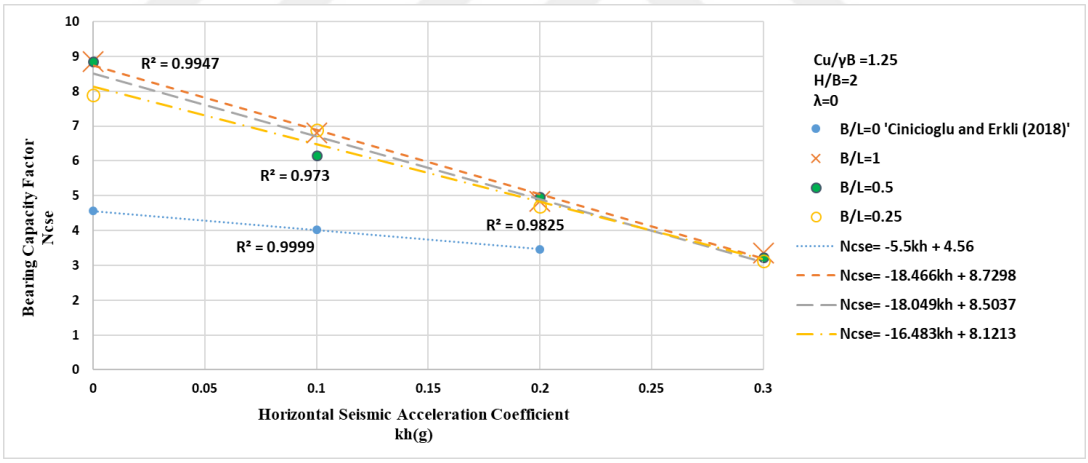


Figure 4.13. Variation of bearing capacity factor with horizontal seismic acceleration coefficient for $\beta=15^{o}$.

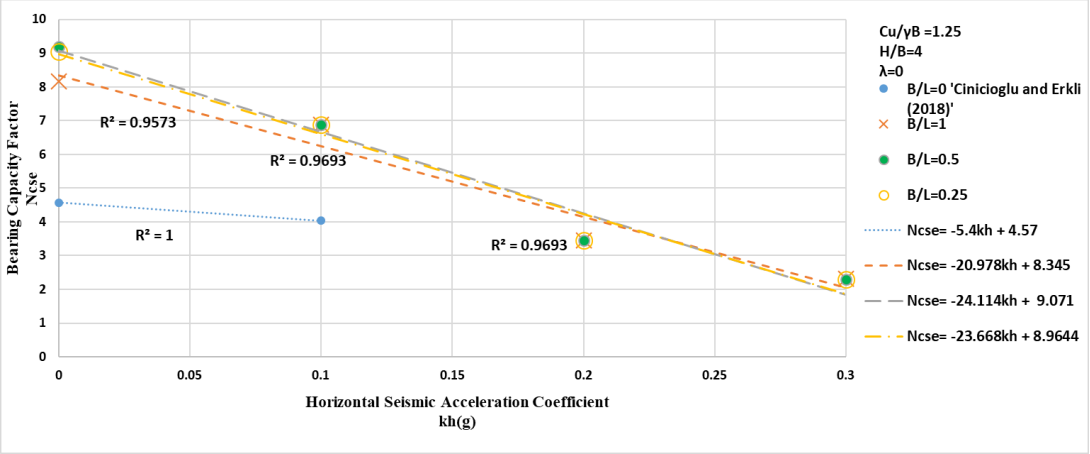


Figure 4.14. Variation of bearing capacity factor with horizontal seismic acceleration coefficient for $\beta=15^{o}$.

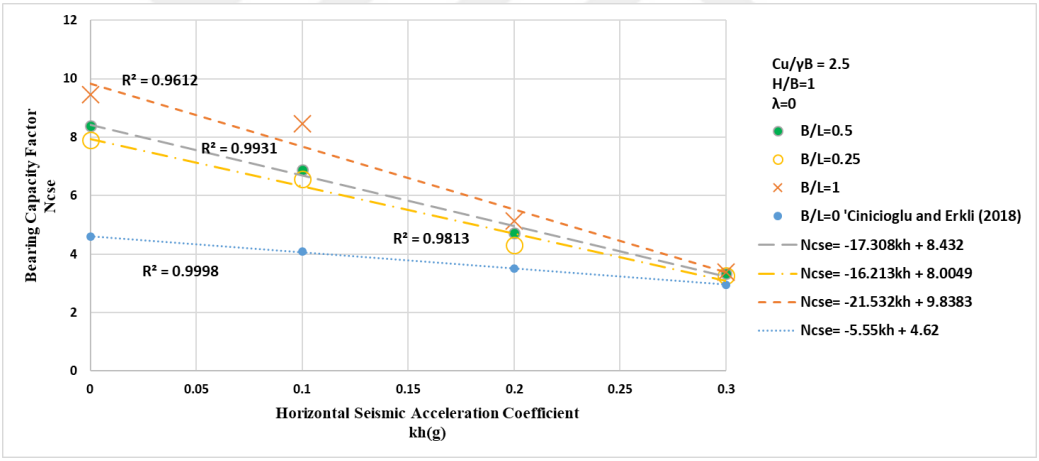


Figure 4.15. Variation of bearing capacity factor with horizontal seismic acceleration coefficient for $\beta=15^{o}$.

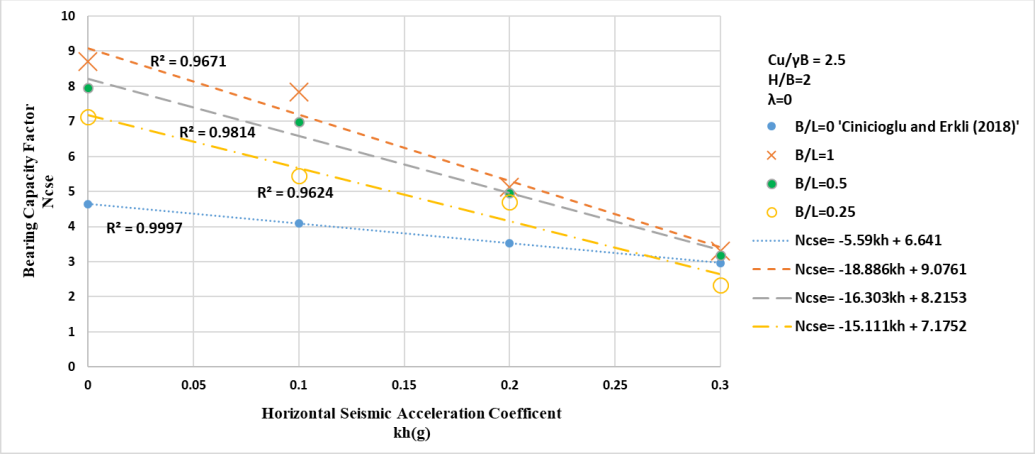


Figure 4.16. Variation of bearing capacity factor with horizontal seismic acceleration coefficient for $\beta=15^{o}$.

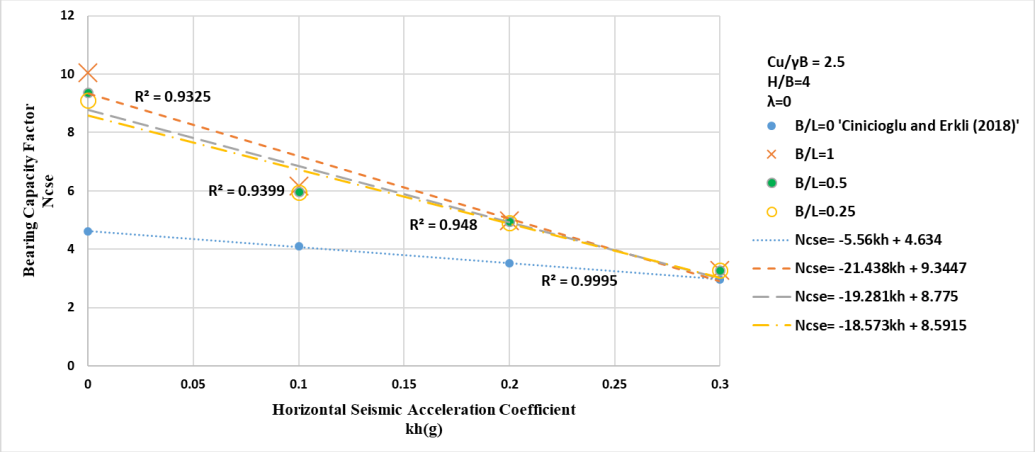


Figure 4.17. Variation of bearing capacity factor with horizontal seismic acceleration coefficient for $\beta=15^{o}$.

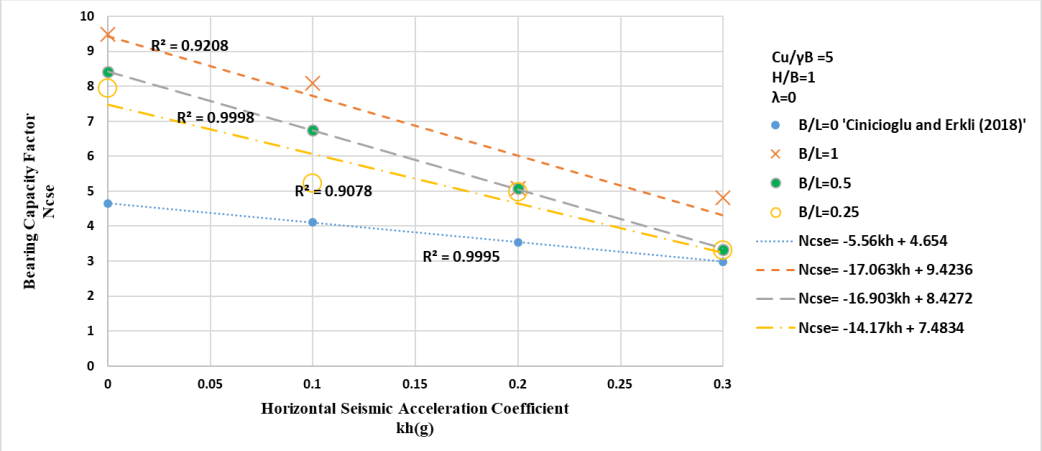


Figure 4.18. Variation of bearing capacity factor with horizontal seismic acceleration coefficient for $\beta=15^{o}$.

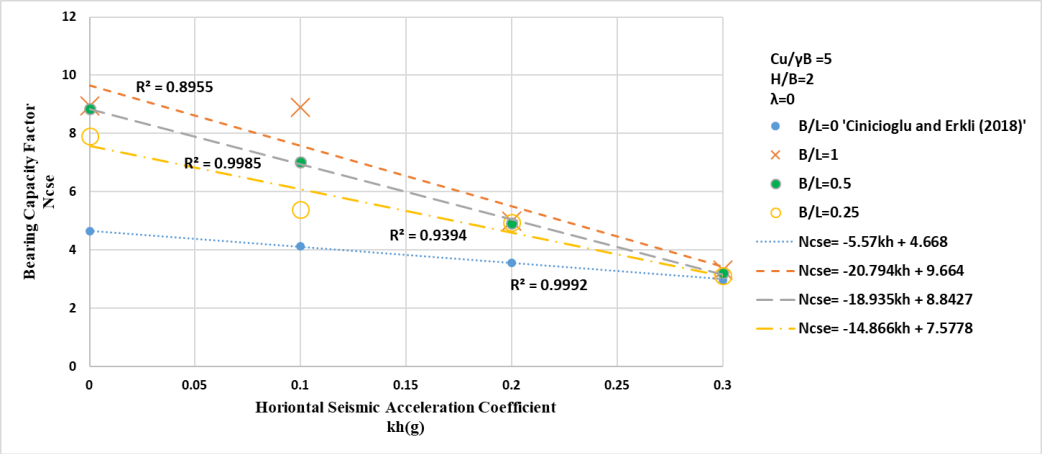


Figure 4.19. Variation of bearing capacity factor with horizontal seismic acceleration coefficient for $\beta=15^{o}$.

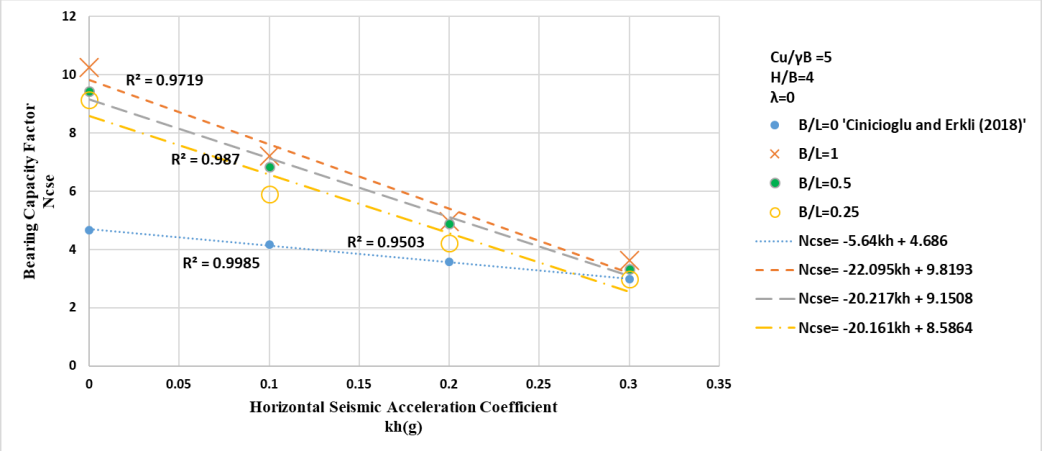


Figure 4.20. Variation of bearing capacity factor with horizontal seismic acceleration coefficient for $\beta=15^{o}$.

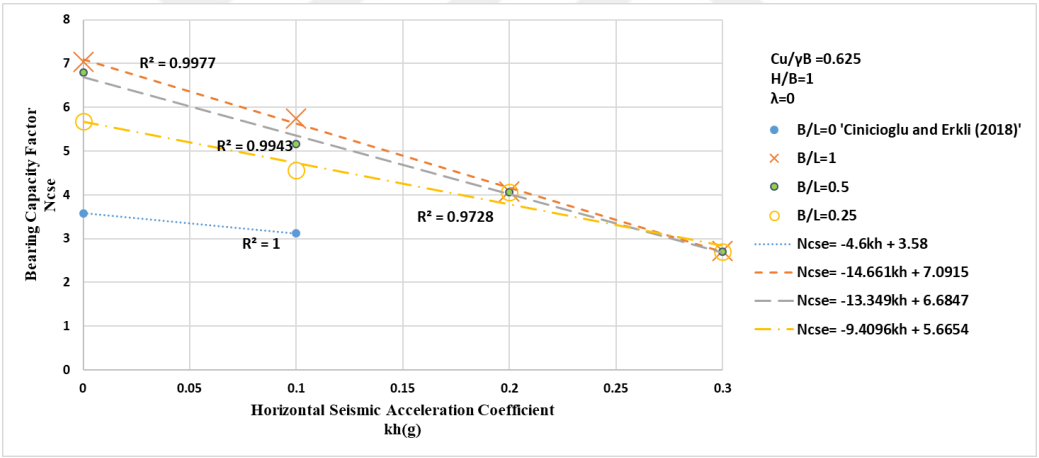


Figure 4.21. Variation of bearing capacity factor with horizontal seismic acceleration coefficient for $\beta=30^{o}$.

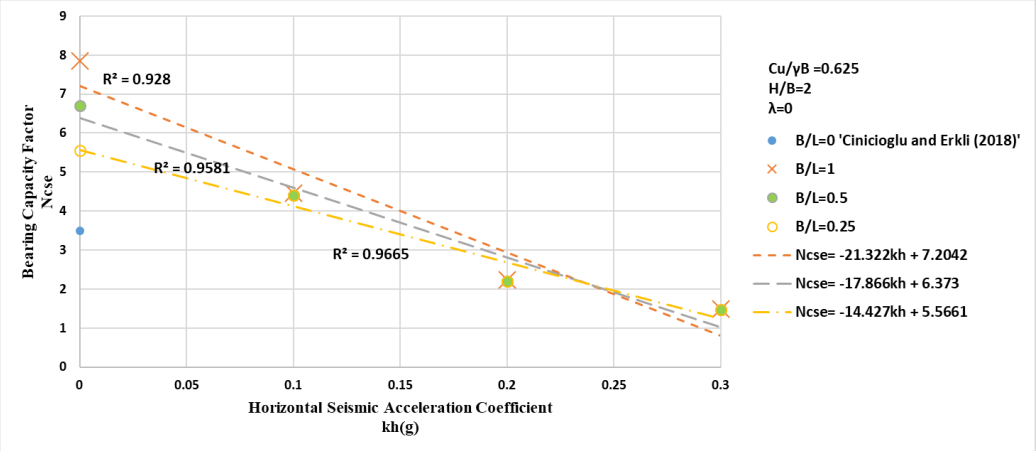


Figure 4.22. Variation of bearing capacity factor with horizontal seismic acceleration coefficient for $\beta=30^{o}$.

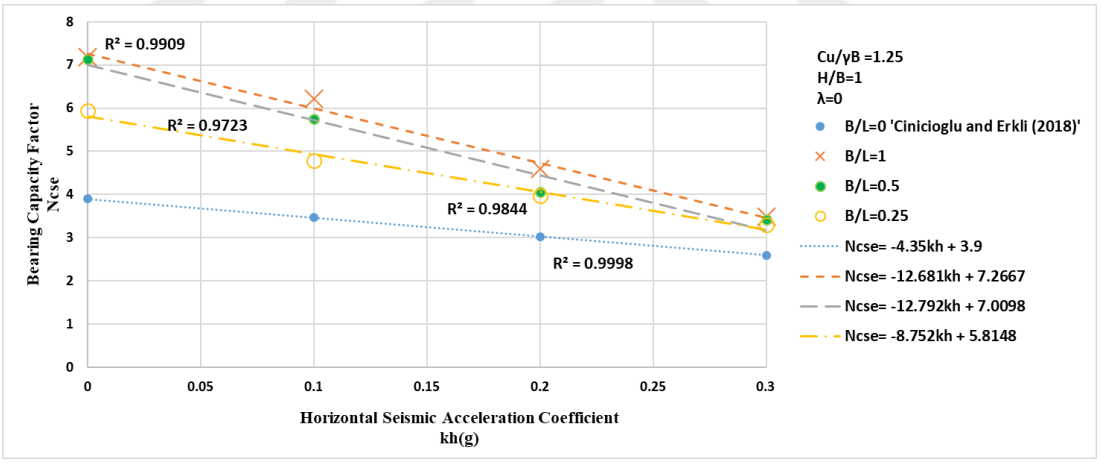


Figure 4.23. Variation of bearing capacity factor with horizontal seismic acceleration coefficient for $\beta=30^{o}$.

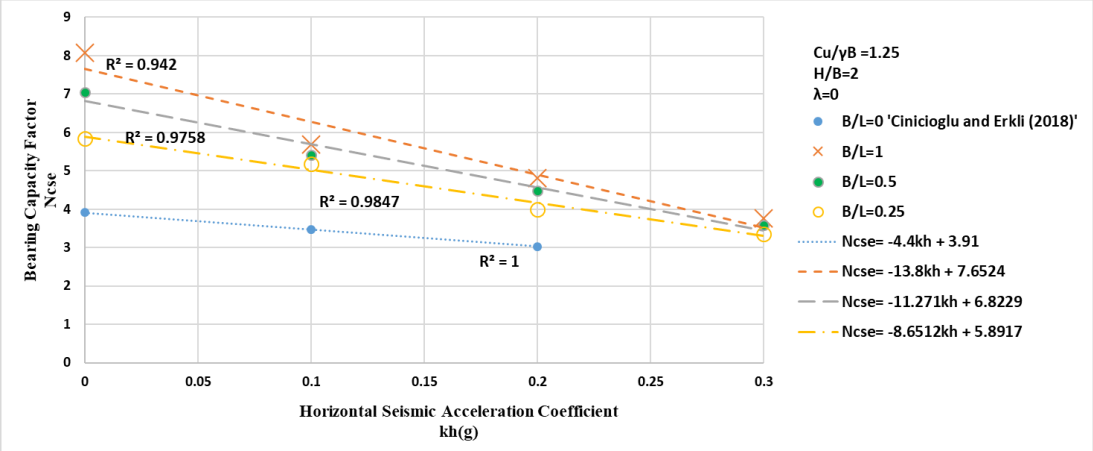


Figure 4.24. Variation of bearing capacity factor with horizontal seismic acceleration coefficient for $\beta=30^{o}$.

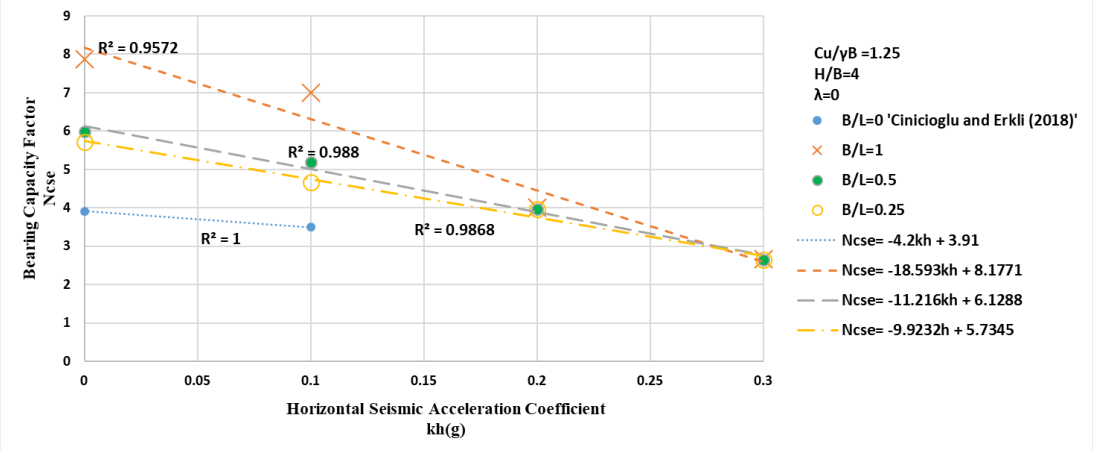


Figure 4.25. Variation of bearing capacity factor with horizontal seismic acceleration coefficient for $\beta=30^{o}$.

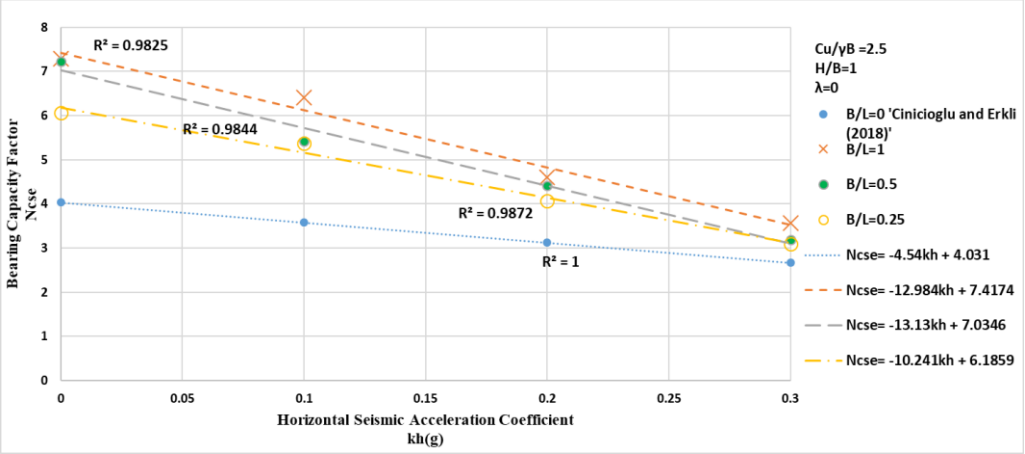


Figure 4.26. Variation of bearing capacity factor with horizontal seismic acceleration coefficient for $\beta=30^{o}$.

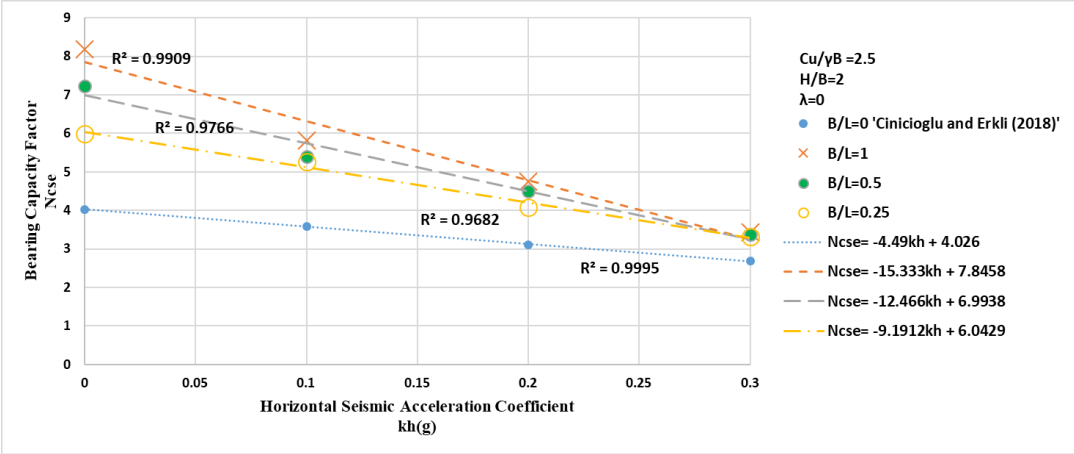


Figure 4.27. variation of bearing capacity factor with horizontal seismic acceleration coefficient for $\beta=30^{o}$.

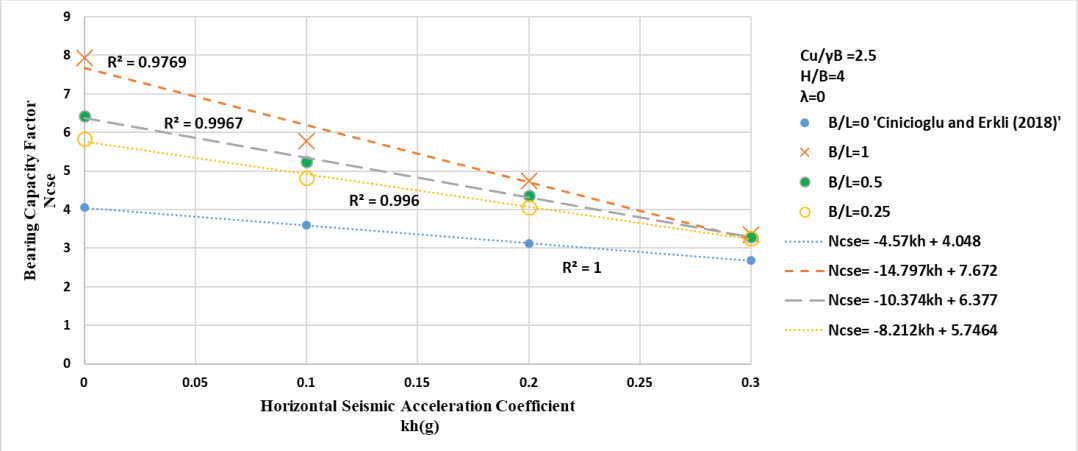


Figure 4.28. Variation of bearing capacity factor with horizontal seismic acceleration coefficient for $\beta=30^{o}$.

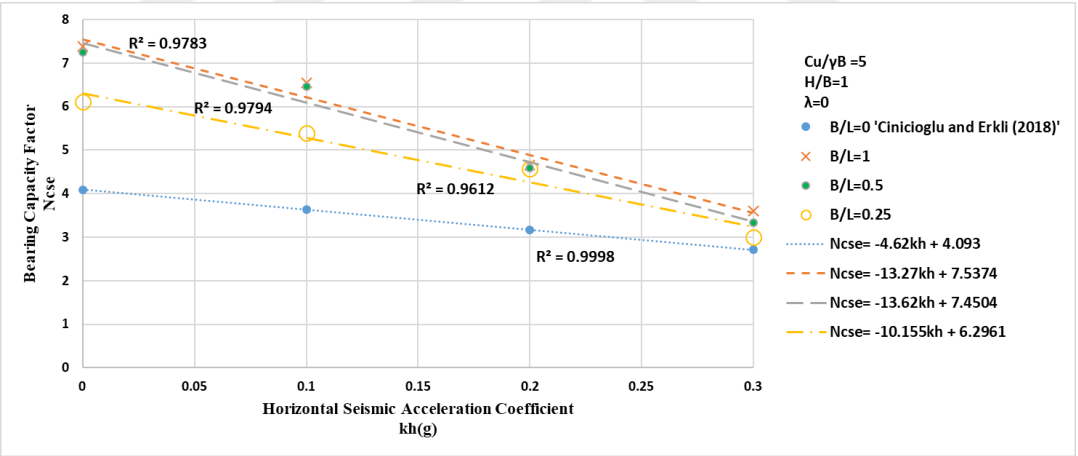


Figure 4.29. Variation of bearing capacity factor with horizontal seismic acceleration coefficient for $\beta=30^{o}$.

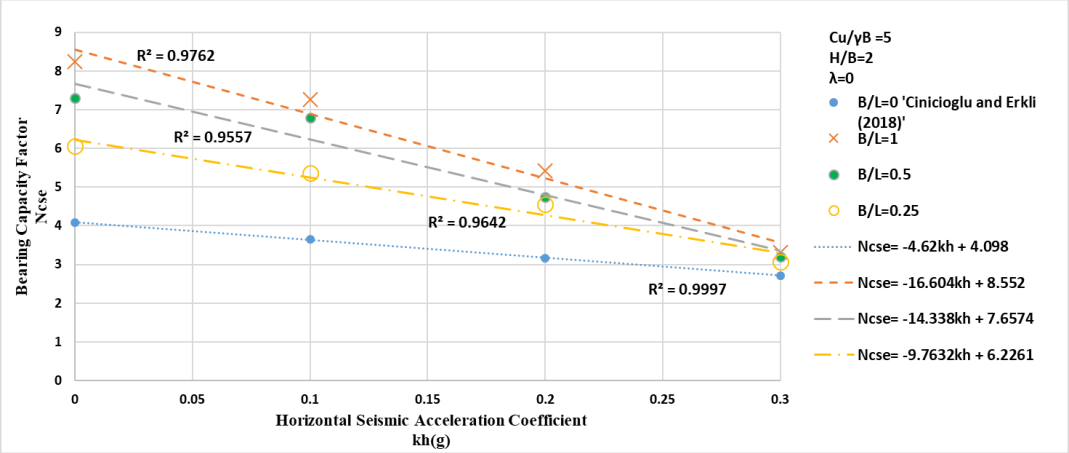


Figure 4.30. Variation of bearing capacity factor with horizontal seismic acceleration coefficient for $\beta=30^{o}$.

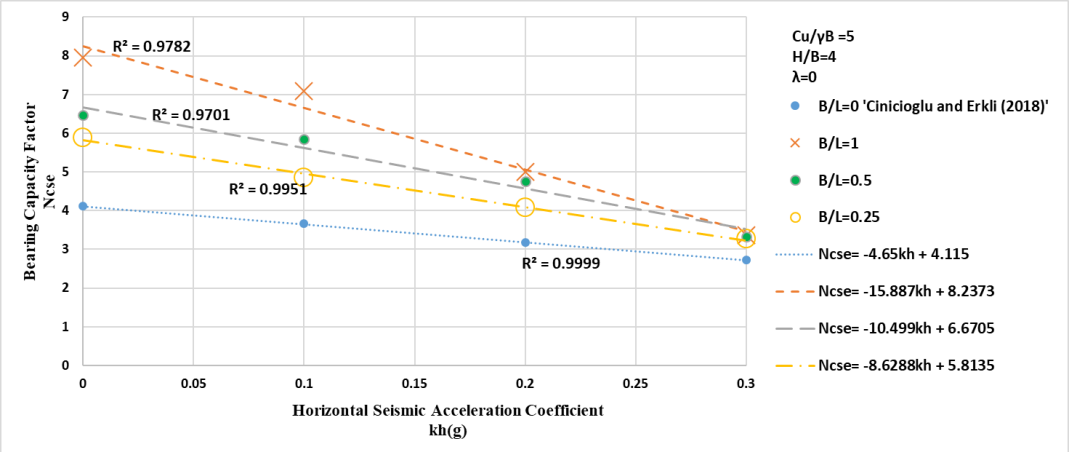


Figure 4.31. Variation of bearing capacity factor with horizontal seismic acceleration coefficient for $\beta=30^{o}$.

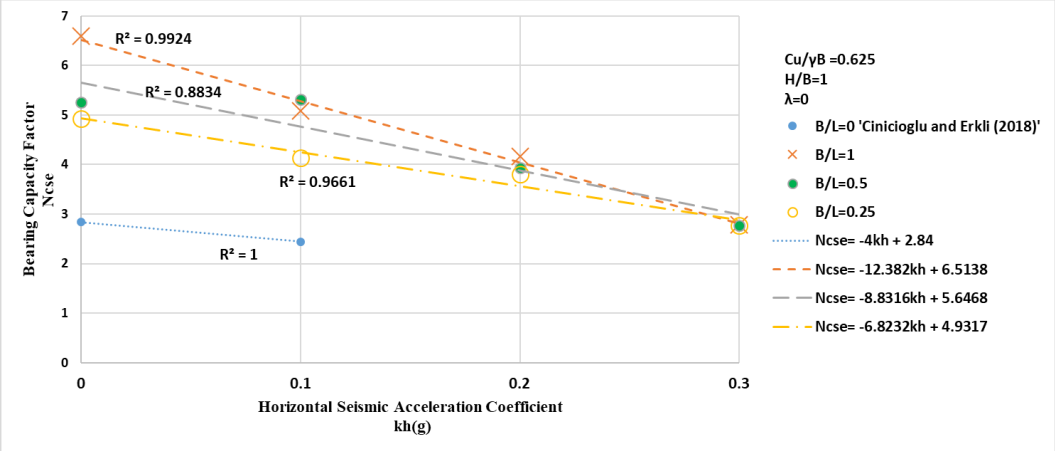


Figure 4.32. Variation of bearing capacity factor with horizontal seismic acceleration coefficient for $\beta=45^{o}$.

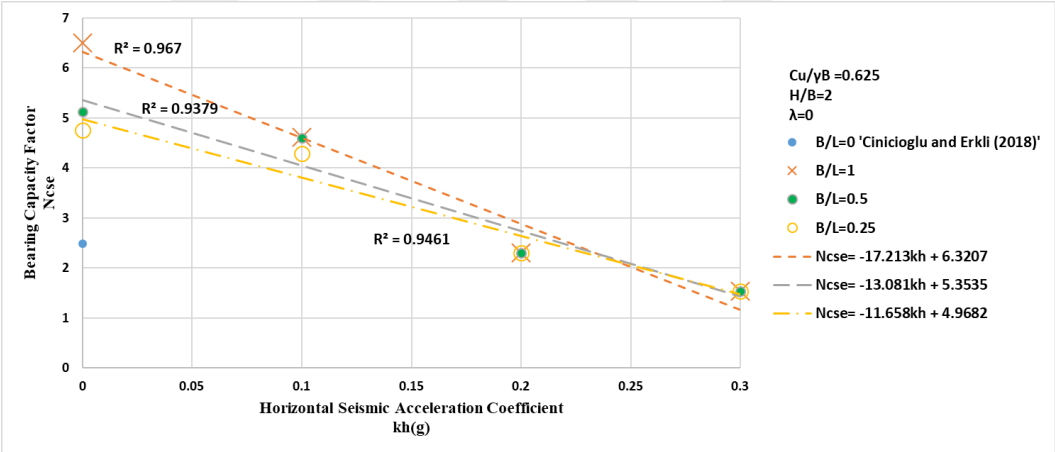


Figure 4.33. Variation of bearing capacity factor with horizontal seismic acceleration coefficient for $\beta=45^{o}$.

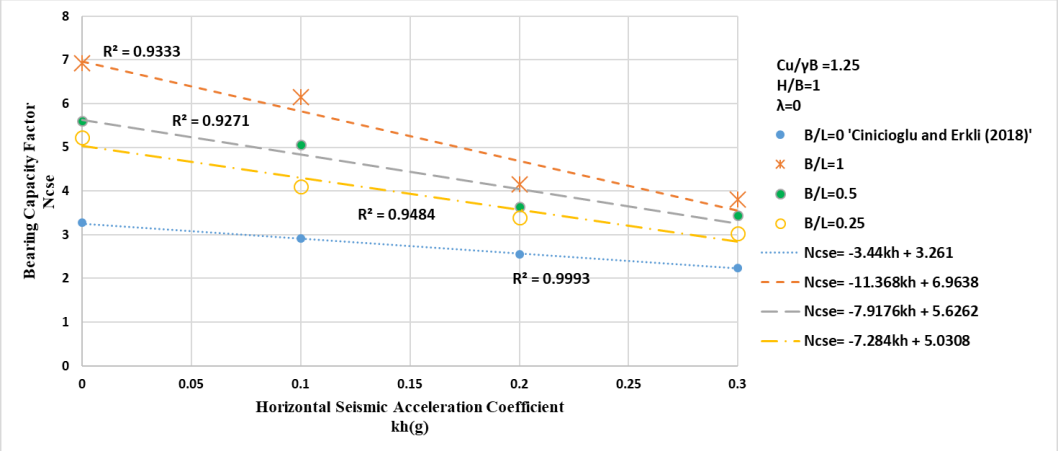


Figure 4.34. Variation of bearing capacity factor with horizontal seismic acceleration coefficient for $\beta=45^{o}$.

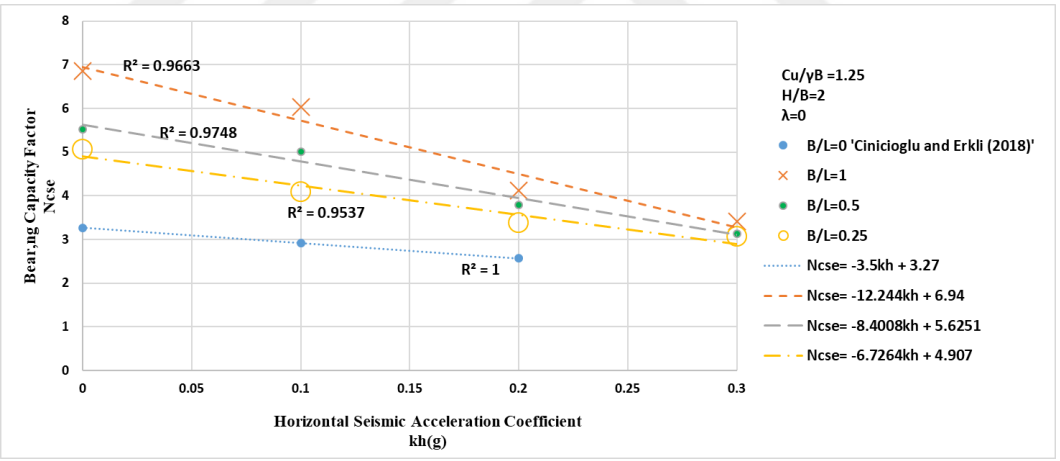


Figure 4.35. Variation of bearing capacity factor with horizontal seismic acceleration coefficient for $\beta=45^{o}$.

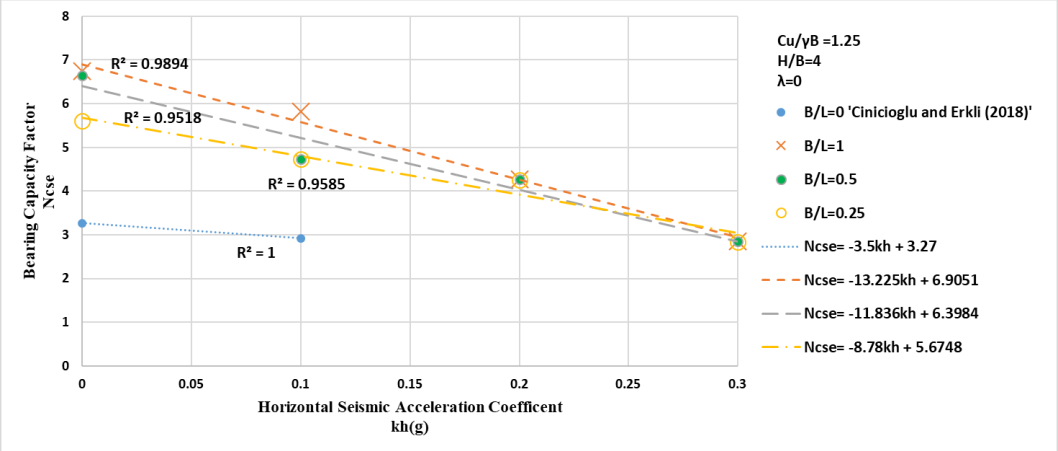


Figure 4.36. Variation of bearing capacity factor with horizontal seismic acceleration coefficient for $\beta=45^{o}$.

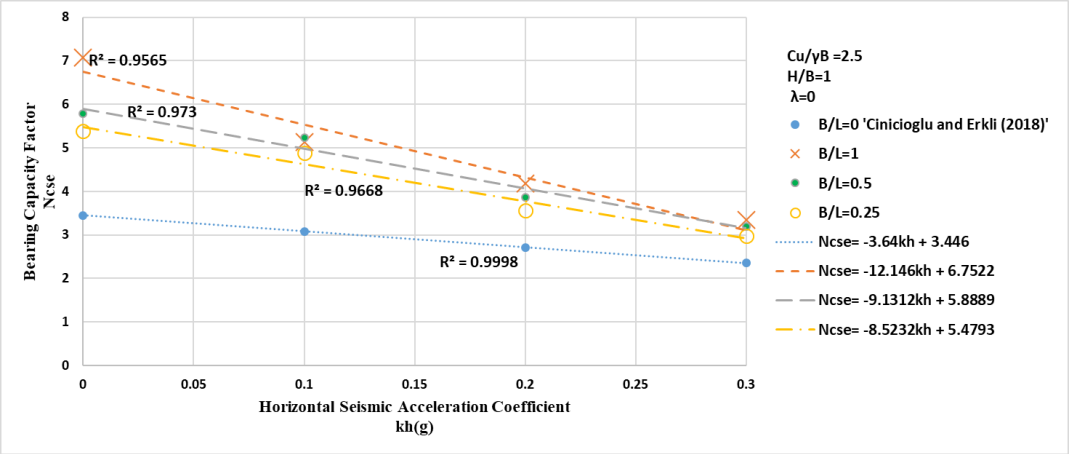


Figure 4.37. Variation of bearing capacity factor with horizontal seismic acceleration coefficient for $\beta=45^{o}$.

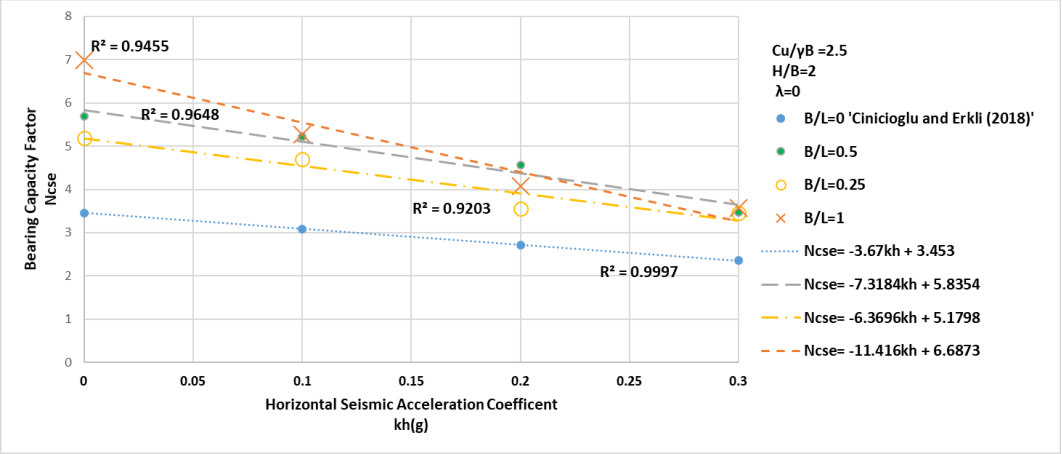


Figure 4.38. Variation of bearing capacity factor with horizontal seismic acceleration coefficient for $\beta=45^{o}$.

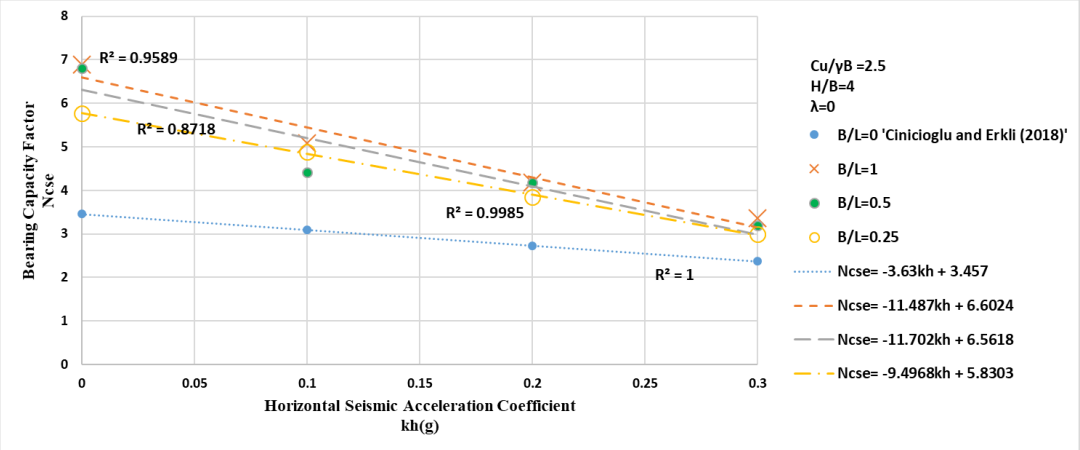


Figure 4.39. Variation of bearing capacity factor with horizontal seismic acceleration coefficient for $\beta=45^{o}$.

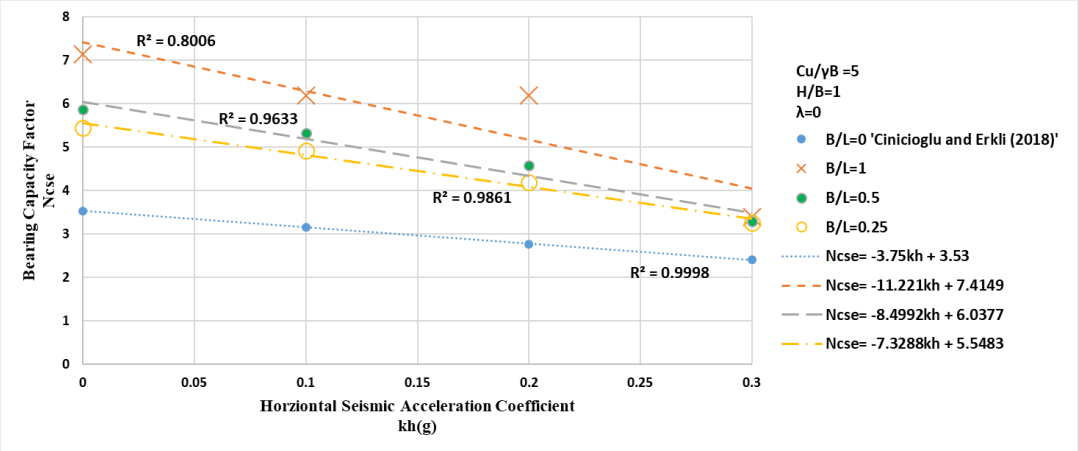


Figure 4.40. Variation of bearing capacity factor with horizontal seismic acceleration coefficient for $\beta=45^{o}$.

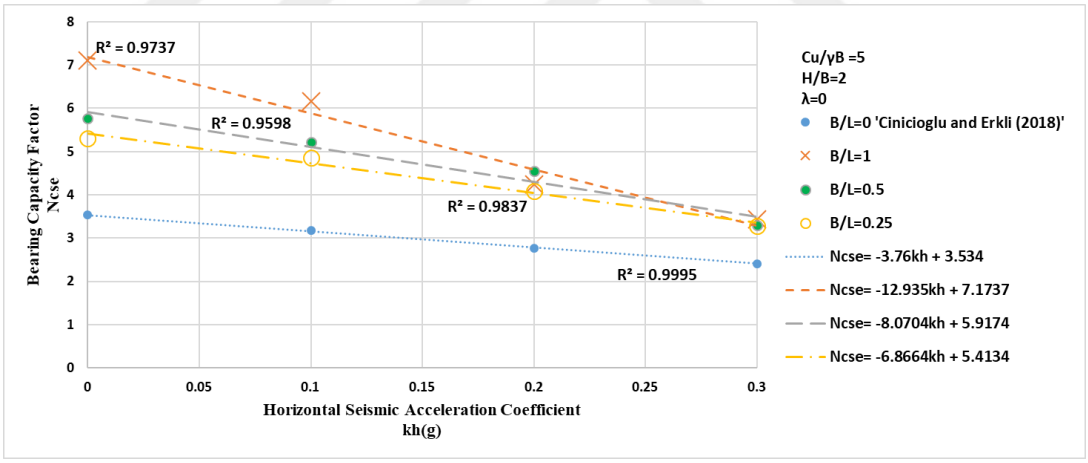


Figure 4.41. Variation of bearing capacity factor with horizontal seismic acceleration coefficient for $\beta=45^{o}$.

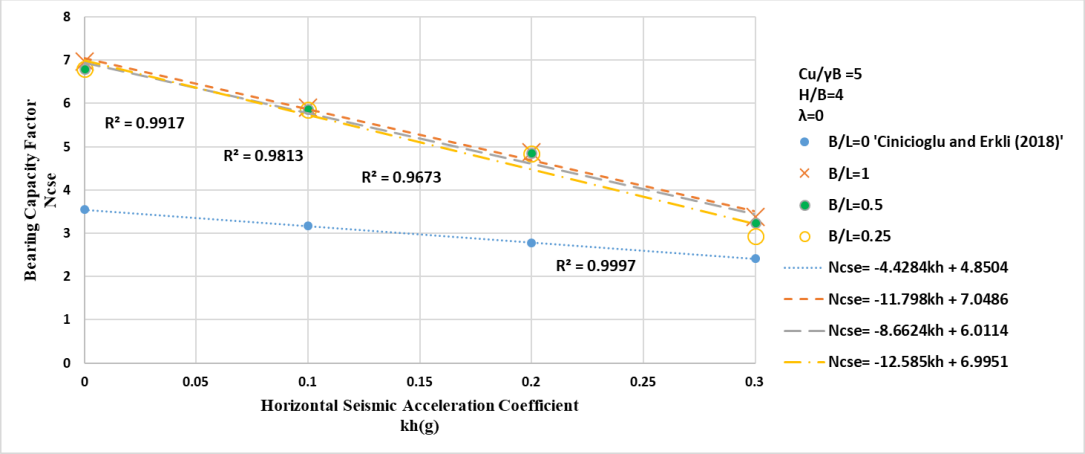


Figure 4.42. Variation of bearing capacity factor with horizontal seismic acceleration coefficient for $\beta=45^{o}$.

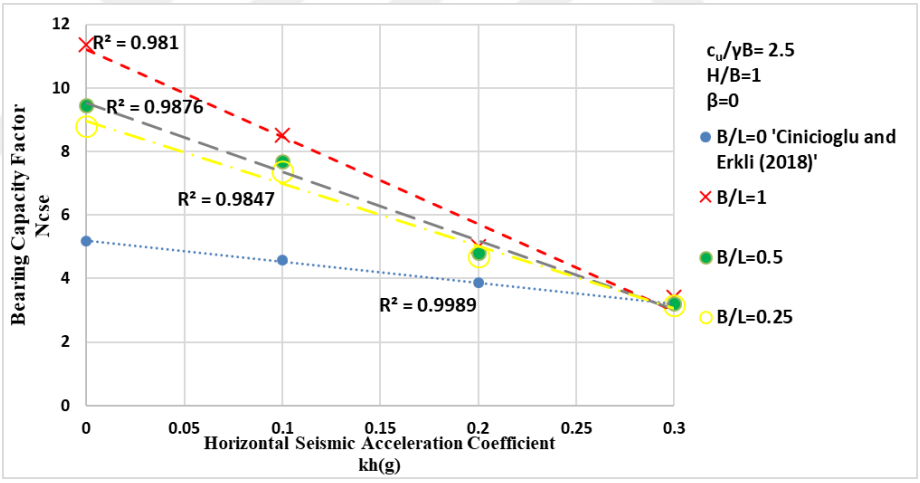


Figure 4.43. Variation of bearing capacity factor with horizontal seismic acceleration coefficient for $\beta=0^{o}$.

5. CONCLUSIONS

Recently, seismic bearing capacity of shallow foundations located on top of or near slopes has become one of the most critical issues for geotechnical designers and engineers. Numerical methods are more commonly used to solve different geotechnical problems. In this study, the finite element technique is used to evaluate the seismic bearing capacity of shallow footings on soil which provides Mohr-Coulomb soil criterion, for different slope angles, size of foundation and seismic coefficient. Therefore, the commercial available code, called Plaxis 3D, based on FEM is used for finite element examinations.

As a result of numerous analyses that were carried out with PLAXIS 3D, the effect of different influential parameters on the undrained seismic bearing capacity of shallow foundations has been investigated. In this study, different from these parameters, size effect plays an important role to draw the relationship between (N_{cse})–k_h. Therefore, seismic bearing capacity coefficient (N_{cse}) can be obtained by the design charts given in Chapter 4.3. All the design charts presented are the result of numerical models performed in this field study. As a conclusion of the assessments, it is observed that the issues given below were achieved.

- Seismic bearing capacity factor (N_{cse}) can be considered as a function of f (k_h ,β, $c_u/\gamma B$, H/B).
- The value of seismic bearing capacity coefficient drops drastically with the increase in horizontal seismic acceleration coefficient. Shape effect has become a minor impact on bearing capacity for the values greater than 0.3g.
- The increase in the slope angle (β) leads to a decrease in seismic bearing capacity factor.
- Due to the increase the in size of foundation (L) with relation to the shape effect and increase in the loading to the system, seismic bearing coefficient decreases.

- According to presented design charts, the slope of each line plotted in graph decreases with the increase in the *B/L* ratio. Likewise, zero intercept of each line decreases with the increase in *B/L* ratio as lineer.
- Three different failure mechanisms (foundation failure, base failure due to inertia effect and base failure due to gravity) were observed.
- For $c_u/\gamma B = 0.625$ and *H/B*=4, the correlation between seismic bearing capacity factor (N_{cse}) and horizontal seismic acceleration coefficient couldn't be drawn because the model failed to reach the final seismic bearing capacity for slope angles. This failure is called 'base failure due to gravity".
- Normalized slope soil strength ($c_u/\gamma B$) has a slight impact on seismic bearing capacity factor.
- *H/B* ratio has a small impact on seismic bearing capacity factor when the foundation failure occurs. Seismic bearing capacity factor (N_{cse}) raises with the decrease for smaller $c_u/\gamma B$ ratio values.
- According to accurate results of Plaxis 3D are larger than the results of Plaxis 2D. It should be kept in mind that there is a dimensional effect in Plaxis 3D while this effect completely is ignored in Plaxis 2D.

REFERENCES

AASHTO, 1996, *Standard Specifications for Highway Bridges*, American Association of State Highway and Transportation Officials, USA.

Bowles, J. E., 1996, *Foundation Analysis and Design*, McGraw-Hill, New York, USA.

Brinkgreve, R. B. J., W. Broere, and D. Waterman, 2006, *Plaxis User's Manual*, Plaxis B. V., Delft, Netherlands.

Castelli, F, and E. Motta, 2010, "Bearing Capacity of Strip Footings Near Slopes" *Geotech Geol Eng*., Vol. 28, pp. 187-198.

Cinicioglu O, and A. Erkli, 2018, “Seismic Bearing Capacity of Surficial Foundations Onsloping Cohesive Ground”, *Soil Dynamics and Earthquake Engineering*, Vol.111, pp. 53-64.

Das, B. M., 2010, *Principles of Geotechnical Engineering*, 7th Edition, Cengage Learning, Stamford.

Das, B. M., and G. V. Ramana, 2011, *Principles of Soil Dymamics*, 2nd Edition, Cengage Leaming, Stamford.

Day, R. W., 2002, *Geotechnical Earthquake Engineering Handbook*, McGraw Hill Professional, New York, USA.

Erkli, A., and O Çinicioğlu, 2012, "Kohezyonlu Sevlerin Üzerindeki Yüzeysel Şerit Temellerin Sismik Taşıma Gücü", *Zemin Mekaniği ve Temel Muhendisliği 14. Ulusal Kongresi*, Isparta.

Farzaneh, O, J. Mofidi, and F. Askari, 2013, "Seismic Bearing Capacity of Strip Footings near Cohesive Slopes Using Lower Bound Limit Analysis", *Proceedings of the 18th International Conference on Soil Mechanies and Geotechnical Engineering*, Paris, pp. 1467-1470.

Georgiadis, K., 2010, "Undrained Bearing Capacity of Strip Footings on Slopes", *Journal of Geotechnical and Geoenviromental Engineering*, Vol. 136, No. 5, pp. 677-685.

Hansen, J. B., 1961, "A General Formula for Bearing Capacity". *Danish Geotechnical Institute Bulletin 11, Copenhagen,* Denmark, pp.38-46.

Islam, M. S., M. Rokonuzzaman, and T. Sakai, 2017, "Shape Effect of Square and Circular Footing under Vertical Loading: Experimental and Numerical Studies", *International Journal of Geomechanics*, Vol.17, No.9, pp. 1-9.

Keshavarz, A., M. Beygi, and R. Vali, 2019, "Undrained Seismic Bearing Capacity of Strip Footing Placed on Homogeneous and Heterogeneous Soil Slopes by Finite Element Limit Analysis", *Computers and Geotechnics*, Vol.113, pp. 1-13.

Koppula, S. D, 1984, "On Stability of Slopes on Clays with Linearly Increasing Strength", *Canadian Geotechnical Journal*, Vol. 21, No. 3, pp. 557-581.

Kramer, S. L., 1996, *Geotechnical Earthquake Engineering,* Prentice Hall, New Jersey.

Kumar, J., and M. Rao, 2003, "Seismic Bearing Capacity of Foundations on Slopes", *Geotechnique*, Vol. 53, No.3, pp. 347-361.

Kusakabe, O., T. Kimura, and H. Yamaguchi, 1981, "Bearing Capacity of Slopes under Strip Loads on the Top Surfaces", *Soils and Foundations,* Vol. 21, No. 4, pp. 29-40.

Li, J.-P., L.-Y. Chen, and F.Y. Liang, 2009, "Effect of Footing Shape on Bearing Capacity of Rectangular Footings", *International Foundation Congress and Equipment Expo*, Orlando, Florida, United States.

Merlos, J., and M. P. Romo, 2006, "Fluctuant Bearing Capacity of Shallow Foundations During Earthquakes", *Soil Dynamics and Earthquake Engineering*, Vol. 26, pp. 103-114

Meyerhof, G. G., 1957, "The Ultimate Bearing Capacity of Foundation on Slopes", *Proceedings of the Fourth International Conference on Soil Mechanics*, London, pp. 384-386.

Pathak, S. R., S. N. Kamat, and D. R. Phatak, 2008, "Study of Behaviour of Square and Rectangular Footings Resting on Cohesive Soils Based on Model Tests", *International Conference on Case Histories in Geotechnical Engineering*, p.31.

Potts, D. M., and L. Zdravkovic, 1999, *Finite Element Analysis in Geotechnical Engineering: Theory*, Thomas Telford, London.

Potts, D. M., and L. Zdravkovic, 2001, *Finite Element Analysis in Geotechnical Engineering:* Application, Thomas Telford, London.

Potts, D. M., K. Axelsson, L. Grande, H. Scheweiger, and M. Long, 2002, *Guidelines for the Use of Advanced Numerical Analysis*, Thomas Telford, London.

Prandtl, L., 1920, "Uber die Harte Plastischer Korper", *Nachrichten von der Koniglichen Gesellschaft der Wissenschaften*, Gottingen, Math. Phys., Klasse, pp. 74-85.

Salgado, R., A. V. Lyamin, S. W. Sloan, and H. S. Yu, 2004, “Two and Three Dimensional Bearing Capacity of Foundations in Clay.” *Geotechnique*, Vol. 54 No.5, pp. 297-306.

Shiau, J., A. Lyamin, and S. Sloan, 2006, "Application of Pseudo-Static Limit Analysis in Geotechnical Earthquake Design", *Numerical Methods in Geotechnical Engineering-Schweiger (ed),* Taylor&Francis Group, LLC., London.

Shiau, J., R. S. Merifield, A. V. Lyamin, and S. Sloan, 2011, “Undrained Stability of Footings on Slopes”, *International Journal of Geomechanics*, Vol.11, pp. 381-390.

Skempton, A. W., 1951, "The Bearing Capacity of Clays", *Building Research Congress*, London, pp. 180-189.

Sloan, S. W., 1988, "Lower Bound Limit Analysis Using Finite Elements and Linear Programming", *International Journal for Numerical and Analytical Methods in Geomechanics*, Vol. 12, pp. 61-67.

Taiebat, H. A., and J. P. Carter, 2008, "Flow Rule Effects in the Tresca Model", *Computers and Geotechnics*, Vol. 35, pp. 500-503.

Taylor, D. W., 1937, "Stability of Earth Slopes", *Journal of the Boston Society of Civil Engineers*, Vol. 24, pp. 197-246.

Terzaghi, K., 1943, *Theoretical Soil Mechanics*, John Wiley& Sons, Inc., New York, USA.

U.S. Army Corps of Engineers, 1995, *Engineering and Design: Geotechnical Analysis by The Finite Element Method*, Washington, DC.

Vesic, A.S., 1975, *Foundation Engineering Handbook*, H.F. Winterkorn and H. Y Fang, eds., Van Nostrand Reinhold, New York, USA.

Washington State Department of Transportation, 2005, *Geotechnical Design Manual*, Washington, DC.

Yamamoto, K., 2010 “Seismic Bearing Capacity of Shallow Foundations near Slopes Using the Upper-Bound Method’’, I*nternational Journal of Geotechnical Engineering*, Vol. 4, No. 2, pp. 255-267.

Yang, H., Z. Shen, and J. Wang, 2003, “3D Lower Bound Bearing Capacity of Smooth Rectangular Surface Footings”, *Mechanics Research Communications*, Vol.30, No.5, pp. 481-492.

Yu, L., J. Liu, X.-J. Kong, and Y. Hu, M. ASCE, 2011, “Three-dimensional Large Deformation FE Analysis of Square Footings in Two-Layered Clays”, *Journal of Geotechnical and Geoenvironmental Engineering*, Vol.137, No.1, pp. 52-58.

Zhu, M., and R. L. Michalowski, 2005, “Shape Factors For Limit Loads on Square and Rectangular Footings”, *Journal of Geotechnical and Geoenvironmental Engineering*, Vol.131, No.2, pp. 223–231.

APPENDIX A: LIST OF RESULTS OF FINITE ELEMENTS MODELS CREATED FOR STATIC CONDITION

List of results for finite element models created for static condition is given in Table A.1, Table A.2 and Table A.3.

Table A.1. List of results of finite elements models created for static condition (β= 15°).

Model No.	GEOTECHNICAL PROPERTIES					SLOPE SOIL PROPERTIES				SEISMIC EFFECT	FILE NAME	ANALYSIS RESULTS FOR STATIC LOADING							
	β (°)	H (m)	λ	B (m)	L (m)	γ (kN/m³)	c_u (kN/m³)	ϕ_u (°)	E_u (kPa)	ν_u	k_h		H/B	β (°)	Load	M stage	q_f (kPa)	N_{cs}	cu/γB	Failure Mode
1	0	2	0	2	2	20	100	0	20000	0,35	0	C_0_2_0_2_100_S	1	0	2000	0,5688	1138	11,376	2,5	Foundation Failure
2	0	2	0	2	4	20	100	0	20000	0,35	0	C_0_2_0_4_100_S	1	0	2000	0,4724	945	9,448	2,5	Foundation Failure
3	0	2	0	2	8	20	100	0	20000	0,35	0	C_0_2_0_8_100_S	1	0	2000	0,4396	879	8,792	2,5	Foundation Failure
4	0	2	0	2	16	20	100	0	20000	0,35	0	C_0_2_0_16_100_S	1	0	2000	0,3882	776	7,764	2,5	Foundation Failure
5	15	2	0	2	2	20	25	0	5000	0,35	0	C_15_2_0_2_25_S	1	15	300	0,7768	233,04	9	0,63	Foundation Failure
6	15	4	0	2	2	20	25	0	5000	0,35	0	C_15_4_0_2_25_S	2	15	300	0,7066	212	8,48	0,63	Foundation Failure
7	15	8	0	2	2	20	25	0	5000	0,35	0	C_15_8_0_2_25_S	4	15	200	N.F.	N.F.	N.F.	0,63	Base failure_GR
8	15	2	0	2	4	20	25	0	5000	0,35	0	C_15_2_0_4_25_S	1	15	300	0,6788	204	8,15	0,63	Foundation Failure
9	15	4	0	2	4	20	25	0	5000	0,35	0	C_15_4_0_4_25_S	2	15	300	0,7219	217	8,66	0,63	Foundation Failure
10	15	8	0	2	4	20	25	0	5000	0,35	0	C_15_8_0_4_25_S	4	15	200	N.F.	N.F.	N.F.	0,63	Base failure_GR
11	15	2	0	2	8	20	25	0	5000	0,35	0	C_15_2_0_8_25_S	1	15	200	0,9542	191	7,63	0,63	Foundation Failure
12	15	4	0	2	8	20	25	0	5000	0,35	0	C_15_4_0_8_25_S	2	15	200	0,9704	194	7,76	0,63	Foundation Failure
13	15	8	0	2	8	20	25	0	5000	0,35	0	C_15_8_0_8_25_S	4	15	200	N.F.	N.F.	N.F.	0,63	Base failure_GR
14	15	2	0	2	16	20	25	0	5000	0,35	0	C_15_2_0_16_25_S	1	15	300	0,6834	205	8,20	0,63	Foundation Failure
15	15	4	0	2	16	20	25	0	5000	0,35	0	C_15_4_0_16_25_S	2	15	200	0,9823	196	7,86	0,63	Foundation Failure
16	15	8	0	2	16	20	25	0	5000	0,35	0	C_15_8_0_16_25_S	4	15	200	N.F.	N.F.	N.F.	0,63	Base failure_GR
17	15	2	0	2	2	20	50	0	10000	0,35	0	C_15_2_0_2_50_S	1	15	600	0,7868	472	9,44	1,25	Foundation Failure
18	15	4	0	2	2	20	50	0	10000	0,35	0	C_15_4_0_2_50_S	2	15	600	0,7377	443	8,85	1,25	Foundation Failure
19	15	8	0	2	2	20	50	0	10000	0,35	0	C_15_8_0_2_50_S	4	15	600	0,6798	408	8,16	1,25	Foundation Failure
20	15	2	0	2	4	20	50	0	10000	0,35	0	C_15_2_0_4_50_S	1	15	600	0,6944	417	8,33	1,25	Foundation Failure
21	15	4	0	2	4	20	50	0	10000	0,35	0	C_15_4_0_4_50_S	2	15	600	0,7376	443	8,85	1,25	Foundation Failure
22	15	8	0	2	4	20	50	0	10000	0,35	0	C_15_8_0_4_50_S	4	15	600	0,7661	460	9,19	1,25	Foundation Failure
23	15	2	0	2	8	20	50	0	10000	0,35	0	C_15_2_0_8_50_S	1	15	400	0,9781	391	7,82	1,25	Foundation Failure
24	15	4	0	2	8	20	50	0	10000	0,35	0	C_15_4_0_8_50_S	2	15	400	0,9866	395	7,89	1,25	Foundation Failure
25	15	8	0	2	8	20	50	0	10000	0,35	0	C_15_8_0_8_50_S	4	15	600	0,7535	452	9,04	1,25	Foundation Failure
26	15	2	0	2	16	20	50	0	10000	0,35	0	C_15_2_0_16_50_S	1	15	600	0,708	425	8,50	1,25	Foundation Failure
27	15	4	0	2	16	20	50	0	10000	0,35	0	C_15_4_0_16_50_S	2	15	600	0,6711	403	8,05	1,25	Foundation Failure
28	15	8	0	2	16	20	50	0	10000	0,35	0	C_15_8_0_16_50_S	4	15	400	0,9295	372	7,44	1,25	Foundation Failure
29	15	2	0	2	2	20	100	0	20000	0,35	0	C_15_2_0_2_100_S	1	15	1000	0,9451	945	9,45	2,50	Foundation Failure
30	15	4	0	2	2	20	100	0	20000	0,35	0	C_15_4_0_2_100_S	2	15	1000	0,8702	870	8,70	2,50	Foundation Failure
31	15	8	0	2	2	20	100	0	20000	0,35	0	C_15_8_0_2_100_S	4	15	1200	0,8366	1004	10,04	2,50	Foundation Failure
32	15	2	0	2	4	20	100	0	20000	0,35	0	C_15_2_0_4_100_S	1	15	1000	0,8398	840	8,40	2,50	Foundation Failure
33	15	4	0	2	4	20	100	0	20000	0,35	0	C_15_4_0_4_100_S	2	15	800	0,9933	795	7,95	2,50	Foundation Failure
34	15	8	0	2	4	20	100	0	20000	0,35	0	C_15_8_0_4_100_S	4	15	1000	0,9357	936	9,36	2,50	Foundation Failure
35	15	2	0	2	8	20	100	0	20000	0,35	0	C_15_2_0_8_100_S	1	15	800	0,9875	790	7,90	2,50	Foundation Failure
36	15	4	0	2	8	20	100	0	20000	0,35	0	C_15_4_0_8_100_S	2	15	800	0,8912	713	7,13	2,50	Foundation Failure
37	15	8	0	2	8	20	100	0	20000	0,35	0	C_15_8_0_8_100_S	4	15	1000	0,9109	911	9,11	2,50	Foundation Failure
38	15	2	0	2	16	20	100	0	20000	0,35	0	C_15_2_0_16_100_S	1	15	1000	0,8629	863	8,63	2,50	Foundation Failure
39	15	4	0	2	16	20	100	0	20000	0,35	0	C_15_4_0_16_100_S	2	15	1000	0,8151	815	8,15	2,50	Foundation Failure
40	15	8	0	2	16	20	100	0	20000	0,35	0	C_15_8_0_16_100_S	4	15	800	0,9425	754	7,54	2,50	Foundation Failure
41	15	2	0	2	2	20	200	0	40000	0,35	0	C_15_2_0_2_200_S	1	15	2000	0,949	1898	9,49	5,00	Foundation Failure
42	15	4	0	2	2	20	200	0	40000	0,35	0	C_15_4_0_2_200_S	2	15	2000	0,8954	1791	8,95	5,00	Foundation Failure
43	15	8	0	2	2	20	200	0	40000	0,35	0	C_15_8_0_2_200_S	4	15	2200	0,9304	2047	10,23	5,00	Foundation Failure
44	15	2	0	2	4	20	200	0	40000	0,35	0	C_15_2_0_4_200_S	1	15	2000	0,841	1682	8,41	5,00	Foundation Failure
45	15	4	0	2	4	20	200	0	40000	0,35	0	C_15_4_0_4_200_S	2	15	2000	0,8843	1769	8,84	5,00	Foundation Failure
46	15	8	0	2	4	20	200	0	40000	0,35	0	C_15_8_0_4_200_S	4	15	2000	0,942	1884	9,42	5,00	Foundation Failure
47	15	2	0	2	8	20	200	0	40000	0,35	0	C_15_2_0_8_200_S	1	15	1600	0,9923	1588	7,94	5,00	Foundation Failure
48	15	4	0	2	8	20	200	0	40000	0,35	0	C_15_4_0_8_200_S	2	15	1600	0,9898	1584	7,92	5,00	Foundation Failure
49	15	8	0	2	8	20	200	0	40000	0,35	0	C_15_8_0_8_200_S	4	15	2000	0,9142	1828	9,14	5,00	Foundation Failure
50	15	2	0	2	16	20	200	0	40000	0,35	0	C_15_2_0_16_200_S	1	15	2000	0,8697	1739	8,70	5,00	Foundation Failure
51	15	4	0	2	16	20	200	0	40000	0,35	0	C_15_4_0_16_200_S	2	15	2000	0,8131	1626	8,13	5,00	Foundation Failure
52	15	8	0	2	16	20	200	0	40000	0,35	0	C_15_8_0_16_200_S	4	15	1600	0,9525	1524	7,62	5,00	Foundation Failure

N.F. :Not found.
Base failire_EQ:Failed due to earthquake.
Base failire_GR:Failed due to gravity.

Table A.2. List of results of finite elements models created for static condition (β= 30°).

Model No.	GEOTECHNICAL PROPERTIES					SLOPE SOIL PROPERTIES					SEISMIC EFFECT	FILE NAME	ANALYSIS RESULTS FOR STATIC LOADING							
	β (°)	H (m)	λ	B (m)	L (m)	γ (kN/m^3)	c_u (kN/m^3)	ϕ_u (°)	E_u (kPa)	ν_u	k_h		H/B	β (°)	Load	Mstage	q_f (kPa)	N_{cs}	cu/γB	Failure Mode
1	30	2	0	2	2	20	25	0	5000	0,35	0	C_30_2_0_2_25_S	1	30	200	0,8803	176	7,04	0,63	Foundation Failure
2	30	4	0	2	2	20	25	0	5000	0,35	0	C_30_4_0_2_25_S	2	30	200	0,9814	196	7,85	0,63	Foundation Failure
3	30	8	0	2	2	20	25	0	5000	0,35	0	C_30_8_0_2_25_S	4	30	200	N.F.	N.F.	N.F.	0,63	Base failure_GR
4	30	2	0	2	4	20	25	0	5000	0,35	0	C_30_2_0_4_25_S	1	30	200	0,8492	170	6,79	0,63	Foundation Failure
5	30	4	0	2	4	20	25	0	5000	0,35	0	C_30_4_0_4_25_S	2	30	200	0,8364	167	6,69	0,63	Foundation Failure
6	30	8	0	2	4	20	25	0	5000	0,35	0	C_30_8_0_4_25_S	4	30	200	N.F.	N.F.	N.F.	0,63	Base failure_GR
7	30	2	0	2	8	20	25	0	5000	0,35	0	C_30_2_0_8_25_S	1	30	200	0,7098	142	5,68	0,63	Foundation Failure
8	30	4	0	2	8	20	25	0	5000	0,35	0	C_30_4_0_8_25_S	2	30	200	0,6929	139	5,54	0,63	Foundation Failure
9	30	8	0	2	8	20	25	0	5000	0,35	0	C_30_8_0_8_25_S	4	30	200	N.F.	N.F.	N.F.	0,63	Base failure_GR
10	30	2	0	2	16	20	25	0	5000	0,35	0	C_30_2_0_16_25_S	1	30	200	0,7457	149	5,97	0,63	Foundation Failure
11	30	4	0	2	16	20	25	0	5000	0,35	0	C_30_4_0_16_25_S	2	30	200	0,7173	143	5,74	0,63	Foundation Failure
12	30	8	0	2	16	20	25	0	5000	0,35	0	C_30_8_0_16_25_S	4	30	200	N.F.	N.F.	N.F.	0,63	Base failure_GR
13	30	2	0	2	2	20	50	0	10000	0,35	0	C_30_2_0_2_50_S	1	30	400	0,8968	359	7,17	1,25	Foundation Failure
14	30	4	0	2	2	20	50	0	10000	0,35	0	C_30_4_0_2_50_S	2	30	600	0,6725	404	8,07	1,25	Foundation Failure
15	30	8	0	2	2	20	50	0	10000	0,35	0	C_30_8_0_2_50_S	4	30	400	0,9838	394	7,87	1,25	Foundation Failure
16	30	2	0	2	4	20	50	0	10000	0,35	0	C_30_2_0_4_50_S	1	30	400	0,891	356	7,13	1,25	Foundation Failure
17	30	4	0	2	4	20	50	0	10000	0,35	0	C_30_4_0_4_50_S	2	30	400	0,88	352	7,04	1,25	Foundation Failure
18	30	8	0	2	4	20	50	0	10000	0,35	0	C_30_8_0_4_50_S	4	30	400	0,7474	299	5,98	1,25	Foundation Failure
19	30	2	0	2	8	20	50	0	10000	0,35	0	C_30_2_0_8_50_S	1	30	400	0,7432	297	5,95	1,25	Foundation Failure
20	30	4	0	2	8	20	50	0	10000	0,35	0	C_30_4_0_8_50_S	2	30	400	0,7309	292	5,85	1,25	Foundation Failure
21	30	8	0	2	8	20	50	0	10000	0,35	0	C_30_8_0_8_50_S	4	30	400	0,7146	286	5,72	1,25	Foundation Failure
22	30	2	0	2	16	20	50	0	10000	0,35	0	C_30_2_0_16_50_S	1	30	400	0,78	312	6,24	1,25	Foundation Failure
23	30	4	0	2	16	20	50	0	10000	0,35	0	C_30_4_0_16_50_S	2	30	400	0,7637	305	6,11	1,25	Foundation Failure
24	30	8	0	2	16	20	50	0	10000	0,35	0	C_30_8_0_16_50_S	4	30	400	0,7974	319	6,38	1,25	Foundation Failure
25	30	2	0	2	2	20	100	0	20000	0,35	0	C_30_2_0_2_100_S	1	30	800	0,9121	730	7,30	2,50	Foundation Failure
26	30	4	0	2	2	20	100	0	20000	0,35	0	C_30_4_0_2_100_S	2	30	1000	0,8181	818	8,18	2,50	Foundation Failure
27	30	8	0	2	2	20	100	0	20000	0,35	0	C_30_8_0_2_100_S	4	30	800	0,9924	794	7,94	2,50	Foundation Failure
28	30	2	0	2	4	20	100	0	20000	0,35	0	C_30_2_0_4_100_S	1	30	800	0,904	723	7,23	2,50	Foundation Failure
29	30	4	0	2	4	20	100	0	20000	0,35	0	C_30_4_0_4_100_S	2	30	800	0,903	722	7,22	2,50	Foundation Failure
30	30	8	0	2	4	20	100	0	20000	0,35	0	C_30_8_0_4_100_S	4	30	800	0,8033	643	6,43	2,50	Foundation Failure
31	30	2	0	2	8	20	100	0	20000	0,35	0	C_30_2_0_8_100_S	1	30	800	0,758	606	6,06	2,50	Foundation Failure
32	30	4	0	2	8	20	100	0	20000	0,35	0	C_30_4_0_8_100_S	2	30	800	0,749	599	5,99	2,50	Foundation Failure
33	30	8	0	2	8	20	100	0	20000	0,35	0	C_30_8_0_8_100_S	4	30	800	0,7289	583	5,83	2,50	Foundation Failure
34	30	2	0	2	16	20	100	0	20000	0,35	0	C_30_2_0_16_100_S	1	30	800	0,8053	644	6,44	2,50	Foundation Failure
35	30	4	0	2	16	20	100	0	20000	0,35	0	C_30_4_0_16_100_S	2	30	800	0,7815	625	6,25	2,50	Foundation Failure
36	30	8	0	2	16	20	100	0	20000	0,35	0	C_30_8_0_16_100_S	4	30	800	0,8204	656	6,56	2,50	Foundation Failure
37	30	2	0	2	2	20	200	0	40000	0,35	0	C_30_2_0_2_200_S	1	30	1600	0,9236	1478	7,39	5,00	Foundation Failure
38	30	4	0	2	2	20	200	0	40000	0,35	0	C_30_4_0_2_200_S	2	30	2000	0,824	1648	8,24	5,00	Foundation Failure
39	30	8	0	2	2	20	200	0	40000	0,35	0	C_30_8_0_2_200_S	4	30	1600	0,9955	1593	7,96	5,00	Foundation Failure
40	30	2	0	2	4	20	200	0	40000	0,35	0	C_30_2_0_4_200_S	1	30	1600	0,9061	1450	7,25	5,00	Foundation Failure
41	30	4	0	2	4	20	200	0	40000	0,35	0	C_30_4_0_4_200_S	2	30	1600	0,912	1459	7,30	5,00	Foundation Failure
42	30	8	0	2	4	20	200	0	40000	0,35	0	C_30_8_0_4_200_S	4	30	1600	0,8075	1292	6,46	5,00	Foundation Failure
43	30	2	0	2	8	20	200	0	40000	0,35	0	C_30_2_0_8_200_S	1	30	1600	0,7642	1223	6,11	5,00	Foundation Failure
44	30	4	0	2	8	20	200	0	40000	0,35	0	C_30_4_0_8_200_S	2	30	1600	0,7564	1210	6,05	5,00	Foundation Failure
45	30	8	0	2	8	20	200	0	40000	0,35	0	C_30_8_0_8_200_S	4	30	1600	0,7359	1177	5,89	5,00	Foundation Failure
46	30	2	0	2	16	20	200	0	40000	0,35	0	C_30_2_0_16_200_S	1	30	1600	0,8148	1304	6,52	5,00	Foundation Failure
47	30	4	0	2	16	20	200	0	40000	0,35	0	C_30_4_0_16_200_S	2	30	1600	0,7919	1267	6,34	5,00	Foundation Failure
48	30	8	0	2	16	20	200	0	40000	0,35	0	C_30_8_0_16_200_S	4	30	1600	0,8306	1329	6,64	5,00	Foundation Failure

N.F. :Not found.
Base failıre_EQ:Failed due to earthquake.
Base failıre_GR:Failed due to gravity.

Table A.3. List of results of finite elements models created for static condition (β= 45°).

Model No.	GEOTECHNICAL PROPERTIES					SLOPE SOIL PROPERTIES					SEISMIC EFFECT	FILE NAME	ANALYSIS RESULTS FOR STATIC LOADING							
	β (°)	H (m)	λ	B (m)	L (m)	γ (kN/m³)	c_u (kN/m³)	ϕ_u (°)	E_u (kPa)	v_u	k_h		H/B	β (°)	Load	Mstage	q_f (kPa)	N_{cs}	cu/γB	Failure Mode
1	45	2	0	2	2	20	25	0	5000	0,35	0	C_45_2_0_2_25_S	1	45	200	0,8246	165	6,60	0,63	Foundation Failure
2	45	4	0	2	2	20	25	0	5000	0,35	0	C_45_4_0_2_25_S	2	45	200	0,8129	163	6,50	0,63	Foundation Failure
3	45	8	0	2	2	20	25	0	5000	0,35	0	C_45_8_0_2_25_S	4	45	200	N.F.	N.F.	N.F.	0,63	Base failure_GR
4	45	2	0	2	4	20	25	0	5000	0,35	0	C_45_2_0_4_25_S	1	45	200	0,6571	131	5,26	0,63	Foundation Failure
5	45	4	0	2	4	20	25	0	5000	0,35	0	C_45_4_0_4_25_S	2	45	200	0,6409	128	5,13	0,63	Foundation Failure
6	45	8	0	2	4	20	25	0	5000	0,35	0	C_45_8_0_4_25_S	4	45	200	N.F.	N.F.	N.F.	0,63	Base failure_GR
7	45	2	0	2	8	20	25	0	5000	0,35	0	C_45_2_0_8_25_S	1	45	200	0,616	123	4,93	0,63	Foundation Failure
8	45	4	0	2	8	20	25	0	5000	0,35	0	C_45_4_0_8_25_S	2	45	200	0,5952	119	4,76	0,63	Foundation Failure
9	45	8	0	2	8	20	25	0	5000	0,35	0	C_45_8_0_8_25_S	4	45	200	N.F.	N.F.	N.F.	0,63	Base failure_GR
10	45	2	0	2	16	20	25	0	5000	0,35	0	C_45_2_0_16_25_S	1	45	200	0,6716	134	5,37	0,63	Foundation Failure
11	45	4	0	2	16	20	25	0	5000	0,35	0	C_45_4_0_16_25_S	2	45	200	0,561	112	4,49	0,63	Foundation Failure
12	45	8	0	2	16	20	25	0	5000	0,35	0	C_45_8_0_16_25_S	4	45	200	N.F.	N.F.	N.F.	0,63	Base failure_GR
13	45	2	0	2	2	20	50	0	10000	0,35	0	C_45_2_0_2_50_S	1	45	400	0,8655	346	6,92	1,25	Foundation Failure
14	45	4	0	2	2	20	50	0	10000	0,35	0	C_45_4_0_2_50_S	2	45	400	0,8562	342	6,85	1,25	Foundation Failure
15	45	8	0	2	2	20	50	0	10000	0,35	0	C_45_8_0_2_50_S	4	45	400	0,8425	337	6,74	1,25	Foundation Failure
16	45	2	0	2	4	20	50	0	10000	0,35	0	C_45_2_0_4_50_S	1	45	400	0,7013	281	5,61	1,25	Foundation Failure
17	45	4	0	2	4	20	50	0	10000	0,35	0	C_45_4_0_4_50_S	2	45	400	0,6905	276	5,52	1,25	Foundation Failure
18	45	8	0	2	4	20	50	0	10000	0,35	0	C_45_8_0_4_50_S	4	45	400	0,8303	332	6,64	1,25	Foundation Failure
19	45	2	0	2	8	20	50	0	10000	0,35	0	C_45_2_0_8_50_S	1	45	400	0,6529	261	5,22	1,25	Foundation Failure
20	45	4	0	2	8	20	50	0	10000	0,35	0	C_45_4_0_8_50_S	2	45	400	0,6333	253	5,07	1,25	Foundation Failure
21	45	8	0	2	8	20	50	0	10000	0,35	0	C_45_8_0_8_50_S	4	45	400	0,7009	280	5,61	1,25	Foundation Failure
22	45	2	0	2	16	20	50	0	10000	0,35	0	C_45_2_0_16_50_S	1	45	400	0,7254	290	5,80	1,25	Foundation Failure
23	45	4	0	2	16	20	50	0	10000	0,35	0	C_45_4_0_16_50_S	2	45	400	0,6533	261	5,23	1,25	Foundation Failure
24	45	8	0	2	16	20	50	0	10000	0,35	0	C_45_8_0_16_50_S	4	45	400	0,6899	276	5,52	1,25	Foundation Failure
25	45	2	0	2	2	20	100	0	20000	0,35	0	C_45_2_0_2_100_S	1	45	800	0,8836	707	7,07	2,50	Foundation Failure
26	45	4	0	2	2	20	100	0	20000	0,35	0	C_45_4_0_2_100_S	2	45	800	0,8729	698	6,98	2,50	Foundation Failure
27	45	8	0	2	2	20	100	0	20000	0,35	0	C_45_8_0_2_100_S	4	45	800	0,8616	689	6,89	2,50	Foundation Failure
28	45	2	0	2	4	20	100	0	20000	0,35	0	C_45_2_0_4_100_S	1	45	800	0,7236	579	5,79	2,50	Foundation Failure
29	45	4	0	2	4	20	100	0	20000	0,35	0	C_45_4_0_4_100_S	2	45	800	0,7113	569	5,69	2,50	Foundation Failure
30	45	8	0	2	4	20	100	0	20000	0,35	0	C_45_8_0_4_100_S	4	45	800	0,8498	680	6,80	2,50	Foundation Failure
31	45	2	0	2	8	20	100	0	20000	0,35	0	C_45_2_0_8_100_S	1	45	800	0,6726	538	5,38	2,50	Foundation Failure
32	45	4	0	2	8	20	100	0	20000	0,35	0	C_45_4_0_8_100_S	2	45	800	0,6487	519	5,19	2,50	Foundation Failure
33	45	8	0	2	8	20	100	0	20000	0,35	0	C_45_8_0_8_100_S	4	45	800	0,7212	577	5,77	2,50	Foundation Failure
34	45	2	0	2	16	20	100	0	20000	0,35	0	C_45_2_0_16_100_S	1	45	800	0,7419	594	5,94	2,50	Foundation Failure
35	45	4	0	2	16	20	100	0	20000	0,35	0	C_45_4_0_16_100_S	2	45	800	0,692	554	5,54	2,50	Foundation Failure
36	45	8	0	2	16	20	100	0	20000	0,35	0	C_45_8_0_16_100_S	4	45	800	0,7267	581	5,81	2,50	Foundation Failure
37	45	2	0	2	2	20	200	0	40000	0,35	0	C_45_2_0_2_200_S	1	45	1600	0,892	1427	7,14	5,00	Foundation Failure
38	45	4	0	2	2	20	200	0	40000	0,35	0	C_45_4_0_2_200_S	2	45	1600	0,8874	1420	7,10	5,00	Foundation Failure
39	45	8	0	2	2	20	200	0	40000	0,35	0	C_45_8_0_2_200_S	4	45	1600	0,8705	1393	6,96	5,00	Foundation Failure
40	45	2	0	2	4	20	200	0	40000	0,35	0	C_45_2_0_4_200_S	1	45	1600	0,7341	1175	5,87	5,00	Foundation Failure
41	45	4	0	2	4	20	200	0	40000	0,35	0	C_45_4_0_4_200_S	2	45	1600	0,7208	1153	5,77	5,00	Foundation Failure
42	45	8	0	2	4	20	200	0	40000	0,35	0	C_45_8_0_4_200_S	4	45	1600	0,8505	1361	6,80	5,00	Foundation Failure
43	45	2	0	2	8	20	200	0	40000	0,35	0	C_45_2_0_8_200_S	1	45	1600	0,6814	1090	5,45	5,00	Foundation Failure
44	45	4	0	2	8	20	200	0	40000	0,35	0	C_45_4_0_8_200_S	2	45	1600	0,6632	1061	5,31	5,00	Foundation Failure
45	45	8	0	2	8	20	200	0	40000	0,35	0	C_45_8_0_8_200_S	4	45	1600	0,849	1358	6,79	5,00	Foundation Failure
46	45	2	0	2	16	20	200	0	40000	0,35	0	C_45_2_0_16_200_S	1	45	1600	0,7616	1219	6,09	5,00	Foundation Failure
47	45	4	0	2	16	20	200	0	40000	0,35	0	C_45_4_0_16_200_S	2	45	1600	0,7091	1135	5,67	5,00	Foundation Failure
48	45	8	0	2	16	20	200	0	40000	0,35	0	C_45_8_0_16_200_S	4	45	1600	0,7377	1180	5,90	5,00	Foundation Failure

N.F. :Not found.
Base failure_EQ:Failed due to earthquake.
Base failure_GR:Failed due to gravity.

APPENDIX B: LIST OF RESULTS OF FINITE ELEMENTS MODELS CREATED FOR SEISMIC CONDITION

List of results for finite element models created for seismic condition is given in Table B.1, Table B.2 and Table B.3.

Table B.1. List of results of finite elements models created for seismic condition (β= 15°).

Model No.	GEOTECHNICAL PROPERTIES					SLOPE SOIL PROPERTIES				SEISMIC EFFECT	FILE NAME	ANALYSIS RESULTS FOR SEISMIC LOADING							
	β (°)	H (m)	λ	B (m)	L (m)	γ (kN/m³)	c_u (kN/m²)	ϕ_u (°)	E_u (kPa)	v_u	k_h		H/B	β (°)	Load	Ms tage	q_f (kPa)	N_s	cu/γB	Failure Mode
1	0	2	0	2	2	20	100	0	20000	0,35	0,1	C_0_2_0_2_100_0.1_D	1	0	2000	0,4261	852,2	8,522	2,5	Foundation Failure
2	0	2	0	2	4	20	100	0	20000	0,35	0,1	C_0_2_0_4_100_0.1_D	1	0	2000	0,3841	768,2	7,682	2,5	Foundation Failure
3	0	2	0	2	8	20	100	0	20000	0,35	0,1	C_0_2_0_8_100_0.1_D	1	0	2000	0,3688	737,6	7,376	2,5	Foundation Failure
4	0	2	0	2	16	20	100	0	20000	0,35	0,1	C_0_2_0_16_100_0.1_D	1	0	2000	0,3574	714,8	7,148	2,5	Foundation Failure
5	15	2	0	2	2	20	25	0	5000	0,35	0,1	C_15_2_0_2_25_0.1_D	1	15	200	0,9611	192,22	7,69	0,63	Base failure_EQ
6	15	4	0	2	2	20	25	0	5000	0,35	0,1	C_15_4_0_2_25_0.1_D	2	15	200	0,4968	99,36	3,97	0,63	Base failure_EQ
7	15	8	0	2	2	20	25	0	5000	0,35	0,1	C_15_8_0_2_25_0.1_D	4	15	200	N.F.	N.F.	N.F.	0,63	Base failure_GR
8	15	2	0	2	4	20	25	0	5000	0,35	0,1	C_15_2_0_4_25_0.1_D	1	15	200	0,9605	192,1	7,68	0,63	Base failure_EQ
9	15	4	0	2	4	20	25	0	5000	0,35	0,1	C_15_4_0_4_25_0.1_D	2	15	200	0,4976	99,52	3,98	0,63	Base failure_EQ
10	15	8	0	2	4	20	25	0	5000	0,35	0,1	C_15_8_0_4_25_0.1_D	4	15	200	N.F.	N.F.	N.F.	0,63	Base failure_GR
11	15	2	0	2	8	20	25	0	5000	0,35	0,1	C_15_2_0_8_25_0.1_D	1	15	200	0,6932	138,64	5,55	0,63	Foundation Failure
12	15	4	0	2	8	20	25	0	5000	0,35	0,1	C_15_4_0_8_25_0.1_D	2	15	200	0,5037	100,74	4,03	0,63	Base failure_EQ
13	15	8	0	2	8	20	25	0	5000	0,35	0,1	C_15_8_0_8_25_0.1_D	4	15	200	N.F.	N.F.	N.F.	0,63	Base failure_GR
14	15	2	0	2	16	20	25	0	5000	0,35	0,1	C_15_2_0_16_25_0.1_D	1	15	200	0,882	176,4	7,06	0,63	Foundation Failure
15	15	4	0	2	16	20	25	0	5000	0,35	0,1	C_15_4_0_16_25_0.1_D	2	15	200	0,5033	100,66	4,03	0,63	Base failure_EQ
16	15	8	0	2	16	20	25	0	5000	0,35	0,1	C_15_8_0_16_25_0.1_D	4	15	200	N.F.	N.F.	N.F.	0,63	Base failure_GR
17	15	2	0	2	2	20	50	0	10000	0,35	0,1	C_15_2_0_2_50_0.1_D	1	15	600	0,7125	427,5	8,55	1,25	Foundation Failure
18	15	4	0	2	2	20	50	0	10000	0,35	0,1	C_15_4_0_2_50_0.1_D	2	15	600	0,5668	340,08	6,80	1,25	Foundation Failure
19	15	8	0	2	2	20	50	0	10000	0,35	0,1	C_15_8_0_2_50_0.1_D	4	15	400	0,8596	343,84	6,88	1,25	Base failure_EQ
20	15	2	0	2	4	20	50	0	10000	0,35	0,1	C_15_2_0_4_50_0.1_D	1	15	600	0,6772	406,32	8,13	1,25	Foundation Failure
21	15	4	0	2	4	20	50	0	10000	0,35	0,1	C_15_4_0_4_50_0.1_D	2	15	600	0,8605	516,3	10,33	1,25	Foundation Failure
22	15	8	0	2	4	20	50	0	10000	0,35	0,1	C_15_8_0_4_50_0.1_D	4	15	400	0,8593	343,72	6,87	1,25	Base failure_EQ
23	15	2	0	2	8	20	50	0	10000	0,35	0,1	C_15_2_0_8_50_0.1_D	1	15	400	0,8327	333,08	6,66	1,25	foundation Failure
24	15	4	0	2	8	20	50	0	10000	0,35	0,1	C_15_4_0_8_50_0.1_D	2	15	400	0,5121	204,84	4,10	1,25	Foundation Failure
25	15	8	0	2	8	20	50	0	10000	0,35	0,1	C_15_8_0_8_50_0.1_D	4	15	400	0,8597	343,88	6,88	1,25	Foundation Failure
26	15	2	0	2	16	20	50	0	10000	0,35	0,1	C_15_2_0_16_50_0.1_D	1	15	400	0,918	367,2	7,34	1,25	Foundation Failure
27	15	4	0	2	16	20	50	0	10000	0,35	0,1	C_15_4_0_16_50_0.1_D	2	15	400	0,8934	357,36	7,15	1,25	Foundation Failure
28	15	8	0	2	16	20	50	0	10000	0,35	0,1	C_15_8_0_16_50_0.1_D	4	15	400	0,7424	296,96	5,94	1,25	Foundation Failure
29	15	2	0	2	2	20	100	0	20000	0,35	0,1	C_15_2_0_2_100_0.1_D	1	15	1000	0,8471	847,1	8,47	2,50	Foundation Failure
30	15	4	0	2	2	20	100	0	20000	0,35	0,1	C_15_4_0_2_100_0.1_D	2	15	1000	0,9839	983,9	9,84	2,50	Foundation Failure
31	15	8	0	2	2	20	100	0	20000	0,35	0,1	C_15_8_0_2_100_0.1_D	4	15	1000	0,6177	617,7	6,18	2,50	Foundation Failure
32	15	2	0	2	4	20	100	0	20000	0,35	0,1	C_15_2_0_4_100_0.1_D	1	15	1000	0,6876	687,6	6,88	2,50	Foundation Failure
33	15	4	0	2	4	20	100	0	20000	0,35	0,1	C_15_4_0_4_100_0.1_D	2	15	800	0,8733	698,64	6,99	2,50	Foundation Failure
34	15	8	0	2	4	20	100	0	20000	0,35	0,1	C_15_8_0_4_100_0.1_D	4	15	1000	0,597	597	5,97	2,50	Foundation Failure
35	15	2	0	2	8	20	100	0	20000	0,35	0,1	C_15_2_0_8_100_0.1_D	1	15	800	0,6561	524,88	5,25	2,50	Foundation Failure
36	15	4	0	2	8	20	100	0	20000	0,35	0,1	C_15_4_0_8_100_0.1_D	2	15	800	0,6818	545,44	5,45	2,50	Foundation Failure
37	15	8	0	2	8	20	100	0	20000	0,35	0,1	C_15_8_0_8_100_0.1_D	4	15	1000	0,595	595	5,95	2,50	Foundation Failure
38	15	2	0	2	16	20	100	0	20000	0,35	0,1	C_15_2_0_16_100_0.1_D	1	15	800	0,9347	747,76	7,48	2,50	Foundation Failure
39	15	4	0	2	16	20	100	0	20000	0,35	0,1	C_15_4_0_16_100_0.1_D	2	15	800	0,9006	720,48	7,20	2,50	Foundation Failure
40	15	8	0	2	16	20	100	0	20000	0,35	0,1	C_15_8_0_16_100_0.1_D	4	15	800	0,8588	687,04	6,87	2,50	Foundation Failure
41	15	2	0	2	2	20	200	0	40000	0,35	0,1	C_15_2_0_2_200_0.1_D	1	15	2000	0,8083	1616,6	8,08	5,00	Foundation Failure
42	15	4	0	2	2	20	200	0	40000	0,35	0,1	C_15_4_0_2_200_0.1_D	2	15	2000	0,8906	1781,2	8,91	5,00	Foundation Failure
43	15	8	0	2	2	20	200	0	40000	0,35	0,1	C_15_8_0_2_200_0.1_D	4	15	1600	0,9006	1440,96	7,20	5,00	Foundation Failure
44	15	2	0	2	4	20	200	0	40000	0,35	0,1	C_15_2_0_4_200_0.1_D	1	15	2000	0,6743	1348,6	6,74	5,00	Foundation Failure
45	15	4	0	2	4	20	200	0	40000	0,35	0,1	C_15_4_0_4_200_0.1_D	2	15	1600	0,877	1403,2	7,02	5,00	Foundation Failure
46	15	8	0	2	4	20	200	0	40000	0,35	0,1	C_15_8_0_4_200_0.1_D	4	15	2000	0,6837	1367,4	6,84	5,00	Foundation Failure
47	15	2	0	2	8	20	200	0	40000	0,35	0,1	C_15_2_0_8_200_0.1_D	1	15	1600	0,6532	1045,12	5,23	5,00	Foundation Failure
48	15	4	0	2	8	20	200	0	40000	0,35	0,1	C_15_4_0_8_200_0.1_D	2	15	1600	0,6755	1080,8	5,40	5,00	Foundation Failure
49	15	8	0	2	8	20	200	0	40000	0,35	0,1	C_15_8_0_8_200_0.1_D	4	15	2000	0,5904	1180,8	5,90	5,00	Foundation Failure
50	15	2	0	2	16	20	200	0	40000	0,35	0,1	C_15_2_0_16_200_0.1_D	1	15	1600	0,9559	1529,44	7,65	5,00	Foundation Failure
51	15	4	0	2	16	20	200	0	40000	0,35	0,1	C_15_4_0_16_200_0.1_D	2	15	1600	0,91	1456	7,28	5,00	Foundation Failure
52	15	8	0	2	16	20	200	0	40000	0,35	0,1	C_15_8_0_16_200_0.1_D	4	15	1600	0,8722	1395,52	6,98	5,00	Foundation Failure

N.F. :Not found.
Base failure_EQ:Failed due to earthquake.
Base failure_GR:Failed due to gravity.

Table B.1. List of results of finite elements models created for seismic condition (β= 15°) (Cont.).

Model No.	GEOTECHNICAL PROPERTIES					SLOPE SOIL PROPERTIES				SEISMIC EFFECT	FILE NAME	ANALYSIS RESULTS FOR SEISMIC LOADING							
	β (°)	H (m)	λ	B (m)	L (m)	γ (kN/m³)	c_u (kN/m³)	ϕ_u (°)	E_u (kPa)	ν_u	k_h		H/B	β (°)	Load	Mstage	q_f (kPa)	N_{cs}	cu/γB	Failure Mode
53	0	2	0	2	2	20	100	0	20000	0,35	0,2	C_0_2_0_2_100_0.2_D	1	0	2000	0,256	512	5,12	2,5	Foundation Failure
54	0	2	0	2	4	20	100	0	20000	0,35	0,2	C_0_2_0_4_100_0.2_D	1	0	2000	0,24	480	4,8	2,5	Foundation Failure
55	0	2	0	2	8	20	100	0	20000	0,35	0,2	C_0_2_0_8_100_0.2_D	1	0	2000	0,2345	469	4,69	2,5	Foundation Failure
56	0	2	0	2	16	20	100	0	20000	0,35	0,2	C_0_2_0_16_100_0.2_D	1	0	2000	0,2497	499,4	4,994	2,5	Foundation Failure
57	15	2	0	2	2	20	25	0	5000	0,35	0,2	C_15_2_0_2_25_0.2_D	1	15	200	0,4781	95,62	3,82	0,63	Base failure_EQ
58	15	4	0	2	2	20	25	0	5000	0,35	0,2	C_15_4_0_2_25_0.2_D	2	15	200	0,2488	49,76	1,99	0,63	Base failure_EQ
59	15	8	0	2	2	20	25	0	5000	0,35	0,2	C_15_8_0_2_25_0.2_D	4	15	200	N.F.	N.F.	N.F.	0,63	Base failure_GR
60	15	2	0	2	4	20	25	0	5000	0,35	0,2	C_15_2_0_4_25_0.2_D	1	15	200	0,4781	95,62	3,82	0,63	Base failure_EQ
61	15	4	0	2	4	20	25	0	5000	0,35	0,2	C_15_4_0_4_25_0.2_D	2	15	200	0,2489	49,78	1,99	0,63	Base failure_EQ
62	15	8	0	2	4	20	25	0	5000	0,35	0,2	C_15_8_0_4_25_0.2_D	4	15	200	N.F.	N.F.	N.F.	0,63	Base failure_GR
63	15	2	0	2	8	20	25	0	5000	0,35	0,2	C_15_2_0_8_25_0.2_D	1	15	200	0,482	96,4	3,86	0,63	Base failure_EQ
64	15	4	0	2	8	20	25	0	5000	0,35	0,2	C_15_4_0_8_25_0.2_D	2	15	200	0,2524	50,48	2,02	0,63	Base failure_EQ
65	15	8	0	2	8	20	25	0	5000	0,35	0,2	C_15_8_0_8_25_0.2_D	4	15	200	N.F.	N.F.	N.F.	0,63	Base failure_GR
66	15	2	0	2	16	20	25	0	5000	0,35	0,2	C_15_2_0_16_25_0.2_D	1	15	200	0,4825	96,5	3,86	0,63	Base failure_EQ
67	15	4	0	2	16	20	25	0	5000	0,35	0,2	C_15_4_0_16_25_0.2_D	2	15	200	0,2517	50,34	2,01	0,63	Base failure_EQ
68	15	8	0	2	16	20	25	0	5000	0,35	0,2	C_15_8_0_16_25_0.2_D	4	15	200	N.F.	N.F.	N.F.	0,63	Base failure_GR
69	15	2	0	2	2	20	50	0	10000	0,35	0,2	C_15_2_0_2_50_0.2_D	1	15	600	0,3996	239,76	4,80	1,25	Foundation Failure
70	15	4	0	2	2	20	50	0	10000	0,35	0,2	C_15_4_0_2_50_0.2_D	2	15	400	0,604	241,6	4,83	1,25	Base failure_EQ
71	15	8	0	2	2	20	50	0	10000	0,35	0,2	C_15_8_0_2_50_0.2_D	4	15	400	0,4316	172,64	3,45	1,25	Base failure_EQ
72	15	2	0	2	4	20	50	0	10000	0,35	0,2	C_15_2_0_4_50_0.2_D	1	15	600	0,3888	233,28	4,67	1,25	Foundation Failure
73	15	4	0	2	4	20	50	0	10000	0,35	0,2	C_15_4_0_4_50_0.2_D	2	15	400	0,6198	247,92	4,96	1,25	Foundation Failure
74	15	8	0	2	4	20	50	0	10000	0,35	0,2	C_15_8_0_4_50_0.2_D	4	15	400	0,4316	172,64	3,45	1,25	Base failure_EQ
75	15	2	0	2	8	20	50	0	10000	0,35	0,2	C_15_2_0_8_50_0.2_D	1	15	400	0,582	232,8	4,66	1,25	Foundation Failure
76	15	4	0	2	8	20	50	0	10000	0,35	0,2	C_15_4_0_8_50_0.2_D	2	15	400	0,586	234,4	4,69	1,25	Foundation Failure
77	15	8	0	2	8	20	50	0	10000	0,35	0,2	C_15_8_0_8_50_0.2_D	4	15	400	0,4306	172,24	3,44	1,25	Base failure_EQ
78	15	2	0	2	16	20	50	0	10000	0,35	0,2	C_15_2_0_16_50_0.2_D	1	15	400	0,6184	247,36	4,95	1,25	Foundation Failure
79	15	4	0	2	16	20	50	0	10000	0,35	0,2	C_15_4_0_16_50_0.2_D	2	15	400	0,6175	247	4,94	1,25	Foundation Failure
80	15	8	0	2	16	20	50	0	10000	0,35	0,2	C_15_8_0_16_50_0.2_D	4	15	400	0,4336	173,44	3,47	1,25	Base failure_EQ
81	15	2	0	2	2	20	100	0	20000	0,35	0,2	C_15_2_0_2_100_0.2_D	1	15	1000	0,4912	491,2	4,91	2,50	Foundation Failure
82	15	4	0	2	2	20	100	0	20000	0,35	0,2	C_15_4_0_2_100_0.2_D	2	15	1000	0,5	500	5,00	2,50	Foundation Failure
83	15	8	0	2	2	20	100	0	20000	0,35	0,2	C_15_8_0_2_100_0.2_D	4	15	1200	0,4155	498,6	4,99	2,50	Foundation Failure
84	15	2	0	2	4	20	100	0	20000	0,35	0,2	C_15_2_0_4_100_0.2_D	1	15	800	0,5903	472,24	4,72	2,50	Base failure_EQ
85	15	4	0	2	4	20	100	0	20000	0,35	0,2	C_15_4_0_4_100_0.2_D	2	15	800	0,6198	495,84	4,96	2,50	Foundation Failure
86	15	8	0	2	4	20	100	0	20000	0,35	0,2	C_15_8_0_4_100_0.2_D	4	15	800	0,6177	494,16	4,94	2,50	Foundation Failure
87	15	2	0	2	8	20	100	0	20000	0,35	0,2	C_15_2_0_8_100_0.2_D	1	15	800	0,5383	430,64	4,31	2,50	Foundation Failure
88	15	4	0	2	8	20	100	0	20000	0,35	0,2	C_15_4_0_8_100_0.2_D	2	15	800	0,5886	470,88	4,71	2,50	Foundation Failure
89	15	8	0	2	8	20	100	0	20000	0,35	0,2	C_15_8_0_8_100_0.2_D	4	15	800	0,6116	489,28	4,89	2,50	Foundation Failure
90	15	2	0	2	16	20	100	0	20000	0,35	0,2	C_15_2_0_16_100_0.2_D	1	15	800	0,6825	546	5,46	2,50	Base failure_EQ
91	15	4	0	2	16	20	100	0	20000	0,35	0,2	C_15_4_0_16_100_0.2_D	2	15	800	0,6776	542,08	5,42	2,50	Base failure_EQ
92	15	8	0	2	16	20	100	0	20000	0,35	0,2	C_15_8_0_16_100_0.2_D	4	15	800	0,6057	484,56	4,85	2,50	Base failure_EQ
93	15	2	0	2	2	20	200	0	40000	0,35	0,2	C_15_2_0_2_200_0.2_D	1	15	1600	0,6351	1016,16	5,08	5,00	Foundation Failure
94	15	4	0	2	2	20	200	0	40000	0,35	0,2	C_15_4_0_2_200_0.2_D	2	15	1600	0,6241	998,56	4,99	5,00	Foundation Failure
95	15	8	0	2	2	20	200	0	40000	0,35	0,2	C_15_8_0_2_200_0.2_D	4	15	2000	0,4965	993	4,97	5,00	Foundation Failure
96	15	2	0	2	4	20	200	0	40000	0,35	0,2	C_15_2_0_4_200_0.2_D	1	15	1600	0,6358	1017,28	5,09	5,00	Base failure_EQ
97	15	4	0	2	4	20	200	0	40000	0,35	0,2	C_15_4_0_4_200_0.2_D	2	15	1600	0,6152	984,32	4,92	5,00	Base failure_EQ
98	15	8	0	2	4	20	200	0	40000	0,35	0,2	C_15_8_0_4_200_0.2_D	4	15	1600	0,6105	976,8	4,88	5,00	Foundation Failure
99	15	2	0	2	8	20	200	0	40000	0,35	0,2	C_15_2_0_8_200_0.2_D	1	15	1600	0,6208	993,28	4,97	5,00	Foundation Failure
100	15	4	0	2	8	20	200	0	40000	0,35	0,2	C_15_4_0_8_200_0.2_D	2	15	1600	0,6197	991,52	4,96	5,00	Base failure_EQ
101	15	8	0	2	8	20	200	0	40000	0,35	0,2	C_15_8_0_8_200_0.2_D	4	15	1600	0,5275	844	4,22	5,00	Base failure_EQ
102	15	2	0	2	16	20	200	0	40000	0,35	0,2	C_15_2_0_16_200_0.2_D	1	15	1600	0,5626	900,16	4,50	5,00	Foundation Failure
103	15	4	0	2	16	20	200	0	40000	0,35	0,2	C_15_4_0_16_200_0.2_D	2	15	1600	0,6219	995,04	4,98	5,00	Base failure_EQ
104	15	8	0	2	16	20	200	0	40000	0,35	0,2	C_15_8_0_16_200_0.2_D	4	15	1600	0,6151	984,16	4,92	5,00	Base failure_EQ

N.F. :Not found.
Base failure_EQ:Failed due to earthquake.
Base failure_GR:Failed due to gravity.

Table B.1. List of results of finite elements models created for seismic condition (β= 15°) (Cont.).

Model No.	GEOTECHNICAL PROPERTIES					SLOPE SOIL PROPERTIES				SEISMIC EFFECT	FILE NAME	ANALYSIS RESULTS FOR SEISMIC LOADING								
	β (°)	H (m)	λ	B (m)	L (m)	γ (kN/m³)	c_u (kN/m²)	ϕ_u (°)	E_u (kPa)	ν_u	k_h		H/B	β (°)	Load	Mstage	q_f (kPa)	N_{cs}	cu/γB	Failure Mode
105	0	2	0	2	2	20	100	0	20000	0,35	0,3	C_0_2_0_2_100_0.3_D	1	0	2000	0,17	340	3,4	2,5	Foundation Failure
106	0	2	0	2	4	20	100	0	20000	0,35	0,3	C_0_2_0_4_100_0.3_D	1	0	2000	0,16	320	3,2	2,5	Foundation Failure
107	0	2	0	2	8	20	100	0	20000	0,35	0,3	C_0_2_0_8_100_0.3_D	1	0	2000	0,158	316	3,16	2,5	Foundation Failure
108	0	2	0	2	16	20	100	0	20000	0,35	0,3	C_0_2_0_16_100_0.3_D	1	0	2000	0,15	300	3	2,5	Foundation Failure
109	15	2	0	2	2	20	25	0	5000	0,35	0,3	C_15_2_0_2_25_0.3_D	1	15	200	0,3188	63,76	2,5504	0,63	Base failure_EQ
110	15	4	0	2	2	20	25	0	5000	0,35	0,3	C_15_4_0_2_25_0.3_D	2	15	200	0,1662	33,24	1,33	0,63	Base failure_EQ
111	15	8	0	2	2	20	25	0	5000	0,35	0,3	C_15_8_0_2_25_0.3_D	4	15	200	N.F.	N.F.	N.F.	0,63	Base failure_GR
112	15	2	0	2	4	20	25	0	5000	0,35	0,3	C_15_2_0_4_25_0.3_D	1	15	200	0,319	63,8	2,55	0,63	Base failure_EQ
113	15	4	0	2	4	20	25	0	5000	0,35	0,3	C_15_4_0_4_25_0.3_D	2	15	200	0,166	33,2	1,33	0,63	Base failure_EQ
114	15	8	0	2	4	20	25	0	5000	0,35	0,3	C_15_8_0_4_25_0.3_D	4	15	200	N.F.	N.F.	N.F.	0,63	Base failure_GR
115	15	2	0	2	8	20	25	0	5000	0,35	0,3	C_15_2_0_8_25_0.3_D	1	15	200	0,3212	64,24	2,57	0,63	Base failure_EQ
116	15	4	0	2	8	20	25	0	5000	0,35	0,3	C_15_4_0_8_25_0.3_D	2	15	200	0,1682	33,64	1,35	0,63	Base failure_EQ
117	15	8	0	2	8	20	25	0	5000	0,35	0,3	C_15_8_0_8_25_0.3_D	4	15	200	N.F.	N.F.	N.F.	0,63	Base failure_GR
118	15	2	0	2	16	20	25	0	5000	0,35	0,3	C_15_2_0_16_25_0.3_D	1	15	200	0,3216	64,32	2,57	0,63	Base failure_EQ
119	15	4	0	2	16	20	25	0	5000	0,35	0,3	C_15_4_0_16_25_0.3_D	2	15	200	0,1678	33,56	1,34	0,63	Base failure_EQ
120	15	8	0	2	16	20	25	0	5000	0,35	0,3	C_15_8_0_16_25_0.3_D	4	15	200	N.F.	N.F.	N.F.	0,63	Base failure_GR
121	15	2	0	2	2	20	50	0	10000	0,35	0,3	C_15_2_0_2_50_0.3_D	1	15	300	0,7696	230,88	4,62	1,25	Base failure_EQ
122	15	4	0	2	2	20	50	0	10000	0,35	0,3	C_15_4_0_2_50_0.3_D	2	15	400	0,4192	167,68	3,35	1,25	Base failure_EQ
123	15	8	0	2	2	20	50	0	10000	0,35	0,3	C_15_8_0_2_50_0.3_D	4	15	400	0,2883	115,32	2,31	1,25	Base failure_EQ
124	15	2	0	2	4	20	50	0	10000	0,35	0,3	C_15_2_0_4_50_0.3_D	1	15	400	0,4643	185,72	3,71	1,25	Base failure_EQ
125	15	4	0	2	4	20	50	0	10000	0,35	0,3	C_15_4_0_4_50_0.3_D	2	15	400	0,4038	161,52	3,23	1,25	Base failure_EQ
126	15	8	0	2	4	20	50	0	10000	0,35	0,3	C_15_8_0_4_50_0.3_D	4	15	400	0,2874	114,96	2,30	1,25	Base failure_EQ
127	15	2	0	2	8	20	50	0	10000	0,35	0,3	C_15_2_0_8_50_0.3_D	1	15	400	0,3526	141,04	2,82	1,25	Base failure_EQ
128	15	4	0	2	8	20	50	0	10000	0,35	0,3	C_15_4_0_8_50_0.3_D	2	15	400	0,3913	156,52	3,13	1,25	Base failure_EQ
129	15	8	0	2	8	20	50	0	10000	0,35	0,3	C_15_8_0_8_50_0.3_D	4	15	400	0,287	114,8	2,30	1,25	Base failure_EQ
130	15	2	0	2	16	20	50	0	10000	0,35	0,3	C_15_2_0_16_50_0.3_D	1	15	400	0,6179	247,16	4,94	1,25	Base failure_EQ
131	15	4	0	2	16	20	50	0	10000	0,35	0,3	C_15_4_0_16_50_0.3_D	2	15	400	0,4277	171,08	3,42	1,25	Base failure_EQ
132	15	8	0	2	16	20	50	0	10000	0,35	0,3	C_15_8_0_16_50_0.3_D	4	15	400	0,2892	115,68	2,31	1,25	Base failure_EQ
133	15	2	0	2	2	20	100	0	20000	0,35	0,3	C_15_2_0_2_100_0.3_D	1	15	1000	0,339	339	3,39	2,50	Base failure_EQ
134	15	4	0	2	2	20	100	0	20000	0,35	0,3	C_15_4_0_2_100_0.3_D	2	15	800	0,4142	331,36	3,31	2,50	Base failure_EQ
135	15	8	0	2	2	20	100	0	20000	0,35	0,3	C_15_8_0_2_100_0.3_D	4	15	800	0,4098	327,84	3,28	2,50	Base failure_EQ
136	15	2	0	2	4	20	100	0	20000	0,35	0,3	C_15_2_0_4_100_0.3_D	1	15	800	0,4	320	3,20	2,50	Base failure_EQ
137	15	4	0	2	4	20	100	0	20000	0,35	0,3	C_15_4_0_4_100_0.3_D	2	15	800	0,3985	318,8	3,19	2,50	Base failure_EQ
138	15	8	0	2	4	20	100	0	20000	0,35	0,3	C_15_8_0_4_100_0.3_D	4	15	800	0,4091	327,28	3,27	2,50	Base failure_EQ
139	15	2	0	2	8	20	100	0	20000	0,35	0,3	C_15_2_0_8_100_0.3_D	1	15	800	0,3912	312,96	3,13	2,50	Base failure_EQ
140	15	4	0	2	8	20	100	0	20000	0,35	0,3	C_15_4_0_8_100_0.3_D	2	15	1000	0,2341	234,1	2,34	2,50	Base failure_EQ
141	15	8	0	2	8	20	100	0	20000	0,35	0,3	C_15_8_0_8_100_0.3_D	4	15	800	0,4088	327,04	3,27	2,50	Base failure_EQ
142	15	2	0	2	16	20	100	0	20000	0,35	0,3	C_15_2_0_16_100_0.3_D	1	15	800	0,3847	307,76	3,08	2,50	Base failure_EQ
143	15	4	0	2	16	20	100	0	20000	0,35	0,3	C_15_4_0_16_100_0.3_D	2	15	800	0,4193	335,44	3,35	2,50	Base failure_EQ
144	15	8	0	2	16	20	100	0	20000	0,35	0,3	C_15_8_0_16_100_0.3_D	4	15	800	0,5515	441,2	4,41	2,50	Base failure_EQ
145	15	2	0	2	2	20	200	0	40000	0,35	0,3	C_15_2_0_2_200_0.3_D	1	15	1600	0,6004	960,64	4,80	5,00	Base failure_EQ
146	15	4	0	2	2	20	200	0	40000	0,35	0,3	C_15_4_0_2_200_0.3_D	2	15	1600	0,4159	665,44	3,33	5,00	Base failure_EQ
147	15	8	0	2	2	20	200	0	40000	0,35	0,3	C_15_8_0_2_200_0.3_D	4	15	2000	0,3616	723,2	3,62	5,00	Base failure_EQ
148	15	2	0	2	4	20	200	0	40000	0,35	0,3	C_15_2_0_4_200_0.3_D	1	15	1600	0,416	665,6	3,33	5,00	Base failure_EQ
149	15	4	0	2	4	20	200	0	40000	0,35	0,3	C_15_4_0_4_200_0.3_D	2	15	1600	0,4037	645,92	3,23	5,00	Base failure_EQ
150	15	8	0	2	4	20	200	0	40000	0,35	0,3	C_15_8_0_4_200_0.3_D	4	15	1600	0,4165	666,4	3,33	5,00	Base failure_EQ
151	15	2	0	2	8	20	200	0	40000	0,35	0,3	C_15_2_0_8_200_0.3_D	1	15	1600	0,4127	660,32	3,30	5,00	Base failure_EQ
152	15	4	0	2	8	20	200	0	40000	0,35	0,3	C_15_4_0_8_200_0.3_D	2	15	1600	0,389	622,4	3,11	5,00	Base failure_EQ
153	15	8	0	2	8	20	200	0	40000	0,35	0,3	C_15_8_0_8_200_0.3_D	4	15	2000	0,2983	596,6	2,98	5,00	Base failure_EQ
154	15	2	0	2	16	20	200	0	40000	0,35	0,3	C_15_2_0_16_200_0.3_D	1	15	1600	0,4097	655,52	3,28	5,00	Base failure_EQ
155	15	4	0	2	16	20	200	0	40000	0,35	0,3	C_15_4_0_16_200_0.3_D	2	15	1600	0,4106	656,96	3,28	5,00	Base failure_EQ
156	15	8	0	2	16	20	200	0	40000	0,35	0,3	C_15_8_0_16_200_0.3_D	4	15	1600	0,4009	641,44	3,21	5,00	Base failure_EQ

N.F. :Not found.
Base failıre_EQ:Failed due to earthquake.
Base failıre_GR:Failed due to gravity.

Table B.2. List of results of finite elements models created for seismic condition (β= 30°)

Model No.	GEOTECHNICAL PROPERTIES					SLOPE SOIL PROPERTIES				SEISMIC EFFECT	FILE NAME	ANALYSIS RESULTS FOR SEISMIC LOADING							
	β (°)	H (m)	λ	B (m)	L (m)	γ (kN/m³)	c_u (kN/m²)	ϕ_u (°)	E_u (kPa)	ν_u	k_h		H/B	β (°)	Load	Mstage	q_f (kPa)	N_{cs}	cu/γB	Failure Mode
1	30	2	0	2	2	20	25	0	5000	0,35	0,1	C_30_2_0_2_25_0.1_D	1	30	200	0,718	143,6	5,74	0,63	Foundation Failure
2	30	4	0	2	2	20	25	0	5000	0,35	0,1	C_30_4_0_2_25_0.1_D	2	30	200	0,5571	111,42	4,46	0,63	Base failure_EQ
3	30	8	0	2	2	20	25	0	5000	0,35	0,1	C_30_8_0_2_25_0.1_D	4	30	200	N.F.	N.F.	N.F.	0,63	Base failure_GR
4	30	2	0	2	4	20	25	0	5000	0,35	0,1	C_30_2_0_4_25_0.1_D	1	30	200	0,6451	129,02	5,16	0,63	Foundation Failure
5	30	4	0	2	4	20	25	0	5000	0,35	0,1	C_30_4_0_4_25_0.1_D	2	30	200	0,5498	109,96	4,40	0,63	Base failure_EQ
6	30	8	0	2	4	20	25	0	5000	0,35	0,1	C_30_8_0_4_25_0.1_D	4	30	200	N.F.	N.F.	N.F.	0,63	Base failure_GR
7	30	2	0	2	8	20	25	0	5000	0,35	0,1	C_30_2_0_8_25_0.1_D	1	30	200	0,5705	114,1	4,56	0,63	Base failure_EQ
8	30	4	0	2	8	20	25	0	5000	0,35	0,1	C_30_4_0_8_25_0.1_D	2	30	200	0,5498	109,96	4,40	0,63	Base failure_EQ
9	30	8	0	2	8	20	25	0	5000	0,35	0,1	C_30_8_0_8_25_0.1_D	4	30	200	N.F.	N.F.	N.F.	0,63	Base failure_GR
10	30	2	0	2	16	20	25	0	5000	0,35	0,1	C_30_2_0_16_25_0.1_D	1	30	200	0,574	114,8	4,59	0,63	Foundation Failure
11	30	4	0	2	16	20	25	0	5000	0,35	0,1	C_30_4_0_16_25_0.1_D	2	30	200	0,5635	112,7	4,51	0,63	Base failure_EQ
12	30	8	0	2	16	20	25	0	5000	0,35	0,1	C_30_8_0_16_25_0.1_D	4	30	200	N.F.	N.F.	N.F.	0,63	Base failure_GR
13	30	2	0	2	2	20	50	0	10000	0,35	0,1	C_30_2_0_2_50_0.1_D	1	30	600	0,5174	310,44	6,21	1,25	Foundation Failure
14	30	4	0	2	2	20	50	0	10000	0,35	0,1	C_30_4_0_2_50_0.1_D	2	30	600	0,4738	284,28	5,69	1,25	Foundation Failure
15	30	8	0	2	2	20	50	0	10000	0,35	0,1	C_30_8_0_2_50_0.1_D	4	30	400	0,8754	350,16	7,00	1,25	Base failure_EQ
16	30	2	0	2	4	20	50	0	10000	0,35	0,1	C_30_2_0_4_50_0.1_D	1	30	600	0,4791	287,46	5,75	1,25	Foundation Failure
17	30	4	0	2	4	20	50	0	10000	0,35	0,1	C_30_4_0_4_50_0.1_D	2	30	600	0,4512	270,72	5,41	1,25	Foundation Failure
18	30	8	0	2	4	20	50	0	10000	0,35	0,1	C_30_8_0_4_50_0.1_D	4	30	400	0,6485	259,4	5,19	1,25	Foundation Failure
19	30	2	0	2	8	20	50	0	10000	0,35	0,1	C_30_2_0_8_50_0.1_D	1	30	400	0,5987	239,48	4,79	1,25	Foundation Failure
20	30	4	0	2	8	20	50	0	10000	0,35	0,1	C_30_4_0_8_50_0.1_D	2	30	400	0,6473	258,92	5,18	1,25	Foundation Failure
21	30	8	0	2	8	20	50	0	10000	0,35	0,1	C_30_8_0_8_50_0.1_D	4	30	400	0,5827	233,08	4,66	1,25	Foundation Failure
22	30	2	0	2	16	20	50	0	10000	0,35	0,1	C_30_2_0_16_50_0.1_D	1	30	400	0,7021	280,84	5,62	1,25	Foundation Failure
23	30	4	0	2	16	20	50	0	10000	0,35	0,1	C_30_4_0_16_50_0.1_D	2	30	400	0,6818	272,72	5,45	1,25	Foundation Failure
24	30	8	0	2	16	20	50	0	10000	0,35	0,1	C_30_8_0_16_50_0.1_D	4	30	400	0,7119	284,76	5,70	1,25	Foundation Failure
25	30	2	0	2	2	20	100	0	20000	0,35	0,1	C_30_2_0_2_100_0.1_D	1	30	1000	0,641	641	6,41	2,50	Foundation Failure
26	30	4	0	2	2	20	100	0	20000	0,35	0,1	C_30_4_0_2_100_0.1_D	2	30	1000	0,5821	582,1	5,82	2,50	Foundation Failure
27	30	8	0	2	2	20	100	0	20000	0,35	0,1	C_30_8_0_2_100_0.1_D	4	30	1000	0,5777	577,7	5,78	2,50	Foundation Failure
28	30	2	0	2	4	20	100	0	20000	0,35	0,1	C_30_2_0_4_100_0.1_D	1	30	800	0,6781	542,48	5,42	2,50	Foundation Failure
29	30	4	0	2	4	20	100	0	20000	0,35	0,1	C_30_4_0_4_100_0.1_D	2	30	800	0,675	540	5,40	2,50	Foundation Failure
30	30	8	0	2	4	20	100	0	20000	0,35	0,1	C_30_8_0_4_100_0.1_D	4	30	800	0,6543	523,44	5,23	2,50	Foundation Failure
31	30	2	0	2	8	20	100	0	20000	0,35	0,1	C_30_2_0_8_100_0.1_D	1	30	800	0,6725	538	5,38	2,50	Foundation Failure
32	30	4	0	2	8	20	100	0	20000	0,35	0,1	C_30_4_0_8_100_0.1_D	2	30	800	0,6578	526,24	5,26	2,50	Foundation Failure
33	30	8	0	2	8	20	100	0	20000	0,35	0,1	C_30_8_0_8_100_0.1_D	4	30	800	0,6031	482,48	4,82	2,50	Foundation Failure
34	30	2	0	2	16	20	100	0	20000	0,35	0,1	C_30_2_0_16_100_0.1_D	1	30	800	0,7196	575,68	5,76	2,50	Foundation Failure
35	30	4	0	2	16	20	100	0	20000	0,35	0,1	C_30_4_0_16_100_0.1_D	2	30	800	0,7105	568,4	5,68	2,50	Foundation Failure
36	30	8	0	2	16	20	100	0	20000	0,35	0,1	C_30_8_0_16_100_0.1_D	4	30	800	0,7326	586,08	5,86	2,50	Foundation Failure
37	30	2	0	2	2	20	200	0	40000	0,35	0,1	C_30_2_0_2_200_0.1_D	1	30	1600	0,8189	1310,24	6,55	5,00	Foundation Failure
38	30	4	0	2	2	20	200	0	40000	0,35	0,1	C_30_4_0_2_200_0.1_D	2	30	1600	0,908	1452,8	7,26	5,00	Foundation Failure
39	30	8	0	2	2	20	200	0	40000	0,35	0,1	C_30_8_0_2_200_0.1_D	4	30	1600	0,8858	1417,28	7,09	5,00	Foundation Failure
40	30	2	0	2	4	20	200	0	40000	0,35	0,1	C_30_2_0_4_200_0.1_D	1	30	1600	0,8071	1291,36	6,46	5,00	Foundation Failure
41	30	4	0	2	4	20	200	0	40000	0,35	0,1	C_30_4_0_4_200_0.1_D	2	30	1600	0,8486	1357,76	6,79	5,00	Foundation Failure
42	30	8	0	2	4	20	200	0	40000	0,35	0,1	C_30_8_0_4_200_0.1_D	4	30	1600	0,73	1168	5,84	5,00	Foundation Failure
43	30	2	0	2	8	20	200	0	40000	0,35	0,1	C_30_2_0_8_200_0.1_D	1	30	1600	0,6746	1079,36	5,40	5,00	Foundation Failure
44	30	4	0	2	8	20	200	0	40000	0,35	0,1	C_30_4_0_8_200_0.1_D	2	30	1600	0,6714	1074,24	5,37	5,00	Foundation Failure
45	30	8	0	2	8	20	200	0	40000	0,35	0,1	C_30_8_0_8_200_0.1_D	4	30	1600	0,6055	968,8	4,84	5,00	Foundation Failure
46	30	2	0	2	16	20	200	0	40000	0,35	0,1	C_30_2_0_16_200_0.1_D	1	30	1600	0,7345	1175,2	5,88	5,00	Foundation Failure
47	30	4	0	2	16	20	200	0	40000	0,35	0,1	C_30_4_0_16_200_0.1_D	2	30	1600	0,7177	1148,32	5,74	5,00	Foundation Failure
48	30	8	0	2	16	20	200	0	40000	0,35	0,1	C_30_8_0_16_200_0.1_D	4	30	1600	0,7641	1222,56	6,11	5,00	Foundation Failure

N.F. :Not found.
Base failire_EQ:Failed due to earthquake.
Base failire_GR:Failed due to gravity.

Table B.2. List of results of finite elements models created for seismic condition (β= 30°) (Cont.).

Model No.	GEOTECHNICAL PROPERTIES					SLOPE SOIL PROPERTIES				SEISMIC EFFECT	FILE NAME	ANALYSIS RESULTS FOR SEISMIC LOADING							
	β (°)	H (m)	λ	B (m)	L (m)	γ (kN/m³)	c_u (kN/m²)	ϕ_u (°)	E_u (kPa)	ν_u	k_h		H/B	β (°)	Load	Mstage	q_f (kPa)	N_{cs}	cu/γB	Failure Mode
49	30	2	0	2	2	20	25	0	5000	0,35	0,2	C_30_2_0_2_25_0.2_D	1	30	200	0,5087	101,74	4,07	0,63	Base failure_EQ
50	30	4	0	2	2	20	25	0	5000	0,35	0,2	C_30_4_0_2_25_0.2_D	2	30	200	0,2786	55,72	2,23	0,63	Base failure_EQ
51	30	8	0	2	2	20	25	0	5000	0,35	0,2	C_30_8_0_2_25_0.2_D	4	30	200	N.F.	N.F.	N.F.	0,63	Base failure_GR
52	30	2	0	2	4	20	25	0	5000	0,35	0,2	C_30_2_0_4_25_0.2_D	1	30	200	0,5083	101,66	4,07	0,63	Base failure_EQ
53	30	4	0	2	4	20	25	0	5000	0,35	0,2	C_30_4_0_4_25_0.2_D	2	30	200	0,2754	55,08	2,20	0,63	Base failure_EQ
54	30	8	0	2	4	20	25	0	5000	0,35	0,2	C_30_8_0_4_25_0.2_D	4	30	200	N.F.	N.F.	N.F.	0,63	Base failure_GR
55	30	2	0	2	8	20	25	0	5000	0,35	0,2	C_30_2_0_8_25_0.2_D	1	30	200	0,5082	101,64	4,07	0,63	Base failure_EQ
56	30	4	0	2	8	20	25	0	5000	0,35	0,2	C_30_4_0_8_25_0.2_D	2	30	200	0,2749	54,98	2,20	0,63	Base failure_EQ
57	30	8	0	2	8	20	25	0	5000	0,35	0,2	C_30_8_0_8_25_0.2_D	4	30	200	N.F.	N.F.	N.F.	0,63	Base failure_GR
58	30	2	0	2	16	20	25	0	5000	0,35	0,2	C_30_2_0_16_25_0.2_D	1	30	200	0,5145	102,9	4,12	0,63	Base failure_EQ
59	30	4	0	2	16	20	25	0	5000	0,35	0,2	C_30_4_0_16_25_0.2_D	2	30	200	0,2819	56,38	2,26	0,63	Base failure_EQ
60	30	8	0	2	16	20	25	0	5000	0,35	0,2	C_30_8_0_16_25_0.2_D	4	30	200	N.F.	N.F.	N.F.	0,63	Base failure_GR
61	30	2	0	2	2	20	50	0	10000	0,35	0,2	C_30_2_0_2_50_0.2_D	1	30	750	0,3058	229,35	4,59	1,25	Foundation Failure
62	30	4	0	2	2	20	50	0	10000	0,35	0,2	C_30_4_0_2_50_0.2_D	2	30	400	0,6016	240,64	4,81	1,25	Foundation Failure
63	30	8	0	2	2	20	50	0	10000	0,35	0,2	C_30_8_0_2_50_0.2_D	4	30	400	0,501	200,4	4,01	1,25	Base failure_EQ
64	30	2	0	2	4	20	50	0	10000	0,35	0,2	C_30_2_0_4_50_0.2_D	1	30	400	0,5074	202,96	4,06	1,25	Foundation Failure
65	30	4	0	2	4	20	50	0	10000	0,35	0,2	C_30_4_0_4_50_0.2_D	2	30	400	0,56	224	4,48	1,25	Foundation Failure
66	30	8	0	2	4	20	50	0	10000	0,35	0,2	C_30_8_0_4_50_0.2_D	4	30	400	0,4966	198,64	3,97	1,25	Base failure_EQ
67	30	2	0	2	8	20	50	0	10000	0,35	0,2	C_30_2_0_8_50_0.2_D	1	30	400	0,4965	198,6	3,97	1,25	Foundation Failure
68	30	4	0	2	8	20	50	0	10000	0,35	0,2	C_30_4_0_8_50_0.2_D	2	30	400	0,4989	199,56	3,99	1,25	Foundation Failure
69	30	8	0	2	8	20	50	0	10000	0,35	0,2	C_30_8_0_8_50_0.2_D	4	30	400	0,4955	198,2	3,96	1,25	Base failure_EQ
70	30	2	0	2	16	20	50	0	10000	0,35	0,2	C_30_2_0_16_50_0.2_D	1	30	400	0,5085	203,4	4,07	1,25	Foundation Failure
71	30	4	0	2	16	20	50	0	10000	0,35	0,2	C_30_4_0_16_50_0.2_D	2	30	400	0,5099	203,96	4,08	1,25	Foundation Failure
72	30	8	0	2	16	20	50	0	10000	0,35	0,2	C_30_8_0_16_50_0.2_D	4	30	400	0,5035	201,4	4,03	1,25	Base failure_EQ
73	30	2	0	2	2	20	100	0	20000	0,35	0,2	C_30_2_0_2_100_0.2_D	1	30	1000	0,46	460	4,60	2,50	Foundation Failure
74	30	4	0	2	2	20	100	0	20000	0,35	0,2	C_30_4_0_2_100_0.2_D	2	30	1000	0,4757	475,7	4,76	2,50	Foundation Failure
75	30	8	0	2	2	20	100	0	20000	0,35	0,2	C_30_8_0_2_100_0.2_D	4	30	1000	0,4742	474,2	4,74	2,50	Foundation Failure
76	30	2	0	2	4	20	100	0	20000	0,35	0,2	C_30_2_0_4_100_0.2_D	1	30	800	0,55125	441	4,41	2,50	Foundation Failure
77	30	4	0	2	4	20	100	0	20000	0,35	0,2	C_30_4_0_4_100_0.2_D	2	30	800	0,5631	450,48	4,50	2,50	Foundation Failure
78	30	8	0	2	4	20	100	0	20000	0,35	0,2	C_30_8_0_4_100_0.2_D	4	30	800	0,5455	436,4	4,36	2,50	Foundation Failure
79	30	2	0	2	8	20	100	0	20000	0,35	0,2	C_30_2_0_8_100_0.2_D	1	30	800	0,5084	406,72	4,07	2,50	Foundation Failure
80	30	4	0	2	8	20	100	0	20000	0,35	0,2	C_30_4_0_8_100_0.2_D	2	30	800	0,51	408	4,08	2,50	Foundation Failure
81	30	8	0	2	8	20	100	0	20000	0,35	0,2	C_30_8_0_8_100_0.2_D	4	30	800	0,5063	405,04	4,05	2,50	Foundation Failure
82	30	2	0	2	16	20	100	0	20000	0,35	0,2	C_30_2_0_16_100_0.2_D	1	30	800	0,6213	497,04	4,97	2,50	Foundation Failure
83	30	4	0	2	16	20	100	0	20000	0,35	0,2	C_30_4_0_16_100_0.2_D	2	30	800	0,5214	417,12	4,17	2,50	Foundation Failure
84	30	8	0	2	16	20	100	0	20000	0,35	0,2	C_30_8_0_16_100_0.2_D	4	30	800	0,5158	412,64	4,13	2,50	Foundation Failure
85	30	2	0	2	2	20	200	0	40000	0,35	0,2	C_30_2_0_2_200_0.2_D	1	30	1600	0,581	929,6	4,65	5,00	Foundation Failure
86	30	4	0	2	2	20	200	0	40000	0,35	0,2	C_30_4_0_2_200_0.2_D	2	30	1600	0,6778	1084,48	5,42	5,00	Foundation Failure
87	30	8	0	2	2	20	200	0	40000	0,35	0,2	C_30_8_0_2_200_0.2_D	4	30	1600	0,6255	1000,8	5,00	5,00	Foundation Failure
88	30	2	0	2	4	20	200	0	40000	0,35	0,2	C_30_2_0_4_200_0.2_D	1	30	1600	0,5743	918,88	4,59	5,00	Foundation Failure
89	30	4	0	2	4	20	200	0	40000	0,35	0,2	C_30_4_0_4_200_0.2_D	2	30	1600	0,593	948,8	4,74	5,00	Foundation Failure
90	30	8	0	2	4	20	200	0	40000	0,35	0,2	C_30_8_0_4_200_0.2_D	4	30	2000	0,4763	952,6	4,76	5,00	Foundation Failure
91	30	2	0	2	8	20	200	0	40000	0,35	0,2	C_30_2_0_8_200_0.2_D	1	30	1600	0,5725	916	4,58	5,00	Foundation Failure
92	30	4	0	2	8	20	200	0	40000	0,35	0,2	C_30_4_0_8_200_0.2_D	2	30	1600	0,5694	911,04	4,56	5,00	Foundation Failure
93	30	8	0	2	8	20	200	0	40000	0,35	0,2	C_30_8_0_8_200_0.2_D	4	30	1600	0,51	816	4,08	5,00	Foundation Failure
94	30	2	0	2	16	20	200	0	40000	0,35	0,2	C_30_2_0_16_200_0.2_D	1	30	1600	0,6216	994,56	4,97	5,00	Foundation Failure
95	30	4	0	2	16	20	200	0	40000	0,35	0,2	C_30_4_0_16_200_0.2_D	2	30	1600	0,6098	975,68	4,88	5,00	Foundation Failure
96	30	8	0	2	16	20	200	0	40000	0,35	0,2	C_30_8_0_16_200_0.2_D	4	30	1600	0,6349	1015,84	5,08	5,00	Foundation Failure

N.F. :Not found.
Base failure_EQ:Failed due to earthquake.
Base failure_GR:Failed due to gravity.

Table B.2. List of results of finite elements models created for seismic condition (β= 30°) (Cont.).

Model No.	GEOTECHNICAL PROPERTIES					SLOPE SOIL PROPERTIES				SEISMIC EFFECT	FILE NAME	ANALYSIS RESULTS FOR SEISMIC LOADING								
	β (°)	H (m)	λ	B (m)	L (m)	γ (kN/m³)	c_u (kN/m²)	ϕ_u (°)	E_u (kPa)	ν_u	k_h		H/B	β (°)	Load	Mstage	q_f (kPa)	N_{cs}	cu/γB	Failure Mode
97	30	2	0	2	2	20	25	0	5000	0,35	0,3	C_30_2_0_2_25_0.3_D	1	30	200	0,3392	67,84	2,71	0,63	Base failure_EQ
98	30	4	0	2	2	20	25	0	5000	0,35	0,3	C_30_4_0_2_25_0.3_D	2	30	200	0,1858	37,16	1,49	0,63	Base failure_EQ
99	30	8	0	2	2	20	25	0	5000	0,35	0,3	C_30_8_0_2_25_0.3_D	4	30	200	N.F.	N.F.	N.F.	0,63	Base failure_GR
100	30	2	0	2	4	20	25	0	5000	0,35	0,3	C_30_2_0_4_25_0.3_D	1	30	200	0,3386	67,72	2,71	0,63	Base failure_EQ
101	30	4	0	2	4	20	25	0	5000	0,35	0,3	C_30_4_0_4_25_0.3_D	2	30	200	0,1838	36,76	1,47	0,63	Base failure_EQ
102	30	8	0	2	4	20	25	0	5000	0,35	0,3	C_30_8_0_4_25_0.3_D	4	30	200	N.F.	N.F.	N.F.	0,63	Base failure_GR
103	30	2	0	2	8	20	25	0	5000	0,35	0,3	C_30_2_0_8_25_0.3_D	1	30	200	0,3385	67,7	2,71	0,63	Base failure_EQ
104	30	4	0	2	8	20	25	0	5000	0,35	0,3	C_30_4_0_8_25_0.3_D	2	30	200	0,1834	36,68	1,47	0,63	Base failure_EQ
105	30	8	0	2	8	20	25	0	5000	0,35	0,3	C_30_8_0_8_25_0.3_D	4	30	200	N.F.	N.F.	N.F.	0,63	Base failure_GR
106	30	2	0	2	16	20	25	0	5000	0,35	0,3	C_30_2_0_16_25_0.3_D	1	30	200	0,343	68,6	2,74	0,63	Base failure_EQ
107	30	4	0	2	16	20	25	0	5000	0,35	0,3	C_30_4_0_16_25_0.3_D	2	30	200	0,1879	37,58	1,50	0,63	Base failure_EQ
108	30	8	0	2	16	20	25	0	5000	0,35	0,3	C_30_8_0_16_25_0.3_D	4	30	200	N.F.	N.F.	N.F.	0,63	Base failure_GR
109	30	2	0	2	2	20	50	0	10000	0,35	0,3	C_30_2_0_2_50_0.3_D	1	30	400	0,436	1744	3,49	1,25	Foundation failure
110	30	4	0	2	2	20	50	0	10000	0,35	0,3	C_30_4_0_2_50_0.3_D	2	30	400	0,4701	188,04	3,76	1,25	Foundation failure
111	30	8	0	2	2	20	50	0	10000	0,35	0,3	C_30_8_0_2_50_0.3_D	4	30	400	0,3307	132,28	2,65	1,25	Base failure_EQ
112	30	2	0	2	4	20	50	0	10000	0,35	0,3	C_30_2_0_4_50_0.3_D	1	30	400	0,4284	171,36	3,43	1,25	Foundation failure
113	30	4	0	2	4	20	50	0	10000	0,35	0,3	C_30_4_0_4_50_0.3_D	2	30	400	0,4493	179,72	3,59	1,25	Foundation failure
114	30	8	0	2	4	20	50	0	10000	0,35	0,3	C_30_8_0_4_50_0.3_D	4	30	400	0,3302	132,08	2,64	1,25	Base failure_EQ
115	30	2	0	2	8	20	50	0	10000	0,35	0,3	C_30_2_0_8_50_0.3_D	1	30	400	0,4126	165,04	3,30	1,25	Foundation failure
116	30	4	0	2	8	20	50	0	10000	0,35	0,3	C_30_4_0_8_50_0.3_D	2	30	400	0,4199	167,96	3,36	1,25	Foundation failure
117	30	8	0	2	8	20	50	0	10000	0,35	0,3	C_30_8_0_8_50_0.3_D	4	30	400	0,3339	133,56	2,67	1,25	Base failure_EQ
118	30	2	0	2	16	20	50	0	10000	0,35	0,3	C_30_2_0_16_50_0.3_D	1	30	400	0,4241	169,64	3,39	1,25	Foundation failure
119	30	4	0	2	16	20	50	0	10000	0,35	0,3	C_30_4_0_16_50_0.3_D	2	30	400	0,4179	167,16	3,34	1,25	Base failure_EQ
120	30	8	0	2	16	20	50	0	10000	0,35	0,3	C_30_8_0_16_50_0.3_D	4	30	400	0,3358	134,32	2,69	1,25	Base failure_EQ
121	30	2	0	2	2	20	100	0	20000	0,35	0,3	C_30_2_0_2_100_0.3_D	1	30	800	0,42125	337	3,37	2,50	Base failure_EQ
122	30	4	0	2	2	20	100	0	20000	0,35	0,3	C_30_4_0_2_100_0.3_D	2	30	800	0,4281	342,48	3,42	2,50	Foundation failure
123	30	8	0	2	2	20	100	0	20000	0,35	0,3	C_30_8_0_2_100_0.3_D	4	30	800	0,419	335,2	3,35	2,50	Foundation failure
124	30	2	0	2	4	20	100	0	20000	0,35	0,3	C_30_2_0_4_100_0.3_D	1	30	800	0,3992	319,36	3,19	2,50	Foundation failure
125	30	4	0	2	4	20	100	0	20000	0,35	0,3	C_30_4_0_4_100_0.3_D	2	30	800	0,4209	336,72	3,37	2,50	Foundation failure
126	30	8	0	2	4	20	100	0	20000	0,35	0,3	C_30_8_0_4_100_0.3_D	4	30	800	0,4121	329,68	3,30	2,50	Foundation failure
127	30	2	0	2	8	20	100	0	20000	0,35	0,3	C_30_2_0_8_100_0.3_D	1	30	800	0,38625	309	3,09	2,50	Base failure_EQ
128	30	4	0	2	8	20	100	0	20000	0,35	0,3	C_30_4_0_8_100_0.3_D	2	30	800	0,4153	332,24	3,32	2,50	Foundation failure
129	30	8	0	2	8	20	100	0	20000	0,35	0,3	C_30_8_0_8_100_0.3_D	4	30	800	0,4073	325,84	3,26	2,50	Foundation failure
130	30	2	0	2	16	20	100	0	20000	0,35	0,3	C_30_2_0_16_100_0.3_D	1	30	800	0,425	340	3,40	2,50	Foundation failure
131	30	4	0	2	16	20	100	0	20000	0,35	0,3	C_30_4_0_16_100_0.3_D	2	30	800	0,3982	318,56	3,19	2,50	Base failure_EQ
132	30	8	0	2	16	20	100	0	20000	0,35	0,3	C_30_8_0_16_100_0.3_D	4	30	800	0,3942	315,36	3,15	2,50	Base failure_EQ
133	30	2	0	2	2	20	200	0	40000	0,35	0,3	C_30_2_0_2_200_0.3_D	1	30	1600	0,45	720	3,60	5,00	Base failure_EQ
134	30	4	0	2	2	20	200	0	40000	0,35	0,3	C_30_4_0_2_200_0.3_D	2	30	1600	0,4149	663,84	3,32	5,00	Base failure_EQ
135	30	8	0	2	2	20	200	0	40000	0,35	0,3	C_30_8_0_2_200_0.3_D	4	30	1600	0,4203	672,48	3,36	5,00	Base failure_EQ
136	30	2	0	2	4	20	200	0	40000	0,35	0,3	C_30_2_0_4_200_0.3_D	1	30	1600	0,4162	665,92	3,33	5,00	Base failure_EQ
137	30	4	0	2	4	20	200	0	40000	0,35	0,3	C_30_4_0_4_200_0.3_D	2	30	1600	0,3998	639,68	3,20	5,00	Base failure_EQ
138	30	8	0	2	4	20	200	0	40000	0,35	0,3	C_30_8_0_4_200_0.3_D	4	30	1600	0,4149	663,84	3,32	5,00	Base failure_EQ
139	30	2	0	2	8	20	200	0	40000	0,35	0,3	C_30_2_0_8_200_0.3_D	1	30	1600	0,3751	600,16	3,00	5,00	Base failure_EQ
140	30	4	0	2	8	20	200	0	40000	0,35	0,3	C_30_4_0_8_200_0.3_D	2	30	1600	0,3836	613,76	3,07	5,00	Base failure_EQ
141	30	8	0	2	8	20	200	0	40000	0,35	0,3	C_30_8_0_8_200_0.3_D	4	30	1600	0,4082	653,12	3,27	5,00	Base failure_EQ
142	30	2	0	2	16	20	200	0	40000	0,35	0,3	C_30_2_0_16_200_0.3_D	1	30	1600	0,4099	655,84	3,28	5,00	Base failure_EQ
143	30	4	0	2	16	20	200	0	40000	0,35	0,3	C_30_4_0_16_200_0.3_D	2	30	1600	0,4096	655,36	3,28	5,00	Base failure_EQ
144	30	8	0	2	16	20	200	0	40000	0,35	0,3	C_30_8_0_16_200_0.3_D	4	30	1600	0,4114	658,24	3,29	5,00	Base failure_EQ

N.F. :Not found.
Base failure_EQ:Failed due to earthquake.
Base failure_GR:Failed due to gravity.

Table B.3. List of results of finite elements models created for seismic condition (β= 45°)

Model No.	GEOTECHNICAL PROPERTIES					SLOPE SOIL PROPERTIES					SEISMIC EFFECT	FILE NAME	ANALYSIS RESULTS FOR SEISMIC LOADING							
	β (°)	H (m)	λ	B (m)	L (m)	γ (kN/m³)	c_u (kN/m²)	ϕ_u (°)	E_u (kPa)	ν_u	k_h		H/B	β (°)	Load	Mstage	q_f (kPa)	N_{cs}	cu/γB	Failure Mode
1	45	2	0	2	2	20	25	0	5000	0,35	0,1	C_45_2_0_2_25_0.1_D	1	45	300	0,424	127,2	5,09	0,63	Foundation Failure
2	45	4	0	2	2	20	25	0	5000	0,35	0,1	C_45_4_0_2_25_0.1_D	2	45	200	0,5766	115,32	4,61	0,63	Base failure_EQ
3	45	8	0	2	2	20	25	0	5000	0,35	0,1	C_45_8_0_2_25_0.1_D	4	45	200	N.F.	N.F.	N.F.	0,63	Base failure_GR
4	45	2	0	2	4	20	25	0	5000	0,35	0,1	C_45_2_0_4_25_0.1_D	1	45	200	0,6649	132,98	5,32	0,63	Foundation Failure
5	45	4	0	2	4	20	25	0	5000	0,35	0,1	C_45_4_0_4_25_0.1_D	2	45	200	0,5755	115,1	4,60	0,63	Base failure_EQ
6	45	8	0	2	4	20	25	0	5000	0,35	0,1	C_45_8_0_4_25_0.1_D	4	45	200	N.F.	N.F.	N.F.	0,63	Base failure_GR
7	45	2	0	2	8	20	25	0	5000	0,35	0,1	C_45_2_0_8_25_0.1_D	1	45	200	0,5172	103,44	4,14	0,63	Foundation Failure
8	45	4	0	2	8	20	25	0	5000	0,35	0,1	C_45_4_0_8_25_0.1_D	2	45	200	0,535	107	4,28	0,63	Foundation Failure
9	45	8	0	2	8	20	25	0	5000	0,35	0,1	C_45_8_0_8_25_0.1_D	4	45	200	N.F.	N.F.	N.F.	0,63	Base failure_GR
10	45	2	0	2	16	20	25	0	5000	0,35	0,1	C_45_2_0_16_25_0.1_D	1	45	200	0,4842	96,84	3,87	0,63	Foundation Failure
11	45	4	0	2	16	20	25	0	5000	0,35	0,1	C_45_4_0_16_25_0.1_D	2	45	200	0,5078	101,56	4,06	0,63	Foundation Failure
12	45	8	0	2	16	20	25	0	5000	0,35	0,1	C_45_8_0_16_25_0.1_D	4	45	200	N.F.	N.F.	N.F.	0,63	Base failure_GR
13	45	2	0	2	2	20	50	0	10000	0,35	0,1	C_45_2_0_2_50_0.1_D	1	45	600	0,513	307,8	6,16	1,25	Foundation Failure
14	45	4	0	2	2	20	50	0	10000	0,35	0,1	C_45_4_0_2_50_0.1_D	2	45	600	0,5028	301,68	6,03	1,25	Foundation Failure
15	45	8	0	2	2	20	50	0	10000	0,35	0,1	C_45_8_0_2_50_0.1_D	4	45	400	0,728	291,2	5,82	1,25	Foundation Failure
16	45	2	0	2	4	20	50	0	10000	0,35	0,1	C_45_2_0_4_50_0.1_D	1	45	600	0,4215	252,9	5,06	1,25	Foundation Failure
17	45	4	0	2	4	20	50	0	10000	0,35	0,1	C_45_4_0_4_50_0.1_D	2	45	400	0,6272	250,88	5,02	1,25	Foundation Failure
18	45	8	0	2	4	20	50	0	10000	0,35	0,1	C_45_8_0_4_50_0.1_D	4	45	400	0,7145	285,8	5,72	1,25	Foundation Failure
19	45	2	0	2	8	20	50	0	10000	0,35	0,1	C_45_2_0_8_50_0.1_D	1	45	400	0,5131	205,24	4,10	1,25	Foundation Failure
20	45	4	0	2	8	20	50	0	10000	0,35	0,1	C_45_4_0_8_50_0.1_D	2	45	400	0,5108	204,32	4,09	1,25	Foundation Failure
21	45	8	0	2	8	20	50	0	10000	0,35	0,1	C_45_8_0_8_50_0.1_D	4	45	400	0,591	236,4	4,73	1,25	Foundation Failure
22	45	2	0	2	16	20	50	0	10000	0,35	0,1	C_45_2_0_16_50_0.1_D	1	45	400	0,6573	262,92	5,26	1,25	Foundation Failure
23	45	4	0	2	16	20	50	0	10000	0,35	0,1	C_45_4_0_16_50_0.1_D	2	45	400	0,6016	240,64	4,81	1,25	Foundation Failure
24	45	8	0	2	16	20	50	0	10000	0,35	0,1	C_45_8_0_16_50_0.1_D	4	45	400	0,6341	253,64	5,07	1,25	Foundation Failure
25	45	2	0	2	2	20	100	0	20000	0,35	0,1	C_45_2_0_2_100_0.1_D	1	45	1000	0,5131	513,1	5,13	2,50	Foundation Failure
26	45	4	0	2	2	20	100	0	20000	0,35	0,1	C_45_4_0_2_100_0.1_D	2	45	1000	0,5269	526,9	5,27	2,50	Foundation Failure
27	45	8	0	2	2	20	100	0	20000	0,35	0,1	C_45_8_0_2_100_0.1_D	4	45	1000	0,5083	508,3	5,08	2,50	Foundation Failure
28	45	2	0	2	4	20	100	0	20000	0,35	0,1	C_45_2_0_4_100_0.1_D	1	45	800	0,6533	522,64	5,23	2,50	Foundation Failure
29	45	4	0	2	4	20	100	0	20000	0,35	0,1	C_45_4_0_4_100_0.1_D	2	45	800	0,6536	522,88	5,23	2,50	Foundation Failure
30	45	8	0	2	4	20	100	0	20000	0,35	0,1	C_45_8_0_4_100_0.1_D	4	45	800	0,5525	442	4,42	2,50	Foundation Failure
31	45	2	0	2	8	20	100	0	20000	0,35	0,1	C_45_2_0_8_100_0.1_D	1	45	800	0,6103	488,24	4,88	2,50	Foundation Failure
32	45	4	0	2	8	20	100	0	20000	0,35	0,1	C_45_4_0_8_100_0.1_D	2	45	800	0,5876	470,08	4,70	2,50	Foundation Failure
33	45	8	0	2	8	20	100	0	20000	0,35	0,1	C_45_8_0_8_100_0.1_D	4	45	800	0,6103	488,24	4,88	2,50	Foundation Failure
34	45	2	0	2	16	20	100	0	20000	0,35	0,1	C_45_2_0_16_100_0.1_D	1	45	800	0,6731	538,48	5,38	2,50	Foundation Failure
35	45	4	0	2	16	20	100	0	20000	0,35	0,1	C_45_4_0_16_100_0.1_D	2	45	800	0,6364	509,12	5,09	2,50	Foundation Failure
36	45	8	0	2	16	20	100	0	20000	0,35	0,1	C_45_8_0_16_100_0.1_D	4	45	800	0,6621	529,68	5,30	2,50	Foundation Failure
37	45	2	0	2	2	20	200	0	40000	0,35	0,1	C_45_2_0_2_200_0.1_D	1	45	1600	0,7747	1239,52	6,20	5,00	Foundation Failure
38	45	4	0	2	2	20	200	0	40000	0,35	0,1	C_45_4_0_2_200_0.1_D	2	45	1600	0,7707	1233,12	6,17	5,00	Foundation Failure
39	45	8	0	2	2	20	200	0	40000	0,35	0,1	C_45_8_0_2_200_0.1_D	4	45	1600	0,7383	1181,28	5,91	5,00	Foundation Failure
40	45	2	0	2	4	20	200	0	40000	0,35	0,1	C_45_2_0_4_200_0.1_D	1	45	1600	0,6649	1063,84	5,32	5,00	Foundation Failure
41	45	4	0	2	4	20	200	0	40000	0,35	0,1	C_45_4_0_4_200_0.1_D	2	45	1600	0,6514	1042,24	5,21	5,00	Foundation Failure
42	45	8	0	2	4	20	200	0	40000	0,35	0,1	C_45_8_0_4_200_0.1_D	4	45	1600	0,7333	1173,28	5,87	5,00	Foundation Failure
43	45	2	0	2	8	20	200	0	40000	0,35	0,1	C_45_2_0_8_200_0.1_D	1	45	1600	0,614	982,4	4,91	5,00	Foundation Failure
44	45	4	0	2	8	20	200	0	40000	0,35	0,1	C_45_4_0_8_200_0.1_D	2	45	1600	0,6078	972,48	4,86	5,00	Foundation Failure
45	45	8	0	2	8	20	200	0	40000	0,35	0,1	C_45_8_0_8_200_0.1_D	4	45	1600	0,7325	1172	5,86	5,00	Foundation Failure
46	45	2	0	2	16	20	200	0	40000	0,35	0,1	C_45_2_0_16_200_0.1_D	1	45	1600	0,6935	1109,6	5,55	5,00	Foundation Failure
47	45	4	0	2	16	20	200	0	40000	0,35	0,1	C_45_4_0_16_200_0.1_D	2	45	1600	0,6526	1044,16	5,22	5,00	Foundation Failure
48	45	8	0	2	16	20	200	0	40000	0,35	0,1	C_45_8_0_16_200_0.1_D	4	45	1600	0,6728	1076,48	5,38	5,00	Foundation Failure

N.F. :Not found.
Base failure_EQ:Failed due to earthquake.
Base failure_GR:Failed due to gravity.

Table B.3. List of results of finite elements models created for seismic condition (β= 45°) (Cont.).

Model No.	GEOTECHNICAL PROPERTIES					SLOPE SOIL PROPERTIES				SEISMIC EFFECT	FILE NAME	ANALYSIS RESULTS FOR SEISMIC LOADING								
	β (°)	H (m)	λ	B (m)	L (m)	γ (kN/m³)	c_u (kN/m²)	ϕ_u (°)	E_u (kPa)	ν_u	k_h		H/B	β (°)	Load	Mstage	q_f (kPa)	N_{cs}	cu/γB	Failure Mode
49	45	2	0	2	2	20	25	0	5000	0,35	0,2	C_45_2_0_2_25_0.2_D	1	45	200	0,5204	104,08	4,16	0,63	Base failure_EQ
50	45	4	0	2	2	20	25	0	5000	0,35	0,2	C_45_4_0_2_25_0.2_D	2	45	200	0,288	57,6	2,30	0,63	Base failure_EQ
51	45	8	0	2	2	20	25	0	5000	0,35	0,2	C_45_8_0_2_25_0.2_D	4	45	200	N.F.	N.F.	N.F.	0,63	Base failure_GR
52	45	2	0	2	4	20	25	0	5000	0,35	0,2	C_45_2_0_4_25_0.2_D	1	45	300	0,3283	98,49	3,94	0,63	Foundation Failure
53	45	4	0	2	4	20	25	0	5000	0,35	0,2	C_45_4_0_4_25_0.2_D	2	45	200	0,2874	57,48	2,30	0,63	Base failure_EQ
54	45	8	0	2	4	20	25	0	5000	0,35	0,2	C_45_8_0_4_25_0.2_D	4	45	200	N.F.	N.F.	N.F.	0,63	Base failure_GR
55	45	2	0	2	8	20	25	0	5000	0,35	0,2	C_45_2_0_8_25_0.2_D	1	45	200	0,4752	95,04	3,80	0,63	Foundation Failure
56	45	4	0	2	8	20	25	0	5000	0,35	0,2	C_45_4_0_8_25_0.2_D	2	45	200	0,2877	57,54	2,30	0,63	Base failure_EQ
57	45	8	0	2	8	20	25	0	5000	0,35	0,2	C_45_8_0_8_25_0.2_D	4	45	200	N.F.	N.F.	N.F.	0,63	Base failure_GR
58	45	2	0	2	16	20	25	0	5000	0,35	0,2	C_45_2_0_16_25_0.2_D	1	45	200	0,5253	105,06	4,20	0,63	Base failure_EQ
59	45	4	0	2	16	20	25	0	5000	0,35	0,2	C_45_4_0_16_25_0.2_D	2	45	200	0,2931	58,62	2,34	0,63	Base failure_EQ
60	45	8	0	2	16	20	25	0	5000	0,35	0,2	C_45_8_0_16_25_0.2_D	4	45	200	N.F.	N.F.	N.F.	0,63	Base failure_GR
61	45	2	0	2	2	20	50	0	10000	0,35	0,2	C_45_2_0_2_50_0.2_D	1	45	600	0,346	207,6	4,15	1,25	Foundation Failure
62	45	4	0	2	2	20	50	0	10000	0,35	0,2	C_45_4_0_2_50_0.2_D	2	45	400	0,5158	206,32	4,13	1,25	Foundation Failure
63	45	8	0	2	2	20	50	0	10000	0,35	0,2	C_45_8_0_2_50_0.2_D	4	45	400	0,5341	213,64	4,27	1,25	Base failure_EQ
64	45	2	0	2	4	20	50	0	10000	0,35	0,2	C_45_2_0_4_50_0.2_D	1	45	400	0,4554	182,16	3,64	1,25	Foundation Failure
65	45	4	0	2	4	20	50	0	10000	0,35	0,2	C_45_4_0_4_50_0.2_D	2	45	400	0,4729	189,16	3,78	1,25	Foundation Failure
66	45	8	0	2	4	20	50	0	10000	0,35	0,2	C_45_8_0_4_50_0.2_D	4	45	400	0,5341	213,64	4,27	1,25	Base failure_EQ
67	45	2	0	2	8	20	50	0	10000	0,35	0,2	C_45_2_0_8_50_0.2_D	1	45	400	0,424	169,6	3,39	1,25	Foundation Failure
68	45	4	0	2	8	20	50	0	10000	0,35	0,2	C_45_4_0_8_50_0.2_D	2	45	400	0,4224	168,96	3,38	1,25	Foundation Failure
69	45	8	0	2	8	20	50	0	10000	0,35	0,2	C_45_8_0_8_50_0.2_D	4	45	400	0,5324	212,96	4,26	1,25	Base failure_EQ
70	45	2	0	2	16	20	50	0	10000	0,35	0,2	C_45_2_0_16_50_0.2_D	1	45	400	0,4475	179	3,58	1,25	Foundation Failure
71	45	4	0	2	16	20	50	0	10000	0,35	0,2	C_45_4_0_16_50_0.2_D	2	45	400	0,4424	176,96	3,54	1,25	Foundation Failure
72	45	8	0	2	16	20	50	0	10000	0,35	0,2	C_45_8_0_16_50_0.2_D	4	45	400	0,5406	216,24	4,32	1,25	Base failure_EQ
73	45	2	0	2	2	20	100	0	20000	0,35	0,2	C_45_2_0_2_100_0.2_D	1	45	1000	0,4186	418,6	4,19	2,50	Foundation Failure
74	45	4	0	2	2	20	100	0	20000	0,35	0,2	C_45_4_0_2_100_0.2_D	2	45	800	0,5087	406,96	4,07	2,50	Foundation Failure
75	45	8	0	2	2	20	100	0	20000	0,35	0,2	C_45_8_0_2_100_0.2_D	4	45	1000	0,4175	417,5	4,18	2,50	Foundation Failure
76	45	2	0	2	4	20	100	0	20000	0,35	0,2	C_45_2_0_4_100_0.2_D	1	45	800	0,4827	386,16	3,86	2,50	Foundation Failure
77	45	4	0	2	4	20	100	0	20000	0,35	0,2	C_45_4_0_4_100_0.2_D	2	45	800	0,5695	455,6	4,56	2,50	Foundation Failure
78	45	8	0	2	4	20	100	0	20000	0,35	0,2	C_45_8_0_4_100_0.2_D	4	45	800	0,5219	417,52	4,18	2,50	Foundation Failure
79	45	2	0	2	8	20	100	0	20000	0,35	0,2	C_45_2_0_8_100_0.2_D	1	45	800	0,4449	355,92	3,56	2,50	Foundation Failure
80	45	4	0	2	8	20	100	0	20000	0,35	0,2	C_45_4_0_8_100_0.2_D	2	45	800	0,4451	356,08	3,56	2,50	Foundation Failure
81	45	8	0	2	8	20	100	0	20000	0,35	0,2	C_45_8_0_8_100_0.2_D	4	45	800	0,4803	384,24	3,84	2,50	Foundation Failure
82	45	2	0	2	16	20	100	0	20000	0,35	0,2	C_45_2_0_16_100_0.2_D	1	45	800	0,5913	473,04	4,73	2,50	Foundation Failure
83	45	4	0	2	16	20	100	0	20000	0,35	0,2	C_45_4_0_16_100_0.2_D	2	45	800	0,5655	452,4	4,52	2,50	Foundation Failure
84	45	8	0	2	16	20	100	0	20000	0,35	0,2	C_45_8_0_16_100_0.2_D	4	45	800	0,5696	455,68	4,56	2,50	Foundation Failure
85	45	2	0	2	2	20	200	0	40000	0,35	0,2	C_45_2_0_2_200_0.2_D	1	45	1600	0,7747	1239,52	6,20	5,00	Foundation Failure
86	45	4	0	2	2	20	200	0	40000	0,35	0,2	C_45_4_0_2_200_0.2_D	2	45	1600	0,5299	847,84	4,24	5,00	Foundation Failure
87	45	8	0	2	2	20	200	0	40000	0,35	0,2	C_45_8_0_2_200_0.2_D	4	45	1600	0,6085	973,6	4,87	5,00	Foundation Failure
88	45	2	0	2	4	20	200	0	40000	0,35	0,2	C_45_2_0_4_200_0.2_D	1	45	1600	0,5712	913,92	4,57	5,00	Foundation Failure
89	45	4	0	2	4	20	200	0	40000	0,35	0,2	C_45_4_0_4_200_0.2_D	2	45	1600	0,5693	910,88	4,55	5,00	Foundation Failure
90	45	8	0	2	4	20	200	0	40000	0,35	0,2	C_45_8_0_4_200_0.2_D	4	45	1600	0,6073	971,68	4,86	5,00	Foundation Failure
91	45	2	0	2	8	20	200	0	40000	0,35	0,2	C_45_2_0_8_200_0.2_D	1	45	1600	0,5226	836,16	4,18	5,00	Foundation Failure
92	45	4	0	2	8	20	200	0	40000	0,35	0,2	C_45_4_0_8_200_0.2_D	2	45	1600	0,5115	818,4	4,09	5,00	Foundation Failure
93	45	8	0	2	8	20	200	0	40000	0,35	0,2	C_45_8_0_8_200_0.2_D	4	45	1600	0,6051	968,16	4,84	5,00	Foundation Failure
94	45	2	0	2	16	20	200	0	40000	0,35	0,2	C_45_2_0_16_200_0.2_D	1	45	1600	0,5958	953,28	4,77	5,00	Foundation Failure
95	45	4	0	2	16	20	200	0	40000	0,35	0,2	C_45_4_0_16_200_0.2_D	2	45	1600	0,5748	919,68	4,60	5,00	Foundation Failure
96	45	8	0	2	16	20	200	0	40000	0,35	0,2	C_45_8_0_16_200_0.2_D	4	45	1600	0,5791	926,56	4,63	5,00	Foundation Failure

N.F. :Not found.
Base failure_EQ:Failed due to earthquake.
Base failure_GR:Failed due to gravity.

Table B.3. List of results of finite elements models created for seismic condition (β= 45°) (Cont.).

Model No.	GEOTECHNICAL PROPERTIES					SLOPE SOIL PROPERTIES				SEISMIC EFFECT	FILE NAME	ANALYSIS RESULTS FOR SEISMIC LOADING							
	β (°)	H (m)	λ	B (m)	L (m)	γ (kN/m³)	c_u (kN/m²)	ϕ_u (°)	E_u (kPa)	ν_u	k_h		H/B	β (°)	Load	Mstage	q_f (kPa)	N_{cs}	cu/γB	Failure Mode
97	45	2	0	2	2	20	25	0	5000	0,35	0,3	C_45_2_0_2_25_0.3_D	1	45	200	0,3472	69,44	2,78	0,63	Base failure_EQ
98	45	4	0	2	2	20	25	0	5000	0,35	0,3	C_45_4_0_2_25_0.3_D	2	45	200	0,1919	38,38	1,54	0,63	Base failure_EQ
99	45	8	0	2	2	20	25	0	5000	0,35	0,3	C_45_8_0_2_25_0.3_D	4	45	200	N.F.	N.F.	N.F.	0,63	Base failure_GR
100	45	2	0	2	4	20	25	0	5000	0,35	0,3	C_45_2_0_4_25_0.3_D	1	45	200	0,3466	69,32	2,77	0,63	Base failure_EQ
101	45	4	0	2	4	20	25	0	5000	0,35	0,3	C_45_4_0_4_25_0.3_D	2	45	200	0,1919	38,38	1,54	0,63	Base failure_EQ
102	45	8	0	2	4	20	25	0	5000	0,35	0,3	C_45_8_0_4_25_0.3_D	4	45	200	N.F.	N.F.	N.F.	0,63	Base failure_GR
103	45	2	0	2	8	20	25	0	5000	0,35	0,3	C_45_2_0_8_25_0.3_D	1	45	200	0,3457	69,14	2,77	0,63	Base failure_EQ
104	45	4	0	2	8	20	25	0	5000	0,35	0,3	C_45_4_0_8_25_0.3_D	2	45	200	0,1919	38,38	1,54	0,63	Base failure_EQ
105	45	8	0	2	8	20	25	0	5000	0,35	0,3	C_45_8_0_8_25_0.3_D	4	45	200	N.F.	N.F.	N.F.	0,63	Base failure_GR
106	45	2	0	2	16	20	25	0	5000	0,35	0,3	C_45_2_0_16_25_0.3_D	1	45	200	0,345	69	2,76	0,63	Base failure_EQ
107	45	4	0	2	16	20	25	0	5000	0,35	0,3	C_45_4_0_16_25_0.3_D	2	45	200	0,1954	39,08	1,56	0,63	Base failure_EQ
108	45	8	0	2	16	20	25	0	5000	0,35	0,3	C_45_8_0_16_25_0.3_D	4	45	200	N.F.	N.F.	N.F.	0,63	Base failure_GR
109	45	2	0	2	2	20	50	0	10000	0,35	0,3	C_45_2_0_2_50_0.3_D	1	45	600	0,3169	190,14	3,80	1,25	Foundation Failure
110	45	4	0	2	2	20	50	0	10000	0,35	0,3	C_45_4_0_2_50_0.3_D	2	45	400	0,4255	170,2	3,40	1,25	Foundation Failure
111	45	8	0	2	2	20	50	0	10000	0,35	0,3	C_45_8_0_2_50_0.3_D	4	45	400	0,3561	142,44	2,85	1,25	Base failure_EQ
112	45	2	0	2	4	20	50	0	10000	0,35	0,3	C_45_2_0_4_50_0.3_D	1	45	600	0,2869	172,14	3,44	1,25	Foundation Failure
113	45	4	0	2	4	20	50	0	10000	0,35	0,3	C_45_4_0_4_50_0.3_D	2	45	400	0,3919	156,76	3,14	1,25	Foundation Failure
114	45	8	0	2	4	20	50	0	10000	0,35	0,3	C_45_8_0_4_50_0.3_D	4	45	400	0,3561	142,44	2,85	1,25	Base failure_EQ
115	45	2	0	2	8	20	50	0	10000	0,35	0,3	C_45_2_0_8_50_0.3_D	1	45	400	0,3791	151,64	3,03	1,25	Foundation Failure
116	45	4	0	2	8	20	50	0	10000	0,35	0,3	C_45_4_0_8_50_0.3_D	2	45	400	0,3825	153	3,06	1,25	Foundation Failure
117	45	8	0	2	8	20	50	0	10000	0,35	0,3	C_45_8_0_8_50_0.3_D	4	45	400	0,3546	141,84	2,84	1,25	Base failure_EQ
118	45	2	0	2	16	20	50	0	10000	0,35	0,3	C_45_2_0_16_50_0.3_D	1	45	400	0,3714	148,56	2,97	1,25	Foundation Failure
119	45	4	0	2	16	20	50	0	10000	0,35	0,3	C_45_4_0_16_50_0.3_D	2	45	400	0,3728	149,12	2,98	1,25	Foundation Failure
120	45	8	0	2	16	20	50	0	10000	0,35	0,3	C_45_8_0_16_50_0.3_D	4	45	400	0,3596	143,84	2,88	1,25	Base failure_EQ
121	45	2	0	2	2	20	100	0	20000	0,35	0,3	C_45_2_0_2_100_0.3_D	1	45	1000	0,3335	333,5	3,34	2,50	Foundation Failure
122	45	4	0	2	2	20	100	0	20000	0,35	0,3	C_45_4_0_2_100_0.3_D	2	45	800	0,4472	357,76	3,58	2,50	Foundation Failure
123	45	8	0	2	2	20	100	0	20000	0,35	0,3	C_45_8_0_2_100_0.3_D	4	45	800	0,4208	336,64	3,37	2,50	Foundation Failure
124	45	2	0	2	4	20	100	0	20000	0,35	0,3	C_45_2_0_4_100_0.3_D	1	45	800	0,39625	317	3,17	2,50	Foundation Failure
125	45	4	0	2	4	20	100	0	20000	0,35	0,3	C_45_4_0_4_100_0.3_D	2	45	800	0,4344	347,52	3,48	2,50	Foundation Failure
126	45	8	0	2	4	20	100	0	20000	0,35	0,3	C_45_8_0_4_100_0.3_D	4	45	800	0,3991	319,28	3,19	2,50	Foundation Failure
127	45	2	0	2	8	20	100	0	20000	0,35	0,3	C_45_2_0_8_100_0.3_D	1	45	800	0,3726	298,08	2,98	2,50	Foundation Failure
128	45	4	0	2	8	20	100	0	20000	0,35	0,3	C_45_4_0_8_100_0.3_D	2	45	800	0,4308	344,64	3,45	2,50	Foundation Failure
129	45	8	0	2	8	20	100	0	20000	0,35	0,3	C_45_8_0_8_100_0.3_D	4	45	800	0,3744	299,52	3,00	2,50	Foundation Failure
130	45	2	0	2	16	20	100	0	20000	0,35	0,3	C_45_2_0_16_100_0.3_D	1	45	800	0,3894	311,52	3,12	2,50	Foundation Failure
131	45	4	0	2	16	20	100	0	20000	0,35	0,3	C_45_4_0_16_100_0.3_D	2	45	800	0,3841	307,28	3,07	2,50	Foundation Failure
132	45	8	0	2	16	20	100	0	20000	0,35	0,3	C_45_8_0_16_100_0.3_D	4	45	800	0,3785	302,8	3,03	2,50	Foundation Failure
133	45	2	0	2	2	20	200	0	40000	0,35	0,3	C_45_2_0_2_200_0.3_D	1	45	1800	0,3773	679,14	3,40	5,00	Foundation Failure
134	45	4	0	2	2	20	200	0	40000	0,35	0,3	C_45_4_0_2_200_0.3_D	2	45	1600	0,4287	685,92	3,43	5,00	Foundation Failure
135	45	8	0	2	2	20	200	0	40000	0,35	0,3	C_45_8_0_2_200_0.3_D	4	45	1600	0,4222	675,52	3,38	5,00	Foundation Failure
136	45	2	0	2	4	20	200	0	40000	0,35	0,3	C_45_2_0_4_200_0.3_D	1	45	1600	0,4112	657,92	3,29	5,00	Base failure_EQ
137	45	4	0	2	4	20	200	0	40000	0,35	0,3	C_45_4_0_4_200_0.3_D	2	45	1600	0,4119	659,04	3,30	5,00	Base failure_EQ
138	45	8	0	2	4	20	200	0	40000	0,35	0,3	C_45_8_0_4_200_0.3_D	4	45	1600	0,4049	647,84	3,24	5,00	Foundation Failure
139	45	2	0	2	8	20	200	0	40000	0,35	0,3	C_45_2_0_8_200_0.3_D	1	45	1600	0,4065	650,4	3,25	5,00	Foundation Failure
140	45	4	0	2	8	20	200	0	40000	0,35	0,3	C_45_4_0_8_200_0.3_D	2	45	1600	0,4092	654,72	3,27	5,00	Foundation Failure
141	45	8	0	2	8	20	200	0	40000	0,35	0,3	C_45_8_0_8_200_0.3_D	4	45	1600	0,3671	587,36	2,94	5,00	Base failure_EQ
142	45	2	0	2	16	20	200	0	40000	0,35	0,3	C_45_2_0_16_200_0.3_D	1	45	1600	0,3479	556,64	2,78	5,00	Base failure_EQ
143	45	4	0	2	16	20	200	0	40000	0,35	0,3	C_45_4_0_16_200_0.3_D	2	45	1600	0,339	542,4	2,71	5,00	Foundation Failure
144	45	8	0	2	16	20	200	0	40000	0,35	0,3	C_45_8_0_16_200_0.3_D	4	45	1600	0,415	664	3,32	5,00	Foundation Failure

N.F. :Not found.
Base failire_EQ:Failed due to earthquake.
Base failire_GR:Failed due to gravity.